

Low band gap polymers for solar cells: The influence of chemical structure on electronic structure, interfacial properties and self-organization of thin films

Dissertation

der Mathematisch-Naturwissenschaftlichen Fakultät
der Eberhard Karls Universität Tübingen
zur Erlangung des Grades eines
Doktors der Naturwissenschaften
(Dr. rer. nat.)

vorgelegt von
Milutin Ivanović
Belgrad/Serbien

Tübingen 2019

Gedruckt mit Genehmigung der Mathematisch-Naturwissenschaftlichen Fakultät der
Eberhard Karls Universität Tübingen.

Tag der mündlichen Qualifikation:	12.11.2019
Dekan:	Prof. Dr. Wolfgang Rosenstiel
1. Berichterstatter:	Prof. Dr. Thomas Chassé
2. Berichterstatter:	Prof. Dr. Udo Weimar

**Low band gap polymers for solar cells:
The influence of chemical structure on
electronic structure, interfacial
properties and self-organization of thin
films**

Advisors:

Prof. Dr. Thomas Chassé
apl. Prof. Dr. Heiko Peisert

Candidate:

Milutin Ivanović

*Овај рад је с љубављу и захвалношћу
посвећен мојој породици.*

Contents

Zusammenfassung.....	v
Abstract.....	vii
Acknowledgments.....	ix
Chapter 1 - Introduction.....	1
Chapter 2 - Surfaces, interfaces and thin films of organic semiconductors.....	5
2.1. Electronic structure of conductive surface	5
2.2. Interfaces of organic semiconductors	8
2.2.1. Interaction at interfaces of organic semiconductors	8
2.2.2. Models for description of interfaces made by organic semiconductors	11
The Schottky-Mott rule	11
The Induced Density of Interface States (IDIS) model	14
Integer Charge Transfer (ICT) model.....	16
Application of ICT model to multilayer systems.....	20
2.3. Thin films of organic semiconductors	23
2.3.1. Thin films of conjugated polymers	23
2.3.2. Thin films of conjugated polymer/PCBM blends.....	25
2.3.3. Thin films of fullerene C ₆₀	27
Chapter 3 - Experimental methods	30
3.1. Photoelectron spectroscopy (PES)	30
3.1.1. Principles of photoelectron spectroscopy	30
3.1.2. Short theory of photoemission process	34
3.1.3. Interpretation of XPS spectra.....	36
3.1.4. Ultraviolet photoelectron spectroscopy (UPS)	42
3.1.5. Experimental equipment	45
3.2. Near edge X-ray absorption fine structure (NEXAFS)	47
3.2.1. Principles of NEXAFS and its application	47

3.2.2. Experimental equipment	54
Chapter 4 - Materials and sample preparation techniques	55
4.1. Organic semiconducting materials	55
4.2. Substrate materials	58
4.2.1. Indium tin oxide (ITO)	58
4.2.2. Zinc oxide (ZnO)	60
4.2.3. UV/Ozone treated polycrystalline film of gold (AuO _x /Au)	61
4.2.4. Poly(3,4-ethylenedioxythiophene) polystyrene sulfonate (PEDOT:PSS)	62
4.3. Sample preparation techniques	65
4.3.1. Doctor blade casting	65
4.3.2. Organic molecular beam deposition (OMBD)	67
Chapter 5 - Results and Discussion	69
5.1. Donor/electrode interfaces	70
5.1.1. UV-Vis-NIR absorption spectroscopy of low band gap polymer films	70
5.1.2. PES study of interfaces between thin films of LBG polymers and different electrodes	74
5.1.3. Summary of Section 5.1.	83
5.2. PES study of organic donor/acceptor interfaces for OPV devices	88
5.2.1. Acceptor/electrode interface	90
Fullerene C ₆₀ /electrode interfaces	90
PCBM/electrode interfaces	93
5.2.2. Donor/acceptor interface in planar heterojunction	96
Energetics at C ₆₀ /PCPDTTBT interface prepared on three different substrates	96
Energetics at C ₆₀ /PCPDTBBT interface prepared on PEI/ITO and AuO _x /Au substrates	102
5.2.3. Donor/acceptor interface in bulk heterojunction	105
5.2.4. Summary of Section 5.2.	113
5.3. Controlling the interface energetics of PCPDTBT thin film by p-doping with F-TCNQ	115

5.3.1. Interfaces of pristine and doped PCPDTBT thin films with electrode and acceptor overlayer, in bilayer prototype organic solar cell structure.....	117
5.3.2. Summary of Section 5.3.	125
5.4. Self-organization properties of low band gap polymers in pristine and blend thin films	127
5.4.1. Molecular orientation of low band gap polymers in pristine thin films – influence of introduction of additional thiophene moieties	128
5.4.2. Molecular orientation of PCPDTTBTT and PCPDTTBTT polymers in 1:1 blend films with PCBM – the effect of blending	137
5.4.3. The effect of post-deposition thermal annealing on molecular orientation of PCPDTTBTT and PCPDTTBTT polymers in pristine and blend films	138
5.4.4. Summary of Section 5.4.	141
Chapter 6 - General summary	143
Appendix	147
References	148

Zusammenfassung

Intrinsisch halbleitende Polymere stellen eine interessante Klasse an Materialien für verschiedene elektronische Anwendungen dar. Die elektrischen / elektronischen und morphologischen Eigenschaften dünner Filme der Polymere können durch Parameter der organischen Synthese feinabgestimmt werden. In dieser Arbeit wurden Thiophen basierte Copolymere mit niedriger Bandlücke und ähnlicher Struktur in zwei Paare (anhand der Elektronenakzeptor-Einheit) unterteilt, PCPDTBT & PCPDTTBTT und PCPDTBBT & PCPDTTBTT und als aussichtsreiche Donor Materialien für photovoltaische Anwendungen untersucht.

Hauptaugenmerk der Untersuchung war es, Einblick in das Verhältnis zwischen der chemischen Struktur der Polymere und ihrer elektronischen Struktur, Ausrichtung und Wechselwirkung der Energieniveaus an verschiedenen Grenzflächen und Selbstorganisation der dünnen Filme zu ermöglichen. Zunächst werden die dünnen Polymerfilme auf einer Vielzahl verschiedener Substrate (Modellelektroden) präpariert und ihre elektronische Struktur sowie Wechselwirkungen an den Grenzflächen mittels UV-vis-NIR-Spektroskopie, Röntgen- und UV-Photoelektronenspektroskopie untersucht. Es wurde festgestellt, dass die unterschiedliche elektronenakzeptierende Einheit im monomeren Baustein (z.B. PCPDTBT vs. PCPDTBBT) einen größeren Einfluss auf die elektronische Struktur des Polymers hat als das Vorhandensein zusätzlicher (Hexyl)Thiophenringe (z.B. PCPDTBT vs. PCPDTTBTT). Weiterhin wurde gezeigt, dass die beiden Polymere eines Paares ähnliches (energetisches) Verhalten an der Grenzfläche zeigen, während Abweichungen zwischen den Paaren vorliegen. Diese beobachteten Unterschiede beeinflussen und bestimmen die Wechselwirkungen mit organischen Akzeptor Materialien an den untersuchten Donor/Akzeptor Grenzflächen.

Für den Fall eines dünnen Films von PCPDTBT auf ITO, für den eine Lochinjektionsbarriere von 1,0 eV gefunden wurde, wurde nach der durchgeführten p-Dotierung des PCPDTBT mit F4-TCNQ Molekülen aus den Ergebnissen eine verbesserte (deutlich niedrigere) Lochinjektionsbarriere ermittelt, so dass eine günstigere Ausrichtung der Energieniveaus für die Anwendung in Solarzellen erhalten wird.

Letzten Endes wurde eine Serie von Messungen der Röntgen-Nahkanten-Absorptionsspektroskopie (NEXAFS) der reinen, getemperten und (mit PCBM) vermischten dünnen Filme von PCPDTTBTT und PCPDTTBTT durchgeführt und mit einer ähnlichen Serie von PCPDTBT und PCPDTBBT verglichen. Als hauptsächliche Folgerung konnte geschlossen werden, dass die Anwesenheit von Seitenketten einen starken Effekt auf die Fähigkeit zur Selbstorganisation der untersuchten Polymere im dünnen Film haben könnte.

Abstract

Intrinsically semiconductive polymers are a promising class of materials for the application in various electronic devices. Their electrical/electronic and morphological properties in the thin films can be fine-tuned by the methods of organic synthesis. Hence, in this work, the low band gap thiophene-based copolymers with related chemical structure are selected into two pairs (according to their electron accepting subunit): PCPDTBT & PCPDTTBTT and PCPDTBBT & PCPDTTBTT, and studied as promising donor materials for photovoltaic devices.

The main focus of the study was to provide an insight into the relationship between the chemical structure of studied polymers with their electronic structure, energy level alignment (interaction) at different interfaces, and self-organization properties in the thin films. The thin films of polymers are firstly prepared on the plethora of different substrates (model electrodes) and their electronic structure and interaction/energetics at interfaces were probed by means of UV-vis-NiR , X-ray and ultraviolet photoemission spectroscopy. It was found that the presence of different electron accepting moiety in the monomer unit of the polymer (e.g. PCPDTBT vs. PCPDTBBT) has a greater influence on the electronic structure of polymer than the presence of additional (hexyl)thiophene rings (e.g. PCPDTBT vs. PCPDTTBTT). Also, it was found that polymers within pair show similar behaviour (energetics) at interfaces, but rather different between pairs. This observed differences further effect and determine the interaction with organic accepting materials in studied donor/acceptor interfaces.

Moreover, for the case of the thin film of PCPDTBT on ITO, where the hole injection barrier of 1.0 eV was found, the p-doping of the PCPDTBT thin film by F4-TCNQ molecule was

performed, and collected results showed an improved (much lower) hole injection barrier value, thus favourable energy level alignment for the application in solar cells was obtained.

Lastly, a series of near edge X-ray absorption fine structure spectroscopy (NEXAFS) measurements were done on the pristine, annealed and blend (with PCBM) thin films of PCPDTTBTT and PCPDTTBTT polymers, and compared with the same for PCPDTBT and PCPDTBBT polymers. As a main conclusion, it was inferred that the presence of the side chains may have a strong effect on the self-organization ability of studied polymers in thin films.

Acknowledgments

On this occasion, I would like to acknowledge people who helped me to realize this work until the end.

First of all, I would like to express my deepest gratitude to my advisor Prof. Thomas Chassé, for providing me the opportunity to do doctoral studies at such renowned University as Eberhard Karls Universität Tübingen is, for his trust and support during the studies. Overall for his stance of a gentleman.

Furthermore, my sincere appreciation goes to my advisor Prof. Heiko Peisert, for his infinite patience and kindness, immense help, scientific and life schooling, anecdotes and jokes. Heiko, thank you very much for everything!

I would like also to express my thankfulness to PD. Dr. Maria Benedetta Casu for her kindness, and intuitive feeling to provide support and help when they are critically needed.

However, nothing of this job would have been done without my dear comrades and colleagues: Małgorzata Polek, David Balle, Aurelien Tournebize, Reza Kakavandi, Ulf Dettinger, Andreas Früh, Tanja Wolfer, Mathias Glaser, Johannes Uihlein, Sabine Savu, Hilmar Adler, Jan Stiedl, Peter Grüninger, Mahdi Samadi Khoshkhoo, Sahar Abdalla, Malgorzata Krasowska, Dustin Quinones, Maximilian Winkler, Josip Mihaljević, Reimer Karstens, Axel Belser, Sven Bölke, Ivana Mršić, Florian Latteyer, Martin Essig, Umut Aygül, Francesca Ciccullo, Dr. David Batchelor, Caroline Arantes da Silva, Bruno Borges, Sabine Abb, Christoph Raisch, Leilei Luo, Hasina Ramanitra, Bin Shen, Hugo Santos Silva, Mateusz Paszkiewicz and Iman Errouihi, and many others with whom I worked or at least smoked a cigarette. Guys, you made every day at

IPTC to be a great pleasure for me. Thank you very much for your support, help, and friendship!
Staying in Tübingen with you was one joyful ride!

Here, I would like to thank Mrs. Elke Nadler and Mr. Wolfgang Neu for their technical support in the laboratory.

A very special thank goes to my landlord Mr. Adolf Cwejn in whose home I lived the whole my time in Tübingen. Herr Adolfo, thank you very much for all kindness, hospitality, and friendship you gave me. Staying with you, I have never felt as a subtenant in foreign country, rather as a nephew who came from abroad. I wish you a good health and peaceful retirement.

A big thank goes to my Yugoslav teammates in Tübingen, with whom I played football for four years and who made my adaptation to Germany easier.

I want to thank also my Tübingen friends Munir and Aron for their sincere friendship, a petty that we did not hang out more.

Finally, I am grateful to the IPTC administration staff: Bettina Kappler, Brigitte Doez, Andrea Teufel, Christine Stadler, Diana Strauss, Jochen Mehne and Dr. Wolfgang Langer, for their constant support and help with all kind of administrative things I encountered during my work at IPTC and life in Tübingen.

Chapter 1

Introduction

For the symbolic beginning of the field of (conjugated) polymers as materials for electronics, it can be taken the end of 1970s when it was discovered that doped trans-poly(acetylene) can behave like a semiconductor (although the neutral polymer is an insulator).⁵⁻⁶ Based on this discovery, the later experiments brought for the iodine doped poly(acetylene) conductivity of 10^5 S/cm, which is comparable to that of copper.⁷⁻⁸ This pioneering work, about two decades later led towards The Nobel Prize in Chemistry, awarded in 2000 to Hideki Shirakawa, Alan Heeger, and Alan MacDiarmid, for the discovery and development of the conductive polymers. The initial research done on poly(acetylene) paved the way for the later coming conjugated polymers which found a wide range of application in electronic devices such as: light-emitting diodes (LEDs),⁹⁻¹² photovoltaic cells (PVs),¹³⁻¹⁵ field-effect transistors (FETs),¹⁶⁻¹⁸ photodetectors,¹⁹⁻²⁰ RFID sensors,²¹⁻²² and other.

The conjugated polymers as organic materials mainly consist of carbon atoms, with other low atomic number atoms often present, such as oxygen, sulfur, nitrogen, silicon, etc., and their intrinsic semiconductive behavior is based on the presence of sp^2 hybridization and alternation of single and double bonds along the polymer backbone.²³ After poly(acetylene), other conjugated polymers such as polyaromatic homopolymers poly(p-phenylene) (PPP), polypyrrole (PPy), polythiophene (PTs) as well as polyaromatic copolymers poly(p-phenylene vinylene) (PPV), polyaniline (PANi), were in the focus of research interest. These polymers

greatly helped in an understanding of the relationship between chemical structure and physicochemical properties of conjugated polymers (especially electronic structure); still, they demonstrated a limited potential for the application in electronic devices. Hence, the polythiophene group of conjugated polymers emerged as one of the most studied and applied materials for the organic electronic devices.²⁴⁻²⁷ Generally, they possess promising physical and chemical properties reflected in good thermal and environmental stability, solubility, processability, and high conductivity when doped. These unique, electronic, optical, charge transport and self-organization properties (on solid surfaces and in bulk) qualify them for a broad application in the organic electronic devices. Additionally, polythiophenes have shown huge potential for the structural modification which allows tuning of their physicochemical properties. Thus, all above-listed advantages deepen research interest in polythiophene polymers, and among them especially has been interesting poly(3-hexylthiophene) or abbreviated P3HT, which is, saying without gross exaggeration, the workhorse among conjugated semiconducting polymers in the field of organic electronics for last two decades. However, during the last years, in the field of organic photovoltaic cells (OPVs) has increased interest in the low band gap polymers (LBG polymers). They were perceived as promising materials for the improvement of the efficiency of photovoltaic devices, due to improved absorption of sunlight in the visible and near-infrared spectral regions. Methods, such as grafting of various side chains to the monomer unit²⁸ or exchange of the heteroatom in conjugated ring²⁹ have been demonstrated as useful methods for tuning the HOMO-LUMO energy gap (the band gap E_g).³⁰ Here, the HOMO stays for the Highest Occupied Molecular Orbital (π -molecular orbital), while the LUMO is the Lowest Unoccupied Molecular Orbital (antibonding π^* -molecular orbital), which are together called the frontier orbitals.³⁰ Additionally, size (width) of the band gap can be influenced and modified by various factors: substituents effect, π -conjugation length, intra-chain charge transfer, and so on.³¹

Considering all the aforementioned factors, the need for low band gap polymers led to the new generation of conjugated polymers, called donor-acceptor polymers or shortly D-A copolymers. These conjugated copolymers are rendered by coupling an electron rich and an electron deficient organic subunits into the polymer monomer unit. The fusion of these different subunits lowers the band gap due to several reasons. It is expected that in D-A polymers intra-chain charge transfer between subunits with a different electron affinity,³²⁻³³ increases double bond character between the repeat units. As a result, the polymer backbone is expected to be more planar, providing a greater delocalization of π electrons, i.e. the narrower band gap (HOMO-LUMO gap).³⁴⁻³⁵

Hence, we may infer that the synthesis of new polymers is a steady continuous process, with the idea to get materials with overall better characteristics which will improve the performance of the electronic devices, among them OPVs as well. For these new materials to be utilized in devices, the strong correlation between the chemical structure on the one side, and electronic structure and morphology in thin films (pristine and blends) on the other side, should be as better as possible understood. Because, it is known that the electronic structure parameters of an organic semiconductor such as work function, ionization potential, electron affinity or organization in the thin films are not constant, but rather depend on the material preparation, or contact (interaction) with other materials in the OPV cell. Thus, for the better understanding of the electronic structure (properties) and self-assembly characteristics of polymers in the thin films, a study should be done via mimicking real device architecture, i.e. when they are in contact to other materials found in solar cells, such as electrodes or other functional layers. It has been shown that interfacial energetics has a significant influence on the performance of the OPV device, thitherto an optimization of the energy level alignment through the whole device should be done. Therefore, it necessary that electronic structure parameters, such as the work function of the electrodes in contact with organic material(s), the ionization energy of the donor

and electron affinity of the acceptor in contact with electrodes, interface dipoles at all interface, are determined with respect to a specific configuration of the device. The simple assumption of the energy level alignment upon interface formation, based on separately determined material parameters, can be highly misleading.

In this work, the four low band gap D-A copolymers with related chemical structures, potential donor materials for the OPV device, are presented. The work tried to provide an insight into the correlation between the chemical structure of four particular polythiophene LBG copolymers, with their electronic structure and ability for self-organization in the thin films. Firstly, the experimental determination of the energy levels of polymers, relevant for their interaction at interfaces, is done via preparation of polymers' thin films onto five different model electrodes. Then, the interaction at interfaces with representative acceptor materials are studied, as application-relevant interfaces for the polymer-based OPVs. Afterwards, briefly, as an inset, effect of the molecular p-doping of polymer thin film, on the energy level alignment with the substrate and acceptor organics in a prototype organic solar cell structure, is studied. Finally, it is tried to connect the difference in the chemical structure between polymers to their self-ordering characteristics in the neat and blend thin films.

Chapter 2

Surfaces, interfaces and thin films of organic semiconductors

Chapter 2 introduces a reader to the electronic structure of the solid state surface, electronic structure of interfaces made by organic semiconductor thin films, and models for understanding and interpretation of the interaction and ELA at latter interfaces. Moreover, in this chapter, the physicochemical properties of the exemplary thin films of organic semiconductors, will be reviewed.

2.1. Electronic structure of conductive surface

Before considering processes of interaction at the interfaces of organic semiconductors with different types of substrates (model electrodes), firstly, the electronic structure of the conductive solid state surface will be reviewed. Currently, metallic electrodes are commonly encountered in organic electronic devices. Although there has been implemented different organic (for instance PEDOT:PSS) or metal oxide (such as ITO, FTO) electrodes, it would be useful to adopt a few ideas about metallic (i.e. highly conductive) surface, which can be further adapted to other types of electrodes (substrates). One of the fundamental parameters for describing a

metal surface is the work function, which is defined as the energy needed to take away an electron from the metal Fermi level into the rest at the vacuum level.³⁶⁻³⁷ The work function is characterized by two components. The first is the chemical potential (μ_b) of electrons in the bulk, while the second one is the change in electrostatic potential (ϕ) felt by electrons when passing from the bulk towards the surface and furthermore into the vacuum. For every metal surface there is an existing probability of electrons to reside outside of the surface, hence, some electron density is present in the vacuum, beyond the surface up to several angstroms. As a consequence, the lack of negative charge i.e. the excess of positive charge density is present below the surface, in the bulk. The outcome of this charge distribution is created surface dipole (SD), perpendicular to the surface and pointed towards the bulk of the material. In Jellium model³⁸ which describes well this phenomenon, the bulk of metal is considered to consist of the positive ion cores. This positive charge density is described by the step function, that drops from the constant value inside the metal to zero at the metal surface.³⁹ On the other hand, at the same point where the step function declines abruptly (at the surface), electron charge density decreases exponentially leaving the tail on the vacuum side. How the electron density profile at the surface looks like according to Jellium model, is depicted in Figure 2.1.

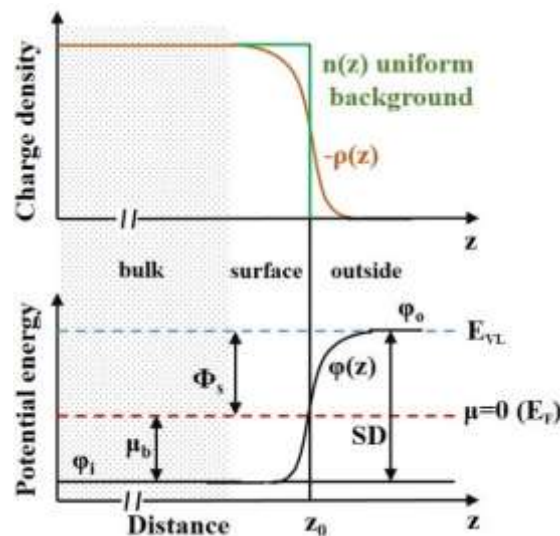


Figure 2.1: In the upper graph are shown positive uniform background charge $n(z)$ and negative electron density $\rho(z)$ as a function of vertical distance (z) relative to the metal surface. In the lower graph is shown a dependence of potential energy $\phi(z)$ on distance z across the metal/vacuum interface.

In the same figure in the graph below, is shown that according to Jellium model, the difference between the potential energy within bulk (ϕ_I) and outside (ϕ_O) of the metal, defines SD which is actually absolute change in the potential energy of electrons. The potential energy difference between ϕ_I and Fermi level (E_F) is defined as the above-mentioned chemical potential (μ_b) of electrons. A corollary from Figure 2.1 stems that the work function of the metal surface equals:

$$\Phi = -\mu_b + SD \quad (2.1)$$

The last equation suggests that an increase in SD gives a higher value of the work function Φ . Indeed, electrons on their way towards the surface and then to the vacuum, move against the electric field created by the surface dipole. Thus, higher SD would imply the higher value of the electric field, and as a consequence, the higher energy is needed to extract an electron from the bulk of metal to a point in the vacuum, on microscopic distance from the solid surface. It can be noticed here, that the last part of the previous sentence is actually the definition of work function.

The connection between the surface dipole and work function can be directly observed in studies of different crystal planes of the same metal. Due to different tailing of electron density outside of the metal surface and corollary different SD, for the (111) and (110) planes of W (tungsten) crystal was observed the difference of 0.78 eV in the work function values.⁴⁰ Moreover, it is theoretically predicted that the contribution of SD to the work function is higher for transition metals in comparison to other metals such as alkali metals.⁴¹

2.2. Interfaces of organic semiconductors

2.2.1. Interaction at interfaces of organic semiconductors

In this section, an insight into the interactions which may occur at interfaces formed by organic semiconductors will be presented. Generally speaking, which energy level alignment (ELA) scenario will occur at the interface of an electrode and organic semiconductor, and which values of interface parameters will emerge, depends highly on the type/strength of interaction among materials involved at/in the interface.

Firstly, the phenomenon colloquially called “push back” or “pillow” effect will be discussed. It has been noticed that upon deposition of organic semiconductors onto clean metal or metal oxide surface, the work function of this type of electrode is reduced. In the previous section we have seen that certain electron density spills out of the metal surface, hence, upon deposition of organic semiconductor it is expected that the electron tail is shortened, i.e. pressed back towards the metal bulk. As a result, SD is reduced, which corresponds with a decrease in the work function of the metal electrode. This phenomenon is attributed in the greatest deal to the physical effect which occur upon adsorption, caused by Pauli repulsion between electron densities of the electrode and adsorbate, due to overlapping of the electronic wave functions of two materials.⁴² The work function reduction assigned to the push back effect can be as large as ~1 eV (organic molecules on metal surfaces), but substantially smaller for the organic molecules on metal oxide surface, due to reduced charge density in the conduction band of an oxide as compared with a metal. The good example for depicting the push back effect is the physisorption of noble gas xenon (Xe) atoms onto various metallic substrates, keeping in mind that noble gases have filled electronic shells. Adsorbed Xe monolayer, for which is expected to interact weakly with substrates via van der Waals forces, decrease substantially work function

of the used substrates.⁴²⁻⁴³ The push back effect can be also nicely observed by the deposition of molecules such as cyclohexane, benzene, organic semiconductor pentacene, etc. onto metal surfaces.⁴⁴⁻⁴⁷ Thus the push back effect is always, up to a certain degree, present upon deposition of the organic conjugated semiconductor on the metallic (inorganic) electrode. It is worthy of note that the work function reduction by the push back effect is not an interface dipole which will be explained in the following text, it only reduces the surface dipole and does not indicate a potential change across the interface. However, the interface dipole may yet occur additionally. In general, the interaction between an organic semiconductor and surface on which it is deposited might be defined as physisorption or chemisorption, or the interaction with mixed characteristics of the latter two. When physisorption occurs at an interface, the interaction is regarded as a weak and no hybridization between orbitals of involved materials is expected to take place. The physisorbed molecules preserve their chemical integrity and orbital structure after adsorption happens, and the charge transfer between two materials at this type of interfaces may occur via quantum mechanical tunneling process. Examples of physisorption can be found at interfaces made by solution processed polymer films on metal oxide and organic substrates.⁴⁸⁻
⁴⁹ On the other side, if chemisorption takes place at the interface, interaction is regarded as a strong. When chemisorption occurs, a chemical bond is formed between two materials. In the case of an organic semiconductor deposited onto the atomically clean metallic electrode surface, the hybridization between molecular orbitals of the organics and electron wave functions of the metal electrode occurs, leading to the chemical bond among two materials as well as partial (non-integer) charge transfer. Hence, the established chemical bond between materials possesses partially covalent and partially ionic character. The chemisorbed species to some extent lose their chemical integrity which consequently changes their electronic structure. Chemisorption, especially the strong one often occurs upon deposition of the strong donor or acceptor molecules, (for instance F4TCNQ and other derivatives of TCNQ), or upon deposition

of organic conjugated semiconductor molecules on the atomically clean reactive metal surface (sputter cleaned), as in the case of Alq₃ on Al substrate.⁵⁰ Additionally, molecules with the intrinsic dipole may strongly interact with the surface onto which are deposited, and they are used for the fine tuning of the underneath electrode work function. Frequently used a group of molecules with intrinsic molecular dipole moment are self-assembled monolayers (SAMs), based on alkyl chains with thiol end groups. Covalent bond with the metal electrode surface due to the presence of the thiol end groups has been reported for these SAMs.⁵¹⁻⁵²

Thus, the two outermost cases of the interaction of organic semiconductor at an interface, according to the strength of interaction, are weak physisorption and strong chemisorption. However, there should be a number of cases of physisorption and chemisorption with a different interaction strength, in between above-named extremes. Hence, interactions with the mixed character of physisorption and chemisorption are expected also to occur. Types of interfaces and potential interactions which can be found in organic electronic devices are listed in Table 2.1 (adapted from ref⁵³), according to the strength of interaction present between materials at the interface.

Table 2.1: Examples of interfaces with interaction types found to be dominant at them.

Example of interface	Interaction type
Saturated hydrocarbon molecules and noble gas atoms onto clean metal surfaces	Physisorption with an absence of charge transfer
π -conjugated molecules and polymers onto organic or passivated metal surfaces	Physisorption with possible integer electron charge transfer through tunneling
π -conjugated molecules prepared on non-reactive clean metal surfaces	Weak chemisorption with possible partial charge transfer
π -conjugated molecules deposited on reactive clean metal surfaces	Strong chemisorption with covalent bonding between molecule and metal, present (partial) charge transfer
π -conjugated molecules with intrinsic dipole and anchoring groups deposited on clean metal surfaces	Strong chemisorption occurs with covalent bond at specific sites of the molecule and metal, present (partial) charge transfer and surface dipole

Ending up this section, the remark should be made that in the case of strong chemisorption at the surface, at the moment there is a lack of unified model which can precisely predict electronic structure and parameters of the interface. Hence, each interface should be studied as a singular case.

2.2.2. Models for description of interfaces made by organic semiconductors

The Schottky-Mott rule

Interface formation and consequent energy level alignment for the organic semiconductors (conjugated polymers and small molecules) do not comply with the same rules as for their inorganic counterparts. Preparation conditions (vacuum, inert or ambient atmosphere) and techniques may have a huge impact on the electronic structure of an interface, hence, on the device performance in which this interface is present. For a gradual introduction into the subject, as a primary example, in Figure 2.2 is schematically depicted the energy level alignment (ELA) between the metallic electrode and organic semiconductor, the frequent interface in organic electronic devices. Established ELA scenario between materials at the presented interface follows Schottky-Mott rule (SM model), where the vacuum levels of both materials are aligned. This model, suitable for the description of non or only weakly interacting interfaces of the organic semiconductors, was firstly introduced in the middle of the last century for metal-inorganic semiconductor interfaces.⁵⁴ The SM model was perceived as the prevalent ELA scenario at the interfaces of organic semiconductors at the beginning of research in the field of organic electronic devices. Nonetheless, today is known that this ELA scenario is just one of the outcomes which may occur at the interface of organic semiconductor and electrode,

where electrode might be either inorganic or organic.^{53, 55-56} However, the last figure may give a good insight into the basic electron structure parameters at the interface, which are defined by the vacuum level alignment (VLA) between the metal electrode surface and organic semiconductor.

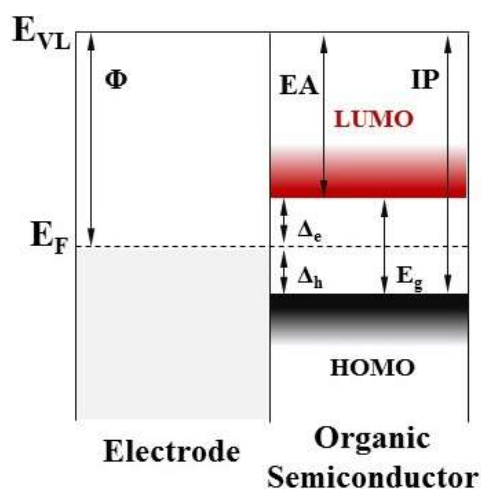


Figure 2.2: Schematic representation on the energy level alignment diagram of the organic semiconductor on electrode interface, with relevant electronic structure parameters.

Firstly, the energy distance between the Fermi level of electrode (E_F) and vacuum level (E_{VL}) determines the value of work function (Φ) of the electrode, where Φ is, as mentioned above, the energy needed to take away an electron from the metal Fermi level into the rest at the vacuum level.³⁶⁻³⁷ Further, the energy distance from the highest occupied molecular orbital (HOMO) and lowest unoccupied molecular orbital (LUMO) to the vacuum level defines ionization potential (IP) and electron affinity (EA) of the organic semiconductor, respectively. Here, it will be recalled that for a molecule, the energy distance from the highest occupied molecular orbital (HOMO) to the lowest unoccupied molecular orbital (LUMO), is regarded as the band gap (E_g). On the other side, in the solid state picture, the band gap can be defined as the energy distance between the top of the valence band and the bottom of the conduction band.³⁰ Within the band gap, the density of states is expected to be zero. However, it has been found for the thin films of organic semiconductors, that some density of states can be present within the band gap. These states might be induced by the different structural imperfections of

the involved polymers and molecules, or the presence of impurities in the material, and they are named trap states.^{57-60,61} It has been shown that trap states have a detrimental effect on the charge transport of these materials.⁶² Turning back to the above discussion, after the contact is made between the electrode and organic semiconductor, new electronic structure parameters characteristic for the interface and substantial for the performance of organic electronic devices, are defined. As can be seen in Figure 2.2 for the case of VLA, the energy offset between E_F of the electrode and HOMO level of the organic semiconductor determines/defines (energy of) hole extraction barrier (Δ_h). On the other hand, the energy offset between the LUMO of organic semiconductor and Fermi level of the electrode determines the electron extraction barrier (Δ_e). Δ_h and Δ_e can be calculated, according to Figure 2.2.:

$$\Delta_h = IP - \Phi \text{ and } \Delta_e = \Phi - EA = E_g - \Delta_h \quad (2.2)$$

Hence, if the vacuum level alignment (Schottky-Mott limit) occurs for the certain range of electrode Φ values (i.e. several different electrodes), then, for the Δ_h and Δ_e is expected to linearly scale with the work function of the electrode, as shown in the equation 2.2.⁶³ Generally, in the case of VLA no charge transfer is expected to happen across the interface, i.e. the electrical potential is not changed across the interface. As a consequence, energy levels on both materials involved in the interface can be calculated to the common vacuum level, and an energy level alignment can be predicted from the properties of individual materials. Although it has been shown that Schottky-Mott limit is not the only scenario which may be found at interfaces of the organic semiconductors, SM limit has been confirmed for a plethora of organic/inorganic and organic/organic interfaces.⁶⁴

The Induced Density of Interface States (IDIS) model

Subsequently, another model was proposed for the interpretation of interaction and corollary energy level alignment at interfaces made by organic semiconductors.⁶⁵⁻⁶⁷ The Induced Density of Interface States (IDIS) model was developed for weakly interacting metal-organic and later for organic-organic interfaces. In this model, moderate chemical interaction (without strong covalent bonds) is perceived at an interface, as it is often the case for interfaces formed by vapor deposited π -conjugated molecules on clean but nonreactive metals such as gold. As a consequence, weak hybridization between the molecular orbitals of π -conjugated molecules with metal substrates is expected to occur.⁶⁸ At this type of interfaces, the charge transfer across the organic/metal interfaces is governed by the alignment of Charge Neutrality level (CNL) of the organic semiconductor with the Fermi level of metal. CNL presents the continuum density of states (DOS) induced in the energy gap (E_g) of organic semiconductor by broadening of molecular orbitals due to electrostatic polarization at the metal surface. The direction and size of charge transfer, hence, the energy level alignment at the organic semiconductor/metal interface is driven by the relative position of the CNL and E_F , with respect to the common vacuum level. If CNL is positioned below the metal Fermi level, charge transfer will occur from the metal to organic semiconductor. Latter scenario is presented in Figure 2.3. Vice versa, if CNL is located above the Fermi level of the metal, charge (electrons) will be transferred to the metal. The CNL of surface states is the position for the Fermi level which renders the surface without a net charge. CNL is calculated considering all molecular levels (rather than just the HOMO and LUMO). As mentioned above, at an interface, CNL would align with the Fermi level, still, the difference between last two is reduced by the interface slope (screening) parameter S_{MO} . The S_{MO} ($1 > S_{MO} > 0$) is a screening parameter which depends on the interfacial

properties, i.e. it is a measure of the strength of interaction at the interface via reflecting the ability of the materials forming the interface to screen electrostatic potential differences.

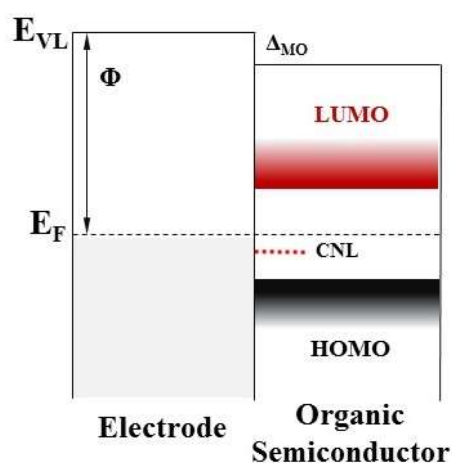


Figure 2.3: Illustration of one energy level alignment diagram for weakly chemisorbed organic semiconductor on inorganic electrode, according to IDIS model. Interface dipole is represented in the figure by the vacuum level shift, i.e. break of the line which represents the vacuum level. It is complex phenomenon which arises due to electrical polarization effect at junction between materials.²

Hence, the position of E_F at the interface as well as interface dipole can be calculated via equations (see Figure 2.3):

$$E_F - \text{CNL} = S_{\text{MO}} (\Phi_{\text{M}} - \text{CNL}) \quad (2.3a)$$

$$\Delta_{\text{MO}} = (1 - S_{\text{MO}}) (\Phi_{\text{M}} - \text{CNL}) \quad (2.3b)$$

It has been shown that the interfaces formed by the thin films of organic semiconductors such as 3,4,9,10-perylenetetracarboxylicdianhydride (PTCDA), 4,4',N,N'-dicarbazolyl biphenyl (CBP), tris-(8-hydroxyquinoline) aluminum (Alq_3), 3,4,9,10-perylenetetracarboxylic bisbenzimidazole (PTCBI), deposited onto gold film substrates, are well explainable via IDIS model.^{64, 69-70} Moreover, since the organic/organic interfaces are perceived as weakly interacting, the IDIS model as mentioned above is also used for elucidation of the energy level alignment at these interfaces. The ELA at the organic/organic interface is expected to be driven by CNLs of the two organic semiconductors, simplistically depicted in Figure 2.4.

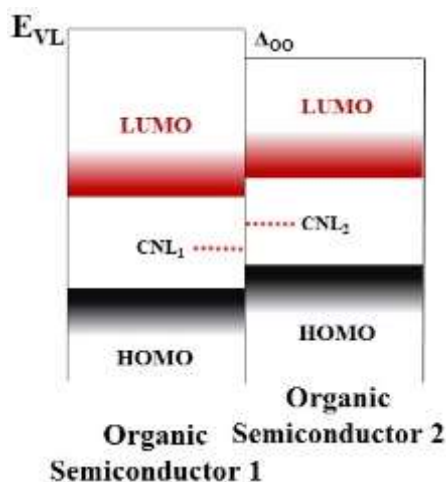


Figure 2.4: Energy level alignment at one organic/organic heterojunction, governed by the difference of CNLs of materials at the interface.

Hence, from the latter figure, the electronic structure parameters such as a difference between CNLs and their positions before and after contact, and interface dipole can be calculated the following way:

$$(CNL_1 - CNL_2)_{final} = S_{OO} (CNL_1 - CNL_2)_{initial} \quad (2.4a)$$

$$\Delta_{OO} = (1 - S_{OO}) (CNL_1 - CNL_2)_{initial} \quad (2.4b)$$

Here also, the S_{OO} presents the screening parameter, obtained the semiempirical way for these type of interfaces, nonetheless, the model has shown good reliability in reproducing experimental data.

Integer Charge Transfer (ICT) model

The last model for the description of interaction and energy level alignment at interfaces of the organic semiconductors, which will be presented is the Integer Charge Transfer (ICT) model. The ICT model has shown to be well appropriate for the description of interfaces prepared by deposition of the organic semiconductors (polymers) from the solution.^{48, 53, 71} Considering that

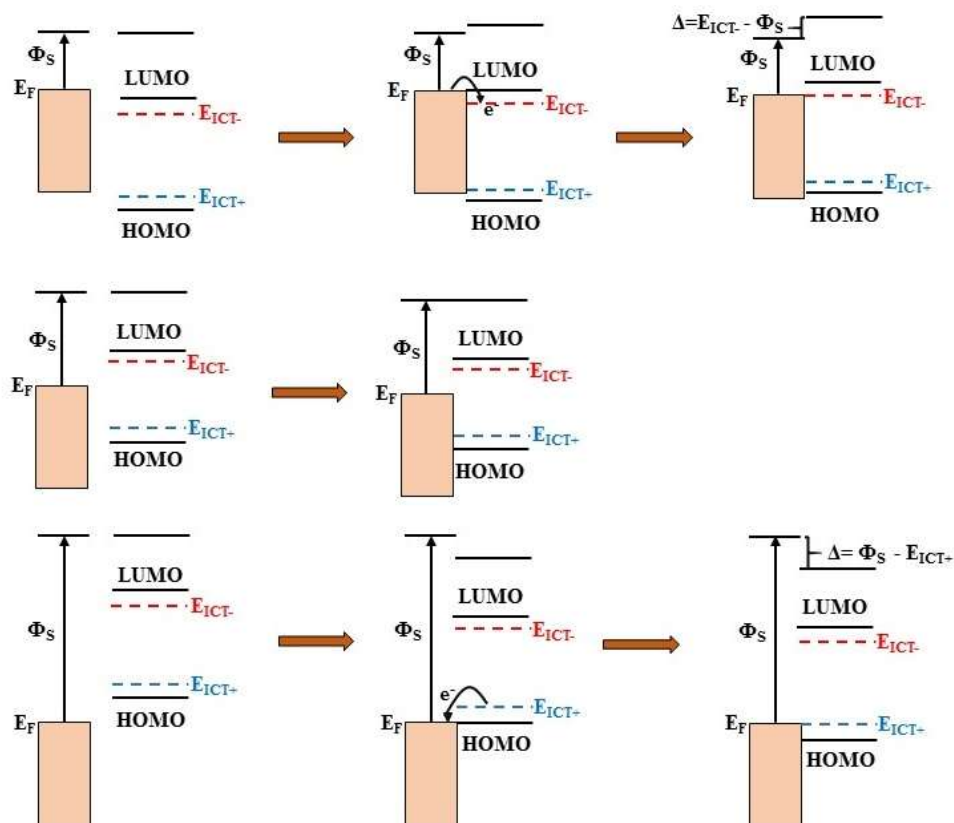
the polymer thin films studied in this work are solution processed, the explanation of the ICT model is especially emphasized. The preparation of organic semiconductor/substrate interfaces via some solution coating technique is done either in the controlled atmosphere of inert gas (N_2 or He filled glove box) or even under ambient conditions. Thus, it is expected that the electrode surface before polymer deposition is already pre-covered by simple hydrocarbons, CO_2 , H_2O and other molecular species from the atmosphere, and undergone the push back effect. Also, in the case of the metal electrode surface, a native oxide might develop on the top. Therefore, the electronic structure of the electrode surface during this thin film preparation procedure is expected to differ from the pristine one. Contamination (passivation) and formation of the oxide layer on the top of the electrode surface reduce interaction between the electrode and organic semiconductor, increasing the probability for VLA at the interface. Nonetheless, for the different types of substrates (electrodes) such as Au (111) (metal), ITO (metal oxide), PEDOT:PSS (organic), it has been shown that the VLA scenario at interface occurs only between two limiting values of the substrate work function. This occurrence/phenomenon is explainable by the ICT model.^{49, 53, 72-74} The model was developed to explain the energy level alignment at organic/inorganic interfaces, where the negligible hybridization of π -molecular orbitals and substrate electronic wave functions is expected to be present. Also, the ICT model is used for the elucidation of organic/organic interfaces where only weak physisorption is expected. In this model, two new electronic states, within the band gap (HOMO-LUMO gap) of the organic semiconductor are defined. These states are called positive (E_{ICT+}) and negative (E_{ICT-}) polaron levels, and occur above the HOMO and below the LUMO, respectively. Their values are expected to be unique and specifically determined for every organic semiconductor. Polaron levels (states) are interpreted as the fully relaxed charge transfer states (both electronic and geometrical relaxation is included), which are created upon integer “amount” of charge is transferred (electron or hole) to the organic semiconductor, taking into account screening from

the electrode (substrate).^{49, 53, 72, 75-77} Three different energy level alignment regimes, which may happen at the interface according to the ICT model, are presented in Figure 2.5a (adapted from ref.⁵³).

First takes place, when the work function of electrode Φ_S is smaller than the energy of formation of the negative polaron level (E_{ICT-}) of the organic semiconductor, or shorten $\Phi_S < E_{ICT-}$. After contact of materials is made, a charge transfer occurs across the interface. The integer number of electrons (holes in the opposite direction) is transferred via quantum mechanical tunneling from the electrode Fermi level to (close to) the LUMO of an organic semiconductor, creating E_{ICT-} state/level. Spontaneous charge transfer across the interface occurs until thermodynamic equilibrium is established. It results in the formation of positive Δ at the interface, alignment of the electrode Fermi level with E_{ICT-} level, and an increase of the work function of the new organic semiconductor on electrode system which is named now the effective work function $\Phi_{org/sub}$. This alignment of the electrode E_F and E_{ICT-} level is denoted as the Fermi level pinning (FLP) regime at the negative polaron level. Hence, the value of newly created $\Phi_{org/sub}$ stands exactly the energy difference between the E_{ICT-} level and the vacuum level (E_{VL}). By the same token, if $\Phi_S > E_{ICT+}$ stands, the integral amount of electrons (holes in the opposite direction) is transferred close to E_F of the electrode from the HOMO of an organic semiconductor. Interface dipole is again created, here in the opposite direction to the first case. The work function $\Phi_{org/sub}$ of the organic semiconductor/electrode system is now lower than the work function of the electrode Φ_S , due to pinning of the electrode E_F at E_{ICT+} , and is equal the energy difference between E_{VL} and E_{ICT+} . Lastly, if the value of Φ_S is in between two threshold values of the formation energies the positive and negative polaron levels, written in short $E_{ICT+} > \Phi_S > E_{ICT-}$, no charge transfer occurs across the interface and the vacuum level alignment (Schottky-Mott limit) is established, with the common vacuum level for two materials and consequently $\Phi_S = \Phi_{org/sub}$. The ICT model predicts for the energy level alignment of an organic semiconductor

with a substrate (electrode), so-called “Mark of Zorro” or “Z” characteristic dependence, depicted in Figure 2.5b.

a)



b)

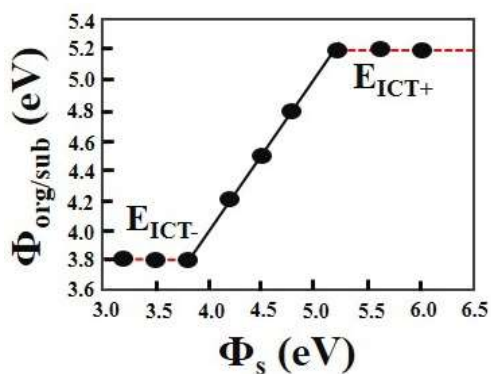


Figure 2.5: Schematic illustration of the evolution of the energy level alignment when a π -conjugated polymer or molecule is physisorbed on the surface of organic or passivated inorganic substrate (a). General dependence of work function of organic semiconductor coated on different substrates, the solid line illustrates expected for vacuum level alignment. The dashed red lines symbolize dependence expected for the Fermi level pinned regime (b).

As can be seen from the graph, the work function of the organics/electrode system as a function of the electrode work function levels off for Φ_S values smaller than E_{ICT-} . As long as Φ_S is smaller than E_{ICT-} level, the value of $\Phi_{org/sub}$ is a constant which equals the E_{ICT-} value. When the value of Φ_S is increasing, and at some point becomes higher than E_{ICT-} , $\Phi_{org/sub}$ starts linearly growing with Φ_S , until again saturates for Φ_S greater than E_{ICT+} . Similarly, as long as Φ_S has a higher value than E_{ICT+} level, the value of $\Phi_{org/sub}$ is a constant which equals the E_{ICT+} value, due to the Fermi level pinning phenomenon. Intuitively it can be inferred, that for the system in the Fermi level pinning regime with constant $\Phi_{org/sub}$, the Δ_h and Δ_e hold constant values as well. On the other hand, for Φ_S having values between E_{ICT+} and E_{ICT-} , the Δ_h and Δ_e linearly scale according to Equations 2.1. This Z graph, theoretically possible for every organic semiconductor to be plotted in praxis is rarely achievable, due to a limited number of appropriate model substrates, especially stable electrodes with the small work function value. Nonetheless, the complete Z graph has been reported for polyfluorene APFO-Green-1 low band gap polymer, which is used for the fabrication of organic solar cells, light emitting diodes and field effect transistors.⁷⁸

Application of ICT model to multilayer systems

According to Table 2.1, at the interface of two organic semiconductors, a pronounced chemical reaction is not expected, also due to lack of dangling bonds at the surface of organic semiconductors. Nonetheless, in the architecture of organic electronic devices, layers of organic semiconductors are often sandwiched between electrodes. Thus, the energy level alignment and parameters at the interface made by deposition of the organic thin film onto organic film(s) precovered electrode (substrate), is expected to heavily depend on the interface made by the first organic layer and electrode.^{53, 79-80} As explained above, after deposition of the organic layer

onto the electrode, the work function of electrode Φ_s might change due to an interaction between materials. The interaction is caused by the charge transfer and creation of the electric potential across the interface, i.e. the Fermi level pinning phenomenon occurs in the proximity of the HOMO or LUMO of the organic material. The present density of states in the proximity of frontier orbitals defines now, as explained above, the new work function so-called effective work function $\Phi_{\text{org/sub}}$. As the outcome, the organic semiconductor on electrode system acts now as a new substrate with the work function $\Phi_{\text{org/sub}}$, which is the reference level for the afterwards deposited organic film. According to the ICT model, the energy level alignment and consequent electronic structure parameters at the organic/organic interface are governed by above-explained conditions. In Figure 2.6a, is depicted scenario at the organic/organic which may occur in an OPV device. The donor organic semiconductor is deposited on the electrode, and the Fermi level is pinned close to the HOMO level. In subsequently prepared organic acceptor thin film, due to condition $\Phi_{\text{org/sub}} < E_{\text{ICT-}}$, the Fermi level pinning happens close to the LUMO. Nonetheless, if the condition was not fulfilled, i.e. $E_{\text{ICT+}} > \Phi_{\text{org/sub}} > E_{\text{ICT-}}$, the vacuum level alignment would take a place at the acceptor/donor interface. The ICT model also predicts that the Fermi level pinning in the second organic layer is not expected if it does not occur in the layer below, hence, if there is no charge transfer at the first interface. This potential situation is depicted in Figure 2.6b. Although the work function of donor/electrode system is (taking into account common vacuum level with the acceptor) smaller than the acceptor LUMO, the vacuum level alignment occurs because no FLP regime occurred in the first organic layer. In this case, no charges are present at the energy symbolized by line extension of the electrode E_F at the organic/organic interface, hence, no Fermi level pinning is expected to take place in the acceptor organic layer. Even if the FLP would have occurred, this most likely would depend on the thickness of the first organic layer, as explained in the work of Brocks et al.⁷⁹ Nonetheless, the interfacial dipole at organic/organic interfaces, has been reported for numerous systems,^{53, 79-82}

such as C₆₀ deposited onto P3HT coated SiO_x/Si substrate,⁸⁰ or good example of C₆₀ evaporated on 6T covered polycrystalline Au electrode and in the same set of experiments 6T on C₆₀ covered Au electrode.⁸³ Situation with energy level alignment and electronic parameters at organic/organic interface becomes even more complicated when the new electrode (cathode) is prepared on the top of acceptor/donor/electrode stack. Then, the built-in field defined by the difference of two work functions of electrodes has a significant influence on the electronic structure of the acceptor/donor interface, and ELA throughout device.⁸⁴

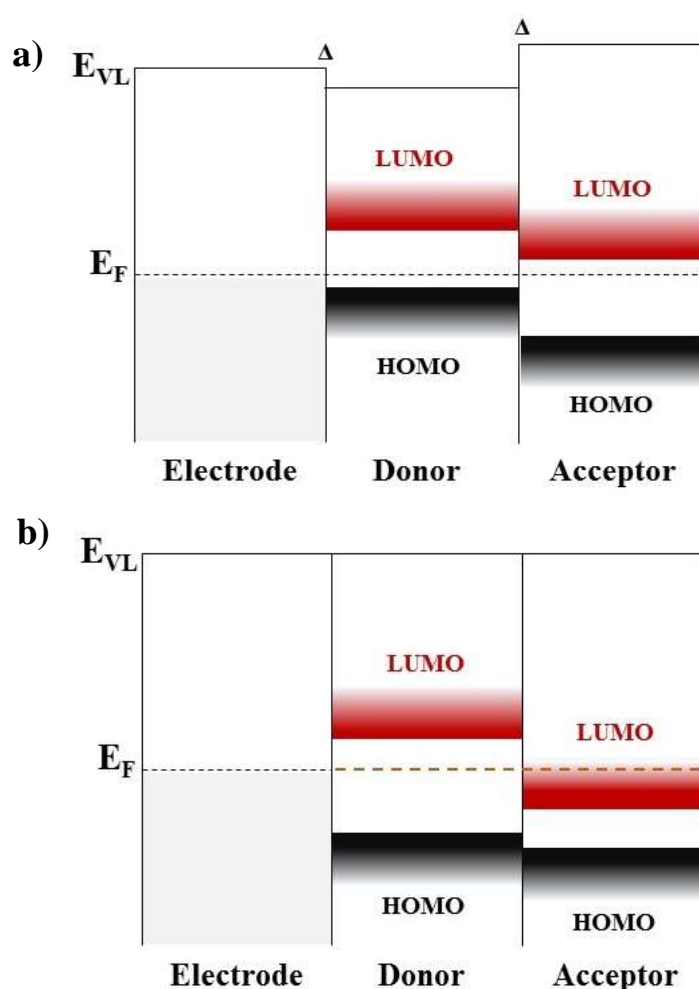


Figure 2.6: Two energy level alignment diagrams of the acceptor/donor bilayer stack, with different alignment outcome scenarios. In (a) as a consequence of FLP at the donor/electrode interface FLP occurs at acceptor/donor interface, while in (b) due to VLA at the first interface also VLA occurs at the acceptor/donor interface.

2.3. Thin films of organic semiconductors

2.3.1. Thin films of conjugated polymers

Conjugated copolymers with the alternating donor and acceptor moieties in their backbone structure, in the last years, have gained great research interest, demonstrating improved charge transport properties and efficiency in OPVs, in comparison to conjugated homopolymers. Nevertheless, understanding and control of the thin film morphology are still a great challenge. It has been shown that properties (electronic, transport, etc.) of organic thin films do not depend only on involved materials (small molecules and polymers) properties but also on the thin film morphology, where intermolecular and molecule-substrate interactions play a crucial role.⁸⁵ Now, among conjugated copolymers in the focus of the research community, the low band gap polymer PCPDTBT is one of the most scrutinized,⁸⁶⁻⁸⁸ demonstrating the huge potential for the utilization in OPV devices. Thus, on the example of PCPDTBT will be reviewed notions of the morphology and molecular orientation in the thin films of conjugated copolymers, regarding that PCPDTBT and other polymers used in this work possess similar chemical structure.

Generally, the morphology of the thin films of PCPDTBT was found to be semicrystalline, with crystalline and amorphous patches present in the film,⁸⁹⁻⁹⁰ whereby the polymer is perceived as marginally crystallizable. However, in the literature different approaches have been reported how to improve the crystallinity and ordering of the thin films, hence, to get better charge transport and gain higher efficiency of the inbuilt device. Some of these methods are post-deposition thermal annealing, the inclusion of additives such as 1,8-diiodooctane (DIO) or 1,8-octanedithiol (ODT) into the polymer solution,^{89,91} choice of the solvent considering its polarity and boiling point and etc. Also, intrinsic polymer properties such as molecular weight (M_w) and polydispersity (PDI) may also have a huge influence on the morphology of their pristine and blend films.⁹²⁻⁹⁵ Observed crystalline phases in the thin film of PCPDTBT are described as fiber

or worm-like looking crystallites.⁸⁹ In order to elucidate ordering and molecular orientation in the thin films of PCPDTBT (in crystalline phases), different techniques such as NEXAFS, GIWAXS, TEM/ED, XRD have been employed.⁹⁶⁻⁹⁹ Within oriented domains of PCPDTBT thin films, the edge-on orientation of the polymer backbone, has been suggested.⁹⁹ For the edge on orientation, illustrated in Figure 2.7, the charge transport is expected to dominantly occur along z and x-axis of the figure. Charge transport in the z-direction is denoted as intrachain charge transport, and it takes a place along the covalently bound polymer backbone (band transport).

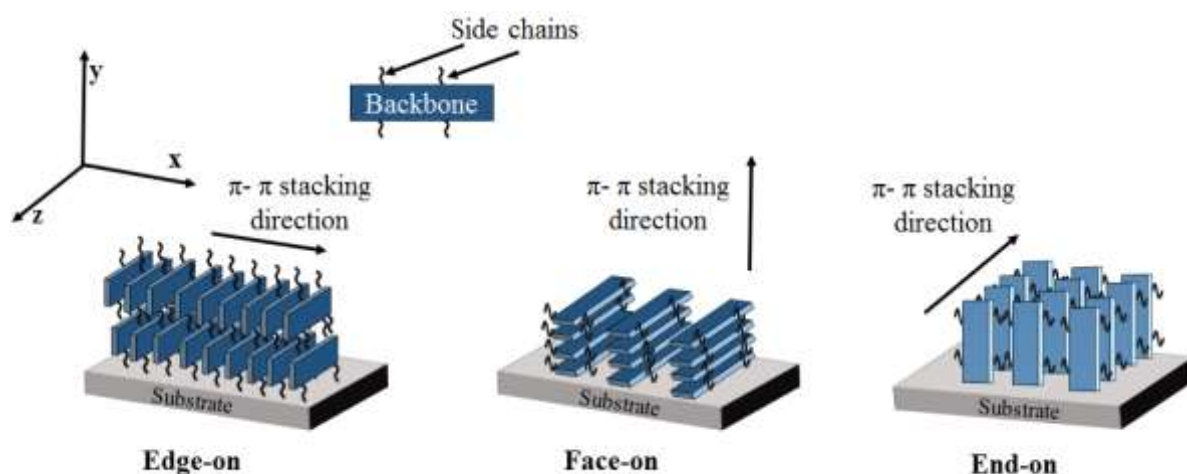


Figure 2.7: Schematic representation of three favorable molecular crystallite orientation, in the thin films of conjugated polymers.

Although the charge transport is highest along the polymer backbone, the intrachain charge transport has shown to be a short distance charge transfer. On the other hand, in the x-direction of the presented edge on orientation is expected to occur interchain charge transport. It occurs due to the overlap of p_z orbitals which jut out of the polymer backbone plane, and this interaction among different polymer chains is called π - π stacking. Interchain charge transport which occurs by the charge hopping is perceived as a long distance charge transport, and it is shown to be the greatest part of the charge transport in solid state devices based on the thin films of conjugated polymers.¹⁰⁰ The hopping transport may occur also along the polymer chain, especially when

there are defects in the chain. Generally, the hopping probability depends on the spatial and energy separation of hopping sites (for instance kinks and coils) involved in this transport mechanism. Furthermore, the less reported molecular orientation of PCPDTBT chains is face-on orientation,¹⁰¹ also shown in Figure 2.7. In the case of face-on molecular orientation, intrachain charge transport is expected to occur in the direction of the z-axis, while, interchain charge transport along the y-axis, due to above-listed reasons. Lastly, for conjugated polymers has also been reported end-on (chain-on) orientation,¹⁰² where the backbone of the polymer is standing perpendicular to the substrate, as shown in Figure 2.7. Here, the interchain charge transport along the z-axis, whilst intrachain charge transport is expected to occur in the direction of the y-axis. Additionally, different orientations with polymer chains tilted for some angle in respect to the substrate were also observed.⁹⁸

2.3.2. Thin films of conjugated polymer/PCBM blends

The morphology of the polymer thin film is generally controlled by two processes: thermodynamically driven self-assembly and the dynamics of self-organization. The first one leads to steady-state structures with the energy minimum, whilst the second process is responsible for various non-equilibrium thin film structures that may occur. Control of the thin film morphology becomes even more complicated in multicomponent thin films, such as bulk heterojunction (BHJ) thin films. The BHJ represents a mixture of two (at least) organic molecules or polymers, where one is acting as electron donor and other as an electron acceptor, and it is employed as an active layer in the organic photovoltaic devices. Prepared by mixing conjugated polymer as a donor material and fullerene derivative PCBM as an acceptor, the BHJ approach has emerged as a promising way to create highly efficient organic solar cells.¹⁰³⁻¹⁰⁶ Considering that charge generation, separation and transport happen in the BHJ thin film of

OPV device, the optimization and control of the BHJ film nanostructure is perceived as the crucial for the functioning of the device. After casting of the polymer:PCBM blend solution onto a substrate, it was shown that before formation and solidification of the thin film, phase separation first takes place in the liquid mixture.¹⁰⁷⁻¹⁰⁸ The BHJ morphology formation is influenced by interaction and ordering of each component of the blend, and this interplay is regarded as crucial. For example, vertical phase separation in the blend films can occur due to the stronger interaction of one material of the blend with the used substrate,¹⁰⁹ or by the increased solubility of one component in the solvent, and its accumulation at the surface of the film during the solvent evaporation.¹¹⁰⁻¹¹¹ If we first concentrate on one component of the blend, initial nucleation of a conjugated polymer as the primary step of crystallization is the process with an energy barrier, and upon crystallization, semicrystalline and amorphous domains of the polymer can be found in the polymer:PCBM blend thin films. This is recognized as a favorable scenario to get BHJ with high-performance characteristics.¹¹² Considering now the acceptor material, after processing of the blend thin films, PCBM shows a lower rate of nucleation, giving disordered nanostructure sometimes with large lateral domains (even micrometer size) within polymer:PCBM blend films. These huge patches which protrude from the film surface are detrimental for the performance of BHJ in solar cells.¹¹³ Thus, thinking about conjugated polymer:PCBM blend films, one should consider it as a three-phase system with domains of pure polymer and fullerene and third which is a mixture of latter two materials. Pictorial representation of one BHJ (polymer:fullerene blend) thin film is shown in Figure 2.8. In order to obtain BHJ with a morphology which can lead to efficient charge generation and transport i.e. efficient solar cell, enough domains of pure (semi)crystalline polymer and fullerene should be present in the thin film as a counterbalance to domains with mixed materials. It has been demonstrated that an improved crystallinity of the blend constituents increases π - π stacking (π overlap) within them, which increases electronic delocalization and charge mobility within

these phases.^{27, 114} Increase of the polymer crystallinity improves connection and charge transport with the pure acceptor phase, knowing that the proximity of fullerene phase is necessary for exciton dissociation. Hence, in order to improve crystallinity and ordering of the polymer in polymer:fullerene blends, post-processing treatments such as thermal and solvent annealing, or the inclusion of small amounts of an extra solvent so-called additive, have been successfully used for various conjugated polymers such as P3HT, PCPDTBT etc.^{115-117 118-121} In general, presence of the fullerene derivative in the BHJ, suppresses ordering of the used polymer, hence, decreases quality of the polymer network important for the performance in OPV device.

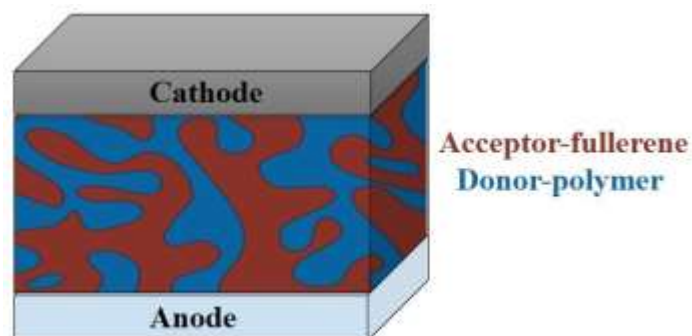


Figure 2.8: Presentation of the three dimensional network of the bulk heterojunction thin film, within the simple solar cell architecture.

2.3.3. Thin films of fullerene C₆₀

Fullerene C₆₀ presents the prototypical molecular organic semiconductor (n-type material), which has been frequently used in high performance organic electronic devices: organic thin film transistors (OTFTs)¹²²⁻¹²⁴ organic light emitting diodes (OLEDs)¹²⁵⁻¹²⁶ and organic photovoltaics (OPVs).¹²⁷⁻¹²⁸ Because of the specific chemical and electronic structure (open shell configuration of π -electrons and high electron affinity), C₆₀ and its derivatives (PCBM,

ICBA etc.) are up to now the electron accepting/transport materials of choice for organic photovoltaic devices.^{13, 129-130} Thin films of fullerene C₆₀ were studied on a plethora of different inorganic and organic substrates (electrodes). The symmetric structure of C₆₀ molecules with a quasi-spherical shape, makes thin films of this material easily processable, with well-ordered often face-centered cubic structure (fcc). The Van der Waals diameter of a C₆₀ molecule is about 1.01 nm, thus, a monolayer might be roughly approximated to be 1 nm thick. Usual preparation method for C₆₀ thin films is organic molecular beam deposition abbreviated OMBD (sublimation of microcrystalline C₆₀ powder), but other methods such as supersonic molecular beam deposition¹³¹⁻¹³² or ionized cluster beam deposition,¹³³ were successfully employed. It has been shown, that the structure and morphology of the thin films of C₆₀ depend very much on the used substrate, i.e. C₆₀-substrate interaction. Ordered polycrystalline films of C₆₀ were successfully prepared on various substrates, where fullerene-substrate interaction is expected to be relatively weak (physisorption with eventual charge transfer). Used substrates were Au,¹³⁴⁻¹³⁵ Ag,¹³⁴ Si (111) single crystal¹³⁶ and ITO¹³⁶ where the substrate temperature was kept high enough to provide sufficient mobility of C₆₀ molecules during nucleation of the monolayer and the following film growth. Well-ordered thin films of C₆₀ have been also deposited successfully onto substrates, pre-covered with other organic semiconductors such as pentacene,¹³⁷⁻¹³⁸ copper(II)phthalocyanine (CuPc),¹³⁹ para-sexiphenyl (6P),¹⁴⁰⁻¹⁴¹ diindenoperylene (DIP),¹⁴² P3HT.¹⁴³ Unlike for the first set of substrates, substrates pre-covered with organics were at room temperature during deposition of fullerene C₆₀, which gives to C₆₀ certain freedom in motions at the top. For these “organic” substrates, fullerene-substrate interaction is expected to be even weaker than in the case of the aforementioned inorganic substrates. Furthermore, self-assembling monolayers, for example, alkyl-thiol¹⁴⁴⁻¹⁴⁵ or 11-phenoxyundecanethiol¹⁴⁶ were also used for the growth facilitation of fullerene C₆₀ thin films. Overall, the C₆₀ films demonstrate all three growth models: layer by layer (or Frank-Van der Merwe),¹⁴⁷ layer plus

island growth mode (or Stranski-Krastanov)¹⁴⁸ and island growth mode (or Volmer-Weber).¹⁴⁹ Which growth mode will dominate, in general, depends on C₆₀-substrate interaction as a primary factor.¹⁵⁰ Moreover, it is known that ordering of the thin film of C₆₀ may have a high impact on its electronic properties.¹⁵¹

Chapter 3

Experimental methods

The experimental methods employed for the characterization of the thin films of organic semiconductors, substrates (model electrodes), and their interfaces presented in this work, are listed in the upcoming chapter. The chapter begins with a description of main principles of photoelectron spectroscopy (PES) and used experimental setup, followed by the same agenda for X-ray absorption spectroscopy, more precisely its subtype called near edge X-ray absorption fine structure (NEXAFS). Because the latter two experimental methods provided the majority of experimental data, the focus of this chapter will be entirely on them.

3.1. Photoelectron spectroscopy (PES)

3.1.1. Principles of photoelectron spectroscopy

Currently, photoelectron spectroscopy is one of the most prominent experimental methods used for studying the electronic structure, bonding states and chemical properties of materials in the different aggregate state, their surfaces, and interfaces. The PES is based on photoelectric effect discovered and described first by Heinrich Hertz in 1887, and then later in 1905 theoretically

elucidated by Albert Einstein. The Nobel Prize in Physics 1921 was awarded to Albert Einstein also “for his discovery of the law of the photoelectric effect“. For the development of photoelectron spectroscopy as an experimental technique, colossal acknowledgment goes to Kai Siegbahn and his coworkers, who during the 1960s constructed a high-resolution spectrometer. Because of this achievement, PES became a well-recognized technique for qualitative and quantitative chemical analysis, still frequently called electron spectroscopy for chemical analysis (ESCA), the name given by Kai Siegbahn. We turn back now to photoelectric effect as the essence of PES, where the matter is irradiated by a (monochromatic) light beam of energy $h\nu$ (h -Planck constant, ν -frequency). If $h\nu$ is higher than binding energy which keeps electron bound inside of material (matter), the electron is emitted with specific kinetic energy, leaving ionized entity (molecule, atom) behind. This process formulated according to the law of conservation of energy is written:



Here, S stands for the total energy of the neutral system (atom, molecule), e^- for the (kinetic) energy of the emitted electron, while S^+ accounts for the total energy of the ionized system (atom, molecule). Depending on the radiation energy ($h\nu$) and energy level from which photoelectron is emitted, the kinetic energy (velocity) of photoelectron may vary. Hence, the difference in energy between S and S^+ quantities can be related to the energy necessary to photoionize studied material, which is frequently defined as the binding energy of an electron, formulated as:

$$E_b = S^+ - S \quad (3.2)$$

Considering that the radiation of different energy can be used in an experiment, and photoexcited electron might belong to the different energy level of an atom (molecule), the emitted electron may have different kinetic energy leaving studied material.

The kinetic energy of the escaping electron is written as:

$$E_k = h\nu - \Phi_s - E_b \quad (3.3)$$

In the latter equation with E_b is designated the binding energy of the emitted electron, while with Φ_s the work function of the studied material. Thus, an electron is emitted from the sample material upon irradiation with the monochromatic light beam of the excitation energy $h\nu$, if $h\nu$ is greater than the sum of the binding energy of the electron and work function of material ($E_b + \Phi_s$). This can be intuitively comprehended from Figure 3.1, where the kinetic energy (E_k) of photoexcited electrons is related to their binding energy in the solid material, i.e. photoelectron distribution $I(E_k)$ is related to the occupied density of electronic states $N(E_b)$ in the sample. In photoelectron spectroscopy, as the reference level in measurements is usually taken the Fermi level (E_F) of the sample, which is aligned with the spectrometer Fermi level.

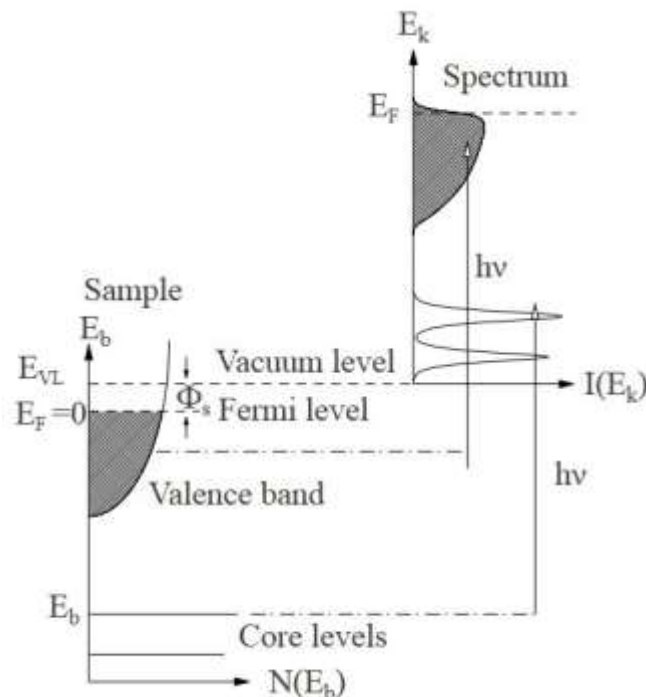


Figure 3.1: Scheme of the photoemission process in the single-particle picture.¹

In Figure 3.2, the energy level alignment between the conductive sample and spectrometer is depicted. The sample and spectrometer are electrically connected and in thermal equilibrium.

As can be seen in the figure, which is most often the case in practice, work functions of the sample and spectrometer have different values. In this situation, all electrons with E_k smaller than difference $\Phi_a - \Phi_s$, are unable to reach analyzer part of the spectrometer, and a constant negative potential is applied to accelerate electrons in order to obtain SECO (which will be later discussed).

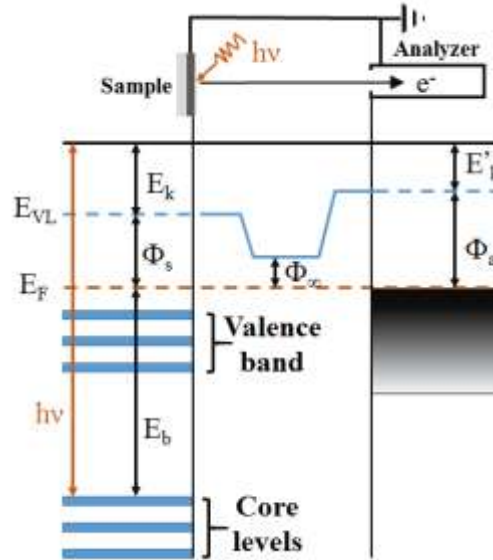


Figure 3.2: Illustration of the energy level alignment between a conducting sample and spectrometer. Due to electrical contact between the sample and spectrometer, the Fermi level of the sample is aligned to the Fermi level of the spectrometer, hence, the Fermi level of spectrometer is the reference level for measurements due to a much higher amount of electrons present in apparatus.

Also, the difference between Φ_s and Φ_a is the reason for a variation in the vacuum level E_{VL} along the path of electrons, as depicted in the latter figure. When the equilibrium is established between the sample (Φ_s) and spectrometer (Φ_a), the photoemitted electron from the irradiated sample has a kinetic energy E'_k . Hence, the kinetic energy of photoelectrons measured by the analyzer can be expressed in the following way:

$$E'_k = hv - E_b - \Phi_s - (\Phi_a - \Phi_s) = hv - E_b - \Phi_a \quad (3.4)$$

As a consequence, when the excitation energy (hv) and spectrometer work function are known, a measurement of the kinetic energy of emitted electrons can be related to the binding energy

of these electrons referenced to E_F . Problems might occur if the conductivity of the solid sample is low, and positive charges which are left behind emitted electrons are accumulated at the surface and cannot be dissipated and neutralized. This phenomenon is known as the static charging or charging effect, and in this case, the common Fermi level of the sample and spectrometer presumption is no longer valid. The Fermi level of the sample is shifted versus the spectrometer Fermi level, so that measured binding energy of photoelectrons (peak) is always higher than in the case when charging does not occur.

Generally, PES can be divided into the two main subtypes, Ultraviolet photoelectron spectroscopy (UPS) and X-ray photoelectron spectroscopy (XPS). In UPS is used excitation energy of ≈ 10 -100 eV to probe valence energy levels of materials. On the other side, in XPS is used $h\nu > 100$ eV, for the excitation of electrons from core levels in order to study film compositions and chemical reactions. Although, if used excitation energy is above 2000 eV, then the technique is denoted as Hard X-ray photoelectron spectroscopy (HAXPES).

3.1.2. Short theory of photoemission process

The brief theory of the photoelectron emission process will be reviewed in this section. Firstly, the single-particle model will be considered, where the principle of conservation of energy connects E_k of the photoemitted electron to the excitation energy, as shown in Equation 3.3. Koopmans' theorem approximates that the binding energy of an electron is equal to the ground-state energy of the emitted electron.¹⁵² It is best applied for the free-electron band-like electronic states, assuming that excitation does not change any other orbital, hence, it disregards the relaxation energy. Hence, the binding energy of an electron in PES is actually the energy

difference between the total energy of ionized final state with $N-1$ electrons ($E(N-1)$) and total energy of the initial state with N electrons ($E(N)$):

$$E_b = E(N - 1) - E(N) \quad (3.5)$$

However, to obtain the total energies of these states is not an easy task, and quantum-chemical calculations must be employed, regarding that eigenstates of the system in the initial state are not the same with the eigenstates of the system in the final state. The reason is that the photoexcited electron and the hole left behind are interacting with the surrounding charges in the solid. Upon hole creation, the system is affected by the existence of the created core-hole and reacts by minimizing the energy of its ionized state. Energy reduction caused by this rearrangement is the relaxation energy of the molecular electronic wave function (relaxation energy).¹⁵³

Although the PES does not probe the ground state directly, it is recognized as one of the most powerful experimental tools to study the electronic structure of materials. For the description of the photoemission process in PES, as an inherently quantum mechanical phenomenon, the semi-classical model proposed by Berglund and Spicer might be used.¹⁵⁴ In this model, the photoemission process is divided into three independent and sequential steps, with each being associated with a specific parameter. In the first step, after the absorption of a photon, an electron is excited within the bulk of solid. The photoexcitation of the electron from the initial to the final state can be described by the transition probability given by Fermi's golden rule:

$$\omega_{fi} = 2\pi/\hbar |\langle \Psi_f | H | \Psi_i \rangle|^2 \delta(E_f - E_i - h\nu) \quad (3.6)$$

where H is the Hamiltonian which describes the interaction between the electromagnetic radiation and the electron. The Ψ_f and Ψ_i are the wave functions of the final and initial states with energies E_f and E_i , respectively. If using the correct wave functions for the initial and final states and the dipole operator as H , Fermi's Golden Rule gives a correct description of the photoelectron process, however, approximations are needed to solve it.¹⁵⁵

The second step describes diffusion of the excited electron through the sample bulk towards the surface. On its way, the emitted electron might undergo elastic and inelastic scattering (collisions) with other electrons or even with atoms. Inelastic collisions lead to loss of the energy of photoelectrons on their way towards the surface, and as a result, the depth from which a piece of information can be obtained is reduced. That is why photoelectron spectroscopy is regarded as one of the most surface sensitive analytic methods.

The last step explains the transfer of photoelectron through the solid surface into the vacuum, where it will be detected. During the escape through the surface, an electron has to overcome barrier grown by the difference in potential inside and outside the solid at the surface (see Section 2.1.), i.e. to exceed the work function of the solid sample. This barrier can also cause the additional scattering at the surface, which may introduce problems in detection especially in the angle-resolved measurements.

In spite of some simplifications which were adopted for the description of the individual processes in the three-step model, the photoionization process can be well explained by the three-step model.¹⁵⁵

3.1.3. Interpretation of XPS spectra

In Figure 3.3, the XPS overview spectrum of indium tin oxide (ITO) film on glass is shown, where different signals (peaks) can be observed. The photoemission spectrum is basically a replica of the electronic structure (distribution of occupied states) of the solid material, shifted on the energy scale by the excitation photon energy ($h\nu$). Due to generally well-separated peaks of photoelectrons stemming from different atoms, PES is recognized as a reliable technique for the composition analysis of the specimen surface. The intensity of a particular XPS core level

peak is proportional to the content of element the peak represents, and its photoionization cross section (this will be explained later in the text). Most of the signals, such as In3d, In3p, O1s and Sn3d in Figure 3.3a, come from the photoelectrons created according to the simple illustration of photophysical processes shown in Figure 3.3b, where core-level electron is ejected by irradiating the sample with X-rays, leaving an ionized atom in the ground state.

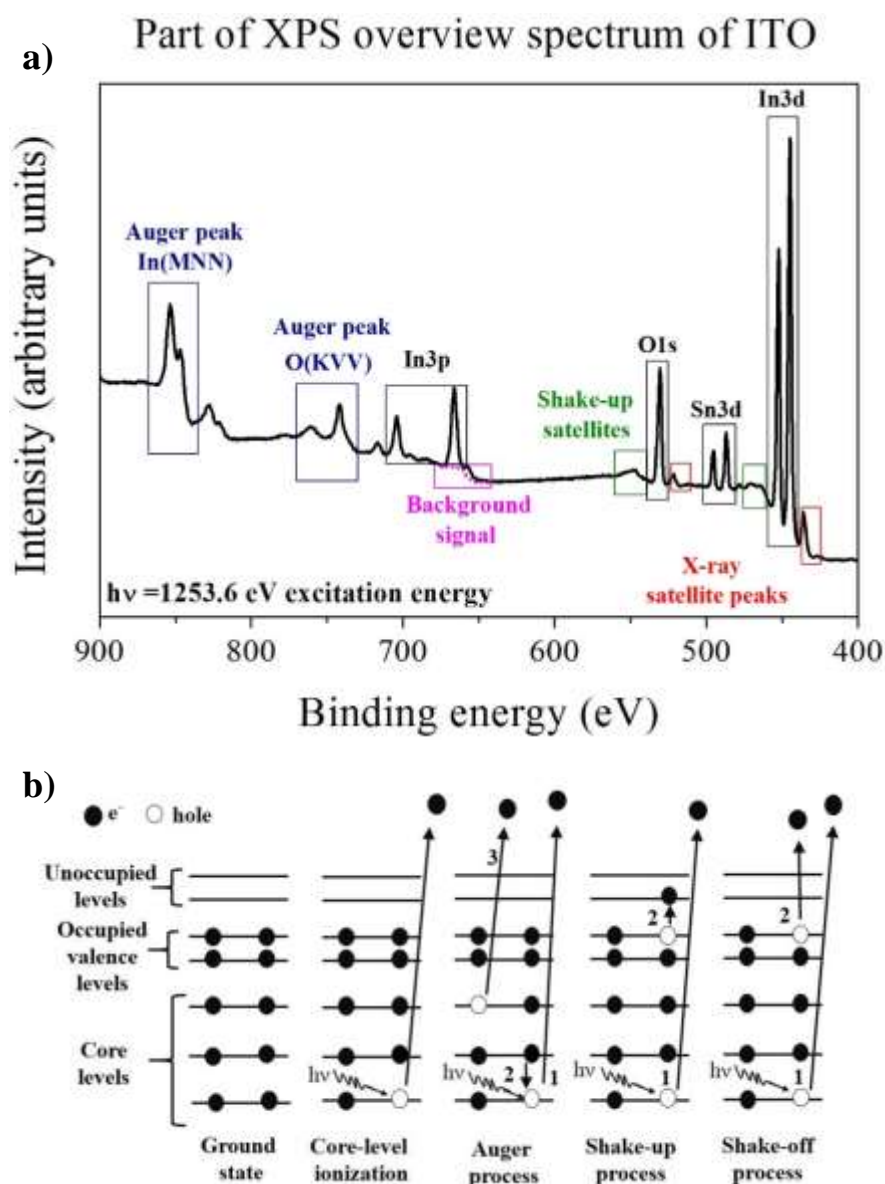


Figure 3.3: Overview spectrum of ITO surface, recorded with Mg Ka radiation ($h\nu = 1253.6 \text{ eV}$) of a standard source, with marked various contributions to the spectrum (a). Illustration of corresponding photoionization processes, which leave the studied system in different finale states upon photoionization (b).

Nonetheless, as stated above, photoelectrons along their path towards the outside of the sample interact with their surroundings, causing different photophysical processes. They might undergo one or more inelastic scattering processes, which will result in the loss of their kinetic energy and as a consequence the loss of information about their initial state. These electrons are called secondary electrons, and they are the major contribution to the background signal in XPS. The background signal in the XPS spectrum is designated in Figure 3.3a and presents one of the main problems in the quantitative chemical XPS analysis.¹⁵⁶ Thus, it can be inferred that a signal in PES stems from both types of electrons, those which elastically interacted with surroundings and preserved their E_k (i.e. information about their initial state), and others which due to inelastic interaction have reduced kinetic energy (loss or limit information about their initial state).

Additionally, the photoexcited electron traversing inside the bulk of a material, excite valence electrons of an already ionized atom which will consequently reduce its kinetic energy. The outcome of this process is depicted in the spectrum as a so-called shake-up peak, with a few eV higher binding energy comparing to the main signal (peak). Also, the photoexcited core electron may pass enough energy to the valence electron to be ejected from the sample. This phenomenon is regarded as a shake-off process, which also gives an additional peak with higher binding energy in comparison to the main line (peak). The shake-up and shake-off processes are regarded as two main final state effects in XPS.¹⁵⁷ Moreover, the created core hole can be filled with an electron from the outer core level, and as the outcome, a photon with energy equal to the difference in energy between involved levels is emitted. On the other hand, that difference in energy can cause another electron from the outer level to be ejected, leading again to the doubly ionized atom. The last process is called Auger decay of the hole, which is non-radiative multi-electron decay process, which results in a filled core hole and ejected electron with known kinetic energy independent on the variation of the excitation energy. Thus, the peak from Auger

electron in the spectrum plotted with the kinetic energy on abscise, always show the same position, independent on the value of excitation energy. Signals of photoemitted and Auger electrons, as well as, implications on the spectrum look of shake-up and shake-off processes, are summarized in Figure 3.3, together with corresponding energy level schemes of produced final states. Additional contributions to the XPS spectrum are so-called X-ray satellite peaks, marked in Figure 3.3a, which may appear if the sample is irradiated with the non-monochromatic X-ray beam (from so-called standard source) which possesses minor resonance lines of higher energy and lower intensity in its spectrum. Therefore, resulting satellite peaks pattern with lower and defined intensity in comparison to the main signal, are displaced on the lower binding energy side from the main signal (peak). On the other hand, some physicochemical phenomena which influence the core level peak appearance in the XPS spectrum are inherent to every system. One of them is the spin-orbit coupling which stems from the electromagnetic interaction between an electron's spin angular momentum and its orbital angular momentum. Thus, energy levels with the same principal quantum number (n) and non-zero angular momentum quantum numbers (l), (all orbitals but s-orbitals) show spin-orbit coupling. The spin-orbit coupling of the orbital and spin angular moment results in the splitting of the energy levels with same n and l quantum numbers. Hence, the photoelectron peak stemming from an orbital other than s, appears as a doublet peak in the XPS spectrum. The look of the In3d doublet peak is shown in Figure 3.4.

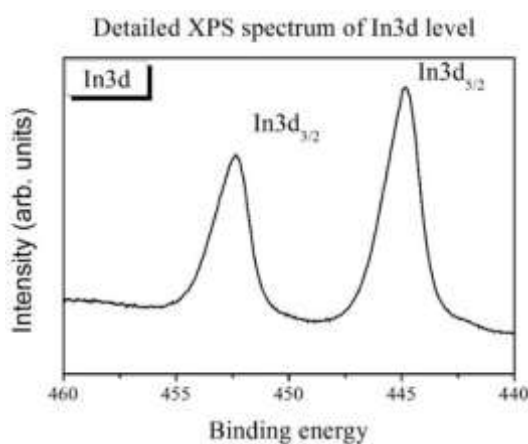


Figure 3.4: The In3d core level spectrum from ITO sample.

The relative intensity of peaks in the doublet is defined by the total angular momentum quantum number, expressed by $j = l + s$ where s is the spin angular momentum quantum number which can be $\pm 1/2$. Hence, the photoelectron signal stemming from some d-orbital ($l = 2$) such as the case in Figure 3.4, will have $j = 3/2$ or $5/2$. A single peak of the doublet will have multiplicity defined by expression $2j+1$, which in the considered case will be 4 and 6, hence, the ratio of intensities will be 2:3. For example, in the case of the photoelectron signal from the p-orbital ($l = 1$), from the calculation above, the intensity ratio would be 1:2. Generally, the probability of transition between the initial and final state wavefunctions, expressed by Fermi's golden rule in Equation 3.6 (see above section), determines the intensity of signals in PES. If the photoelectron cross section is known, the intensity of a particular signal can also be written as:¹⁵⁷

$$I = J * c_a * \alpha_{pc} * K_f * \lambda_{IMFP} \quad (3.7)$$

where J represents the X-ray flux striking the sample; c_a is the concentration of the photoelectrons emitted from an atom (ion) within the sampled volume (a is the element of interest). The α_{pc} is the photoelectron cross section, while K_f includes all instrumental factors such as the transmission function, and λ_{IMFP} is the inelastic mean free path of the photoemitted electron.

The inelastic mean free path (IMFP or λ) also called the escape depth, stands for the average distance passed by an electron between two inelastic collisions in particular single-layered homogeneous amorphous solid. The IMFP of an electron from a certain electronic level depends on its kinetic energy, which on the other side depends on the excitation energy. Therefore, varying the excitation energy, the depth from where electrons escape can be tuned. Yet, the very high surface sensitivity of the photoelectron spectroscopy technique comes from the relatively short IMPF of electrons in the condensed matter,¹⁵⁸ knowing that even for the electrons with high kinetic energy (> 1000 eV), IMPF does not exceeds 10 nm. The IMPF measured for different materials as a function of the electron kinetic energy forms the universal

curve, presented in Figure 3.5. Another important parameter in Equation 3.7 is photoionization (photoelectron) cross section. The photoionization cross section in the photoemission process is defined as the probability of an electron to be emitted from its electronic level.^{155, 159-160} It may vary from the element to element and from the level to level, but stays constant for a particular set of analytical conditions, such as excitation energy.¹⁶¹ As mentioned above, relatively short IMPF of electron limits the sampling depth of XPS, which is highly obscured by the absorption of the studied material. Hence, the absorption of a certain medium is a complex issue, which depends on the kinetic energy of photoelectrons and properties of the

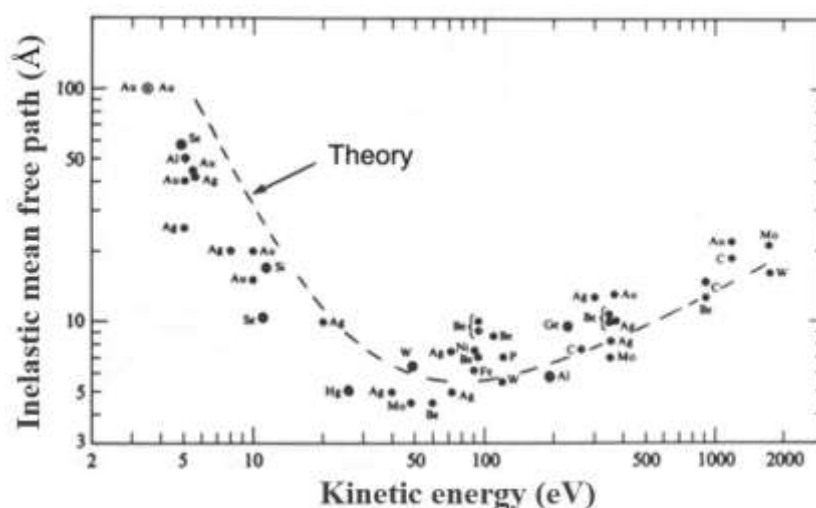


Figure 3.5: The universal curve of inelastic mean free path of electrons, based on experimental data for various materials, as a function of the kinetic energy of studied material.¹⁶²

Nonetheless, in XPS measurements, for the determination of the thickness of an organic layer, the exponential equation, similar to Lambert-Beer law, is used. In this work, it is used for assessment of the thickness (d) of prepared overlayers (thin films) of the organic semiconductors. The equation stands:

$$I_0/I_S = \exp(-d/(\lambda_0 * \cos \theta)) \text{ from which stands, } d = \lambda_0 * \cos \theta * \ln(I_S/I_0) \quad (3.8)$$

here, I_S stands for the intensity of substrate signal (particular substrate peak) when no organic layer is deposited onto the substrate, while I_0 presents intensity of the same peak after

deposition of the organic thin film. The θ denotes the takeoff angle measured with respect to the surface normal and its relationship with angle φ shown in Figure 3.6 holds: $\theta = 90^\circ - \varphi$. The inelastic mean free path in the organic material is designated with λ_o , while with E_k is marked the kinetic energy of the photoelectron peak.^{158, 163}

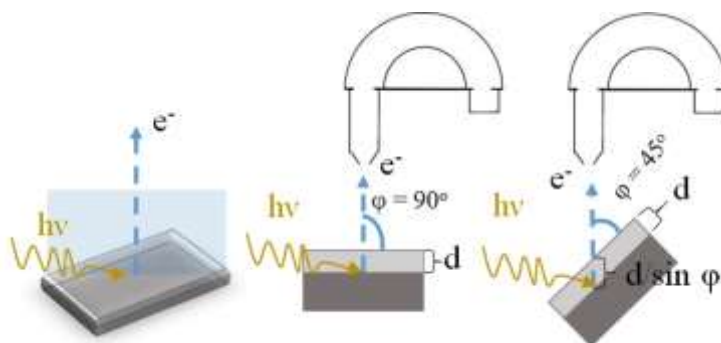


Figure 3.6: Geometry of measurements, depicted for the sample aligned perpendicular to the analyzer (central illustration) and tilted to the analyzer (right illustration). By tilting the sample, the exit angle of the detected photoemitted electrons and thus the surface sensitivity of the measurement can be changed. The path d that an emitted electron has to travel within the sample before it reaches the sample surface depends on the angle φ . If the measuring geometry is tilted ($0^\circ < \varphi < 90^\circ$), this changes by the factor $(\sin \varphi)^{-1}$ in comparison to the vertical outlet ($\varphi = 90^\circ$).

3.1.4. Ultraviolet photoelectron spectroscopy (UPS)

In order to get insight into the physical phenomena which occurs at the interface of two materials, Ultraviolet photoelectron spectroscopy (UPS) is frequently used. The UPS measurements provide valuable information about the electronic structure of studied material such as the origin of specific orbitals and bands in the valence band, work function, and ionization potential. For UPS measurements in home labs, it is often used Helium (He) gas discharge lamp with excitation photons of energy $h\nu = 21.2 \text{ eV}$ or 40.8 eV , called He I α and He II α lines, respectively. Both α -excitation energy lines are followed by β and γ lines with higher excitation energy and lower intensity. Thus, the main signal produced by α line is followed by signals from excitation lines β and γ , which possess lower binding energy and lower relative intensity. Hence, signals in the UPS spectrum produced by β and γ lines, called satellites, should

be removed during the spectrum evaluation procedure. Due to very short inelastic mean free path of photoelectrons in UPS which is approximately 2-3nm, the technique is regarded as very surface sensitive, with the depth resolution $\geq 2\text{nm}$. In Figure 3.7 are presented principles of the UPS study of the interface prepared via deposition of the organic thin film onto the conductive substrate. For the UPS measurement of the organic thin film (and any other), as can be inferred from at the last figure, the position of the substrate Fermi level (in equilibrium with E_F of the spectrometer) is also used as the reference for measurement of the kinetic (or binding) energy of photoelectrons. Going down the axis of the kinetic energy of the organic film spectrum, a signal which first arises (with highest kinetic energy) stems from various σ and π molecular orbitals for small molecules or valence bands of an extended conjugated system for polymers. The valence band signal (peak) from the organic thin film with the highest kinetic energy (lowest binding) energy stems from the HOMO level. The energy distance between the onset (leading edge) of the first HOMO peak ($E_b(\text{HOMO})$) and Fermi level of the substrate defines the interface parameter called the hole injection barrier (Δ_h) (introduced in Section 2.2.2.). As can be seen in the figure, for a broader purpose of understanding UPS technique and electronic structure of an interface, with a dashed line is shown part of the conduction band, i.e. the LUMO signal. Here should be mentioned, that the LUMO position cannot be obtained by UPS since it is unoccupied molecular orbital. For that purpose, and corollary to obtain values of the band gap of organic material (E_g) as the energy distance between the HOMO and LUMO levels, and electron injection barrier (Δ_e) as the energy distance between the Fermi level and LUMO level, e.g., inverse photoemission spectroscopy (IPES) might be employed. Broaden signal at the lower kinetic energy arises from secondary electrons, which does not carry information about the initial state they originate. The secondary electron signal with the lowest kinetic energy finishes with tail-like abrupt cutoff, which is frequently denoted as the secondary electron cutoff or shorten SECO. The SECO stems from the photoemitted electrons with the lowest kinetic

energy, still higher than the vacuum level, which are capable to leave the sample. The SECO position represents a direct measure of the local vacuum level (E_{VL}) position. Thus, change in the SECO position after measurement of an overlayer would mean the formation of interface dipole (Δ) at that particular interface. According to Figure 3.7, the difference between excitation energy and SECO, stands the value of the work function (Φ), i.e. $\Phi = h\nu - \text{SECO}$. On the other hand, ionization potential (IP) of the organic material is obtained through the equation $\text{IP} = \Phi + E_b(\text{HOMO}) = h\nu - W$, where W stands for the spectrum width from the $E_b(\text{HOMO})$ to SECO. This way obtained IP value is based on Koopmans' theorem (briefly discussed above), hence, the calculated binding energy of photoelectrons emitted from the HOMO is considered as a threshold ionization potential of the studied material.

It is worth noting here, what can be seen in Figure 3.2, that if the sample has higher work function than the spectrometer which is seldom the case, E_{VL} can be measured directly from the low kinetic energy electron onset. On the other hand, if opposite, the vacuum level of the measured sample cannot be obtained from the low energy electrons tail. In that case, the sample is biased to a known negative voltage with respect to the analyzer, in such a way that sample E_{VL} is higher than E_{VL} of the spectrometer. The BIAS voltage is applied since the complex electric field in the spectrometer chamber affects electrons with the low kinetic energy with respect to the analyzer. This way the low kinetic energy electrons get additional energy to reach the analyzer. After UPS spectra of the substrate (electrode) and sequentially deposited organic or inorganic overlayers are collected, obtained information might be converted into the energy level alignment diagram (introduced in Section 2.2.2.). The hypothetical situation at one interface, depicted by taken UPS spectra, is also shown in Figure 3.7 by integrated energy level alignment diagrams. From the ELA diagram can be more readily comprehended position and meaning of the interface structure parameters, important for the understanding of operation of the organic electronic devices such as OPVs and OLEDs.

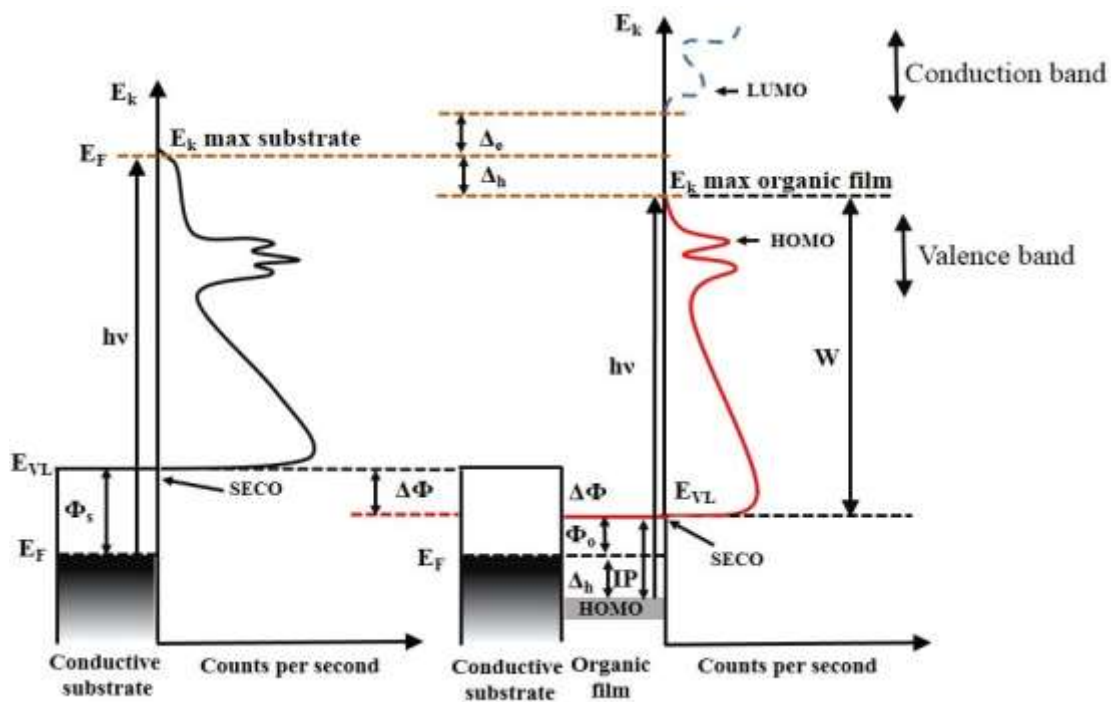


Figure 3.7: Principles of UPS presented on example of interface made by deposition of organic thin film onto conductive substrate.

3.1.5. Experimental equipment

Upon X-ray or UV irradiation of the sample, electrons are ejected and separated in the analyzer according to their speed (kinetic energy) and, depending on the analyzer, according to their angle of incidence. At the detector, the number of electrons is registered with the respective energy and then processed. The central part of the UHV system used for photoemission measurements is the energy analyzer. In Figure 3.8 is shown a simple illustration which explains the basics of photoemission measurements, where can be seen that the analyzer consists of three elements: the (electronic) lens system, concentric hemispherical analyzer (CHA) (two hemispheres at different voltages, within which electrons travel and separate according to their

kinetic energy) and detector. It should be mentioned here that cylindrical mirror analyzer (CMA) and other analyzer constructions are also often used in PES setups.

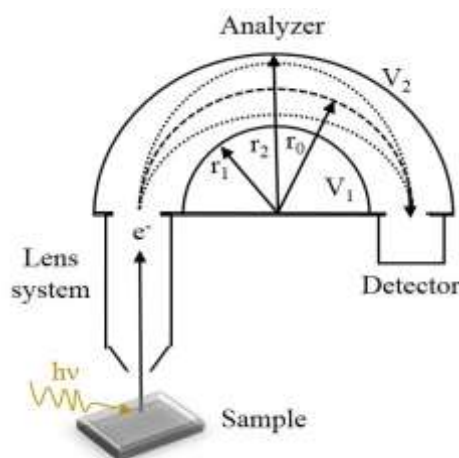


Figure 3.8: Cross section of the main part of PES spectrometer. The emitted electrons first pass through the lens system, where they are focused and decelerated to the pass energy. Due to the potential difference of the two hemispheres, only electrons whose kinetic energy corresponds to the pass energy can reach the detector.

Nonetheless, every analyzer has its own specific advantages which can be used dependently on the demand and goal of the experiment. The PES spectrometer is a sealed system which most of the parts are kept under high or ultrahigh vacuum! In this work, XPS and UPS measurements were performed in a multichamber UHV system with the analyzer made by Omicron NanoTechnology, located at the Institute of Physical and Theoretical Chemistry at the University of Tübingen. The photo of the UHV system can be seen in Figure 3.9. The system is equipped with an X-ray tube type DAR 400 and a hemispheric analyzer type EA 125. The base pressure of the analysis chamber and the subsequent preparation chamber separated is about $7 \cdot 10^{-10}$ mbar. In the X-ray tube, an Mg/Al twin anode is available, thus non-monochromatic Mg $K\alpha$ and Al $K\alpha$ radiation of the energies 1253.6 eV and 1486.6 eV, respectively, might be used. The UHV system is also equipped with a helium gas discharge lamp of the type UVS 10/35, which emits UV radiation with energies of 21.22 eV (He I α) and 40.81 eV (He II α), for Ultraviolet photoemission spectroscopy measurements. During the UPS

measurements, the pressure in the analysis chamber is $\sim 2 \cdot 10^{-8}$ mbar. For the work function determination via UPS measurements, a bias voltage of -10.0 or -12.0 V was applied to the

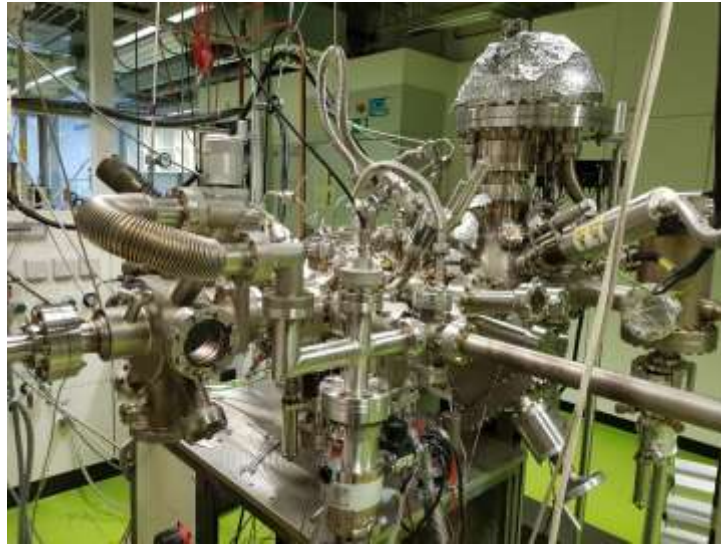


Figure 3.9: Photo of the photoelectron spectrometer used for our UPS and XPS measurements. sample.

3.2. Near edge X-ray absorption fine structure (NEXAFS)

3.2.1. Principles of NEXAFS and its application

The X-ray absorption spectroscopy (XAS) is a widely used technique for a determination of the local geometric and electronic structure of matter, which like photoelectron spectroscopy, roots in the photoelectric effect. In this technique, a sample is irradiated with monochromatic X-ray photons from the tunable source of high intensity, such as radiation provided in synchrotron facilities. In XAS, after absorption of radiation, the transition of an electron from the initial to the final state is the subject of well-defined quantum mechanical selection rules based on the symmetry of the final and initial states. Thus, the selection rules apply such as a change in the angular momentum quantum number ($\Delta l = \pm 1$) or the orientation of the electric field vector E

of the linearly polarized synchrotron radiation. After the sample is irradiated with X-rays, transitions of electrons from occupied core levels to unoccupied valence levels are recorded as a function of the excitation energy, as shown in Figure 3.10. As can be seen in the figure, XAS can be generally divided into two main subtechniques, based on the studied region of the XAS spectrum, and studied physicochemical phenomena behind the spectral features in the particular region. The subtechnique which studies region about 10 eV before and up to ~ 50 eV above the atomic absorption edge is called near edge X-ray absorption fine structure (NEXAFS) or X-ray absorption near edge structure (XANES), and it is the subject of the following text. In NEXAFS, the energy of soft X-ray excitation beam is varied around the ionization threshold of the certain atom of the investigated sample. The resonance energy of transition in NEXAFS spectrum is depicted by the absorption edge, denoted usually according to the electronic shell from which excited electron originates (i.e. K-edge, L-edge) or just core level (i.e. 1s-edge, 2s-edge). The first near edge X-ray absorption fine structure experiments, with used acronym XANES, were published around the beginning of the 1980s.¹⁶⁴⁻¹⁶⁶

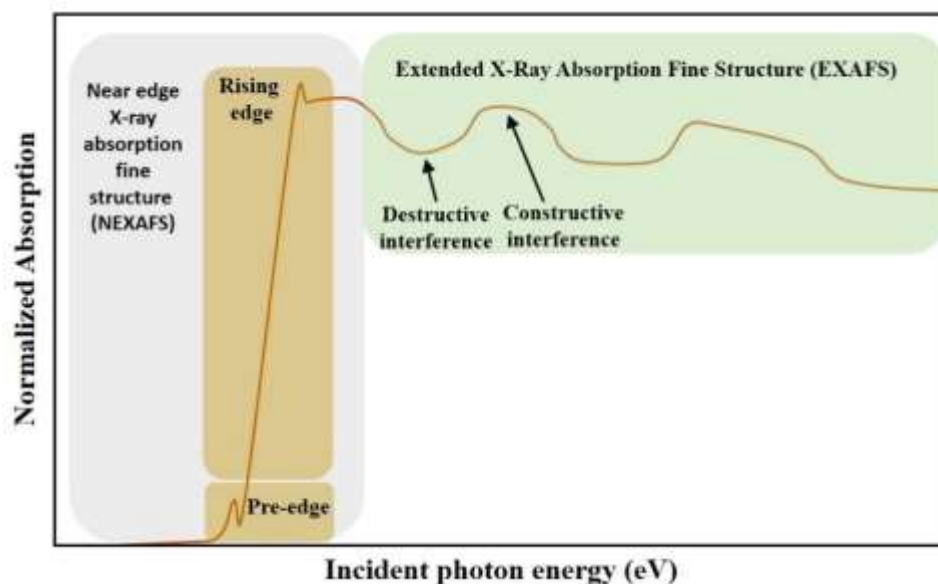


Figure 3.10: Different regions of the XAS spectrum, with designated subtechniques which study corresponding parts of spectrum.

The physicochemical principles of NEXAFS are depicted in an illustration, shown in Figure 3.11. Let us, for instance, imagine a diatomic organic molecule to be the subject of study in the latter figure. There, the core levels are almost unaffected keeping their initial structure and identity from the atom they belong, whilst electrons from the outer shells (valence electrons) take part in the formation of molecular orbitals, bonding σ and π , and antibonding σ^* and π^* orbitals. When the sample (molecule) is irradiated with the soft X-rays of enough energy, an electron is ejected from the core level. In the proximity of the absorption edge, the kinetic energy of photoelectron is small and approximated by equation $E_k = h\nu - E_b$, where $h\nu$ stands for the excitation energy, while E_b for the binding energy of the electron in the core level (shell).

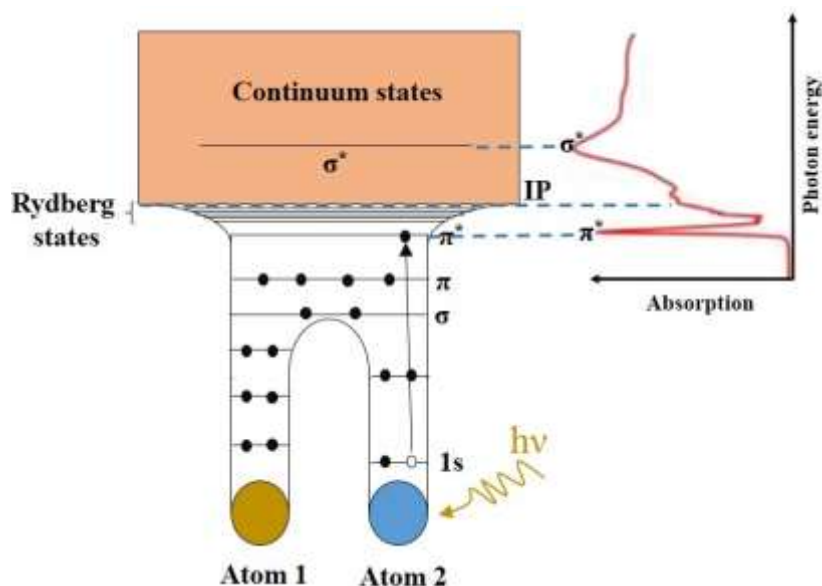


Figure 3.11: Illustration of fundamental physicochemical principles of NEXAFS.

Thus, the ejected core level electron is excited into the unoccupied π^* - molecular orbital of discrete energy which is below the atomic ionization potential (the vacuum level) and excited states with energies that follow the Rydberg formula (Rydberg states), as shown in Figure 3.11. Hence, the aforementioned transition of the electron from the 1s core level to π^* antibonding orbital is named π^* transition, which is usually reflected in the NEXAFS spectrum as a sharp peak just after the absorption edge. On the other hand, increasing the energy of X-rays from the tunable source, photoexcited electrons may finish above the ionization threshold (potential) in

the unbound continuum-like states, denoted in Figure 3.11 as σ^* state. In the continuum, a photoemitted electron is regarded as “free”, and can take any energy value, not only discrete. The σ^* transition in NEXAFS spectrum is reflected as a broader peak (series of peaks) which arises on the higher photon energy side than the π^* transition peak.¹⁶⁷⁻¹⁶⁸ The probability of transition, for a photoexcited electron from the initial state i (core level) to the final state f (unoccupied level), is quantum-mechanically described by Fermi’s Golden rule. The transition probability of the X-ray absorption ω_{fi} is proportional to the product of the absolute square of the matrix element of the perturbation operator and the density of states $\rho(E)$, where the perturbation operator $H'(t)$ considers the photon field as a time-dependent perturbation.

The transition probability is described by Equation 3.9:

$$\omega_{fi} \sim |\langle \Psi_f | H' | \Psi_i \rangle|^2 \rho_f(E) \quad (3.9)$$

where $H'(t)$ can be presented by product of the electric field vector E of the incoming light beam at the excitation place and transition dipole moment μ , which furthermore might be approximated by product of the elementary charge e and radius vector r . Hence, the above equation might be rewritten:

$$\omega_{fi} \sim |\langle \Psi_f | E e r | \Psi_i \rangle|^2 \rho_f(E) \quad (3.10)$$

The NEXAFS, as relatively young technique, has shown to be proven experimental surface science method to explore the electronic structure of different kinds of molecular species, especially their unoccupied density of states. It allows studying particular atomic species, charge distribution and bonding properties. Moreover, by probing the orientation of specific bonds by NEXAFS, the conclusion about orientation of the entire molecule may be drawn. This is commonly used for studying the orientation of the thin films of organic semiconducting molecules (small molecules and polymers) on different substrates.¹⁶⁹⁻¹⁷⁵ The highly oriented thin films of the organic semiconductors are very important for the efficient exciton diffusion,

charge separation and charge transport in organic electronic devices.¹⁷⁶⁻¹⁷⁸ As can be inferred from the above-presented equations, the magnitude of X-ray absorption depends on the component of polarization vector (electric field vector) of the incoming linearly polarized X-rays parallel to the transition dipole moment of the molecule. Thus, for the studied system which shows pronounced structural order, the measured NEXAFS spectra show a strong dependence on the angle between the incident light and sample surface, which can be observed in the change of intensity of the probed transition peaks. If the signal in NEXAFS spectrum is associated with the transition to particular antibonding orbital, which position is known in the structure of the studied molecular system, a conclusion about that orbital orientation, hence, the whole molecule orientation might be inferred.¹⁷⁴⁻¹⁷⁵ Figure 3.12 shows the effect of the mutual orientation of the polarization electric field vector and transition dipole moment of the probed molecular orbital, on the appearance of NEXAFS spectra.

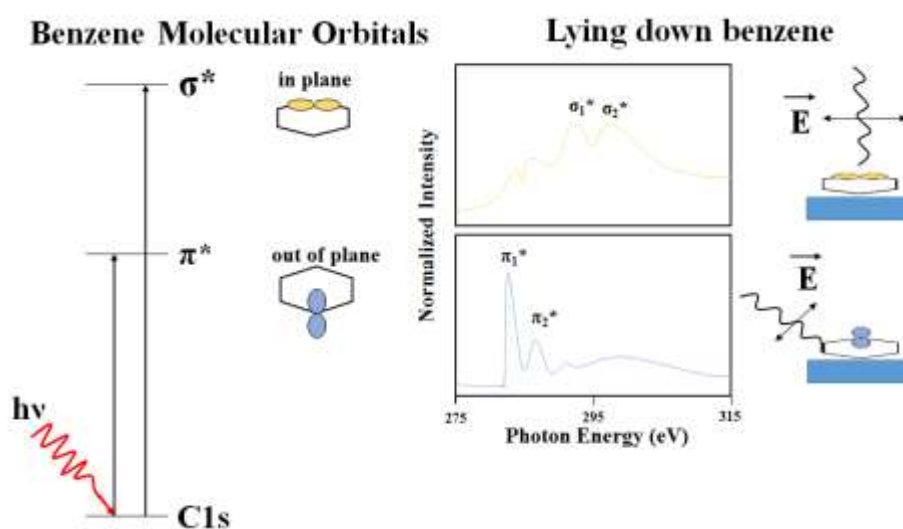


Figure 3.12: Dependence of NEXAFS spectra on the relative orientation of polarization vector and transition dipole moments, depicted by the hypothetical example of benzene.

The latter physical phenomenon observed in NEXAFS spectra is called linear dichroism. The determination of the molecular orientation as briefly indicated above, is based on the general notion of dipole selection rule.¹⁶⁷ Because, the π^* orbital have maximum orbital amplitude

normal to the bond direction (molecular plane), from this can be inferred that the dipole moment of the π^* transition is oriented normal to the molecule plane, for the flat-lying π -conjugated carbon system. On the other hand, the maximum orbital amplitude of the σ^* orbitals is along the bond axis, hence, the σ^* transition is aligned in parallel with the molecular plane. Thus, the intensity of π^* or σ^* transition is the strongest if the electric field vector of the linearly polarized X-ray beam is along π^* or σ^* orbitals, respectively, which is further related to the orientation of the probed molecular system. The NEXAFS has shown to be a convenient technique for probing the molecular orientation of the π -conjugated molecular systems (small molecules and polymers). For that purpose, NEXAFS spectra should be obtained for at least for two extreme values of θ angle, where θ is defined as the angle between the sample surface plane and the incident light. For example, in this work are used $\theta = 15^\circ$ and $\theta = 75^\circ$, defined as grazing and normal incidence angles, respectively. Hence, from the NEXAFS measurements, the tilt angle between the substrate surface and molecular plane might be determined.¹⁷¹ The intensity expression, might be reduced to $\cos^2\theta$ for perfectly lying (“face on”), or $\sin^2\theta$ for perfectly standing (“edge on”) planar π -conjugated system, orientations which could be seen in the graphical representation in Section 2.3.1.

In the NEXAFS technique, different detection methods can be used to record a spectrum. If the transparent sample is used, then the detection of the transmitted X-ray beam might be applied. However, it is rarely the case to deal with transparent samples, hence the other indirect methods of detection have to be used. Upon X-ray absorption, the core hole is created, and afterwards, it is filled by an electron from the higher energy level. The created excess of energy, after falling of the electron from the higher energy level into the core hole, might be released either radiatively or nonradiatively. In the former case, the fluorescence radiation is emitted, whilst in the latter Auger and photoelectrons are ejected.¹⁷⁹⁻¹⁸⁰ Detection modes based on emitted electrons are named: Total Electron Yield (TEY), Partial Electron Yield (PEY) and Auger

Electron Yield (AEY). While in the TEY mode, the signal is composed of all emitted electrons including Auger and secondary electrons, in the PEY detection mode electrons with lower kinetic energies (secondary electrons) are filtered out. In the AEY mode, only Auger electrons are detected. Thus, considering the depth from which different electrons originate in the solid sample (Auger electrons ~ 1 nm and ~ 5 nm for secondary electrons), the surface sensitivity increases for these three detection modes the way they are presented. The AEY mode is the most and TEY the least surface sensitive. Yet, all three detection modes based on electrons collections are much more surface sensitive (used for NEXAFS studies of the ultrathin films) than mode based on the detection of fluorescence radiation, named Fluorescence Yield (FY). In comparison to electrons which cannot travel far in a matter being prone to interact with their surroundings, photons may travel much longer. The mean free path of fluorescence X-rays is more than $1\mu\text{m}$ hence, the FY is much more bulk sensitive, i.e. less surface sensitive.²¹ In general, for soft X-ray region such as K-edges of C, N, O and F, detection modes based on electron yield are superior to the Fluorescence Yield (FY), although signal to background ratio is much higher in FY, the probability for the fluorescent decay process decreases with atomic number of the atom. On the other hand, for the higher energy soft X-ray region, such as K absorption edges of elements in the third row of the periodic table of elements (such as Sulfur K-edge), the FY mode is frequently used due to a higher probability to occur and much better signal to background ratio.

Hence, the FY mode in comparison to above-listed detection modes is the most bulk sensitive, which qualified the FY mode as a detection mode of choice for studying the polymer thin films in this work.¹⁷⁹

3.2.2. Experimental equipment

The XAS measurements are performed at high-performance X-ray absorption spectroscopy (XAS) beamline on a bending magnet source at ANKA (abbreviation for “Angströmquelle Karlsruhe”), the synchrotron light source facility at the Karlsruhe Institute of Technology (KIT). The beamline covers an energy range of 2.4 - 27 keV. Hence, the K-edges from sulfur to cadmium, and up till the L-edge of uranium can be probed. The double crystal monochromator with two parallelly mounted Si(111) and Si(311) crystals, exchangeable within minutes, is available for measurements. The beamline at the sulfur K edge has a typical energy resolution of about 300 meV (Si(111)) and a polarization degree higher than 0.95 (p-polarized). For the experiments presented in this work, the fluorescence detector of type 5 element LEGe (Canberra-Eurisys) is used. The standard sample holder (manual) used for our fluorescence measurements, is designed for plate samples (max. 8 mm thickness, 4 cm length, 5 cm high). Spectra are taken using a setup that enables the variation of the incidence angle to the sample surface, in the chamber filled with Ar gas.

Chapter 4

Materials and sample preparation techniques

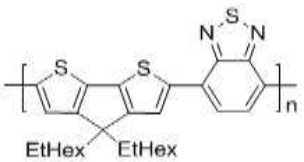
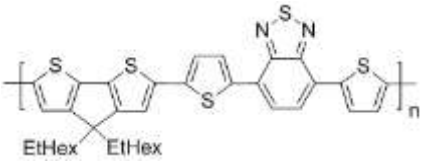
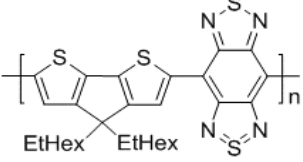
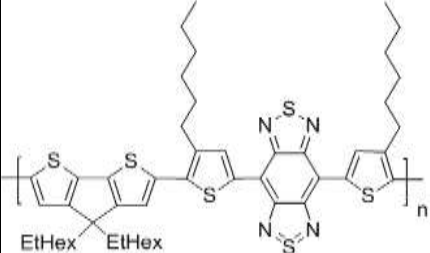

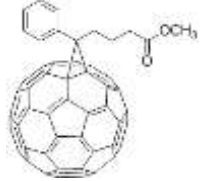
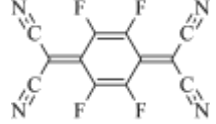
In this chapter, organic semiconducting materials and substrates (model electrodes) used in this work, will be reviewed. Also, the preparation techniques, used for the fabrication of samples of latter organic polymers and molecules, will be presented.

4.1. Organic semiconducting materials

Since presented for the first time some 25 years ago, the bulk heterojunction based on the conjugated polymer as the donor and fullerene as the acceptor material is still a deep inspiration for researchers around the world, to find the “winning” combination(s) of donor and acceptor materials. What will be regarded as the winning combination depends on a lot of factors, where the electronic structure of constituent materials is one of the most fundamental. The electronic structure of the donor and acceptor materials, especially condition their mutual interaction as the crucial point for functioning of organic photovoltaic devices based either on planar (PHJ) or bulk (BHJ) heterojunctions. Moreover, the interaction of donor and acceptor materials with other materials embedded in the photovoltaic device (such as electrodes, hole and electron

transport layers, dopants, additives, etc.), is affecting the overall device performance. The electronic and chemical structure of the used materials in a photovoltaic device may have a substantial influence on the morphology of the prepared films. This is of highest importance knowing that the architecture of current photovoltaic devices is based on stacking of differently functionalized layers (films), and that transport properties of the π -conjugated polymers and molecules highly depend on the molecular orientation and ordering in thin films. In this work, fullerene C₆₀ (Sigma Aldrich) and its derivate PCBM (Solenne) are used as acceptor materials. In the doping experiments as a dopant is used a strong electron accepting (oxidizing) molecule (molecular p-dopant) F4-TCNQ (Sigma Aldrich). Lastly, as the donor materials in this work are used four π -conjugated donor-acceptor copolymers, named by acronyms: PCPDTBT, PCPDTTBTT, PCPDTBBT and PCPDTTBTT. All four polymers are based on dithiophene (PCPDT) as the electron donating (electron rich) subunit and, benzothiadiazole (BT) or stronger benzobisthiadiazole (BBT) as the electron withdrawing (electron deficient) subunit. Also, studied polymers differ by the presence of the additional thiophene rings (T) (with and without side chains) within their monomer unit, as can be inferred from the above presented abbreviated names. These subtle changes in the chemical structure of polymers may have an influence on their electronic structure, and the complexification of the monomer unit structure might affect organization properties of these in the thin films. All copolymers presented here except PCPDTBT (purchased from Sigma Aldrich), were synthesized and kindly provided by the research group of Prof. Ullrich Scherf (Fachbereich C-Makromolekulare Chemie, Bergische Universität Wuppertal). Full names and chemical structures, of all organic semiconducting polymers and molecules used in this work, are listed below in Table 4.1.

Table 4.1: Acronyms, chemical structures, full names and molecular weights of the organic semiconductors used in this work.

Acronyme	Chemical structure	Full name	Molecular weight
PCPDTBT		Poly[2,6-(4,4-bis(2-ethylhexyl)-4H-cyclopenta[2,1-b:3,4-b']di-thiophene)-alt-4,7-(2,1,3-benzothiadiazole)]	Mw = 56 kg/mol
PCPDTTBT		Poly[2,6-(4,4-bis(2-ethylhexyl)-4H-cyclopenta[2,1-b:3,4-b']-dithiophene)- alt-4,7-(bis (thiophene-2-yl)-2,1,3-benzothiadiazole)]	Mw = 7.7 kg/mol
PCPDTBBT		Poly [2,6-(4,4-bis(2-ethylhexyl)-4H-cyclopenta[2,1-b:3,4-b']dithio- phene)-alt-4,8-(benzobis[1,2-c:4,5-c']thiadiazole)]	Mw = 18 kg/mol
PCPDTTBBTT		Poly[2,6-(4,4-bis(2-ethylhexyl)-4H-cyclopenta- [2,1-b:3,4-b']-dithiophene)-alt-4,8-(bis(thiophene-2-yl)- benzobis [1,2-c:4,5-c']thiadiazole)]	Mw = 12 kg/mol
C ₆₀		Fullerene C ₆₀ H ₆₀	Mw = 0.7206 kg/mol
PCBM		[6,6]-phenyl-C ₆₁ -butyric acid methyl ester	Mw = 0.911 kg/mol
F4-TCNQ		(2,3,5,6-Tetrafluoro-2,5-cyclohexadiene-1,4-diylidene)dimalononitrile	Mw = 0.276 kg/mol

4.2. Substrate materials

4.2.1. Indium tin oxide (ITO)

Indium tin oxide (ITO) is a wide band gap n-type semiconductor extensively studied for the last couple of decades in the optoelectronic industry. Its unique properties, notably low resistivity and high transparency in the visible and near-infrared regions of the electromagnetic spectrum made ITO the material of choice for a transparent electrode in the organic optoelectronic devices.¹⁸¹⁻¹⁸³ For experiments presented in this manuscript, the ITO coated glass samples with the sheet resistance $R=10 \text{ } \Omega/\square$ (Hoya Corporation) were used for the NEXAFS and AFM measurements, whilst samples with $R=33.1 \text{ } \Omega/\square$ (unknown producer) for the photoemission measurements. The ITO plates were cleaned prior to deposition of organic semiconductors in the glove box or introduction into the UHV system. The cleaning procedure consisted firstly of the sweeping of ITO plates with the nitrogen gas stream in order to remove all mechanical dirt from the surface. Then, the sonication in acetone for 15 min. and subsequently in isopropanol for the same time is done. This wet chemical prepared ITO substrate results in the work function value of 3.8 eV. On the other hand, if the additional step of 5 min. UV/ozone treatment is included as the last step in the above explained cleaning procedure, the obtained Φ stands 4.0 eV. It was shown that UV irradiation step if included enough long in the preparation procedure, may produce an atomically clean ITO surface.¹⁸⁴⁻¹⁸⁵

Here, it should be mentioned that the preparation/cleaning procedure of the ITO plates has a great influence on its surface stoichiometry, hence, the work function value.¹⁸⁴⁻¹⁸⁵ The approach to tune the surface properties of the ITO film, for application in the organic electronics, is also the introduction of an ultrathin film overlayer of another chemical compound. Those

compounds being chemically or physically adsorbed on the surface of an ITO thin film, due to their intrinsic physicochemical properties modify the surface electronic structure properties of the substrate beneath. In Figure 4.1 can be seen the chemical structure of the branched polymer poly(ethylenimine) or abbreviated PEI. The PEI polymer due to its large band gap (it is an insulator) and dipole moment associated with amine groups, recently has been extensively used as an overlayer with the task to lower the work function of conductive substrates beneath. Cast as a thin film up to 10 nm thick, PEI substantially reduces the work function of a wide range of conductive substrates, such as transparent metal oxides, metallic and organic substrates.¹⁸⁶⁻¹⁸⁸ For the experiments presented in this work, PEI films on ITO (PEI/ITO) from 1 mg/ml PEI solution in isobutanol were prepared by doctor blade casting and subsequently annealed at 110 °C in N₂ atmosphere for 10 min. Here, it is important to consider this compound as a surface modifier and its thin film on ITO as a modified surface of the used substrate, rather than a newly introduced substrate.

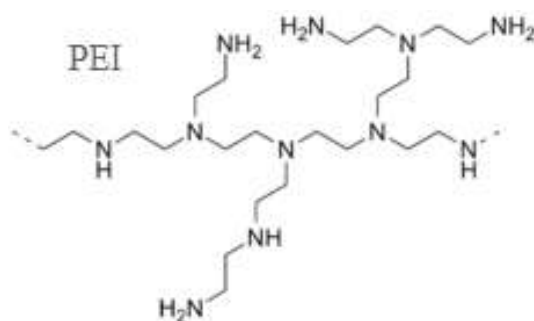


Figure 4.1: Chemical structure of polyethylenimine or abbreviated PEI.

Being a wide band gap polymer, for the technological application as a surface modifier in the organic electronic devices,¹⁸⁸⁻¹⁹² thickness of the PEI film should be kept under around 10 nm, for the reason that tunneling of charge carriers is possible between substrate and overlayer.¹⁸⁶ Strong XPS signals which originate from the used substrate (In3d, Sn3d, O1s) suggest us that the PEI is present in ultrathin film on ITO (not shown here), in experiments presented in this manuscript. The calculated thickness of the PEI layer using Equation 3.8, and the intensity of

In3d peak of the XPS overview spectrum before and after a PEI casting, brings a thickness for the PEI layer ≈ 6 nm which might advocate that the tunneling of charges is possible between the ITO substrate and subsequent polymer overlayer.¹⁸⁶ This way modified ITO substrate by the ultrathin film of PEI, shows Φ_s of 3.2 eV measured by UPS. Hence, clearly can be seen that ITO work function is decreased by 0.8 eV due to PEI deposition (ITO with Φ_s of 4.0 eV was exclusively used for PEI deposition), as a result of physic-chemical phenomena explained in Section 2.2.

4.2.2. Zinc oxide (ZnO)

The method to decrease the work function of the substrate/electrode beneath greatly exploited in the preparation of inverted solar cell structures is the deposition of ZnO thin films as interfacial electron transport layer.¹⁹³⁻¹⁹⁴ ZnO is a wide band gap n-type semiconductor because of the presence of oxygen vacancies or zinc interstitials, which possesses high transparency, environmental stability, and relatively high electron mobility. Due to its high natural abundance and inexpensive solution-based thin film deposition at low temperatures, a thin film of ZnO is in the focus of recent research efforts, as an electron transport layer, which might be also used as electrode modifier.¹⁹⁴⁻¹⁹⁶ For the preparation of zinc oxide thin film on ITO (ZnO/ITO) in this work, zinc oxide nanoparticles sonicated in ethanol for 30 min. are used. The ZnO films on ITO were produced by the doctor-blade casting of ZnO solution, followed by an annealing step in N₂ atmosphere (140 °C for 10 min) of the glove box. Although ZnO films in this work were prepared on ITO substrates, they are considered as new substrates. In XPS spectra, the signal from ITO beneath could not be observed due to the thickness of ZnO film. This way produced

ZnO substrates show Φ_s of 3.3 eV, which is lower than the original work function value of bare ITO substrate.

4.2.3. UV/Ozone treated polycrystalline film of gold (AuO_x/Au)

In order to determine energy levels of polymers relevant for their energy level alignment at interfaces in electronic devices, substrates with a wide range of the work functions are needed. The UV/ozone treated gold film (named AuO_x/Au) due to its high work function is the substrate which may allow determination of E_{ICT^+} level, important for conjugated polymers which are considered as potential donor materials in OPVs or OLEDs.

Although literature values for the gold work function are rather high (5.1-5.5 eV),³⁷ this magnitude of values is usually reported for different atomically cleaned monocrystalline and polycrystalline Au surfaces. To achieve these work function values, usually, a long-term ion sputtering in UHV is necessary.³⁷ On the other hand, *ex situ* prepared Au surfaces have substantially lower Φ values than 5 eV, due to adsorption of gasses from the atmosphere and well known “push back” effect.¹⁹⁷ It has been reported, that original high work function can be recovered after treatment in the UV/ozone (UV/O₃) chamber, and stay the same for at least half an hour of ambient exposure.¹⁹⁸ For experiments presented in this work, Au films were evaporated onto Si wafers in a specially assembled UHV system for that purpose, with a thickness around \approx 200 nm estimated by monitoring Quartz microbalance. The film of Au on Si wafer was then transferred to UV Photo Surface Processor PL16-110B-1 by SEN LIGHT Corporation for 30 min. long treatment in UV/ozone atmosphere. Afterwards, the sample was exposed to the atmosphere for < 3 min. on the way to the glove box for the polymer casting or

insertion into UHV measuring system. The UPS measurements, bring the stable work function value of 5.0 eV for this substrate.

4.2.4. Poly(3,4-ethylenedioxythiophene) polystyrene sulfonate (PEDOT:PSS)

It has been demonstrated, that a thin film of PEDOT:PSS conducting polymer coated atop ITO anode is a successful method to optimize the charge transport across the active material/ITO interface.¹⁹⁹⁻²⁰¹ One of the reasons is that PEDOT:PSS film has a high work function, which better matches with energy levels of the hole conducting material relevant for the charge transfer and energy level alignment at the interface. As a result, OPV and OLED devices fabricated with PEDOT:PSS layer atop an ITO anode, have a longer lifetime and better photovoltaic performance than those using only bare ITO anode.²⁰² The PEDOT:PSS deposited on the ITO anode has shown to be an effective combination for the performance of organic photovoltaic devices, due to decrease of the surface roughness of ITO (i.e. decreasing number of micro-shorts) and increase of the work function of system (which might lead to lower hole injection barrier), while minorly influencing the original transmittance of bare ITO.^{201, 203} The PEDOT:PSS is the dispersion of the π -conjugated, highly conductive and transparent polymer PEDOT, stabilized by charge balancing dopant PSS. Here, PSS behaves as a p-type doping counter ion which promotes hole mobility along the PEDOT conjugated backbone and improves the dispersion of the complex in polar solvents. Chemical structure of PEDOT:PSS can be seen in Figure 4.2. For the PEDOT:PSS thin film, it has been demonstrated that a lot of its properties, such as morphology and consequently conductivity and work function, tightly depend on the content of polymer mixture, i.e. the PEDOT to PSS ratio. Moreover, properties

of PEDOT:PSS can also be changed by blending with additives or by the chemical change of the structure of original compounds. Thus, on the market exists a wide variety of PEDOT:PSS analogs, with nuanced physicochemical properties. Generally, the film produced by deposition of PEDOT:PSS from the aqueous dispersion leads to the formation of grain like structures in the film, which surface is mostly made of PSS whilst core of PEDOT. Nevertheless, PEDOT and PSS distribution is expected to be more homogeneous throughout the film.²⁰⁴⁻²⁰⁵ It was shown that an increase of the content of PSS in the mixture improves the film morphology, but on the other side decreases the film conductivity.²⁰⁶

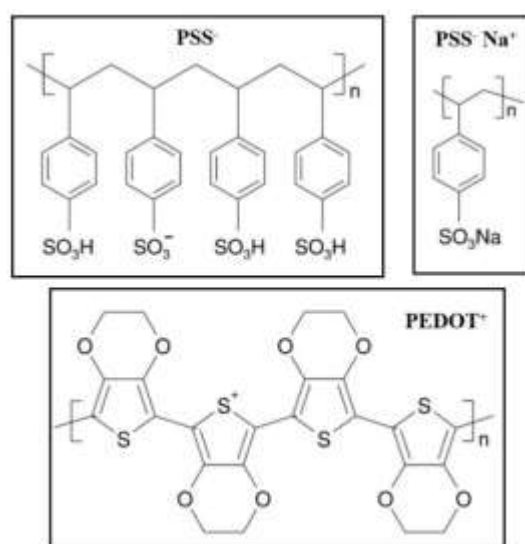


Figure 4.2: Chemical structures of consist parts of PEDOT:PSS blend.

Also, it has been observed that in the PEDOT:PSS thin film, PSS segregates at the surface of thin film²⁰⁵, and this excess of the nonconductive PSS part at the surface is expected to decrease the work function of PEDOT:PSS thin film²⁰⁷. For experiments presented in this manuscript, thin films of PEDOT:PSS were prepared via spin-coating (1000 rpm for 20 seconds) under ambient conditions on precleaned ITO, with $\Phi = 4.0$ eV, from the solution with mixing ratio 1:6 provided by H.C.Starck company. After coating of PEDOT: PSS, the film was annealed in N₂ atmosphere of the glove-box at 120 °C for 20 min. The thickness of the PEDOT:PSS thin film obtained from the XPS overview spectrum using Equation 3.8, is ≈ 20 nm. In Figure 4.3,

are shown fitted XPS spectra of S2p and O1s signals, to particular contributions from PEDOT and PSS parts, according to approach published elsewhere.²⁰⁵

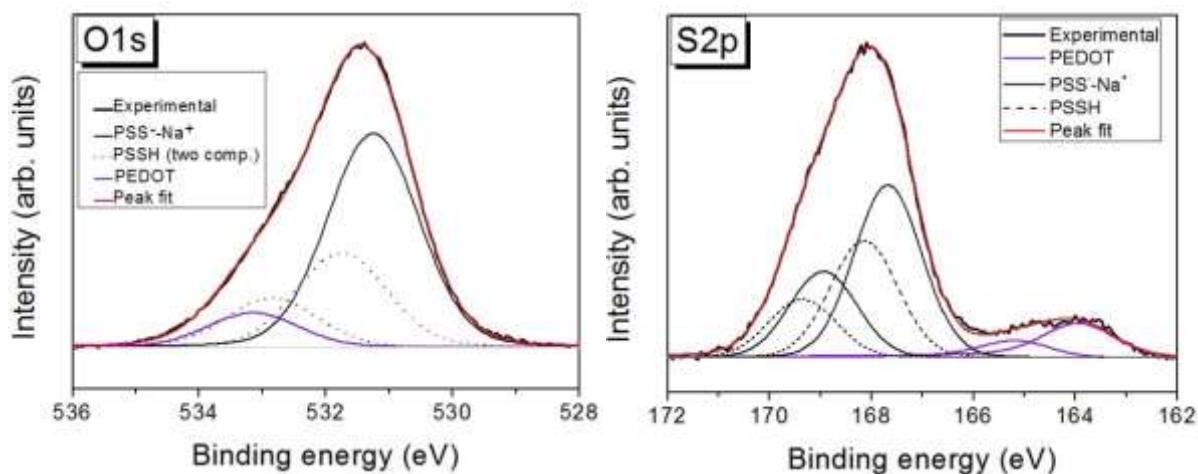


Figure 4.3: Fitted spectra of S2p (left) and O1s (right), of PEDOT:PSS thin film prepared on ITO.

Fitting of signals is done in order to evaluate the exact ratio between PEDOT and PSS parts in the mixture. The PEDOT to PSS ratio obtained from integrated areas of PEDOT and PSS parts of S2p and O1s signals is 1:6.2, which is in excellent agreement with the information provided from the supplier of 1:6 ratio. Obtained amount of sodium in the PEDOT:PSS thin film from the integration of signals in XPS overview spectrum is 2.1% in absolute atomic concentration. While the absolute stoichiometry of the PEDOT:PSS thin film is in agreement with the chemical formula of the PEDOT:PSS mixture, a considerable amount of sodium present at the sample surface might stem from $\text{Na}_2\text{S}_2\text{O}_8$ oxidizing agent used during the polymerization of PEDOT.²⁰⁷ Measured UPS overview spectrum of the thin film of PEDOT:PSS on ITO is shown in Figure 4.4. The obtained spectrum somehow reminds on that measured for a neat PSSH film on ITO.²⁰⁵ The intensity of the spectrum is extended close to zero (Fermi level) and then decreases rapidly. This observation is a clear sign of the Fermi level of PEDOT:PSS, stemming from the PEDOT

part, and a kind of metallic character of PEDOT:PSS material. For this way prepared PEDOT:PSS film on ITO substrate, the work function was found to be 5.2 eV.

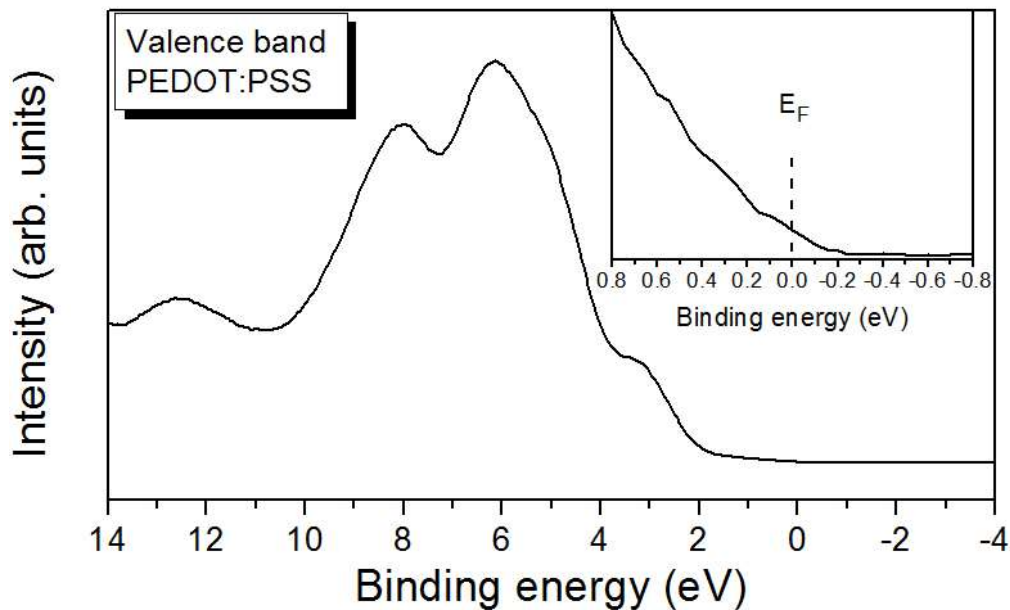


Figure 4.4: The UPS valence band spectrum of the PEDOT:PSS thin film prepared on ITO. Inset shows that density of states can be found up to the Fermi level (0 eV) and then abruptly vanishes.

4.3. Sample preparation techniques

4.3.1. Doctor-blade casting

The doctor-blade casting is well known as a precise coating technique for preparation of the thin films on the large area surfaces, originating from the 40s of the last century when it was first used for the production of the thin sheets of piezoelectric materials and capacitors.²⁰⁸ In doctor blade casting technique, the thin film is created by spreading the solution of studied material over the substrate with uniform thickness at a constant speed, using “doctor” blade. The basic principle of doctor blading and setup of the used device in this work, are shown in Figure 4.5. Thin films are produced by the movement of the blade over the stationary plate onto which the substrate for coating is fixed. After casting of the material solution, evaporation of

the solvent is promoted or reduced by the temperature control of the plate on which substrate is placed for coating. This way experimenter has an influence on the morphology of the produced thin film. The polymer thin films produced in this work, according to experience based on combined AFM and UV-Vis absorption measurements are between 20 and 40 nm thick, however, it should be noted that the film thickness might vary depending on the different substrates used in this study. The thickness of the film can be varied by adjusting the space between the blade and substrate, via precise micrometer screw bolt.

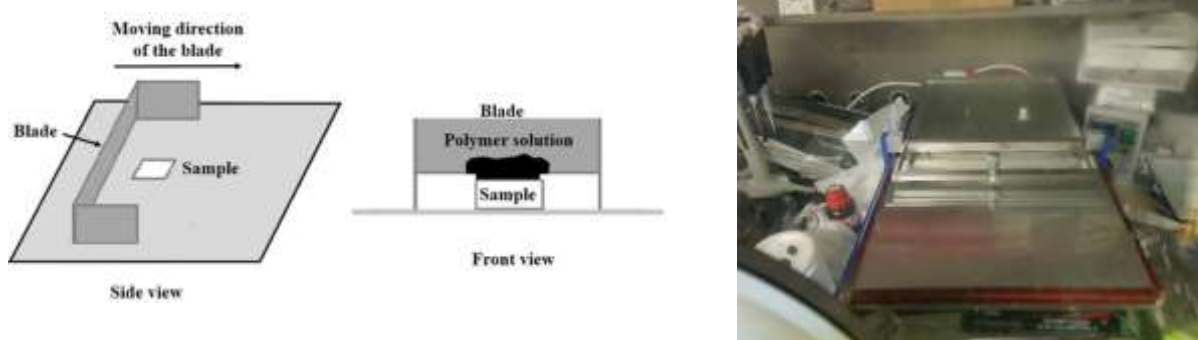


Figure 4.5: Simple illustrations which depict principles of doctor blade casting are shown in left and central part of the figure, while photo of used apparatus is shown right.

Additionally, the film thickness might be varied by change of concentration of the used solution, or by changing the velocity of the blade which spreads the solution. Doctor-blade casting technique is successfully used for the production of conjugated polymer-based photovoltaic devices, providing films of good quality and showing certain advantages in comparison to related solution coating methods, such as spin coating.²⁰⁹ This coating technique is more comparable to real device preparation conditions, using for example polymers and PCBM for application in OPVs, in comparison to other methods such as vacuum sublimation or electro spray deposition. For experiments presented in this text, the doctor-blade casting was always done within the nitrogen filled glove box. Solutions of polymers and polymer:PCBM blends were prepared as the 1 w% solutions in 1,2-dichlorobenzene

(orthodichlorobenzene (ODCB)), stirred and heated at 80°C overnight (about 10h) before the casting. On the other hand, thin films of PCBM were prepared from the solution with chloroform (trichloromethane) used as a solvent, stirred and heated overnight at 50°C, before the film preparation.

4.3.2. Organic molecular beam deposition (OMBD)

Organic molecular beam deposition (OMBD) is a frequently used deposition technique for the preparation of the thin films of organic semiconducting small molecules, from submonolayer to multilayer films.²¹⁰⁻²¹³ The advantage of OMBD is that it enables fabrication of multilayer devices in which the thickness of each layer can be controlled more easily, in comparison for instance to the doctor-blade casting. In OMBD, molecules are thermally evaporated from the evaporation cell, usually in ultrahigh vacuum (UHV) condition. Preparation in UHV provides clean and controlled preparation conditions, which are crucial for the investigation of the interaction between the prepared film and surface onto which is deposited. The evaporation (effusion) cell designed on the basis of Knudsen cell is an especially suited tool for the well governable vapor deposition process, from the resistively heated crucible (container) filled with the deposition material.²¹⁴⁻²¹⁵ The control and monitoring of the deposition rate are done by the power supply, via adjusting the voltage or current, and also by monitoring pressure via pressure readout device. Finally, the deposition rate in praxis is almost always monitored by the quartz microbalance. Photo of the evaporation cell used for OMBD experiments is shown in Figure 4.6. Thin films of fullerene C₆₀ presented in this thesis, were prepared within the UHV system, at pressures lower than $1 \cdot 10^{-8}$ mbar.



Figure 4.6: Photo of the evaporator used in experiments presented in this work.

Chapter 5

Results and Discussion

The polymer thin film solar cells have attracted great attention due to the wide diversity of potential fields of application, counting on their main advantages: low cost, light weight, environment friendly, simple and large-scale processability from solution. These advantages rely on π -conjugated polymers as promising semiconducting materials, which physicochemical and electronic properties can be tailored through versatile chemical modifications of their structure. These chemical modifications can be subtle, such as grafting of different subunits (electron donating or accepting) or side chains within/on the polymer backbone, or larger such as dimerization for example. In π -conjugated polymers, changes in the chemical structure can be used for fine tuning of the position (energy) of energy levels, interaction with light, solubility, chemical stability, thin film formation, and etc. It should be kept in mind that the improvement of one physicochemical property by modification of the chemical structure without affecting other(s) (even worsening) is a challenging task. Moreover, the knowledge of electronic properties of these materials and their interaction with materials found in electronic devices (such as organic or inorganic layers and electrodes) is essential for the understanding of their self-organization properties in (thin) films. This all would imply that physicochemical interaction at all interfaces throughout device should be comprehended, and the energy level alignment at the junction between different materials optimized and predictable, as well as consequential molecular orientation (of conjugated polymers) in the thin film based organic

electronic devices. Hence, the aim of this work is to relate how the distinction in the chemical structure between two low band gap (LBG) “polymer pairs” PCPDTBBT & PCPDTTBTT and PCPDTBT & PCPDTTBTT (different electron withdrawing subunit) and within pairs (addition of extra (hexyl)thiophene rings) affects physicochemical properties important for the implementation of these polymers as electron donor materials (hole conductors) in OPVs.

5.1. Donor/electrode interfaces

Low band gap copolymers are widely used as promising donor materials for OPVs. One of the ways to improve the performance of polymer-based solar cells is a comprehensive understanding of the electronic properties of organic materials, especially when these materials are in contact with other materials. Hence, the predictability of their interaction (i.e. charge transfer, energy level alignment or even chemical reaction) at different organic-inorganic and organic-organic functional interfaces present in electronic devices is of high importance. Therefore, in this section, the thin films of four LBG polymers with similar and related chemical structures are probed, in order to grasp the interplay between their chemical structure and electronic properties at interfaces with different model electrodes.

5.1.1. UV-Vis-NIR absorption spectroscopy of low band gap polymer films

The focus of this section will be on the influence of changes of the chemical structure on the optical gap of four LBG polymers: PCPDTBT, PCPDTTBTT, PCPDTBBT, and

PCPDTTBBTT, studied via UV-Vis-NIR absorption spectroscopy. Thin films of polymers were prepared via doctor-blade casting of the 1 w% solution in orthodichlorobenzene on the quartz substrate, using the same parameters of the deposition technique as it is the case for polymer thin films prepared on different model electrodes. The UV-Vis-NIR absorption spectroscopy measurements were performed in order to assess the optical band gap (E_g^{opt}) of each polymer, where E_g^{opt} corresponds to the energy of the lowest (HOMO – LUMO) electronic transition accessible via absorption of a single photon.³⁰ For a full understanding of the properties of organic materials and their implementation in electronic devices, it is very important to know the size of the optical band gap. In π -conjugated systems, the presence of C=C bond causes light absorption which initiates the electronic transition from the valence into the conduction band of the studied system. These are electronic transitions from the highest occupied molecular orbitals (HOMO, HOMO –1, and etc.) to the lowest unoccupied molecular orbitals (LUMO, LUMO+1, and etc.), where the lowest HOMO to LUMO transition is designated as electronic the $\pi \rightarrow \pi^*$ transition. Hence, upon absorption of a photon, an electron is excited from the HOMO to LUMO level of the organic semiconductor, still being bound to the formed hole via strong Coulombic attraction force. This way formed, the bound electron-hole pair is referred as exciton, with binding energy in organic semiconductors even up to 1.4 eV,¹⁰³ (for different conjugated polymers it has been reported in the range from a few tens of meV to 1 eV).²¹⁶⁻²²⁰ The energy difference between the optical gap and the band gap (electronic or transport gap) of the considered polymer is regarded as the value of the electron-hole pair binding energy, i.e. the exciton binding energy (ϵ_b).²²¹⁻²²² While the HOMO position of the polymer thin films is accurately accessible via ultraviolet photoemission spectroscopy (more precisely N–1 final state),³⁰ the direct measurement of the LUMO position of polymers (more precisely N+1 final state) is not possible in our laboratory. Here, with N is represented N-electron ground state of the molecule, while with $N \pm 1$ is described electron ionized state of

that molecule. Therefore, the UV-Vis-NIR absorption measurements of four semiconductive LBG polymers were performed in order to be able to estimate LUMO positions of these polymers. Both the HOMO and LUMO level positions are equally important in order to correctly predict the energy level alignment at the functional interface in electronic devices.

In Figure 5.1 the UV-Vis-NIR absorption spectra of the thin films of four LBG polymers are shown. The thickness of produced films is expected to be in the range reported in Section 4.3.1. Generally, in the UV-Vis-NIR absorption spectrum of D-A polymer, an alternation of subunits in the backbone rises two bands (spectral features). The one with lower energy which extends to NIR region of the spectrum belongs to internal charge transfer transition between subunits, while high energy band represents π - π^* transition. First, what can be noticed in Figure 5.1 is that absorption spectra of PCPDTBBT and PCPDTTBTT films are widened towards the NIR region (higher wavelength/lower energy) due to a presence of the stronger electron withdrawing subunit (BBT),²²³ bringing the half smaller value of E_g^{opt} for these in comparison to PCPDTBT and PCPDTTBTT, respectively. The optical band gap values are determined from the onset of an absorption peak in the spectrum. In the case of PCPDTBT and PCPDTTBTT, E_g^{opt} is 1.44 and 1.58 eV, respectively, while, for PCPDTBBT and PCPDTTBTT it is 0.69 and 0.78 eV, respectively. This substantial decrease of E_g^{opt} for the “polymer pair” possessing stronger electron accepting (BBT) subunit, could also mean that the band gap of this pair is also substantially lower than in the case of PCPDTBT and PCPDTTBTT pair.

It might be expected that a presence of BBT subunit in the polymer structure, more effectively reduces bond-length alternation and the HOMO-LUMO (π - π^*) energy separation, hence, the width of the band gap.²²⁴ On the other hand, it is observed that the introduction of thiophene (hexylthiophene) spacer rings into the structure of PCPDTBT (PCPDTBBT), only slightly increases E_g^{opt} of the newly formed polymer structure PCPDTTBTT (PCPDTTBTT). This might be a sign that the introduction of thiophene (hexylthiophene) rings does not have such a

strong effect on the electronic structure of polymers as the presence of different acceptor subunit.

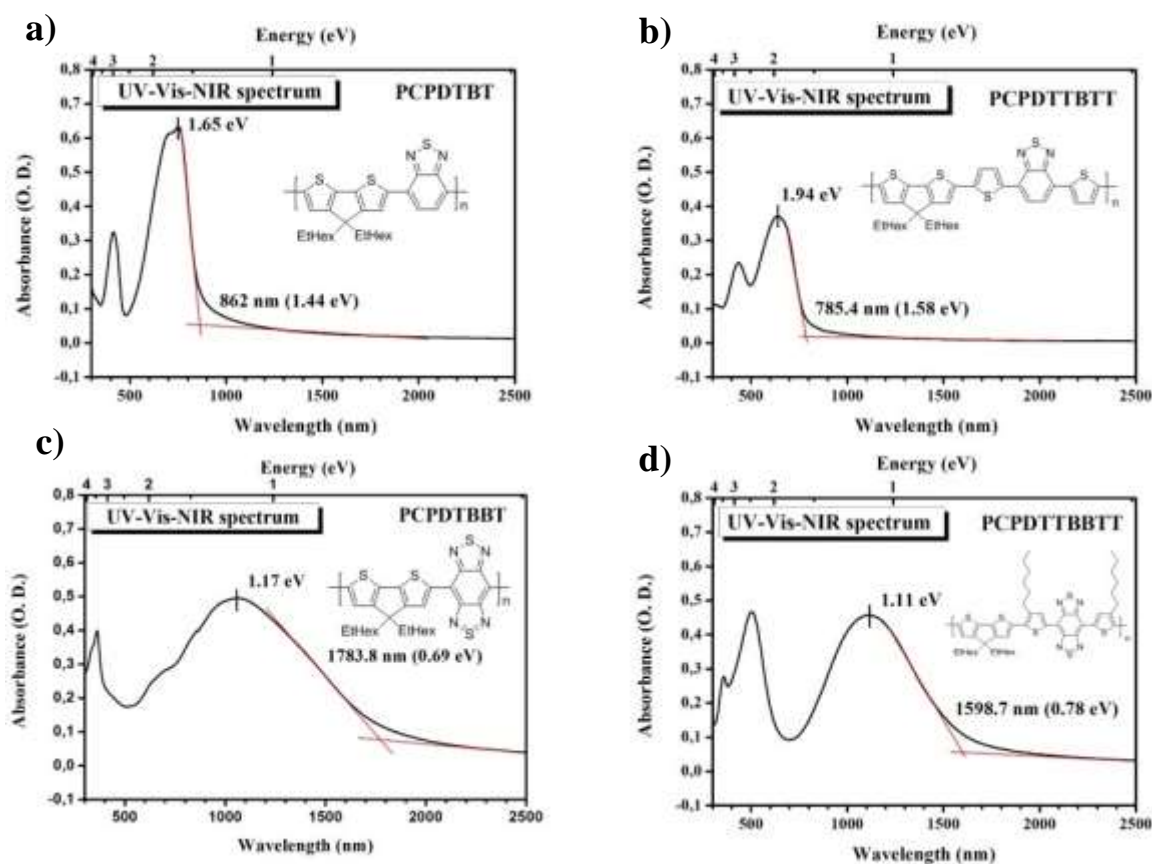


Figure 5.1: UV-Vis-NIR absorption spectra of (a) PCPDTBT (b) PCPDTTBTT (c) PCPDTBBT and (d) PCPDTTBTT. Onset of the absorption is presented on figures by intersection of red lines, with also designated maximum of absorption.

In Table 5.1 are listed values of E_g^{opt} obtained for four studied polymers.

Table 5.1: Obtained values of the optical band gap for four studied polymers.

Polymer	Optical band gap (E_g^{opt})
PCPDTBT	1.44 eV
PCPDTTBTT	1.58 eV
PCPDTBBT	0.69 eV
PCPDTTBTT	0.78 eV

The UV-Vis-NIR spectroscopy measurements presented in this work were performed in the transmission mode using Lambda 9/19 spectrophotometer (Perkin-Elmer). The apparatus possesses double monochromator. The wavelength range of the spectrophotometer is from 185

nm to 3200 nm. The step is settable to 0.1 nm, and spectral bandpass might be varied from 0.05 to 5 nm in the UV/vis and 0.2 to 20 nm in NIR range. The scan speed can be varied from 0.9 to 960 nm per min. The absorbance accuracy can be measured with $\pm 0.003\%$.

5.1.2. PES study of interfaces between thin films of LBG polymers and different electrodes

Chemical substitutions significantly affect the electronic structure of organic molecules; an impressive example is fluorination which results in a distinct increase of the ionization potential.²²⁵⁻²²⁶ Therefore, we study first, how the introduction of additional (hexyl)thiophene moieties affects the electronic structure of the polymers and their interfaces. In general, it was demonstrated for organic semiconductors that the energy level alignment (ELA) at interfaces does not necessarily follow the vacuum level alignment (VLA) regime. Rather, as previously mentioned, depending on electronic parameters of the organic thin film and substrate, the formation of an interface dipole (Δ) is observed, which is the outcome of the charge transfer across the interface.^{53, 227} Additionally it should be noted, that both the morphology and the molecular orientation may have a distinct impact on the interface electronic properties of organic semiconductors.^{74, 228}

In Section 2.2. models for the interpretation of weakly interacting interfaces formed by organic semiconductors were proposed. One of the proposed models is the Integer Charge Transfer (ICT) model,^{53, 73, 79} which is found to be the most appropriate for description and interpretation of interfaces formed via blade casting of polymer thin films onto substrates which are expected to possess nonreactive (due to preparation conditions) surfaces. In this model, depending on the relative position of the work function of the substrate (Φ_{sub}), pinning of the Fermi level at the

so-called ICT⁺ or ICT⁻ levels (states) of the organic semiconductor may happen, i.e. charge transfer across the interface occurs until thermodynamic equilibrium is reached. In order to gain more information about the energetic position of these pinning levels, we study by UPS, the ELA of four LBG polymers PCPDTBT, PCPDTBBT, PCPDTTBTT and PCPDTTBTT on substrates with a wide span of the work function values (PEI/ITO = 3.3, ZnO = 3.5 eV, ITO = 3.8, AuO_x/Au = 5.0 eV and PEDOT:PSS = 5.2 eV). In Figure 5.2 (a-e), the corresponding UPS spectra of later polymers and substrates are shown, zooming into the region of the secondary electron cutoff (SECO, left window) and the highest occupied molecular orbital (HOMO, right window). Values of the measured $\Phi_{\text{poly/sub}}$ and position of the HOMO onset ($E_{\text{b}}(\text{HOMO})$) are summarized in Table 5.2, together with the ionization potential $\text{IP} = E_{\text{b}}(\text{HOMO}) + \Phi_{\text{poly/sub}}$. It is interesting to notice here, that the appearance of the VB region (strictly, bands derived from dispersive states in crystals or periodic structures) spectra of four LBG polymers somehow reminds to the one of P3HT. In the case of valence band spectrum of P3HT (spectrum is shown in Appendix 1), an extended spectral feature with lower binding energy is subscribed to delocalized frontier π -states, while more pronounced peak on the higher binding energy side is expected to stem from localized π -states,²²⁹⁻²³¹ which is reminiscent to what can be nicely seen for (for example) PCPDTBT on ITO. The reason could be, that for four LBG copolymers the valence band, hence, the VB spectral features have the major contribution from thiophene subunits.²³² Nevertheless, the level of contribution of BT or BBT subunits to the VB spectral features of polymers cannot be realized without further theoretical and experimental studies. Importantly, it is clearly visible that the introduction of additional (hexyl)thiophene moieties only slightly changes the IP (averaged for all substrates) for the “polymer pairs” PCPDTBBT & PCPDTTBTT and PCPDTBT & PCPDTTBTT within the error bars of ± 0.1 eV, what can be seen in Table 5.2.

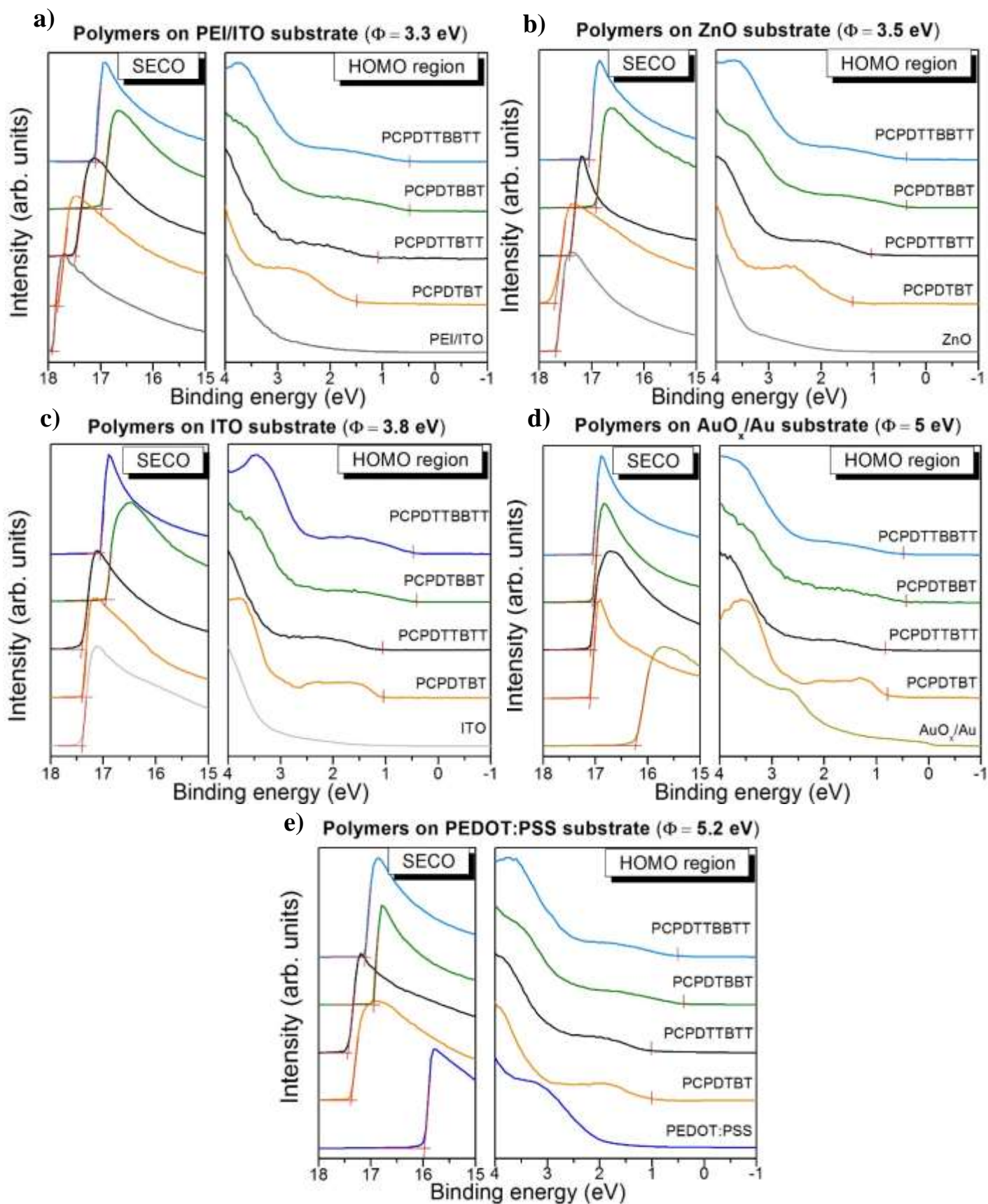


Figure 5.2: UPS spectra of studied LBG polymers (PCPDTBT, PCPDTTBTT, PCPDTBBT and PCPDTTBBTT) deposited on four different substrates with a wide range of work function a) PEI/ITO, $\Phi_{\text{sub}}=3.3$ eV, b) ZnO, $\Phi_{\text{sub}}=3.5$ eV, c) PEI/ITO, $\Phi_{\text{sub}}=3.8$ eV, d) AuO_x/Au , $\Phi_{\text{sub}}=5.0$ eV and e) PEDOT:PSS, $\Phi_{\text{sub}}=5.2$ eV. Where SECO and HOMO onsets are designated with red lines.

Also, we could see in previous section that the increase of the optical gap (E_g^{opt}) is very small (0.09 eV from PCPDTBBT to PCPDTTBTT and 0.14 eV from PCPDTBT to PCPDTTBTT) with the introduction of additional (hexyl)thiophene moieties. An increase of E_g^{opt} upon the introduction of thiophene moieties might be expected due to the enlargement of the electron donating subunits of the LBG polymer, nevertheless, the size of this effect is rather small as mentioned.

Table 5.2: Collected electronic structure parameters of the LBG polymers PCPDTBT, PCPDTTBTT, PCPDTBBT and PCPDTTBTT on five different substrates, as obtained from UPS spectra.

Polymer	IP (eV)	Work function on substrate (eV) ($E_b(\text{HOMO})$ and Δ_h on substrate (eV))				
		PEI/ITO	ZnO	ITO	AuO _x /Au	PEDOT:PSS
PCPDTBT	4.8-4.9	3.4 (1.5)	3.5 (1.4)	3.8 (1.0)	4.1 (0.8)	3.8 (1.0)
PCPDTTBTT	4.8-4.9	3.7 (1.1)	3.8 (1.1)	3.8 (1.0)	4.1 (0.8)	3.8 (1.0)
PCPDTBBT	4.6	4.2 (0.4)	4.3 (0.3)	4.3 (0.3)	4.2 (0.4)	4.2 (0.4)
PCPDTTBTT	4.6	4.1 (0.5)	4.2 (0.4)	4.2 (0.4)	4.1 (0.5)	4.1 (0.5)

Note that the IP cannot be generally regarded as a material constant, because, variations due to charge transfer, molecular orientation, and the morphology have been observed.²³³⁻²³⁵ Nevertheless, the ionization potential of the polymer thin film, as an inherently “disordered” system, is not so prone to changes induced by the change in molecular orientation on different substrates (different interaction with the substrate), as in the case of thin films of small molecules.^{74, 235-236} This may explain the slight substrate-dependent variations in the sum IP ($E_{\text{HOMO}} = E_b(\text{HOMO}) + \Phi_{\text{poly/sub}}$ (cf. Table 5.2), observed in this work. Thus, observed energy level alignment on the different substrates is very similar within two “polymer pairs” PCPDTBBT & PCPDTTBTT and PCPDTBT & PCPDTTBTT, but as we will see, highly different between them. The corresponding energy level diagrams are shown in Figure 5.3. For the low work function substrates PEI/ITO and ZnO (with $\Phi_{\text{sub}} = 3.3$ eV and 3.5 eV,

respectively), pinning is expected if the ICT- level exceeds the work function of the substrate. In many cases the ICT- level (i.e. the fully relaxed negative polaron level) is found 0.3-0.6 eV below the LUMO level referenced to the vacuum level (also labeled, E_{LUMO} or electron affinity-EA), where EA is determined from inverse photoemission.^{72, 237-238} Due to lack of inverse photoemission data for the studied polymers, we use for a rough estimation of the upper limit of the LUMO position, the optical gap according to $E_{\text{LUMO}} = \text{IP} - E_{\text{g}}^{\text{opt}}$. The difference between EA and ICT- level might partly compensate the neglect of excitonic effects (for instance, exciton binding energy $\epsilon_{\text{b}} = 0.5$ eV for P3HT²⁶¹) in the estimation presented above. We arrive now, for PCPDTBT and PCPDTTBTT at the LUMO level position of about 3.46 eV and 3.22 eV below the vacuum level, respectively, i.e. values in the range of the substrate work function of PEI/ITO and ZnO, and thus a charge transfer is not necessarily expected. Indeed, in the case of the PCPDTBT thin film, no or minor interface dipole of 0.1 eV are observed on PEI/ITO and ZnO, respectively, from which we cannot unambiguously conclude that the system is in the pinning regime. Nonetheless, in the case of thin films of PCPDTTBTT polymer on PEI/ITO and ZnO substrates, interface dipoles of 0.4 and 0.3 eV are found, respectively, and the pinning position is found at 3.7-3.8 eV below E_{VL} , which might be regarded as the ICT- level of the polymer. The FLP has been more expected in the case of PCPDTBT than for PCPDTTBTT, due to narrower $E_{\text{g}}^{\text{opt}}$ of the former, hence, expected narrower E_{g} , higher EA, and potentially higher mismatch between the substrate Fermi level and potential polymer ICT- level. Nevertheless, to remind once again that rather simplified method to estimate LUMO position was used. Thus, in the case of PCPDTTBTT, it might be that the Fermi level of PEI/ITO is not above the LUMO position of the polymer, but in between the LUMO and ICT- level, still fulfilling conditions for spontaneous electron transfer from the substrate into the organic film at the interface.⁵³

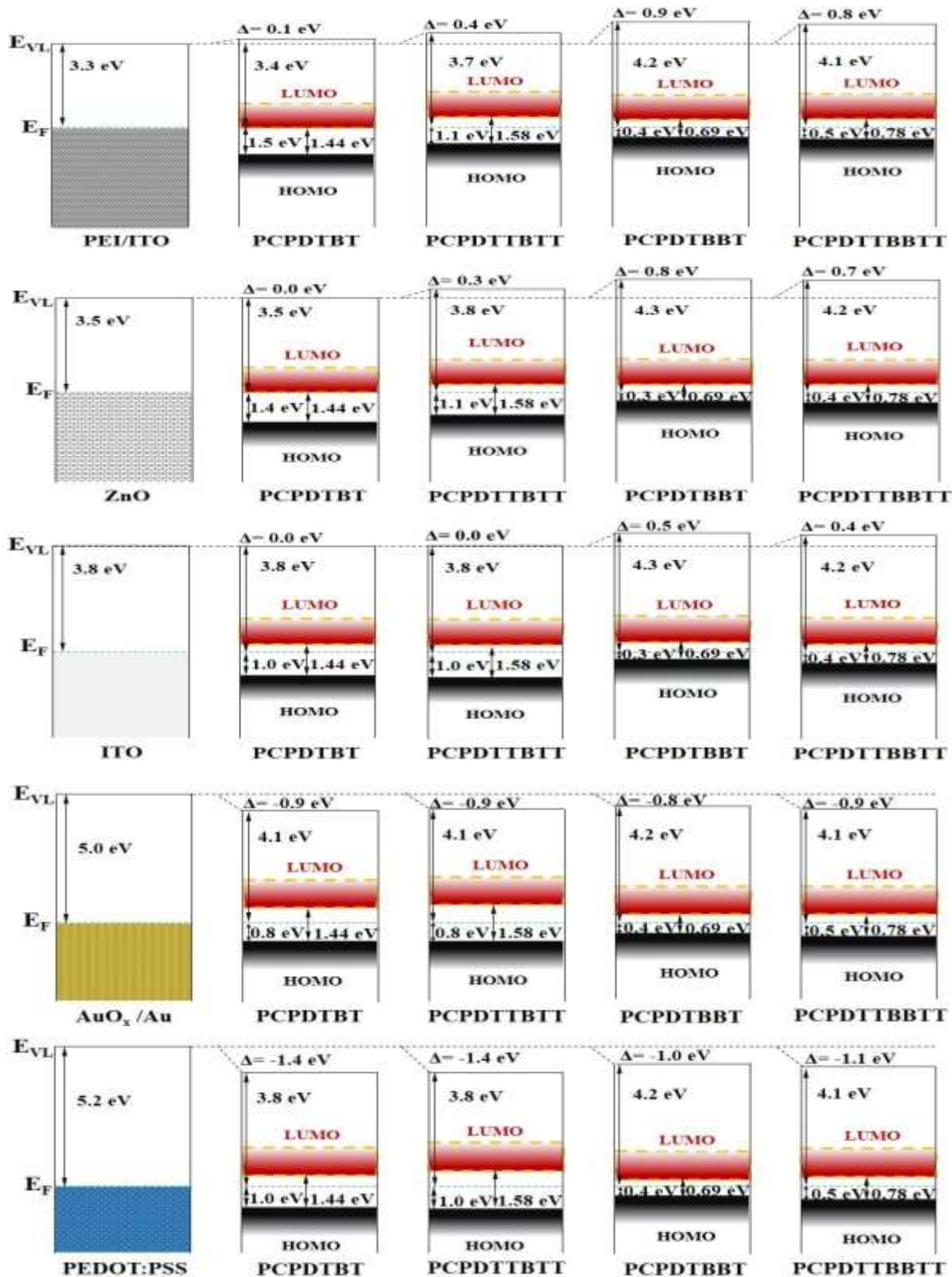


Figure 5.3: Energy level diagrams of LBG polymers PCPDTBT, PCPDTTBTT, PCPDTBBT and PCPDTTBTT on five different substrates with a wide range of work function a) PEI/ITO, $\Phi_{sub} = 3.3$ eV b) ZnO, $\Phi_{sub} = 3.5$ eV, c) ITO, $\Phi_{sub} = 3.8$ eV, d) AuO_x/Au, $\Phi_{sub} = 5.0$ eV and e) PEDOT:PSS, $\Phi_{sub} = 5.2$ eV as obtained from the UPS measurements. The LUMO levels in the figure are approximated from optical band gaps of polymers.

Further, for the pair PCPDTBBT & PCPDTTBBT the LUMO position (we calculate E_{LUMO} (EA) at ~ 3.91 eV for PCPDTBBT, whilst at around 3.82 eV for PCPDTTBBT) is significantly lowered due to the smaller band gap and consequently, we observe distinct interface dipoles for these polymers of around 0.9 and 0.8 eV, respectively, on PEI/ITO and ZnO substrates. We expect that the condition $\Phi_{sub} < E_{ICT-}$ is fulfilled at interfaces of the BBT polymers prepared onto PEI/ITO and ZnO substrates. The values of $\Phi_{poly/sub}$ found for PCPDTBBT and PCPDTTBBT are 4.2-4.3 and 4.1-4.2 eV, respectively, and they might be assigned to the pinning positions (negative polaron levels) of these polymers. We note that values obtained for $\Phi_{poly/sub}$ and Δ are very similar for the pair PCPDTBBT and PCPDTTBBT.

In order to study the electronic structure relevant for four LBG copolymers as potential donor materials for OPVs, substrates with the higher work function value are subsequently used. Hence, the chemically cleaned ITO film on glass, with the work function of 3.8 eV, was the next used substrate. As can be seen in Figure 5.2, after deposition of the thin films of PCPDTBT and PCPDTTBT polymers, no change in the SECO value can be observed. This finding implies that upon deposition, no change in the value of the work function happens ($\Phi_{sub} = \Phi_{poly/sub}$), and interface dipole equals zero. Hence, the vacuum level alignment has occurred, due to the lack of charge transfer across the interfaces. Here, according to ICT model, the condition $E_{ICT+} > \Phi_{sub} > E_{ICT-}$ is fulfilled. On the other hand, after deposition of the second “polymer pair” PCPDTBBT and PCPDTTBBT, significant Δ values of 0.5 and 0.4 eV, respectively, are found. The $\Phi_{poly/sub}$ value found for PCPDTBBT film was 4.3 eV, whilst for PCPDTTBBT was 4.2 eV. Hence, the Fermi level pinning scenario occurred, with pinning positions very similar to what was found for these films prepared on ZnO and PEI/ITO.

Since the investigated polymers are potential materials for the donor component in solar cells, in particular, the position of the positively charged ICT+ level is important. For the high work function substrates AuO_x/Au and PEDOT:PSS (with Φ_{sub} of 5.0 and 5.2 eV), pinning at the

ICT⁺ level is expected since according to obtained results stands $\Phi_{\text{sub}} > \text{IP}$ for all polymers, thus also $\Phi_{\text{sub}} > E_{\text{ICT}^+}$ is expected. Indeed, the change of work function upon polymer deposition (effective work function $\Phi_{\text{poly/sub}}$) is observed, indicating the formation of an interface dipole Δ which corresponds to the difference $\Phi_{\text{sub}} - \Phi_{\text{poly/sub}}$. Most importantly, within both “polymer pairs” (PCPDTBT & PCPDTTBTT and PCPDTBBT & PCPDTTBTT), values for $\Phi_{\text{poly/sub}}$ and Δ are almost the same within the error bar of about ± 0.1 eV for a particular substrate (see also Table 5.2) suggesting that the position of the pinning levels is practically unaffected by the introduction of (hexyl)thiophene spacer rings. Nevertheless, for the polymer pair PCPDTBT and PCPDTTBTT, $\Phi_{\text{poly/sub}}$ of thin films prepared on AuO_x/Au has a higher value (in both cases 4.1 eV) in comparison to films prepared on PEDOT:PSS (c.f. Table 5.2) (in both cases 3.8 eV), while being expected to have the same/very similar values. This difference in the ELA outcome may be due to particular interaction (n-doping) at the respective interfaces with organic substrate PEDOT:PSS. It has been shown that at the very top of PEDOT:PSS films, a non-negligible amount of Na is present not only in the form of PSS-Na.²³⁹ In this work, sodium is also found to be present at the surface of PEDOT:PSS film. After blade casting of polymer films, might happened that due to the formation of an interlayer, close contact between materials is achieved and the reaction of electron transfer from Na to polymer overlayers occurred. As a result of n-type of doping at the interfaces, the HOMO and core levels which belong to polymer films are shifted towards higher binding energy for about same number of eV, as shown in Figure 5.4a, having in mind that the distance core level to HOMO should be constant in a first approximation. Nevertheless, the energy level alignment with the polymer PEDOT:PSS electrode, which is expected to be driven by the VB derived states of PCPDTBT and PCPDTTBTT, seems not affected by the difference in their chemical structure. Hence, the relevant electronic structure parameter at the interface with PEDOT:PSS, such as hole injection barrier, is found to be the same for PCPDTBT and PCPDTTBTT. The value found for the pinning

position close to the HOMO level of PCPDTBT polymer on AuO_x/Au (ICT+ level of 4.1 eV) is somewhat lower compared to the reported ICT+ level of spin-coated PCPDTBT (4.37 eV),⁷³ which could be due to the different preparation procedure.

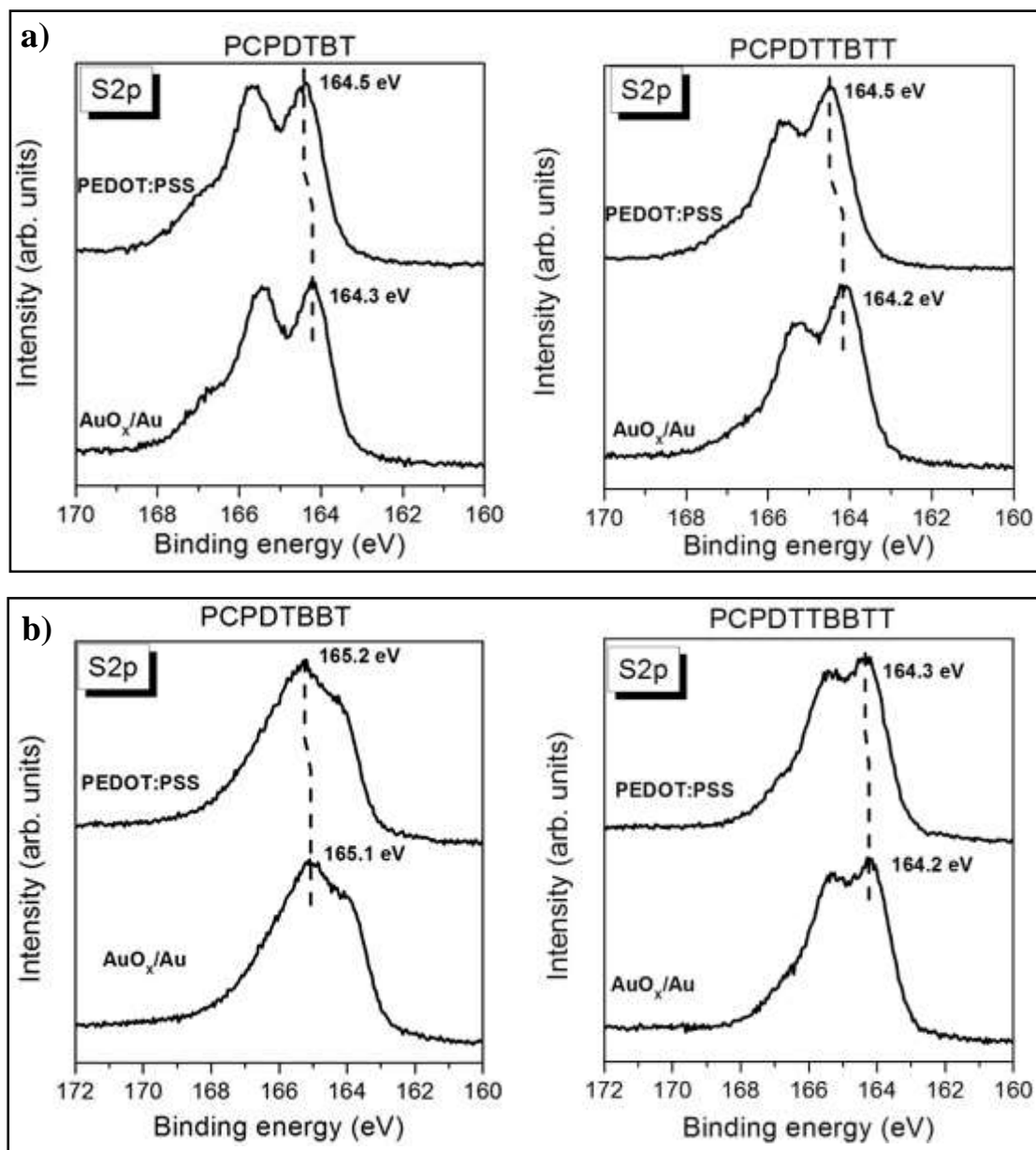


Figure 5.4: The XPS S2p signals of (a) PCPDTBT and PCPDTTBTT, and (b) PCPDTBBT and PCPDTTBTT polymer films deposited on AuO_x/Au and PEDOT:PSS substrates.

On the other hand, interestingly, in Figure 5.4b is presented that S2p signals of PCPDTBBT and PCPDTTBTT films on AuO_x/Au and PEDOT:PSS substrates do not show the difference in the binding energy position in magnitude observed for BT carrying polymers on the same

substrates. This finding is very interesting, considering that electron affinity is anticipated to have higher values for the BBT polymer pair, hence, n-doping might be expected to have a more pronounced effect than in the case of BT polymers. Still, the effect of n-doping, in particular, might depend on an electronic structure of the LUMO level of the molecule. It has been noticed that for the p-doping of conjugated polymers, the same amount of the same dopant has a different influence on the ELA pictures for different polymers.^{27,32} Also, it has been observed that p-doping of conjugated copolymers with the same/similar electron donating group has a similar effect on electronic structure, i.e. the formation of the HOMO derived states.³³ Thus, in view of aforementioned things, and expected very small band gap of BBT polymers, the effect of n-doping is less observable in the case of BBT polymers than for the BT counterpart polymers where E_g is expected to be wider. It should be mentioned here, that in XPS spectra of all studied polymers, there is no evidence of signals which stem from the products of a strong chemical reaction (chemisorption, hence, the covalent bond formation) at presented polymer/substrate interfaces. Thus, physisorption like interactions are regarded to be prevalent at studied interfaces, and responsible for observed ELA at them.

As a brief conclusion, electronic structure parameters IP (HOMO level and derived states) and E_g^{opt} , and the energy level alignment at interfaces are very similar within each “polymer pair”, suggesting that the introduction of additional (hexyl)thiophene moieties has only minor effect on these electronic parameters of polymers relevant for the application in OPVs.

5.1.3. Summary of Section 5.1.

At the very beginning of this section, information collected by UV-Vis-NIR absorption spectroscopy done on polymer thin films were presented. Afterwards, UPS and XPS data of

four LBG polymers doctor-blade cast on five different substrates with a wide span of the work function (Φ_{sub}), were considered. Polymers were selected in two groups, according to the electron-withdrawing moiety in the structure of the monomer unit. The first polymer pair consists of PCPDTBT and PCPDTTBTT, while PCPDTBBT and PCPDTTBBTT polymers represent the second pair. In Section 5.1.1. could be seen that BBT subunit holding polymers have about twice smaller optical band gap in comparison to their BT carrying counterparts. The E_g^{opt} values found for PCPDTBT and PCPDTTBTT are 1.44 and 1.58 eV, whilst for the second pair PCPDTBBT and PCPDTTBBTT are 0.69 and 0.78 eV, respectively. From this finding, two things can be clearly comprehended. First one is that the presence of stronger electron accepting subunit benzobisthiadiazole (BBT) in the structure of PCPDTBBT and PCPDTTBBTT narrows their optical band gaps in comparison to similar polymer systems PCPDTBT and PCPDTTBTT, as a result of the extended conjugation length along the backbone of the BBT polymers. Lower E_g^{opt} values of PCPDTBBT and PCPDTTBBTT polymers were also commented as a sign of expected lower (electronic) band gaps for this polymer pair in comparison to benzothiadiazole (BT) subunit carrying polymers. The second thing is that the insertion of additional thiophene (hexylthiophene) rings into the structure of PCPDTBT (PCPDTBBT), which leads to derived structure PCPDTTBTT (PCPDTTBBTT), only slightly increases the optical band gap of the new polymer. Nevertheless, extended UPS measurements of thin films of four LBG polymers showed that last discussed change in the chemical structure within the polymer pair, has no influence on their E_{HOMO} , i.e. ionization potential measured for both PCPDTBT and PCPDTTBTT was 4.8-4.9 eV, whereas for PCPDTBBT and PCPDTTBBTT was about 4.6 eV, for all used substrates. This might be supported by Density functional theory (DFT) calculations, which suggest that the electron accepting subunit in donor-acceptor copolymers has a generally greater influence on the position (energy) of the LUMO level, whilst the HOMO level is delocalized along the polymer backbone.^{232, 240} Thus,

very generally might be said that in a D-A polymer the LUMO level is determined by the LUMO of the electron accepting subunit, whilst the HOMO level mostly resembles in value to the HOMO of the electron donor moiety, altogether leading to lower band gap. Furthermore, in this section it could be seen, that the energy level alignment pictures obtained for the prepared interfaces show a high dependency on the electronic structure of the considered polymer and substrate. In general, a deviation from the Schottky-Mott limit (vacuum level alignment), formerly considered as a prevalent ELA for this kind of weakly interacting interfaces, was observed. The polymer/electrode interfaces within one polymer pair showed similar ELA outcomes, while in between pairs distinctively different. For the BBT polymer pair, where the band gap is expected to be smaller compared to BT moiety-holding polymer pair, the work function of polymer/substrate stack ($\Phi_{\text{org/sub}}$) shows almost constant value (within range of ± 0.1 eV) independent of the work function of the substrate beneath (Φ_{sub}). On the other side, values of $\Phi_{\text{org/sub}}$ show greater dispersion in the case of PCPDTBT and PCPDTTBT thin films, with a clear dependence on the underlying substrate work function value. How the work function $\Phi_{\text{org/sub}}$, of the four LBG polymers changes with the underlying substrate's work functions Φ_{sub} , can be seen in Figure 5.5 where characteristic, "Z-like" dependence plots are presented. On the left-hand side, the plot for the BT polymer pair can be seen. In the black symbols drawn, we notice that obtained points for PCPDTBT follow the line of slope = 1 dependence expected for the vacuum level alignment with three substrates with the lowest Φ_{sub} , while they deviate from this trend for two substrates with higher work functions, where the slope is expected to be zero. For the polymer film prepared on AuO_x/Au substrate, it was found that $\Phi_{\text{org/sub}}$ does not scale linearly with the substrate work function and that the Fermi level is pinned at 4.1 eV, what was regarded to be the ICT+ (positive polaron) level of PCPDTBT. Thus, according to the ICT model, for $\Phi_{\text{sub}} > 4.1$ eV, we expect FLP regime at the ICT+ level in PCPDTBT film due to electron transfer at the interface from the polymer to the substrate.

We could not assess the ICT- (negative polaron) level of PCPDTBT film due to a limited range of the work function of used substrates, and it is expected to be lower than 3.3 eV. In the case of PCPDTTBTT polymer film, as we can see, the effective work function $\Phi_{\text{org/sub}}$ shows independent behaviour from Φ_{sub} for the substrates with the lowest work function values, PEI/ITO and ZnO. The Fermi level pinning was observed at 3.7-3.8 eV which was perceived as the ICT- level of the polymer, and electron transfer from the substrate to the polymer film at the interface was expected. For the same polymer film, deviation from the slope = 1 is also expected for Φ_{sub} higher than 4.1 eV, as it was the case with PCPDTBT. The Fermi level pinning regime is established, and E_F is pinned at 4.1 eV below the vacuum level (0.7 eV above HOMO), what can be regarded as an ICT+ level of the polymer. The vacuum level alignment at the interface of PCPDTTBTT was only observed for the thin film prepared on ITO with $\Phi_{\text{sub}} = 3.8$ eV, which is similar/same to values found to be negative polaron level of the polymer. This might imply that for the thin film of PCPDTTBTT, VLA can be merely accomplished on substrates with the work function in the range of 3.8 - 4.1 eV, which is interestingly a small range of values. In Figure 5.5a can be seen that the data point for the effective work function of both polymers on the PEDOT:PSS substrate stands 3.8 eV (marked with a red circle). This divergence from the expected value of 4.1 eV, (the ICT+ level of BT-holding polymer pair), was explained by possible n-doping, occurred due to the specificity of interaction with PEDOT:PSS.²⁴¹ At that point remark was made, that ELA with high work function substrates (anodes) which is important from the point of polymers application, is not substantially changed for the thin films of PCPDTBT and PCPDTTBTT, regardless of the difference in chemical structure.

The “Z” dependence plot for the thin films of the second polymer pair PCPDTBBT and PCPDTTBTT, is presented in Figure 5.5b. First thing, which can be immediately noticed for both polymers, is that $\Phi_{\text{org/sub}}$ shows independent behaviour on Φ_{sub} in the whole range of used

substrates (work function values), i.e. the VLA was not observed for all prepared interfaces of these two polymers.

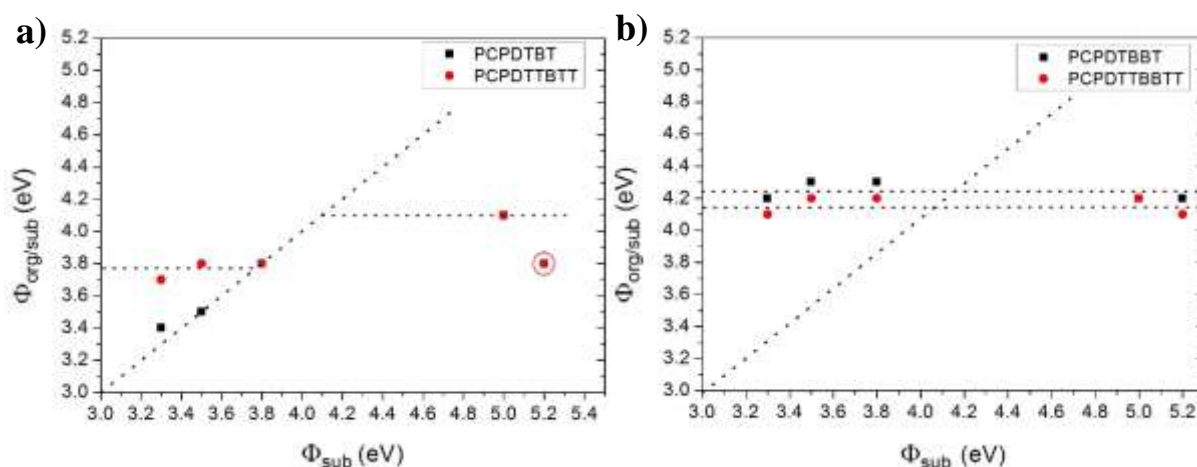


Figure 5.5: Work functions of (a) BT polymer pair and (b) BBT polymer pair thin films prepared on different substrates, displayed as a function of substrate work function.

The FLP regime was established at all interfaces of thin films of BBT polymer pair onto five different substrates with the 1.9 eV span of the work function. Values of the effective work function found for all substrates, in the case of PCPDTBBT is in the range 4.2-4.3 eV, whereas for the thin film of PCPDTTBBTT is 4.1-4.2 eV. For both polymer thin films, E_F was always measured around the midgap position, where LUMO levels were estimated using optical absorption measurements. Thus, for two substrates with the lowest Φ_{sub} , PEI/ITO and ZnO, which work functions are expected to be smaller than LUMO level positions of BBT polymers, FLP was established with the integer electron (hole) charge transfer towards polymer thin films (substrates). The same ELA scenario with the same direction of charge transfer was observed for thin films prepared on ITO, where condition $E_{ICT-} > \Phi_{sub}$ is also expected to be fulfilled. On the other hand, for substrates AuO_x/Au and PEDOT:PSS which work functions were measured to be greater than IP of polymers (automatically $\Phi_{sub} > E_{ICT+}$ realized), interface dipole and charge transfer of opposite direction were found. In the case of thin films of BBT polymers on PEDOT:PSS substrate, substantial shift of the valence band and core level signals towards

higher binding energies was not observed, as it was the case with BT polymer pair. This is understood as a consequence of the electronic and chemical characteristics of BBT polymers.

Finally, based on the ultralow band gaps perceived for the BBT polymers, and Δ_h independent from the substrate work function observed at interfaces of these materials, it would be especially interesting to prepare and study OPV devices utilizing the BBT polymers as donor materials.

5.2. PES study of organic donor/acceptor interfaces for OPV devices

Among OPVs, devices based on bulk heterojunction (BHJ) active layer, where donor and acceptor materials are mixed into a three-dimensional interpenetrating network, have shown promising and constantly improving work efficiency.¹⁰⁵ Since the concept of the organic heterojunction structure for organic solar cells was presented for the first time in 1986 by Tang,¹⁷² the donor/acceptor interface and its properties, are under the permanent scrutiny of researchers working in the field of OPVs. Generally, it can be said that if no significant interfacial chemistry occurs at the organic/organic interface, which is expected not to be the case in this work according to properties of used materials, the interaction between materials is regarded as a rather physisorptive. Hence, the physisorption is expected to control the charge exchange between materials at the junction and determine ELA with all interfacial electronic structure parameters. However, the presumption of the ELA at the organic/organic interface, based on the knowledge of energy positions of frontier orbitals of the donor and acceptor materials individually, and taking into account the common vacuum level, could be highly misleading. Verily, the vast amount of reported data, show that the upward and downward

vacuum shifts at the organic/organic interface, in the magnitude of tens of meV frequently occur.^{165, 290-291} Moreover, it has been reported, that the electrode (substrate) work function has a great influence on ELA throughout whole multilayer stack of an OPV device, hence, on the donor/acceptor interface as well.²⁹²⁻²⁹⁵ The energy level alignment at the acceptor/donor interface has a huge impact on different processes within the solar cell, among which, the efficiency of separation of the light generated charges and their transfer towards electrodes, are of the pivotal importance. Hence, the electronic configuration of the all-organic donor/acceptor interface determines the energy distances between HOMO and LUMO levels of donor and acceptor materials, called HOMO (ΔH) and LUMO (ΔL) offsets, respectively. These should be optimized in the solar cell in order to get effective charge separation at the interface.²¹⁹ An important parameter, also defined by the donor/acceptor interface is the energy distance between the HOMO level of donor and LUMO level of acceptor material, called the photovoltaic gap (Δ_{DA}). The size of the photovoltaic gap presents the potential upper limit of the open circuit voltage (V_{OC}),⁸⁴ i.e. the maximum voltage that solar cell can provide to an external circuit under open circuit conditions. Nonetheless, it has been demonstrated that the open circuit voltage is not fully independent on the work functions of the electrodes.¹⁸⁴⁻¹⁸⁵ Thus, a simple increase in the energy distance between the HOMO of donor and the LUMO of acceptor, does not necessarily lead to the higher open circuit voltage due to different obstacles. In the fabrication of polymer-based solar cells, one of the concepts is to use a conjugated polymer (as the donor material) with the low band gap to maximize the absorption of the solar radiation in the visible and near-infrared regions and to optimize energy distance between relevant frontier orbitals. Also, the higher photon absorption leads to an increased number of photogenerated charge carriers, which is reflected in a higher photocurrent. In the previous section, we could see that the introduction of additional (hexyl)thiophene rings only slightly affects the energy level alignment at interfaces with used substrates, in comparison to the presence of different

electron withdrawing subunit. Hence, it would be highly interesting to check, implications of these differences in the chemical structure of polymer pairs on ELA at the donor/acceptor interface. Moreover, the performance of solar cells based on polymer:fullerene BHJ depend heavily on the electronic interaction of the polymer and fullerene molecular species from which the BHJ is composed. The intermolecular interaction between the constituent polymer and fullerene species tends to be optimized in an efficient OPVs, as evidenced by efficient charge transfer processes and by large changes in the energetics of the polymer and fullerene when they are mixed on the molecular level. Since the bulk heterojunction is generally represented by the mixture of donor and acceptor materials, its interfacial electronic structure properties are not easily characterized, using established surface analysis methods such as UPS, due to potential overlapping/mixing of signals originating in different materials.

Hence, in this work, we first tried to model this donor-acceptor interaction in BHJ via deposition of the thin films of fullerene C_{60} onto the thin films of PCPDTTBTT and PCPDTBBT. The thickness of C_{60} thin can be easily tuned via deposition time and rate, and interaction at an interface can be closely monitored. Then, obtained/collected observations about ELA, electronic structure parameters and interaction at these planar heterojunctions are compared with the data collected in the study of BHJ prepared from PCPDTBT and PCBM materials.

5.2.1. Acceptor/electrode interface

Fullerene C_{60} /electrode interfaces

Before considering closely donor/acceptor interfaces, we should be familiar with the electronic structure of the constituent materials. In the previous section we investigated the electronic structure of four LBG polymers, hence, here we briefly show the study of the electronic

structure of two state of the art acceptor materials, C₆₀ and its derivative PCBM. Obtained results are compared with the literature, where the plethora of data about the latter two molecules exists.

Firstly, the photoemission data of fullerene C₆₀ thin films prepared on three different substrates, with progressively increasing work function: PEI/ITO = 3.3 eV, ITO = 4.0 eV and AuO_x/Au = 5.0 eV, are presented. Thin films of fullerene C₆₀ on all substrates were prepared via molecular beam deposition, using quartz microbalance to assess the nominal thickness of the obtained films. Nominal thicknesses of the deposited films were: 3 nm, 2 nm and 2 nm, following the order of the above-listed substrates. The UPS spectra of fullerene C₆₀ overlayer thin films (plotted in black) on PEI/ITO, ITO, and AuO_x/Au substrates (plotted in gray), are shown in Figure 5.6. From the SECO region spectra presented on the left-side panel of the last figure, it can be seen that the SECO substantially moves towards lower binding energy for the C₆₀ film on PEI/ITO, much less for C₆₀ on ITO, while for the fullerene film on AuO_x/Au only a minor change in SECO position can be observed. On the right panel, where the valence band region is presented, we can see spectra of the vacuum deposited C₆₀ thin film. The spectrum is dominated by two peaks, denoted as HOMO-1 (higher E_b) and HOMO (lower E_b). The HOMO peak with h_u symmetry carries ten electrons, while HOMO-1 has mixed h_g + g_g symmetry is occupied by 18 electrons, and both present pure π molecular orbitals.²⁴² The absence of substrate signals suggests that the thin film of C₆₀ is completely formed. This is supported by the measured ionization potential of ≈ 6.4 eV for all three studied C₆₀ films, which corresponds to the value characteristic for C₆₀ in bulk.²⁴³⁻²⁴⁴ Hence, briefly summarizing measured data here, for C₆₀ films on PEI/ITO and ITO, the Fermi level pinning regime can be confirmed, where the obtained value of Φ_{org/sub} = 4.3 eV in both cases can be regarded as the value of E_{ICT-}, which shows good agreement with literature reported values.⁷³ This is the scenario where the Fermi

level of an electrode is placed closest possible to the LUMO level of a molecule, creating the smallest possible Δ_e for the undoped material.

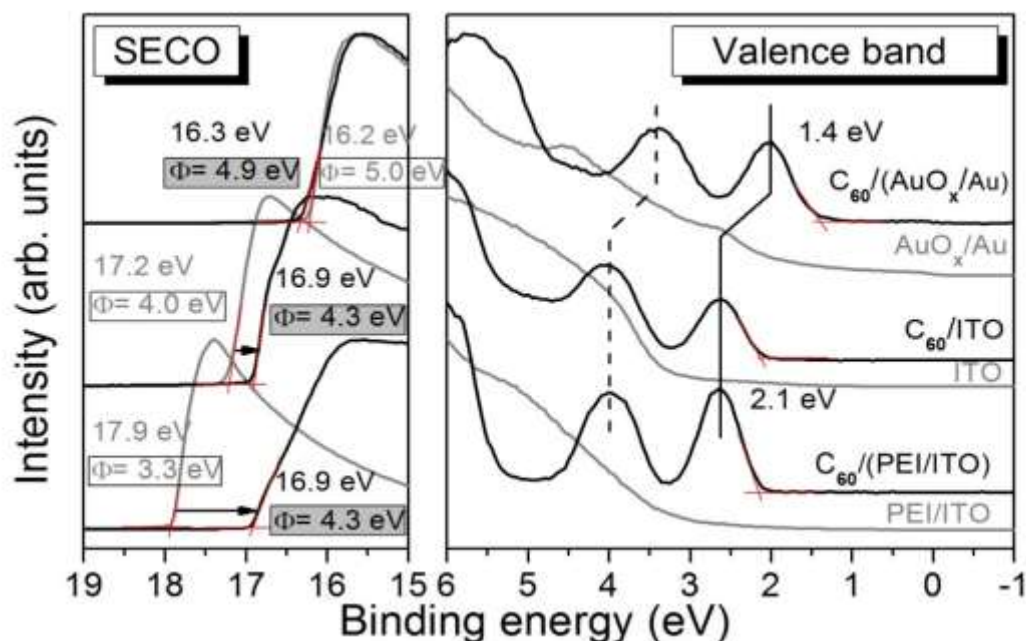


Figure 5.6: The UPS spectra of the fullerene C_{60} thin films, and three corresponding substrates PEI/ITO, ITO and AuO_x/Au , on which C_{60} was deposited.

On the other side, for the fullerene C_{60} on AuO_x/Au , VLA can be inferred at the interface of materials. In Table 5.3 are listed electronic structure parameters obtained from UPS measurements of the C_{60} thin films deposited onto PEI/ITO, ITO and AuO_x/Au substrates, while the ELA diagrams of corresponding interfaces are presented in Figure 5.7.

Table 5.3: Summed up electronic structure parameters of the thin film of C_{60} on three different substrates with the wide span of the work function, as obtained from UPS spectra.

Molecule	IP (eV)	Work function on substrate (eV)			Expected LUMO onset and Δ_e on substrate (eV)		
		PEI/ITO	ITO	AuO_x/Au	PEI/ITO	ITO	AuO_x/Au
C_{60}	6.4	4.3	4.3	4.9	0.3	0.3	0.9

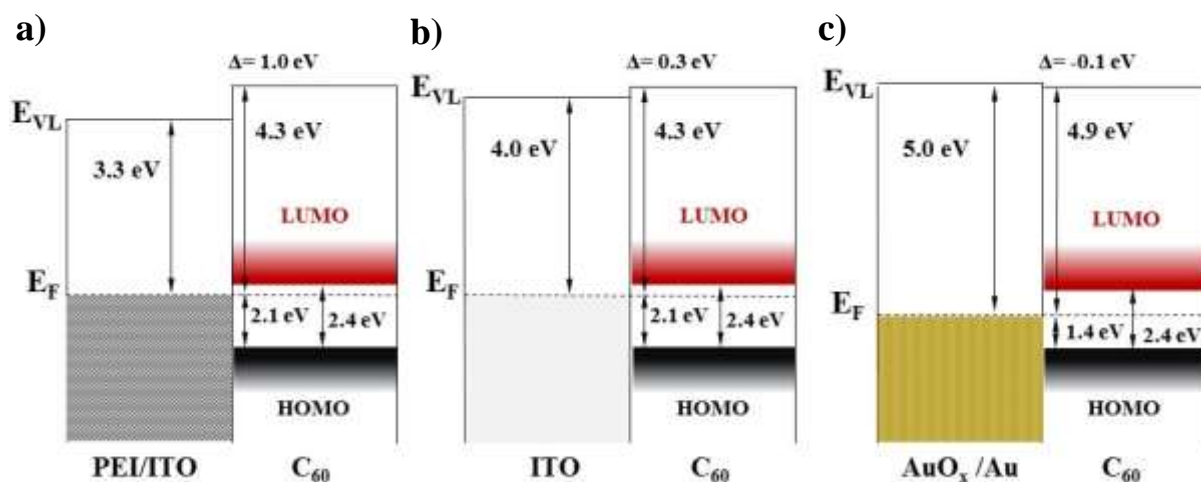


Figure 5.7: Energy level alignment diagrams of fullerene C₆₀ thin films deposited on (a) PEI/ITO, (b) ITO and (c) AuO_x/Au electrodes (substrates). The position of LUMO level of C₆₀ is deduced from the literature taken value of E_g. In cases depicted under a) and b), condition $\Phi_S < E_{ICT-}$ is expected to be fulfilled, whereas in the case under c), condition $E_{ICT+} > \Phi_S > E_{ICT-}$.

PCBM/electrode interfaces

While the solubility of C₆₀ is generally low in organic solvents,²⁴⁵ its derivatives with attached side chains such as PCBM, have shown improved solubility in the wide variety of solvents, which give them a possibility to be processed on the large-scale from solution.^{31, 246-247} It has been also reported that side chains attached to C₆₀ have an effect on the electronic structure of the molecule, as well as the morphology of the film.²⁴⁷⁻²⁵⁰ In this section, the UPS spectra of the fullerene derivative PCBM prepared on PEI/ITO ($\Phi_{\text{sub}} = 3.3$ eV) and ITO ($\Phi_{\text{sub}} = 4.0$ eV) substrates, will be presented. The thin films of PCBM are prepared by doctor-blade casting from 1 w% chloroform solution. As can be noticed from the left frame (SECO position) of Figure 5.8, after casting of the thin film of PCBM on PEI/ITO and ITO substrates, SECO position changes towards lower binding energy in both cases. This SECO decrease for the deposited PCBM film on both substrates depicts the rise of Δ at both created interfaces. In the right panel of Figure 5.8 can be seen UPS spectra of the upper valence levels of PCBM thin films prepared on PEI/ITO and ITO substrates, with corresponding substrate spectra. Obtained

spectra resemble the spectrum of C_{60} , with dominant HOMO (lower E_b) and HOMO-1 (higher E_b) signals, which is the clear sign that valence band signals stem mostly from the C_{60} cage, rather than side chains present in PCBM. The HOMO onset values ($E_b(\text{HOMO})$) are found to be 2.0 eV for PCBM on PEI/ITO and similarly 1.9 eV on ITO substrate, referenced to E_F (0 eV). The ionization potential (IP) of PCBM film obtained from measurements on the two substrates is 6.1 eV, the value which is in excellent agreement with values reported in the literature.^{73, 248}

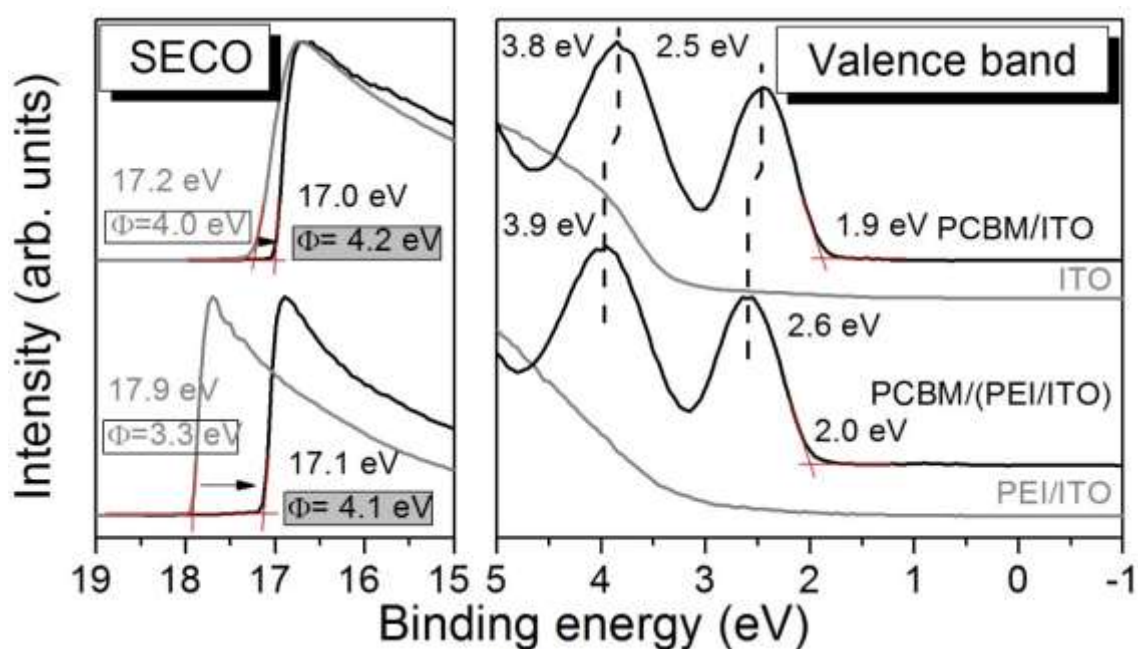


Figure 5.8: The UPS spectra of the fullerene PCBM thin films, and two corresponding substrates PEI/ITO and ITO, on which PCBM was deposited.

The lower IP of PCBM in comparison to C_{60} can be subscribed to the presence of the attached side chains on buckyball. Furthermore, measured effective work functions ($\Phi_{\text{org/sub}}$) are very similar; 4.1 eV for PCBM on PEI/ITO and 4.2 eV for PCBM on ITO. These pinning positions of the Fermi level within the PCBM band gap are recognized as the negative polaron (ICT-) level of PCBM, and they show good agreement with literature reported value of 4.3 eV.⁷³ Here we conclude that Fermi level pinning occurred due to fulfilled condition $E_{\text{ICT}^-} > \Phi_{\text{org/sub}}$. As

mentioned in the section above, this scenario where the Fermi level of electrode is pinned closest to the LUMO level of molecule, creates the smallest possible Δ_e . Electronic structure parameters obtained for two PCBM films, doctor-blade cast onto PEI/ITO and ITO are listed in Table 5.4, whilst resulting energy level alignment diagrams, are presented in Figure 5.9.

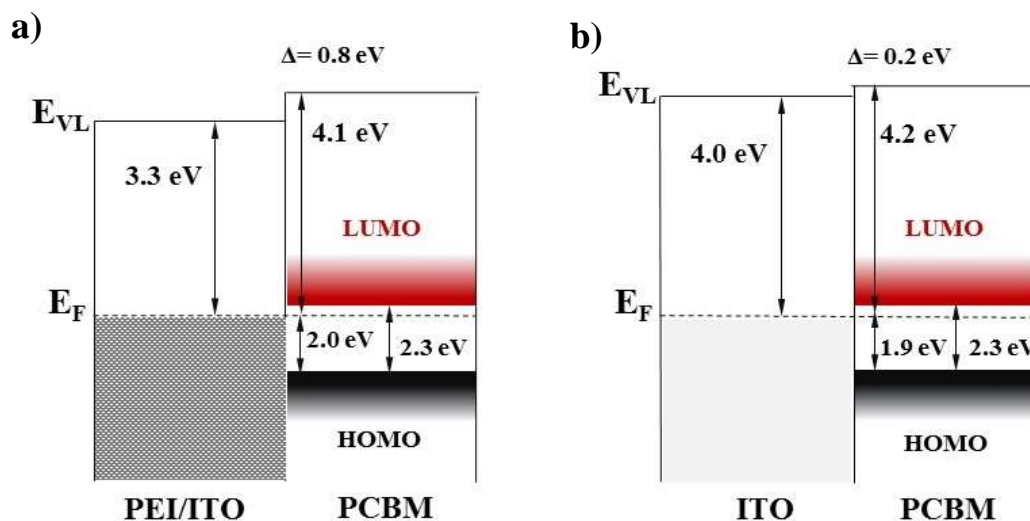


Figure 5.9: Energy level alignment diagrams of fullerene derivative PCBM thin films deposited on (a) PEI/ITO and (b) ITO electrodes (substrates). The position of LUMO level of PCBM is deduced from the literature taken value of E_g .

Table 5.4: Summary of electronic structure parameters of the thin film of PCBM on PEI/ITO and ITO electrodes, as obtained from UPS spectra.

Molecule	IP (eV)	Work function on substrate (eV)		Expected LUMO onset and Δ_e on substrate (eV)	
		PEI/ITO	ITO	PEI/ITO	ITO
PCBM	6.1	4.1	4.2	0.3	0.4

5.2.2. Donor/acceptor interface in planar heterojunction

Energetics at C₆₀/PCPDTTBTT interface prepared on three different substrates

In this section, the thin film overlayer of C₆₀ is prepared onto three thin films of PCPDTTBTT, which have shown three different ELA alignment outcomes with substrates beneath. The thin film deposited on AuO_x/Au has shown FLP close to the HOMO level, on ITO substrate has shown VLA, and on PEI/ITO substrate FLP close to the LUMO level. Now, it would be interesting to check how those differences may affect interaction at the interface with the acceptor material fullerene C₆₀.

Hence, in Figure 5.10 are presented UPS data which are recorded for the overlayer of C₆₀ deposited onto PCPDTTBTT/(PEI/ITO), PCPDTTBTT/ITO and PCPDTTBTT/(AuO_x/Au) stacks. Firstly, from the bottom left spectra for C₆₀ on PCPDTTBTT/(PEI/ITO) can be seen that SECO barely changes its position after evaporation of 3 nm (~ 3 monolayers, ML) thick film of fullerene. This means that no interface dipole is created at this C₆₀/PCPDTTBTT interface, and the VLA regime is established. On the right-hand side panel, bottom spectrum, we can see fully developed HOMO peaks of C₆₀, with onset located at 2.6 eV below E_F (0 eV). Moreover, the weak interaction (vacuum level alignment) can be also perceived for the interface made of about 3 nm fullerene C₆₀ vacuum evaporated onto the PCPDTTBTT/ITO stack. As can be seen from the middle spectra of Figure 5.10 (left panel), the SECO value shows no changes to what was observed for PCPDTTBTT covered ITO. The HOMO onset of fullerene on the PCPDTTBTT/ITO system is again located 2.6 eV below the Fermi level (0 eV), what can be seen in the right middle spectrum. Lastly, from the top left spectra of Figure 5.10 can be seen that after the evaporation of about 4 nm thick fullerene C₆₀ film on the

PCPDTTBTT/(AuO_x/Au) system, the SECO is shifted for 0.2 eV to the lower binding energy creating an interface dipole of the same size. Observed SECO shift (i.e. E_{VL} upward shift), gives the new value of the work function, which is now calculated to be 4.3 eV. On the right panel where the valence band region spectra are presented, the top spectrum of C₆₀ shows the onset value of 2.1 eV. It is interesting to notice here that in the case of the top spectrum, SECO and E_b(HOMO) are shifted for about 0.5 eV towards lower binding energy in comparison to lower two spectra. In all three cases of the thin films of C₆₀, obtained ionization potential was found to be ≈ 6.4 eV, which matches very well with the literature and previously found values.

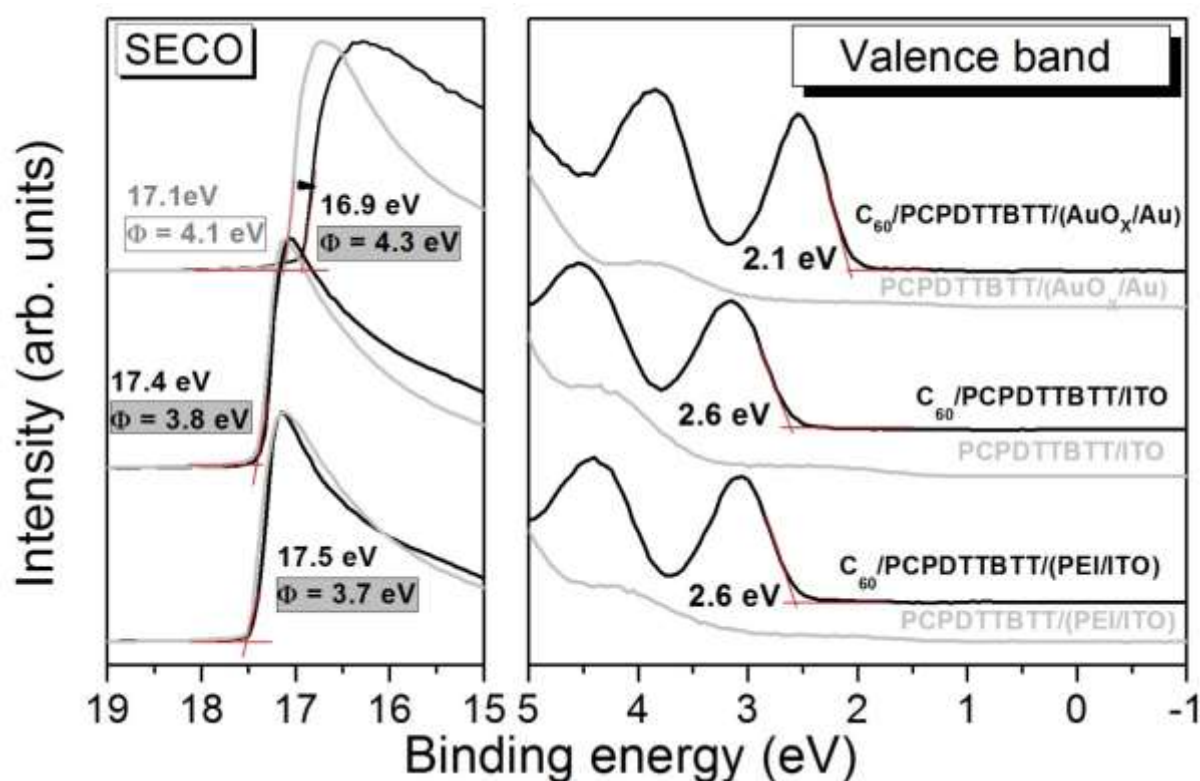


Figure 5.10: The UPS spectra of the fullerene C₆₀ thin films, deposited onto three different PCPDTTBTT stacks.

The above presented UPS data are further converted into the ELA diagrams shown in Figure 5.11, in order to determine the electronic properties of studied C₆₀/PCPDTTBTT interfaces. In Figure 5.11 and all following ELA diagrams in Section 5.2.2., for the determination of energy level alignment scenarios at the mimicked p-n junctions for solar cells (donor-acceptor

interfaces), the optical band gap was used to approximate the position of the LUMO level (represented with yellow dashed line) of donor (polymer) materials, while the transport gap (from the literature) was used for the same reason in the case of the acceptor material (C_{60}). Nonetheless, the approach used here can also give valuable insight into the comprehension of the nature of interaction, energy and charge transfer at these organic/organic interfaces, hence, provide an explanation of the obtained energy level alignment scenarios. Now, the obtained ELA alignment for the bilayer stack $C_{60}/PCPDTTBTT/(PEI/ITO)$ is presented in Figure 5.11a. From the ELA scheme can be seen, that after casting of PCPDTTBTT thin film on PEI/ITO, an interface dipole of 0.4 eV was established at the latter interface. The Fermi level of the substrate was pinned at 3.7 eV below E_{VL} what was at first regarded as the potential ICT- level of PCPDTTBTT polymer. After evaporation of C_{60} , no interface dipole was observed at the $C_{60}/PCPDTTBTT$ interface. What can be also noticed in Figure 5.11a is that the HOMO position of the polymer is below the LUMO position of fullerene, hence, no direct spontaneous charge transfer is expected between materials at the interface. Additionally, a conclusion might be drawn that in the obtained VLA scenario, the effective work function of the PCPDTTBTT/(PEI/ITO) stack is greater than the electron affinity of C_{60} , i.e. the Fermi level of the latter stack (shown as a brown dashed line) is located above the bottom of the conduction band (the LUMO level) of C_{60} , determined by inverse photoemission in the literature to be ~ 4.0 eV.²⁵¹⁻²⁵² This scenario of E_F being placed above the empty part of the conduction band is implausible from the point of view of thermodynamic equilibrium. By the ICT model, if the FLP at polaron (ICT) level occurs in the first organic layer, then, FLP might be expected as well in the organic overlayer if the conditions: $E_{ICT-} > \Phi_{poly/sub}$ or $\Phi_{poly/sub} > E_{ICT+}$ are fulfilled. Additionally, in Section 5.2.1. it was shown that deposition of fullerene C_{60} thin film on a nonreactive substrate with $\Phi_{sub} < 4.3$ eV would lead to pinning of E_F close to LUMO level of C_{60} at 4.3 eV referenced to the vacuum level. Regarding the fact that the conditions mentioned

above are fulfilled, pinning of E_F at 4.3 eV with the formation of a substantial interface dipole (Δ) of 0.6 has been expected. Nevertheless, no E_{VL} shift at the $C_{60}/PCPDTTBTT$ interface was found, and the vacuum level alignment is established, without charge transfer. This finding is further supported by the absence of the charging effect we observed during the photoemission measurements. The explanation for this outcome might be found in FLP regime at the trap states within the previously forbidden band gap of the donor material PCPDTTBTT, rather than at ICT- (negative polaron) level. It has been reported that the trap or gap states are significantly inherent to (especially polymer) organic semiconductor thin films which are far from having an ideal crystal structure, and their density of states is related to the microscopic structural/morphological imperfections and irregularities, to impurities originating from synthetic or material processing, and/or the molecular design of the copolymer itself.^{57-58,61} Moreover, it has been demonstrated that the density of states of the organic semiconductors, particularly gap states, critically influences the pinning position of Fermi level.^{253 254} However, the density of states of trap states is expected to be lower than in the valence band, i.e. trap states are not expected to possess that amount of charge as polymer states.²⁵⁵ Hence, in the case of the thin film of PCPDTTBTT, at the energy of 3.7 eV below the E_{VL} , no significant charges can be found, and charge transfer cannot occur towards the LUMO level of fullerene at the $C_{60}/PCPDTTBTT$ interface. As a consequence, E_F of the PCPDTTBTT/(PEI/ITO) stack is not “pinned” in the proximity of the LUMO level (ICT- level) of C_{60} , and no interface dipole can be observed. Thus, the reason for a different ELA of PCPDTBT and PCPDTTBTT films with low Φ_{sub} substrates PEI/ITO and ZnO, might be in the observed distinction in morphology and orientation properties measured for the thin films of the latter polymers, more precisely, the weaker self-organization properties found for PCPDTTBTT films. These observations about the difference in morphology between PCPDTBT and PCPDTTBTT thin films are going to be discussed in Section 5.4., as closely related to the change in the chemical structure of two

polymers. In addition, the energy level alignment diagram of the C₆₀/PCPDTTBTT/ITO bilayer system is shown in Figure 5.11b. As presented, VLA is found at both donor/substrate and acceptor/donor interfaces. The absence of the E_F pinning in the PCPDTTBTT layer means that no charge carriers are present at the energy of 3.8 eV below the vacuum level (this energy lies in the gap of PCPDTTBTT) and no pinning can occur in the second organic layer, in agreement with the literature.⁵³ Although Fermi level is depicted in polymer and fullerene layers by the brown dashed line, no charge is expected to be at that energy represented by E_F in both organic layers. Thus, as in the case presented above, thermodynamically is impossible that E_F (charge) is present above the lowest unoccupied molecular orbital (LUMO) of the C₆₀ layer. Moreover, the electrostatic interaction between the substrate and fullerene layer is not expected to occur, due to the polymer layer in between them which prevents the tunneling of charges.⁷⁹ Hence, as a result, the vacuum level alignment at the acceptor/donor interface can be enclosed, without charge transfer taking place at the junction. Lastly, the ELA diagram of the C₆₀ film prepared on the PCPDTTBTT/(AuO_x/Au) system will be discussed. The latter diagram is presented in Figure 5.11c and as can be seen, at the PCPDTTBTT/(AuO_x/Au) interface the substrate Fermi level is pinned 0.8 eV above the HOMO level of the polymer (at 4.1 eV below E_{VL}), rising huge interface dipole of -0.9 eV. After the deposition of C₆₀ film, interface dipole with opposite sign of 0.2 eV is measured at the fullerene/polymer interface. This leads to the increase of the effective work function from 4.1 eV to 4.3 eV, due to pinning of E_F at 0.3 eV below the expected LUMO position of fullerene. In this case, where the effective work function of the PCPDTTBTT/(AuO_x/Au) system is smaller than the ICT- level of C₆₀, ICT model predicts FLP close to the LUMO level of fullerene C₆₀. According to the obtained energy level alignment scenario at considered organic/organic interface, the electron transfer has occurred towards the LUMO level of the C₆₀ layer. Truly, as it is shown, the Fermi level of PCPDTTBTT/(AuO_x/Au) stack is pinned in the C₆₀ overlayer at 4.3 eV below the vacuum level, what was found to be the

position of negative polaron level of C_{60} . Thus, the observed pinning position in PCPDTTBTT polymer prepared on AuO_x/Au substrate can be indeed recognized as the ICT+ level. From the analysis of obtained detailed XPS spectra, a chemical reaction between C_{60} and PCPDTTBTT, with measurable products, can be ruled out. From the above listed data, we could see that the largest photovoltaic gap is found for $C_{60}/PCPDTTBTT/(AuO_x/Au)$ bilayer system.

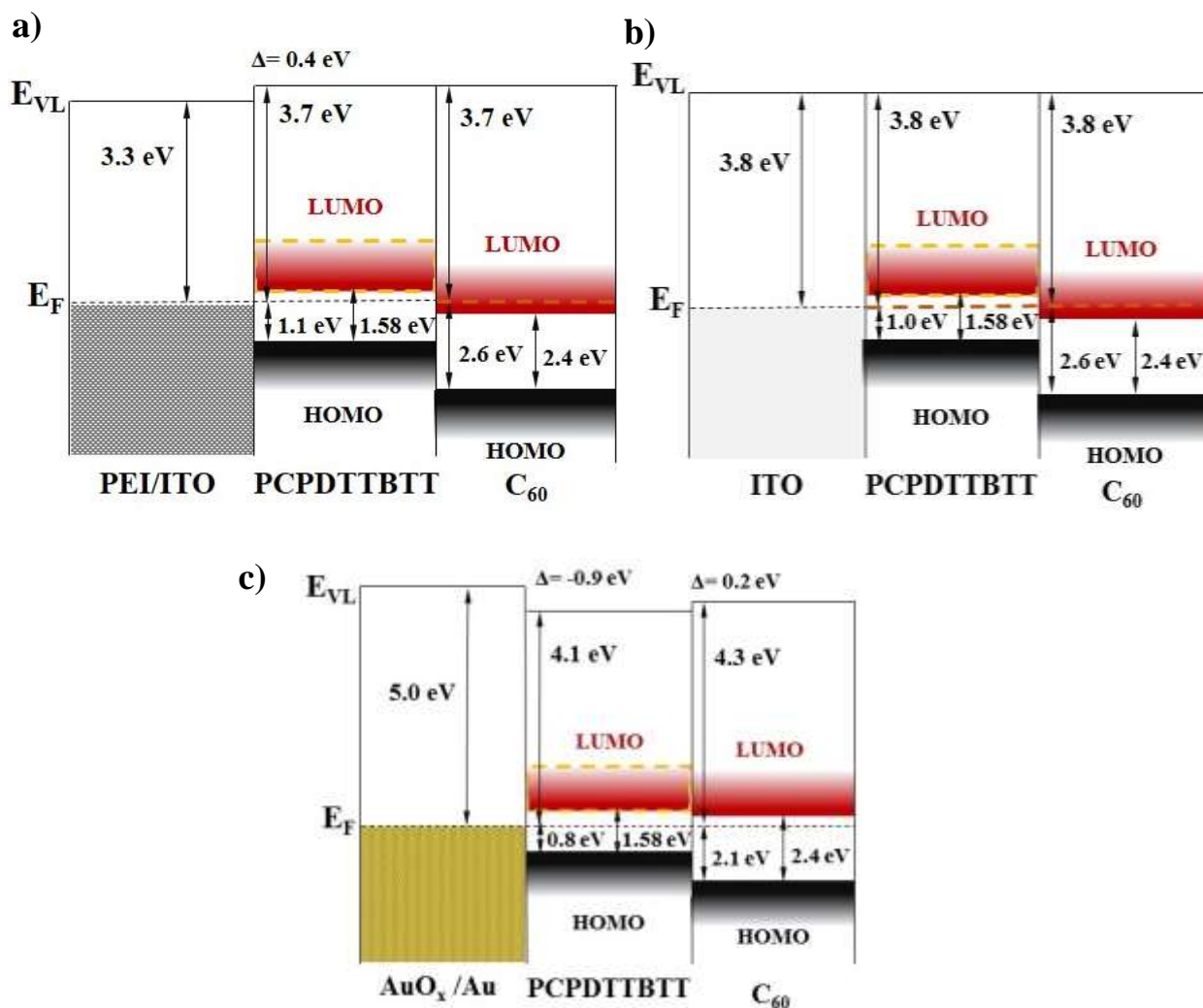


Figure 5.11: Energy level alignment diagrams of the fullerene C_{60} thin films deposited onto (a) PCPDTTBTT/(PEI/ITO), (b) PCPDTTBTT/ITO and (c) PCPDTTBTT/(AuO_x/Au) systems.

Here, the photovoltaic gap ΔE_{DA} is expected to be around 1.0 eV, whilst, for the other two systems, Δ_{DA} value of 0.8 eV is deduced. The interface dipole measured at the $C_{60}/PCPDTTBTT$ interface on the golden substrate is expected to have a positive influence on (i.e increase) the

open-circuit voltage (V_{OC}).²⁰³ Moreover, the smallest Δ_h found for this bilayer system on AuO_x/Au is expected also to boost the performance of a solar cell made of these materials, due to increased the built-in potential and fill factor.⁸⁴

Energetics at $C_{60}/PCPDTBBT$ interface prepared on PEI/ITO and AuO_x/Au substrates

The effective work function of the donor/electrode systems made by preparation of the thin films of BBT polymers on five substrates (with the 1.9 eV huge span of the work function), shows almost the same value. This localization of the position of E_F within the band gap of the BBT polymers, it is believed to be mainly the consequence of the very narrow band gaps expected for these, rather than the presence of trap states. Here, the UPS study of the acceptor/donor interfaces prepared by the vacuum evaporation of fullerene C_{60} onto PCPDTBBT/(PEI/ITO) and PCPDTBBT/(AuO_x/Au) systems, is presented. The aim of the study is to explore the influence of the electronic structure parameters found at the polymer/substrate interface, on interaction at the C_{60} /polymer interface. As aforementioned in the text, for the PCPDTBBT/(PEI/ITO) interface FLP close to the LUMO is expected, whilst for the PCPDTBBT/(AuO_x/Au) interface is anticipated FLP close to the HOMO level. Hence, in Figure 5.12, the UPS spectra are presented for the C_{60} film prepared on PCPDTBBT/(PEI/ITO) and PCPDTBBT/(AuO_x/Au) stacks. From the bottom spectra of the SECO panel, it can be seen that after evaporation of 6-7 ML of C_{60} , onset position is shifted for 0.1 eV to lower binding energy side, taking the new value of 16.9 eV. The observed shift brings an upward deviation of E_{VL} creating an interface dipole, hence, an increase of the work function is found for the new bilayer stack. The new value of the work function is now calculated to be $\Phi_{C60/poly/sub} = 4.3$ eV. On the right-hand side panel, the bottom spectrum of C_{60} shows fully

developed characteristic HOMO features, with onset position of 2.1 eV below the Fermi level (0 eV). Furthermore, after preparation of the 4 nm thick fullerene C_{60} film onto the PCPDTBBT coated AuO_x/Au substrate, the SECO shift of the same magnitude and direction is observed as in the above presented case. It can be seen in Figure 5.12 from the left top spectra, that the SECO onset position decreases for 0.1 eV, i.e. the work function value increases to 4.3 eV. The HOMO onset of the C_{60} film is measured to be at 2.1 eV as can be seen from the top right spectrum. For both fullerene C_{60} films, after addition of the SECO and HOMO onset values, the ionization potential of 6.4 eV is obtained.

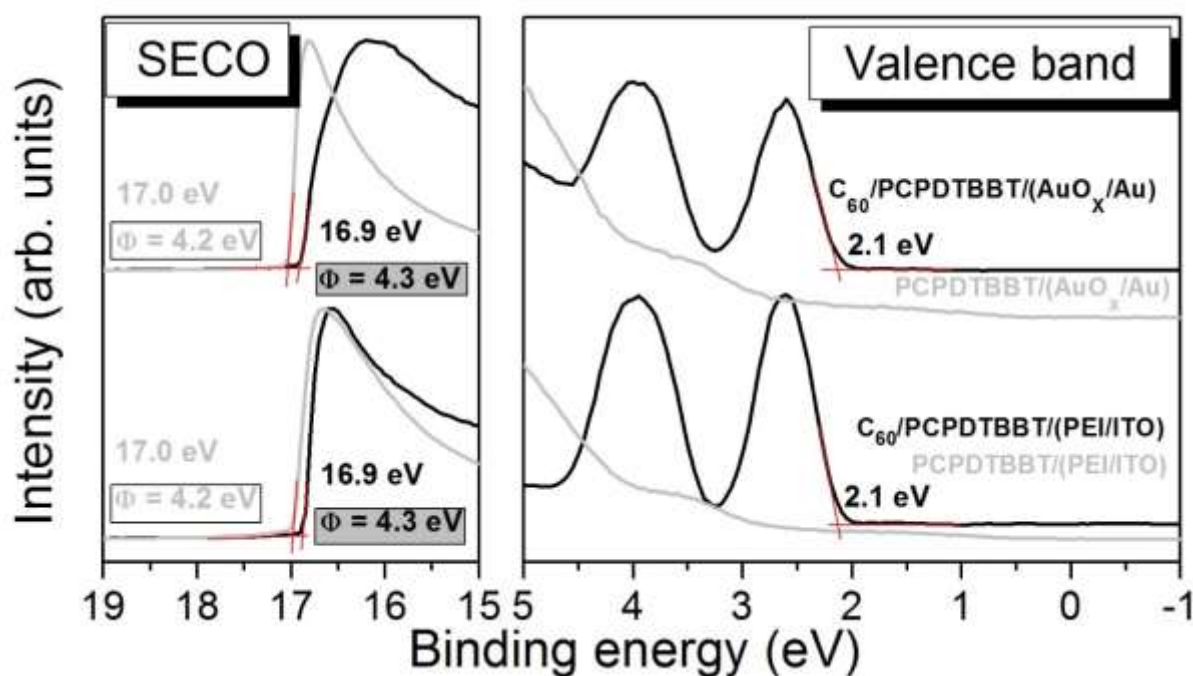


Figure 5.12: The UPS spectra of the fullerene C_{60} thin films, deposited onto PCPDTBBT/ (AuO_x/Au) and PCPDTBBT/(PEI/ITO) stacks.

The obtained ELA diagrams for $C_{60}/PCPDTBBT/(PEI/ITO)$ and $C_{60}/PCPDTBBT/(AuO_x/Au)$ bilayer systems are summarized in Figure 5.13. Firstly, as shown in the left diagram, after the preparation of the thin film of PCPDTBBT onto PEI/ITO, a huge vacuum level shift was observed and Δ of 0.9 eV was measured. The FLP regime was established at this interface, with E_F in the band gap of 4.2 eV beneath E_{VL} , and 0.4 eV above the measured HOMO level of the polymer. After the evaporation of fullerene C_{60} film, E_{VL} shifts upward for 0.1 eV, which is the

value of established interface dipole at the C_{60} /PCPDTBBT interface. Thus, the FLP regime might be deduced at the C_{60} /PCPDTBBT interface, with the interfacial charge transfer of electrons to the C_{60} overlayer. In agreement with ICT model, E_F is found pinned at 4.3 eV referenced to the vacuum level, which is exactly the position of which was regarded as the ICT-level of fullerene C_{60} .

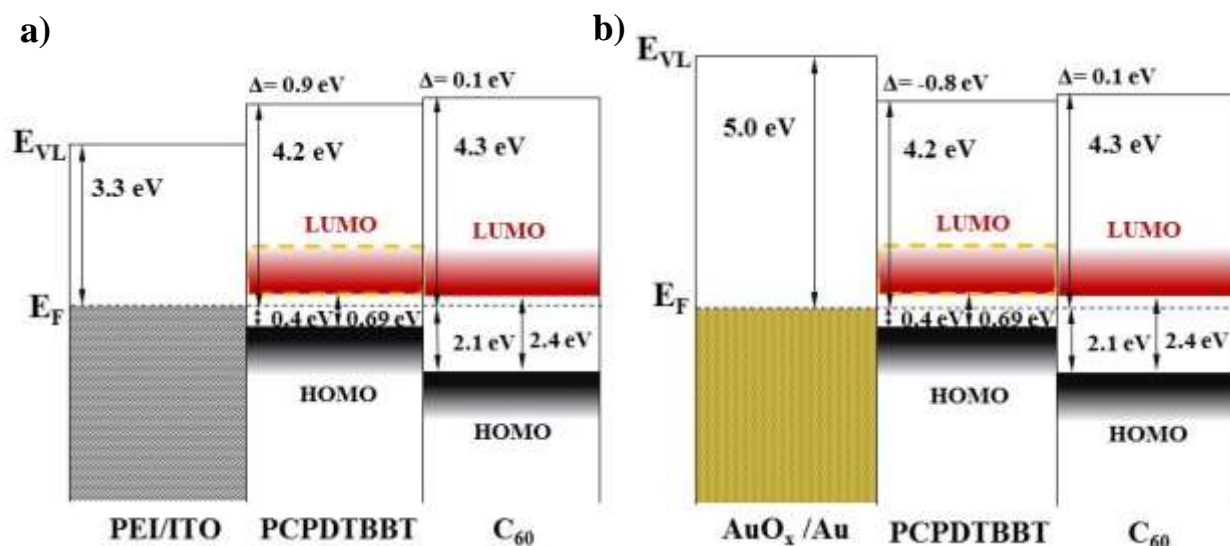


Figure 5.13: Energy level alignment diagrams of the fullerene C_{60} thin films deposited on (a) PCPDTBBT/(PEI/ITO) and (b) PCPDTBBT/(AuO_x /Au) systems.

We find here that the acquired ELA scenario for C_{60} /PCPDTBBT/(PEI/ITO) stack is well explainable by the ICT model. The ELA diagram of the second bilayer stack C_{60} /PCPDTBBT/(AuO_x /Au) is presented in Figure 5.13b. After huge interface dipole (-0.8 eV) was found at the PCPDTBBT/(AuO_x /Au) interface and the effective work function of 4.2 eV was measured, at the C_{60} /PCPDTBBT interface small deviation of the vacuum level is observed ($\Delta = 0.1$ eV), and the work function of 4.3 eV is measured. The diagram shows that after blade casting of the PCPDTBBT thin film onto the electrode AuO_x /Au which work function was found to be higher than the ionization potential of the polymer, the effective work function was acquired to be 4.2 eV, for 0.1 eV lower than the ICT-level of C_{60} . This may explain why the FLP regime is established with a small shift of E_{VL} at the C_{60} /PCPDTBBT interface. From the

obtained ELA scenario, the HOMO (D) – LUMO (A) gap is expected to stay at about 0.7 eV, as in the case of the previous C₆₀/PCPDTBBT interface. As it was the case with donor/acceptor interfaces presented in the previous section, also at C₆₀/PCPDTBBT there is no proof in XPS spectra of the chemical reaction between materials.

5.2.3. Donor/acceptor interface in bulk heterojunction

Unlike the planar heterojunctions (PHJ) presented in the previous section, the interfacial electronic properties of the bulk heterojunction (BHJ) are more complicated for the characterization using established surface analysis methods such as UPS. In the case of above-presented PHJs, due to expected more abrupt separation between donor and acceptor materials, the interface energetics could be studied in a thorough manner. On the other hand, in the blend systems, the work function of a single component is only partially accessible and relevant energy levels are frequently overlapped. Nonetheless, the valence energy level alignment in the BHJ can be studied via core level shifts related to each component, assuming a constant energetic separation between the corresponding core level and the HOMO level.²⁵⁶⁻²⁵⁷ The focus of this section is on the ELA in BHJ, made by LBG semiconducting polymer PCPDTBT as a donor and fullerene derivative PCBM as an acceptor material. Samples of PCPDTBT:PCBM blends with 1:1, 1:2 and 1:3 mixing ratio, as well as pristine film of PCPDTBT, are prepared from 1 w% solution in orthodichlorobenzene on ITO substrates, with the work function of 4.0 eV. The XPS technique is employed for the acquisition of data. The energy level alignment is determined by relating binding energies of signals characteristic for a single component, hence, the S2p peak is taken for PCPDTBT and O1s for PCBM. More precisely, the S2p_{3/2} signal which stems from sulfur atoms of dithiophene part of the polymer, and oxygen O1s from the methoxy group of PCBM, are used. The XPS is recognized to be a

suitable technique for the assessment of ELA in blend films. For the blends of similar polymer systems such as P3HT,²⁵⁸ PCDTBT,²⁵⁹ an accumulation of PCBM close to the substrate is found, even for the 1:1 ratio blends, whilst polymer wetting layer occurred at the surface of the blend films. Thus, according to ref.¹⁵⁸ calculated mean free path of S2p and O1s electrons are estimated to be about 3.3 and 2.6 nm, respectively, indicating that the bulk of the thin film is probed more than just a surface, which should represent the blend faithfully. Yet, before XPS data of the PCPDTBT:PCBM blends are shown, it would be useful to recall findings collected for PCPDTBT and PCBM prepared on ITO substrate, listed in previous sections. In Section 5.1.2. it has been shown, that for the thin film of PCPDTBT, FLP is expected for substrates with $\Phi_{\text{sub}} > 4.1$ eV, whilst on the other three used substrates VLA was found. Hence, for PCPDTBT cast on ITO with $\Phi_{\text{sub}} = 3.8$ eV, vacuum level alignment was inferred. For this PCPDTBT/ITO stack, the binding energy of S2p_{3/2} signal was determined to be 163.5 eV relative to the HOMO onset, and 168.3 eV relative to E_{VL} , where in Figure 5.14 is shown the peak binding energy position related to the Fermi level. On the other side, at the beginning of this section, FLP regime with E_{F} at 4.2 eV below the vacuum level, was found for the PCBM thin film on ITO ($\Phi_{\text{sub}} = 4.0$ eV). For the high binding energy component of the O1s core level (oxygen from the methoxy group), energy distances (O1s-HOMO) and (O1s- E_{VL}) were determined to be 531.6 eV and 537.7 eV, respectively. In Figure 5.14 is presented the aforementioned O1s signal with the binding energy of the oxygen from the methoxy group referenced to E_{F} . Here should be stressed that in the following text, the energetic distance core level to vacuum level will be used for the determination of the ELA of two materials with the substrate and in between them in BHJ, taking into account that the HOMO to core level and the HOMO to vacuum level (IE) are constants. Thus, for the ITO substrate ($\Phi_{\text{sub}} = 4.0$ eV), the vacuum level alignment is expected at the interface with PCPDTBT, but the Fermi level pinning at the junction with PCBM material. Moreover, the vacuum level alignment regime might be

expected between PCPDTBT and PCBM in the blend according to their electronic structure, i.e. the position of relevant frontier orbitals. The energy position of the LUMO level of PCBM is above the HOMO of polymer, hence, no direct ground state charge transfer is expected to occur. In that case of VLA, calculated energy distance between the S2p signal from PCPDTBT and O1s signal from PCBM, should be: $O1s - S2p = 537.7 - 168.3 = 369.4$ eV.

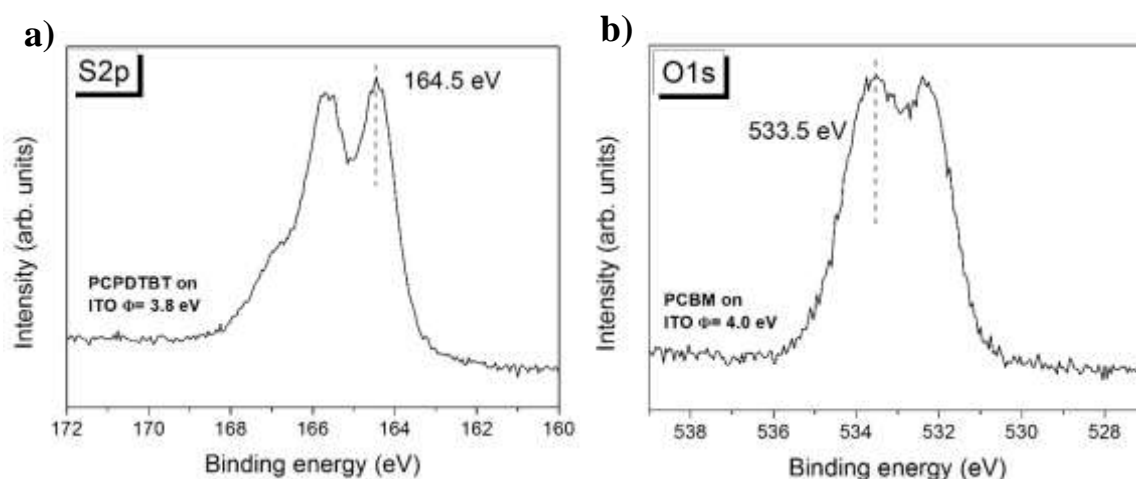


Figure 5.14: The XPS S2p signal of PCPDTBT thin film on ITO with $\Phi_{sub} = 3.8$ eV (left), and O1s signal of PCBM deposited onto ITO with $\Phi_{sub} = 4.0$ eV (right).

Turning back now to XPS data of PCPDTBT:PCBM blends, in Figure 5.15a are presented overview spectra of pristine PCPDTBT and three corresponding blend films, plus detail spectra of S2p and O1s core levels of latter films. The S2p peak binding energy found for the pristine polymer is measured to be 164.4 eV, which is for 0.1 eV smaller than the peak position measured for the same polymer on ITO with $\Phi_{sub} = 3.8$ eV. Considering that peak positions are referenced to E_F (0 eV), this would mean that the HOMO level of the PCPDTBT polymer is for 0.1 eV closer to the substrate Fermi level, in the new experiment. Having in mind that IP of PCPDTBT showed constant value by preparation on different substrates, i.e. the HOMO level to E_{VL} distance is constant, the measured S2p position is expected in terms of the higher value of the work function. Although 0.2 eV smaller binding energy of S2p signal is expected in the new experiment due to the difference in work function values of two ITO substrates, obtained

binding energy of S2p might suggest (taking into account the measurement error of technique) that the foreseen VLA is established at the interface of PCPDTBT with ITO ($\Phi_{\text{sub}} = 4.0$ eV).

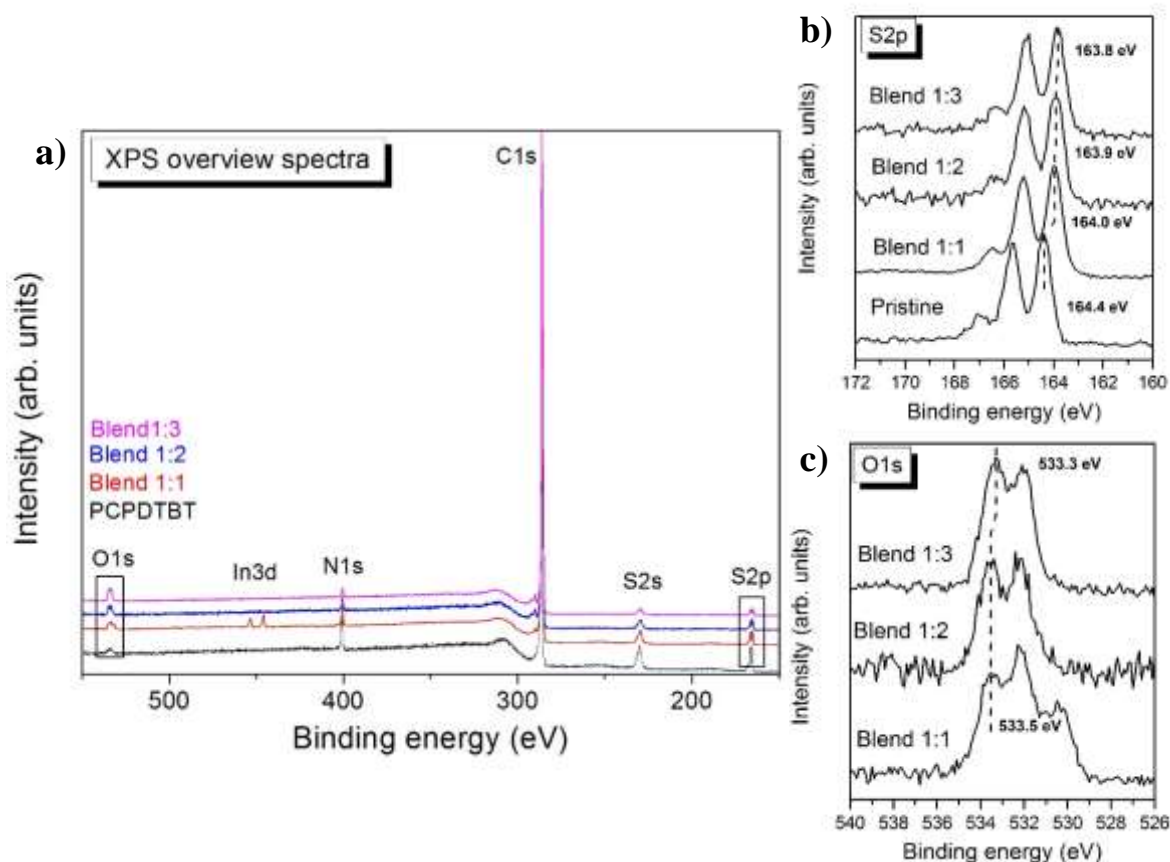


Figure 5.15: The XPS overview spectra of pristine PCPDTBT and two blends with PCBM with designated regions of S2p and O1s peaks are shown in (a), whilst in (b) and (c) are shown enlarged regions of S2p and O1s signals, respectively.

In Figure 5.15 (b and c) can be seen that S2p signal for the blend 1:1 thin film is measured at a binding energy of 164.0 eV, while O1s signal at 533.5 eV. It is noteworthy to remind here that for PCBM deposited on ITO substrate with the same work function value, the O1s peak was found at the same position, as can be seen in the previous figure. This would imply that energy levels of PCBM in the 1:1 blend are measured at the same position relative to the Fermi level, as it was the case for the pristine film. Different shape of the O1s peak observed for this blend is the result of lower film thickness (see the red spectrum with In3d signal in Figure 5.15) and contribution from the substrate oxygen signal (not a signal from the product of chemical

reaction at the interface), and should not have a substantial influence on the ELA in the blend. On the contrary, the obtained binding energy of the $S2p_{3/2}$ peak in the 1:1 blend film is shifted for 0.4 eV to the lower binding energy in comparison to the pristine film, which suggests that PCPDTBT in the blend shows different energy level alignment. Obtained ELA diagram, at the PCPDTBT/PCBM interface for 1:1 blend is shown in Figure 5.16a. Calculated energetic distance between $S2p_{3/2}$ and (methoxy) O1s core levels for 1:1 blend stands 369.5 eV, hence, corresponds to an interface dipole of $\Delta = -0.1$ eV at the interface of PCPDTBT and PCBM in the 1:1 blend. Moreover, while O1s signal preserves the same position in the 1:2 blend, $S2p$ peak is shifted for an additional 0.1 eV to lower binding energy. The energetic distance between $S2p$ and O1s is found to be 369.6 eV in a more diluted blend, which would mean that Δ at the polymer:fullerene interfaces in 1:2 blend is -0.2 eV, depicted in Figure 5.16b. Lastly, in 1:3 blend, $S2p$ signal is shifted by 0.1 eV while O1s by 0.2 eV towards lower binding energy, creating interface dipole at their interface of - 0.1 eV, as shown in Figure 5.16c. Hence, for this blend, neither the polymer nor PCBM is in the vacuum level alignment regime with ITO substrate. From three ELA diagrams shown above, it can be inferred that resulting ELA in the PCPDTBT:PCBM blend seems dependent on the mixing ratio of the blend, causing a variation in energy offsets with E_F , which is found pinned close to the LUMO of PCBM. Observed shift of energy level which belongs to the polymer in prepared blends, in comparison to the pristine polymer film, might be understood as a function of the blending amount of PCBM. Indeed, it was observed that in polymer:fullerene derivative blends, change in the position of the polymer valence band occurs due to polarization effects, i.e. the change in an electrostatic environment of the polymer caused by the presence of fullerene molecules, having in mind that PCBM possesses a permanent dipole moment.²⁶⁰⁻²⁶¹ Minor interface dipoles at the PCPDTBT:PCBM interface in blend films, might be supported by the electronic structure of participating materials, as commented above, and the weak interaction between materials might be inferred,

still, the charge transfer between materials cannot be ruled out. The HOMO level (IP) of PCPDTBT was measured to be around 4.8 eV, while the literature reported LUMO level (EA) value of PCBM, obtained via IPES was 3.8 eV.²⁵¹

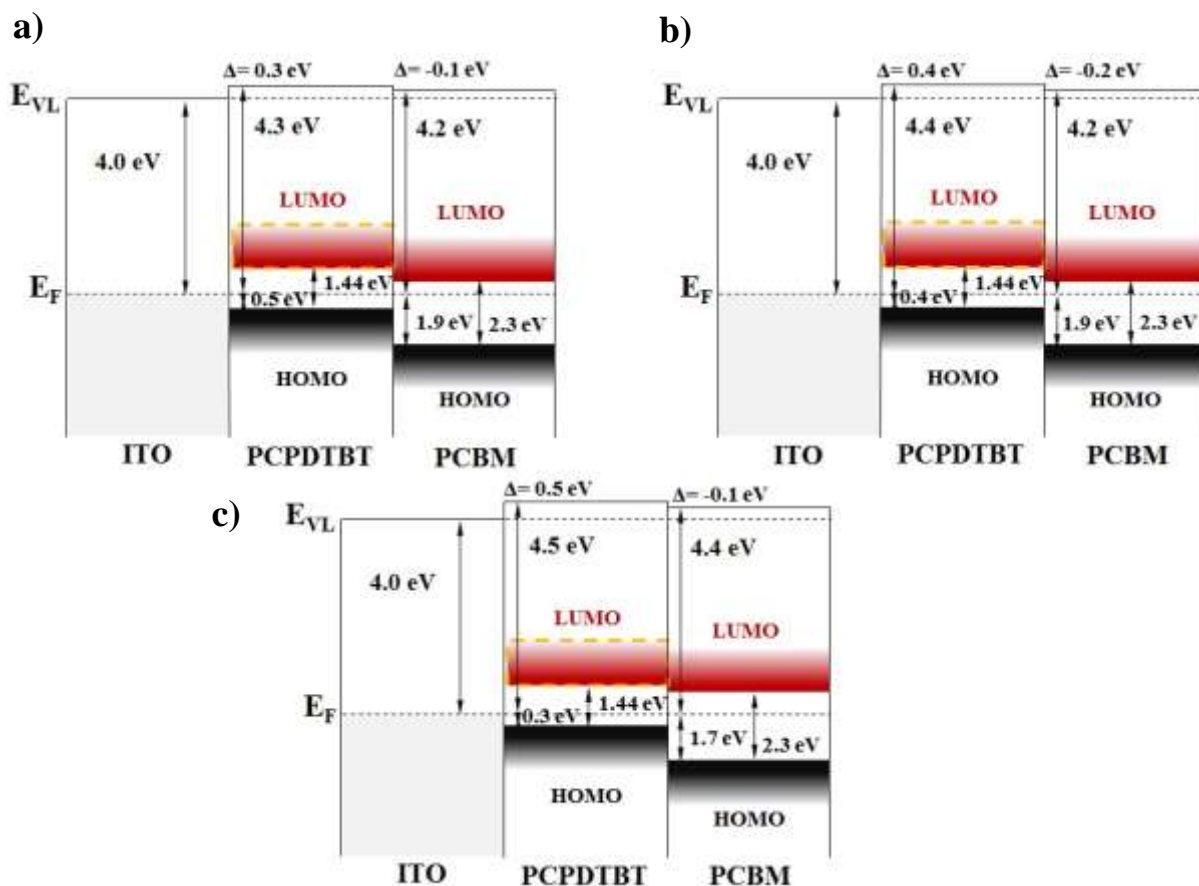


Figure 5.16: Schematic energy level alignment diagrams of the PCPDTBT:PCBM blend with three mixing ratios a) 1:1, b) 1:2 and c) 1:3. Here should be noted that both materials obtain contact with the substrate, hence diagrams might look bit misleading. Nonetheless, from the extended line (dashed) which represents E_{VL} of substrate, reader can easily find the electronic structure parameters at the PCBM/ITO interface. For the polymer is used the optical gap (E_g^{opt}) for an estimation of the LUMO position, while for PCBM is taken literature value of the band gap, obtained via IPES.

Thus, as aforementioned, no direct charge transfer from the HOMO level of donor to the LUMO level of acceptor is expected even in the blend solutions, however, the potential transfer of an excited electron from the LUMO of PCPDTBT to the LUMO of PCBM is expected to be possible for all mixing ratios according to energies of these frontier orbitals. Generally, electron transfer processes occur at different interfaces in various types of (opto)electronic devices such

as solar cells and light emitting diodes, and they are crucial for the functioning of the latter. Thus, for the potential utilization of a certain blend as active layer for an efficient BHJ based solar cell, the information about the efficiency of the local electron dynamics at the interface of constituent parts of BHJ, as an essential point of the solar cell where the initial charge separation occurs, should be obtained. For the presented three PCPDTBT:PCBM blends, the charge transfer time dynamics at the donor:acceptor interfaces was studied by the core-hole clock method.^{22,23,262} This method is frequently used to study the charge transfer dynamics at different interfaces with the core-hole lifetime as an internal time reference to track the charge transfer process. The core-hole clock method can be described as a two step model, with the core excitation as a first and the core-hole decay as the second step. In short, a core electron of the material (in this work PCPDTBT polymer) is excited to the unoccupied orbitals by absorption of a soft x-ray photon. Hence, one valence electron falls to the core hole while another valence electron leaves into the vacuum as an Auger electron. During the lifetime of core-hole, the excited electron can either stay at the core-hole site and screens the decay as a spectator (spectator Auger decay) or can take part in the decay process (participator Auger decay). On the other hand, the excited electron can be transferred to the band or unoccupied state of the contact material (substrate or acceptor material such as PCBM used in this work) in charge transfer decay (CT Auger decay). In this work, PCPDTBT in pristine and in blend films has been studied with the core-hole clock method applied to electron spectra containing kinetic energies in the vicinity of the S KL_{2,3}L_{2,3} normal Auger transition with the X-ray photon energy varied over the S K edge resonance. In the blends, unoccupied electronic states are shared between materials, where the π^* orbital of the thiophene unit (S-C bond) is expected to have a larger overlap with the π^* system of PCBM, in comparison to the π^* orbital that is more localized on the S-N bond of the benzothiadiazole unit. The excitation of the S2p core electron via photon energies below the photoionization threshold close to S-K edge, shows that PCPDTBT:PCBM

favours delocalization of the core-excited electrons via intermolecular charge transfer to PCBM. The charge transfer time decreases with the addition of PCBM, up to mixing ratio somewhere between 1:2 and 1:3 (this ratio is found generally to be the best ratio for the photovoltaic performance), when is expected that an interfacial area does not increase any more, and no further increase of the density of states at the interface occurs. The observed decrease in the charge transfer time for the blend system compared to the pristine polymer is 86%, and the blend also exhibits the fastest charge transfer recorded up to now for the polymer:PCBM blend of 170 as (220 as was previously fastest charge transfer time, measured for the P3HT:PCBM blend).

Finalizing this section, from the above shown and discussed results a few conclusions can be drawn about presented PCPDTBT:PCBM blends. Firstly, obtained ELA scenarios to some extent differ from what is being expected from the electronic structure of materials (energy of frontier orbitals) and substrate (work function) considered separately. The electrostatic polarization in an intimate 3-dimensional mixture such as BHJ is perceived as different than in the PHJ where 2-dimensional contact between materials is expected, hence, the donor:acceptor ratio in BHJ is expected to have an influence on the ELA in between materials and latter with the substrate. For studied thin films, this can be nicely seen on the example of the ELA of PCPDTBT in blends. Furthermore, it is inferred that the ICT model cannot be applied straightforwardly for the explanation of the obtained ELA pictures. Finally, shortly discussed charge transfer dynamics measurements have shown that studied blends have a certain potential for the implementation as active material in solar cells. Additionally, these measurements brought new information about the interaction between PCPDTBT and PCBM in the BHJ.

5.2.4. Summary of Section 5.2.

In this section, an interaction at the organic acceptor/donor interface, prepared in planar and bulk heterojunction, was studied. For the donor/acceptor interfaces presented here, the only weak interaction (physisorption) is found to govern the energy level alignment at the junction between materials.

Firstly, at the beginning of this section, we reviewed the electronic structure of two state of the art acceptor molecules C_{60} and PCBM, important for the further understanding of energetics at the donor/acceptor interfaces. Then, as a model for the description of the interaction at donor/acceptor interface, planar heterojunctions (PHJ) consist of two conjugated polymers with related chemical structures PCPDTTBTT and PCPDTBBT (used as donor materials), and C_{60} as the acceptor material, were prepared. In the case of PCPDTTBTT thin films as donor materials, PEI/ITO and AuO_x/Au were used as the substrates, for which FLP regime with E_F pinned close to LUMO and HOMO level of the polymer, respectively, has been demonstrated. Additionally, a thin film of fullerene C_{60} was sublimated on the vacuum level aligned PCPDTTBTT/ITO stack. Overall, the fullerene C_{60} thin layer was prepared on thin films of PCPDTTBTT polymer which shows three possible ELA scenarios with three different substrates. In the case of C_{60} deposited onto PCPDTTBTT/(PEI/ITO), the VLA was found at the fullerene/polymer interface. Lack of large interface dipole expected at the C_{60} /PCPDTTBTT was explained by FLP at the trap (gap) states at the polymer/substrate interface. From the study of the latter interface, we could also additionally learn about the electronic structure of PCPDTTBTT low band gap polymer. For the following interface of C_{60} prepared on PCPDTTBTT/ITO, the vacuum level alignment was found at the C_{60} /PCPDTTBTT interface, as a result of VLA at the polymer/substrate interface. In the last two cases, the polymer thin film prevents the electrostatic interaction of fullerene with the substrate beneath, which could

lead to electrostatic polarization at the acceptor/donor interface and rise of interface dipole at the latter junction.⁷⁹ Hence, for these two PHJs, the electrostatic potential is not expected to change across the donor/acceptor interface.

Lastly, at the interface of C₆₀ on PCPDTTBTT/(AuO_x/Au), E_F pinning was obtained according to positions of relevant ICT levels of fullerene and polymer. For this interface, charge transfer is expected to occur across the donor/acceptor interface, creating an interface dipole of 0.2 eV. On the other side, for C₆₀ deposited on the thin films of PCPDTBBT, as substrates were used PEI/ITO and AuO_x/Au. These two substrates induce FLP in the proximity of frontier orbitals of PCPDTBBT, two only ELA scenarios found for the BBT polymers. In the case of both C₆₀/PCPDTBBT interfaces, minor interface dipoles of 0.1 eV were measured. Although observed interface dipoles are within the error of measurement technique and the vacuum level alignment might be equally deduced, obtained ELA scenarios are well expected and dictated by determined pinning positions (ICT levels) of fullerene C₆₀ and PCPDTBBT. Hence, for all donor/acceptor flat heterojunctions presented here, only weak interaction might be deduced, with the energy level alignment scenarios well explainable via used ICT model. Based on the electronic structure of all used polymers and fullerenes, no ground state charge transfer is found at the presented donor/acceptor interfaces. Thus, from interfaces made by fullerene C₆₀ with PCPDTTBTT and PCPDTBBT, can be inferred that the difference in electronic structure between BT and BBT polymer pairs, especially substantial difference expected in the band gap, might have essential effect to interaction at interface with potential acceptor molecules, hence, on the performance of potential OPV device. Also, it was shown that the electronic structure of the substrate, has a huge influence on the ELA at the donor/acceptor interface. On the other side, for the series of PCPDTBT:PCBM blends an average interface dipole of about -0.1 eV, was found, which can vouch about weak interaction at the acceptor/donor interface, also in BHJ. Nevertheless, the ELA in the bulk heterojunction made of PCPDTBT and PCBM is found

to be not easily interpretable via ICT model, and different than what might be expected from the electronic structure of pristine materials or potential flat heterojunction created with them. The reason for this energy level shifts, especially referenced to the underneath ITO substrate, we found in electrostatic interactions between the polymer and fullerene different than in PHJ, caused by intimate mixing of materials in BHJ.²⁶⁰ The photovoltaic gap (ΔE_{DA}) is found to be 0.7 eV on average, the value that is lower to what was expected assuming VLA between PCPDTBT and PCBM in potential PCBM/PCPDTBT/ITO bilayer stack. On the other hand, the different ELA of PCPDTBT with model anode ITO is observed than expected for the PHJ between these materials, giving the smaller value of the hole injection barrier which might be regarded as a positive outcome.

5.3. Controlling the interface energetics of PCPDTBT thin film by p-doping with F-TCNQ

One of the main drawbacks in the fabrication of highly efficient OPV devices are nonoptimized organic-inorganic and organic-organic contacts.²⁶³⁻²⁶⁵ In Section 5.1.2., where the focus was on the scrutiny of the ELA between potential donor materials (hole transport layers) for OPVs and different model electrodes, we could see versatile outcome regarding ELA, hence, the magnitude of the hole injection barrier. In the case of the second polymer pair with BBT electron withdrawing subunit, for which ultralow band gaps are perceived, we could see that the hole injection barrier takes almost the same values independently of the used substrate. On the other side, obtained values of the hole injection barrier for the PCPDTBT and PCPDTTBT thin films showed a greater span of values, 0.7-1.5 eV and 0.7-1.1 eV, respectively. For all polymers, the best result, i.e. smallest Δ_h , was obtained when films were prepared on (two) the

highest work function substrates, with Φ_{sub} greater than IP of polymers. Employing the high work function substrate as an anode is a common approach in building OPV devices with regular device architecture.

As earlier mentioned, it has been demonstrated, that for every semiconducting polymer a certain lower limit of the substrate work function should exist, which is expected to bring E_F of the substrate closest possible to the transport (HOMO) level of the polymer. This value is expected to be specific for every used semiconducting polymer, and a further Φ_{sub} increase is not expected to result in a smaller hole injection barrier. Achieving the smallest possible Δ_h (also electron injection barrier i.e. Δ_e) is very important, in order to decrease losses to the open-circuit voltage of an OPV device. It has been reported that when the contact E_F of the anode (cathode) lies close to the HOMO of a donor material (the LUMO of an acceptor material), the V_{OC} is independent of the contact work function.²⁶⁵⁻²⁶⁶ In this case, an Ohmic contact between the electrode and active material is established, and V_{OC} depends more on the width of the relevant density of states (the HOMO of donor and the LUMO of acceptor).²⁶³ Also, smaller Δ_h is expected to promote charge carrier extraction in comparison to detrimental competitive processes like recombination within the bulk of the active material.²⁶⁷

Several approaches have been proposed to reduce the energy level onset between the Fermi level of electrode and transport states of an organic semiconductor, like an introduction of buffer layer at the interface with electrode or molecular doping of the organic semiconductor film. It has been demonstrated, that the molecular doping of the organic semiconductor film, not only (very often) leads to Quasi-Ohmic contacts, but also to the increase of the hole mobility and electrical conductivity for few orders of magnitude demonstrated by means of optical spectroscopy and electronic characterization measurements.^{237, 268-271} Hence, in this section we will describe how F4-TCNQ molecular p-doping of the polymer thin film influences on the energetics and ELA with the electrode beneath and overlayer acceptor material. For that

purpose, a bilayer prototype OPV device structure consisting of the low band gap polymer PCPDTBT as donor material and fullerene C₆₀ as electron accepting material is firstly prepared, using indium tin oxide-ITO (common anode material in organic solar cells) as a substrate with $\Phi_{\text{sub}} = 3.8$ eV. The PCPDTBT and ITO are chosen, because the interface made of these two widely used materials, showed large Δ_{h} of about 1.0 eV (presented in Section 5.1.2.), which is not a favourable scenario for the fabrication of efficient solar cell.

Then, the similar device architecture with F4-TCNQ doped PCPDTBT film is prepared, in order to understand the influence of the doping on the ELA of PCPDTBT thin film with electrode beneath and C₆₀ overlayer, and its potential implications on parameters important for the performance of an OPV device. For the investigation of the interface Ultraviolet photoelectron spectroscopy is used. Also, the distribution of dopant in the polymer thin film is probed by changing the surface sensitivity of X-ray photoelectron spectroscopy, because, it has been shown that electrical parameters and the energy level alignment (ELA) of the materials in thin films clearly depend on the dopant distribution.^{243, 272}

5.3.1. Interfaces of pristine and doped PCPDTBT thin films with electrode and acceptor overlayer, in bilayer prototype organic solar cell structure

The UPS spectra recorded for a prepared C₆₀/PCPDTBT/ITO bilayer stack are shown in Figure 5.17. Although spectra and corresponding ELA of PCPDTBT thin film on ITO have been already discussed, it is worthy to remind on them once again here. In Section 5.1.2. it was shown that for the PCPDTBT thin film blade cast on five different substrates, whose span of the work function stands from 3.3 to 5.2 eV, the Fermi level pinning regime is only observed on two

substrates with Φ_{sub} higher than IP of the polymer. For the PCPDTBT thin film prepared on ITO with the work function of 3.8 eV, VLA was found, because the Fermi level of ITO is expected to be positioned within the band gap in between ICT levels of the polymer. Whereas the pinning position in proximity of the HOMO level of PCPDTBT was deduced to be 0.7 eV above the HOMO level, at 4.1 eV referenced to E_{VL} , the position of the negative polaron (ICT-) level of the PCPDTBT thin film could not be measured.

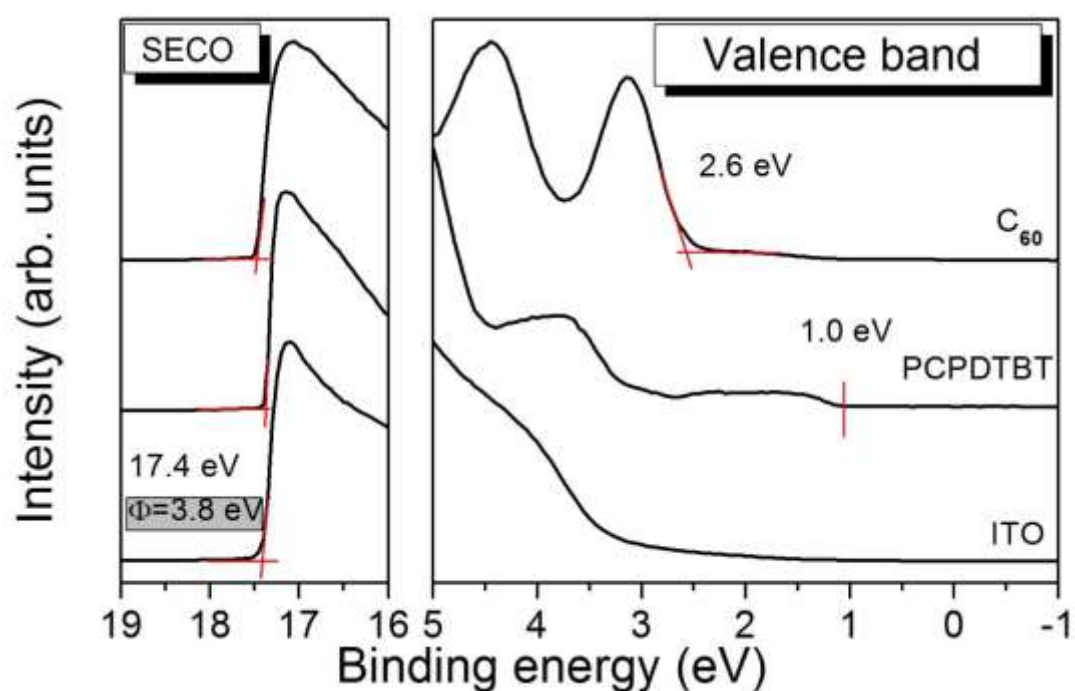


Figure 5.17: The UPS spectra of bilayer stack, made of fullerene C_{60} deposited on thin film of PCPDTBT coated on ITO.

Returning to Figure 5.17, it can be seen that after vacuum sublimation of 4 nm (~ 4 monolayers, ML) C_{60} on the polymer, the position of SECO is not changed (left panel), i.e. the effective work function of the C_{60} /PCPDTBT/ITO stack preserves the value of 3.8 eV afore measured for the PCPDTBT/ITO stack beneath. The right-side panel, of the same figure, shows the HOMO onset at 2.6 eV beneath the E_{F} (0 eV), and we arrive at an ionization potential for C_{60} of 6.4 eV, which indicates that the polymer is entirely covered with C_{60} . The energy level alignment for the complete bilayer stack is summarized in Figure 5.18. As presented, in the case of the undoped PCPDTBT, the Fermi level of ITO is expected to be located between the

ICT levels of PCPDTBT, resulting in the vacuum level alignment (VLA) and hole injection barrier of 1.0 eV. The C₆₀ overlayer follows also the VLA regime, although the Fermi level of ITO substrate is located above the ICT- level of C₆₀ found at 4.3 eV and even above the LUMO determined from inverse photoemission (~ 4.0 eV), both referenced to E_{VL}.²⁵¹ However, due to the absence of Fermi level pinning in the PCPDTBT layer and the polymer film thickness, no charge carriers are present at the energy of 3.8 eV close to the interface with fullerene (this energy lies in the gap of PCPDTBT) and no E_F pinning can occur at this organic-organic junction, in agreement with the literature.^{53, 71}

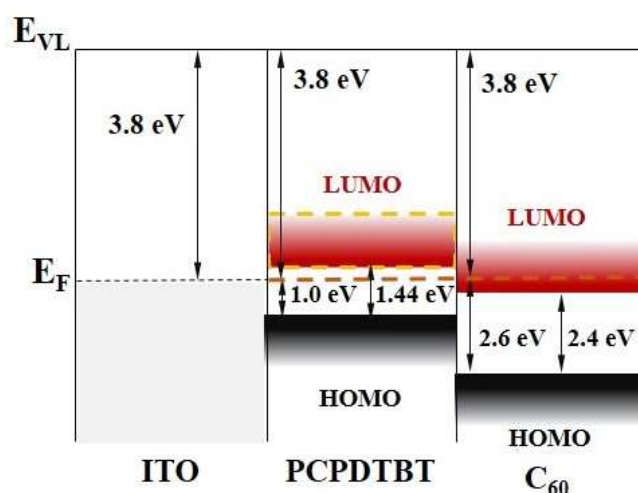


Figure 5.18: Energy level alignment of bilayer stack made by fullerene C₆₀ thin films deposited on undoped PCPDTBBT coated on ITO. The LUMO of polymer is deduced from the optical band gap, shown in Section 5.1.1., while the position of LUMO level of fullerene C₆₀ is taken from the literature.

On the other hand, it has been found that the p-doping of organic semiconductors can distinctly affect the ELA at interfaces with different layers or electrodes in an OPV device,^{237, 273} since the removal of electrons causes significant changes in the electronic structure of the doped material. Hence, for the efficient doping of polymers, complete (integer) charge transfer between the dopant and the organic semiconductor occurs. This can be ensured if the lowest unoccupied molecular orbital (LUMO) of the organic semiconductor is lower than the highest occupied molecular orbital (HOMO) of the dopant (n-doping), or, vice versa, the HOMO of the organic semiconductor is higher than the LUMO of the dopant (p-doping). A simple sketch

which depicts principles of the molecular doping in organic semiconductors is shown in Figure 5.19.

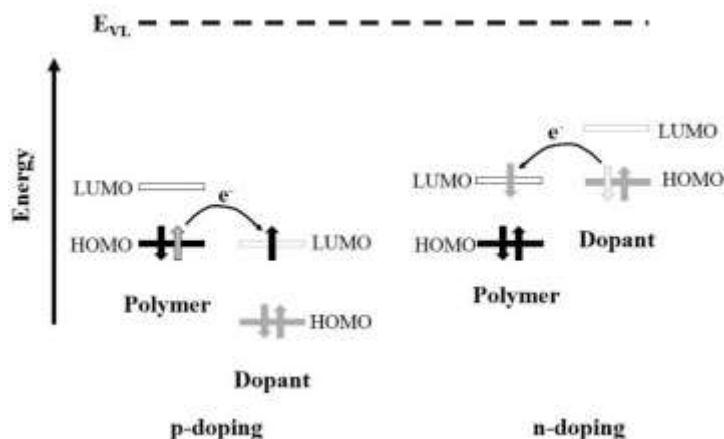


Figure 5.19: Graphic representation of molecular doping in organic semiconductors via integer charge transfer.

Therefore, for the efficient p-doping, an organic dopant with high ionization potential (IP) is needed such as F4-TCNQ, a strong oxidizing agent with high electron affinity (EA) of 5.24 eV and ionization potential (IP) around 8.4 eV.^{238, 274} Several studies have shown that the insertion of a thin interlayer of F4-TCNQ between the electrode and the organic active layer can optimize contact properties, i.e. a significant decrease of the energy level offset between the Fermi level of the electrode and the HOMO of the organic semiconductor was observed.^{81, 183} Such doped intermediate layers can be prepared by both, a premixing of the semiconducting material and the dopant in solution^{237, 275} or by co-evaporation.²⁷⁴ As an example, the doping of polymers with F4-TCNQ has been shown to boost the performance of bulk heterojunction (BHJ) solar cells. The doping can occur either in the bulk of the active layer prepared by mixing TCNQ with the polymer:fullerene blend,²⁷⁶⁻²⁷⁷ or a doped (interface) layer is introduced.²⁷⁸ In some cases, the ability of F4-TCNQ to diffuse in the organic thin films is utilized for the purpose of efficient/guided doping.^{274, 278-279} Indeed, it has been shown, that in some cases upon preparation of the F4-TCNQ doped polymer thin films, dopant segregates atop the polymer film, affecting the alignment of energy levels at the interface with another organic film.²⁴³ Therefore, recent

scientific efforts were also focused on the determination of the distribution of dopants in polymer thin films. It was shown that electrical parameters and the energy level alignment of the materials in thin films clearly depend on the dopant distribution.^{243, 272} Here, the study goal is to investigate the influence of p-doping on the ELA in a bilayer prototype organic solar cell structure, consisting of the polymer PCPDTBT blade cast on ITO substrate as donor material, and fullerene C₆₀ as an electron accepting material.

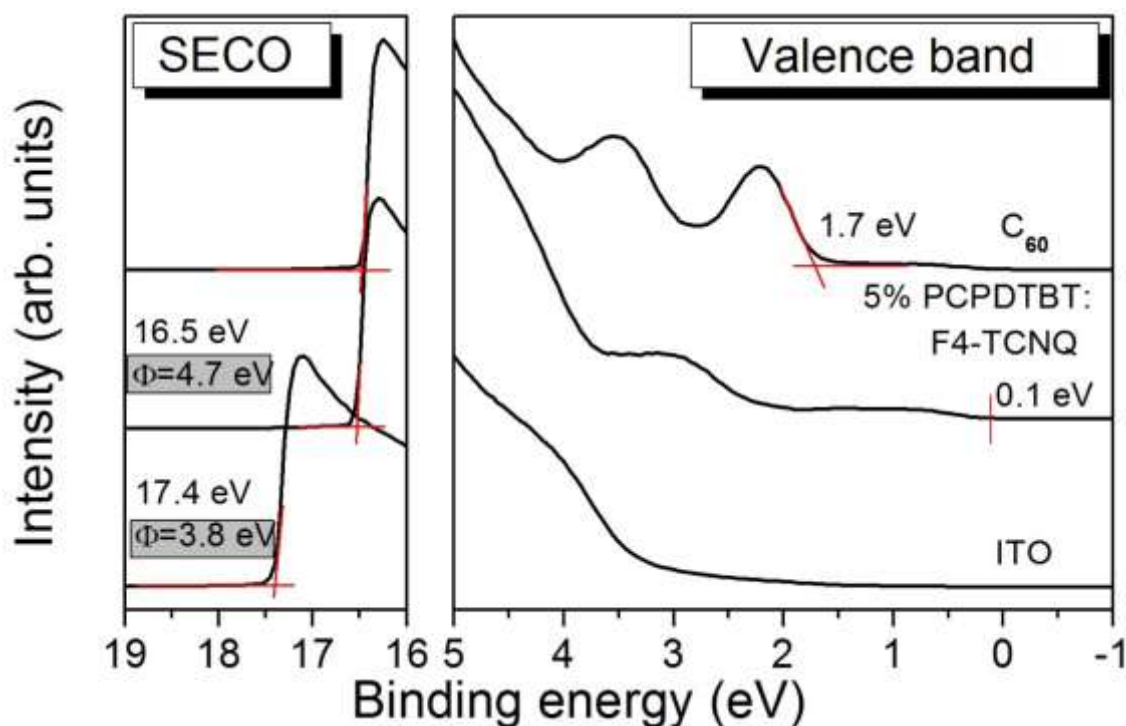


Figure 5.20: The UPS spectra of bilayer stack, made of fullerene C₆₀ deposited on thin film of PCPDTBT 5% doped by F4-TCNQ, coated on ITO.

The p-doping of PCPDTBT was performed by adding F4-TCNQ to the polymer solution, the doping ratio was 5 wt % corresponding to one F4-TCNQ molecule per 10 monomer units of PCPDTBT. The UPS spectra of the C₆₀/F4-TCNQ:PCPDTBT/ITO system is depicted in Figure 5.20. As it can be seen, in opposite to the undoped PCPDTBT film in Figure 5.17, a clear change of the SECO position is visible after deposition of the doped PCPDTBT film on ITO ($\Phi_{\text{sub}} = 3.8 \text{ eV}$). The rigid shift of the SECO and all valence band features (also core levels) by 0.9 eV towards lower binding energy, is observed. This energy shift reveals the formation of an interface dipole Δ of 0.9 eV at the PCPDTBT:F4-TCNQ/ITO interface, whereas the HOMO

onset binding energy is found very close to the Fermi level of ITO. Surprisingly, IP is not affected by the doping of the polymer (IP = 4.8 eV), this might be a first hint that a pronounced aggregation of F4-TCNQ on top of the polymer film, as observed for related systems,²³⁷ did not take place in this case.

The question now arises, whether or not the presence of charges in the polymer and/or the varied ELA for the doped PCPDTBT/ITO interface affects the ELA of the subsequent C₆₀ overlayer. It is clearly visible in the left pane of Figure 5.20 that after deposition of 2 nm (~2 ML) C₆₀, no shift of the SECO is observable, hence, the vacuum level alignment is found at the C₆₀/PCPDTBT:F4-TCNQ interface. The fully developed HOMO feature and the characteristic IP of 6.4 eV for C₆₀, indicates that the doped PCPDTBT film is fully covered with the fullerene. The energy level alignment, for the latter UPS data, is summarized in Figure 5.21. In contrast to the PCPDTBT/ITO system, for PCPDTBT:F4-TCNQ on ITO pinning close to the HOMO occurs, i.e. electrons from the ITO substrate can fill empty states close to the HOMO of the polymer, induced by p-doping. The Fermi level is found close to the HOMO of the polymer, establishing the hole injection barrier of only 0.1 eV which might lead to Ohmic-like contact at the interface. The Fermi level at 4.7 eV below E_{VL}, settles in the band gap of the C₆₀ overlayer, between ICT levels.⁷³

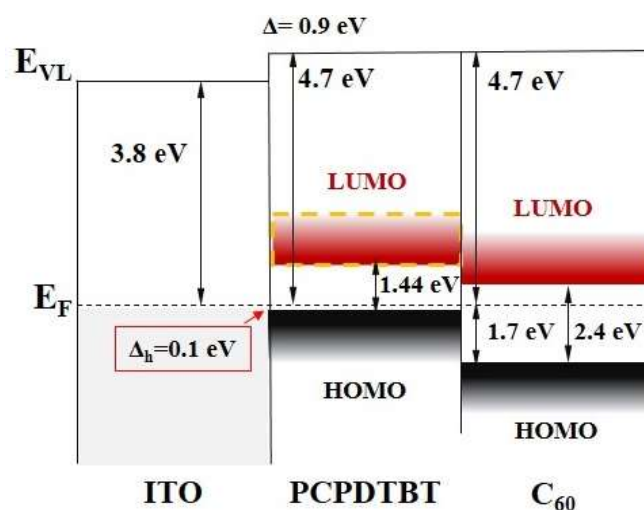


Figure 5.21: Energy level alignment of bilayer stack made by fullerene C₆₀ thin film deposited onto PCPDTBT 5% doped by F4-TCNQ, precoated on ITO.

As a result, at the C₆₀/PCPDTBT:F4-TCNQ interface VLA regime is established, as it was the case for the C₆₀/PCPDTBT interface. This means that the energy difference between the HOMO of PCPDTBT and the HOMO and LUMO of C₆₀ is independent on the p-doping of the polymer with F4-TCNQ. The changed ELA upon doping might have distinct consequences for solar cell devices based on these materials. It is known that the difference between the HOMO of a donor (e.g. PCPDTBT) and the LUMO of an acceptor material (e.g. a fullerene) determines the photovoltaic gap, hence, it can affect the open circuit voltage (V_{OC}) of a solar cell device. In the example shown above, this value is not changed by the doping of the potential donor material PCPDTBT. However, as mentioned above, the energetic barriers at electrode interfaces have to be considered as they represent losses to V_{OC}. More exactly, V_{OC} is discussed to be dependent on the work function differences between the electrodes or the built-in potential.^{265, 280} Thus, a substantial decrease of Δ_h is expected to increase the built-in potential and fill factor in BHJ solar cells, hence, the overall performance of a solar cell.²⁸⁰ It is worth to mention that such a significant decrease of Δ_h has not been observed in the case of F4-TCNQ doped poly-3-hexylthiophene (P3HT, a reference donor material for BHJ solar cells), for equal or even higher doping concentrations.²³⁷ In the case of polyfuran, even an increase of the hole injection barrier is reported after doping with F4-TCNQ, with an increment of the dopant amount.²⁴³ Other approaches reported for the reduction of the HOMO level onset include, on the other hand, the insertion of a buffer layer between the electrode and the polymer²⁸¹ and doping of the polymer at the electrode/polymer interface.²⁸² Therefore, the question arises how the dopant F4-TCNQ is distributed within the polymer film. In order to distinguish between the stoichiometry in the bulk of PCPDTBT:F4-TCNQ film and close to the surface, the angle-dependent XPS measurements at normal and grazing (60° in respect to the surface normal) emission angles, were performed, and can be seen in Figure 5.22a. Thus, the probed depth at normal emission is two times larger compared to grazing emission. According to ref.¹⁵⁸ the mean free path of C1s

electrons is estimated to be about 3.2 nm, indicating that the surface of the organic film is probed. The results of the angle-dependent measurements are summarized in Table 5.5. For the more bulk sensitive measurement at normal emission, the stoichiometry that fits very well to values expected from the atomic composition is obtained. However, in the case of the more surface sensitive measurement, a distinct decrease of nitrogen and fluorine content is visible, indicating a lower concentration of the dopant F4-TCNQ at the surface of the sample. Additionally, there is no evidence that subsequent annealing performed for 5 min at 120°C has an effect on the distribution of the elements. The inhomogeneous distribution of F4-TCNQ in the film could be a result of the well-known ability of this molecule to diffuse in an organic matrix.^{274, 278-279, 283}

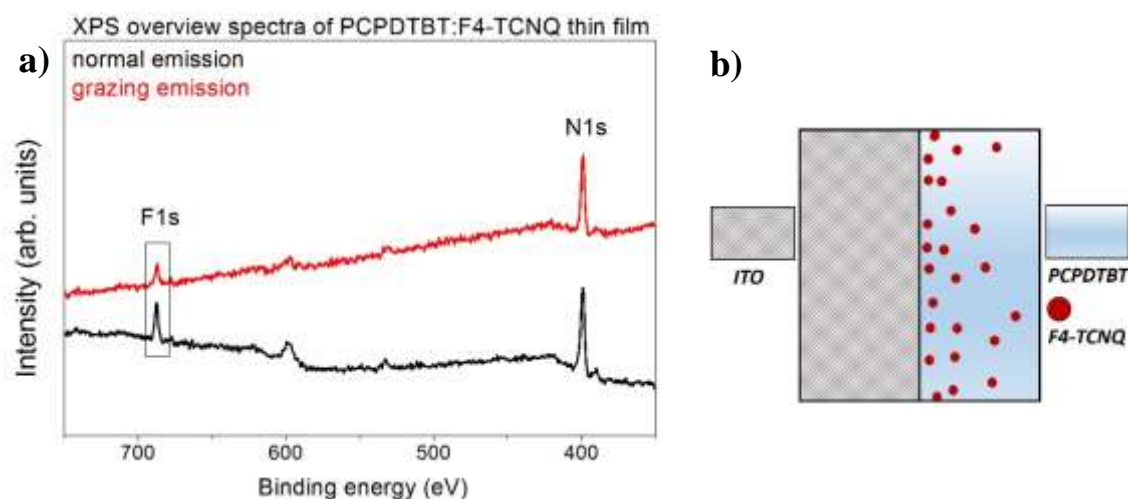


Figure 5.22: The XPS overview spectra (normalized at C1s signal) of 5% doped by F4-TCNQ thin film of PCPDTBT, taken at normal and grazing emission with marked F1s signals, are shown in (a). Sketch of the F4-TCNQ dopant distribution in a thin film of PCPDTBT, illustrating the depletion at the polymer surface, is shown in (b).

Hence, the higher concentration of F4-TCNQ closer to the interface with ITO substrate in combination with the favourable electronic structure of the polymer (HOMO = 4.8 eV) and dopant (LUMO = 5.24 eV) might be reasons for the observed effective doping at this interface. The distribution of F4-TCNQ is illustrated in Figure 5.22b. This behaviour is distinctly different from P3HT:F4-TCNQ and polyfuran:F4-TCNQ where not depletion but an enrichment of F4-

TCNQ was found on the polymer surface for the similar concentrations.^{237, 243} It seems that the structure and chemical properties of the conjugated polymer and dopant are important in this context, i.e. they determine the interaction between materials.²⁸⁴ It has been reported that in particular for PCPDTBT:F4-TCNQ intrinsic on-chain dipoles preserve F4-TCNQ from clustering.²⁷²

Table 5.5: Stoichiometry of the PCPDTBT:F4-TCNQ thin film presented in the relative atomic concentrations, expected from the chemical structure of the polymer monomer unit and dopant molecule, and two obtained values.

Element	C	S	N	F
Expected values	84.7	7.9	6.3	1.1
Normal emission $\varphi = 90^\circ$	85.6	7.6	5.8	1.0
Grazing emission $\varphi = 30^\circ$	86.9	7.8	4.9	0.4

Although the four LBG polymers which are the focus of this whole work, possess similarity in their chemical structures (especially within pairs), the F4-TCNQ doped P3HT films could be the example why the potential prediction of effects of the p-doping on the ELA of other three polymers could be misleading. Nonetheless, the p-doping of PCPDTBT with F4-TCNQ in a prototype planar heterojunction solar cell structure decreases significantly the energetic barrier at the interface to the electrode material ITO, whereas the energy level alignment to C₆₀ is not affected by doping. Since such barriers are expected to represent losses of the open circuit voltage in organic solar cells, a comparably weak molecular p-doping might improve the performance of devices based on these materials. A possible reason for this behaviour is the depletion of the dopant at the surface of the polymer film and homogeneous distribution in the bulk or even an enrichment at the interface to ITO.

5.3.2. Summary of Section 5.3.

The influence of p-doping of the donor material PCPDTBT polymer by F4-TCNQ, on the energy level alignment in a prototype organic solar cell structure with ITO as an anode and fullerene C₆₀ as an electron accepting material, was studied in this section. Firstly, as a reference, the thin film overlayer of fullerene C₆₀ was vacuum deposited onto the PCPDTBT/ITO system with VLA at the interface. After evaporation of the C₆₀ thin film, the VLA is again established, which is believed to be the consequence of the same alignment regime at the polymer/substrate interface. For the following solar cell structure C₆₀/PCPDTBT/ITO, the hole injection barrier of 1.0 eV is found at the polymer/substrate interface, which is expected to cause a significant contribution in losses of the open circuit voltage V_{OC}. Then, the C₆₀/PCPDTBT:F4-TCNQ/ITO system was prepared, where the thin film of PCPDTBT was 5 wt % p-doped with F4-TCNQ. As shown, after casting of the p-doped PCPDTBT thin film onto ITO, a large shift of E_{VL} was observed at the PCPDTBT/ITO interface, bringing interface dipole of 0.9 eV. Now, the Fermi level was found in the close proximity of the HOMO level of the polymer, at 4.7 eV below the vacuum level, and Δ_h was measured to be 0.1 eV, i.e. an almost Ohmic contact was created at the PCPDTBT/ITO interface. After evaporation of the fullerene C₆₀ overlayer, at the newly made C₆₀/PCPDTBT:F4-TCNQ interface, the vacuum level alignment was measured. The reason for this ELA scenario was found in E_F of the PCPDTBT:F4-TCNQ/ITO system being positioned between ICT levels of C₆₀. Therefore, it could be seen that upon p-doping of the donor polymer PCPDTBT, a significant change of ELA occurred at the donor/electrode interface, while the ELA at the acceptor/donor interface stayed the same in as in the case of the undoped film of PCPDTBT. This outcome could be beneficial for the performance of an OPV device, as it is shown to decrease Δ_h whilst preserving the photovoltaic gap Δ_{DA} intact. Substantial decrease of

Δ_h found for the p-doped film, which has not been seen in that magnitude for similar systems, was later elucidated via angle dependent XPS measurements. It was shown that a higher concentration of F4-TCNQ could be expected closer to ITO substrate, and could be the reason for the observed huge decrease of Δ_h , due to the effective doping at this interface. The section was summarized by the inference that the magnitude of (p-) doping effect, and consequent ELA of the doped polymer thin film in a solar cell structure, might substantially depend on the chemical structure of used polymer.

5.4. Self-organization properties of low band gap polymers in pristine and blend thin films

In the previous sections, the interaction energetics and following energy level alignment were scrutinized at donor/substrate, acceptor/substrate, and donor/acceptor interfaces. These sections aimed to explore the electronic structure of organic semiconducting materials, relevant for their interaction at interfaces throughout the whole OPV device, hence, important for the device work and performance. Nevertheless, beside from the high importance of the electronic structure of active materials and electrodes involved in the work of device, the orientation and ordering of the polymer backbone in the active layer of solar cells, have also huge importance. This is especially the case for the bulk heterojunction based (BHJ) solar cells, where the active material is a three-dimensional mixture (network) of the donor and acceptor compounds. The reason is that microscopic ordering of the donor (polymer) material has a significant influence on different processes, such as the exciton diffusion, charge separation, and charge carrier transport.^{118, 228, 285-286} Also, the polymer orientation relative to the donor/acceptor heterointerface might be an important parameter for/regarding the optimization of device

operation, hence efficiency overall.²⁸⁵ Recently, it has been shown via employing near edge X-ray absorption fine structure spectroscopy (NEXAFS) that for the workhorse polymer of community P3HT and also the widely studied PCPDTBT, a preferred orientation in the thin films can be inferred.⁹⁹ Also, it has been demonstrated that the addition of new thiadiazole moiety to PCPDTBT (leading to PCPDTBBT) causes an almost complete loss of the preferred orientation in thin films.²⁸⁷ Thus, it might be concluded that ability for self-organization of LBG polymers depends strongly on the chemical structure. Since the very good self-organization properties were found for poly(3-hexylthiophene) (P3HT),²⁸⁸⁻²⁹¹ the introduction of additional thiophene moieties might positively influence the ability for the ordering of LBG polymers in thin films.

In this section, the influence of the introduction of additional (hexyl)thiophene spacer rings on the ability for self-organization of low band gap polymers in the thin films, is studied. Addition of two thiophene rings to monomer structure of PCPDTBT leads to PCPDTTBTT, while the addition of a pair of hexylthiophene rings into the structure of PCPDTBBT gives the new structure of PCPDTTBTT. Moreover, the influence on the molecular orientation of blending with PCBM and post-processing thermal annealing, is probed.

5.4.1. Molecular orientation of low band gap polymers in pristine thin films – influence of introduction of additional thiophene moieties

Firstly, it will be discussed how the molecular orientation is affected by the introduction of additional thiophene moieties. For the polymer thin film, preferential molecular orientation implies the high degree of ordering due to the ability of self-organization. An appropriate approach to probe the molecular orientation of the π -conjugated moieties of the polymers is the

analysis of the dichroism of sulfur K-edge NEXAFS spectra.^{99, 287} In Figure 5.23, the angle dependent sulfur K-edge absorption spectra are presented for PCPDTBT (a) and PCPDTBBT (c), which will be further compared to PCPDTTBTT (b) and PCPDTTBTTT (d), respectively. Data for PCPDTBT and PCPDTBBT are taken from refs.^{99, 287} In the case of PCPDTTBTTT (Figure 5.23d) an obvious change of the peak shape with the change of the incidence angle of the incoming beam can be easily noticed, whilst it is much less evident for the PCPDTBBT counterpart (Figure 5.23c). On the other hand, for the “polymer pair” PCPDTBT and PCPDTTBTT, the angular dependence is more pronounced in the case of PCPDTBT (Figure 5.23a) than for the new structure PCPDTTBTT (Figure 5.23b) for which a loss of the dichroism is obtained. Observed weak dichroism can be a clear sign of the absence of preferred orientation in the thin film. However, we should have in mind that beside disorder, other ordered films with differently oriented molecules or an orientation close to the magic angle may also be responsible for the decrease or loss of dichroism.

In the following text, the shape of the S-K XAS spectra of PCPDTTBTT (Figure 5.23b) and PCPDTTBTTT (Figure 5.23d) will be analyzed in a more detailed manner. Similar to the spectra of related polymers based on thiophene and thiadiazole moieties: PCPDTBT, Si-PCPDTBT, PCPDTBBT and PSIF-DBT, four main components can be recognized in the energy region between 2470 and 2480 eV.^{4, 99, 287} On the other side, for the polymer P3HT, the spectrum is mainly determined by a single feature T_1 at 2473.8 eV.⁹⁹ Hence, features in the close vicinity to this energy in XAS spectra of LBG polymers can be regarded as thiophene-related, for PCPDTBT found at 2474.1 eV.²⁸⁷ Remaining peaks in the considered LBG polymers might originate predominantly from the electron withdrawing moieties, i.e. benzobisthiadiazole (BBT) and benzothiadiazole (BT). These features are labeled B_1 and B_2 in Figure 5.23 (b and d); shaded green (BBT) and orange (BT) in the corresponding chemical structure (see insets). In particular, for B_2 , a superposition with a thiophene related transition

cannot be ruled out. For feature C, a liable assignment to dominant contributions from a particular subunit is not evident. This kind of assignment of signals according to the part of the molecule from which signal is expected to originate is based on so-called building block approach. The building blocks approach is originally proposed for interpretation and analysis of the larger molecules NEXAFS spectra. In this semi-quantitative method, the NEXAFS spectra are envisioned by the superposition of spectra stemming from building blocks, i.e. from specific atomic groups (simplest is the diatom) where large molecules are viewed as an assembly of such building blocks. Hence, the method is frequently used for an interpretation of the polymer NEXAFS spectra, and followed by theoretical calculations brought considerable insight into understanding of such spectra chemical structure of studied materials.^{171, 292-293}

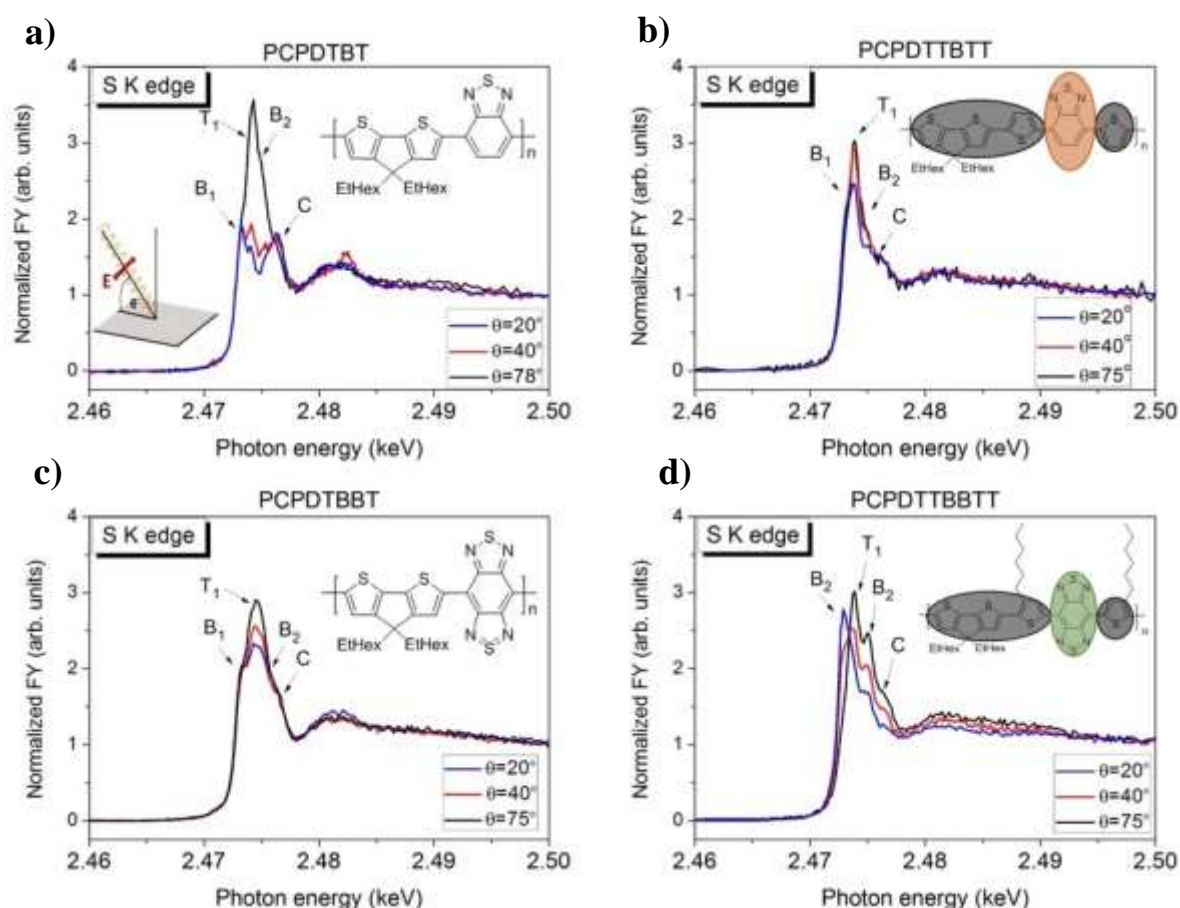


Figure 5.23: (a-d) The S1s excitation spectra of four low band gap polymer films on ITO as a function of the angle θ between the sample surface and direction of the (p-polarized) synchrotron light (see inset of a). The insets of b) and d) illustrate the origin of feature T₁ (thiophene related gray); features B₁ and B₂ are assigned to benzobisthiadiazole (green) and benzothiadiazole (orange). The figure is taken from the reference³.

The results of the peak fit analysis for PCPDTTBBTT and PCPDTTBTT are presented in Figure 5.24 close to normal incidence ($\theta=75^\circ$), for angle in between ($\theta=50^\circ$) and grazing incidence spectra ($\theta=15^\circ$). All NEXAFS spectra were normalized to the same step height and the analysis of the spectra was done by the peak-fit analysis software UNIFIT, using various peaks with the same Voigt profile and a special step background function.²⁹⁴ The step energy position is related to (represents) the ionization threshold energy and was estimated by summing the S1s binding energy and the work function Φ of the sample. The binding energies of S1s were deduced from the measured S2p binding energies assuming a constant energetic separation S1s to S2p of 2307.4 eV (as found for S₈).²⁹⁵ Because of the difference in the S2p binding energy for sulfur in thiophene and benzothiadiazole subunits, the background of the low band gap polymer is described by two step edges with fixed energy. The position of the step edges was determined to be 2475.7 and 2477.1 eV for PCPDTTBBTT, and 2475.8 and 2477.1 eV for PCPDTTBTT. Turning back to the result of the analysis, for the PCPDTTBBTT thin film the peak fit procedure brings following peak positions (energies of transition): B₁=2472.9 eV, T₁=2473.9 eV, B₂=2475.0 eV, C=2476.7eV, while for PCPDTTBTT B₁=2472.9 eV, T₁=2473.9 eV, B₂=2475.0 eV, C=2476.6 eV. The obtained transition energy for T₁ is in very good agreement with the expected values for thiophene moieties (see above); slight changes might be the result of the different chemical structure of the polymers. What can be noticed is that the obtained energies for B₁ and B₂ are exactly the same for the benzobisthiadiazole (BB) and benzothiadiazole (BT) moieties, indicating that the close chemical environment may determine the energy of transition in these cases. In Figure 5.24, where the angle-dependent intensities for the lowest lying transitions in S K NEXAFS spectra of PCPDTTBBTT and PCPDTTBTT as obtained from the peak fit analysis together with the $\cos^2\theta$ and $\sin^2\theta$ are recapped, it can be seen that the highest intensity of T₁ is found for both polymers at normal incidence (75°), particularly for PCPDTTBBTT where the data of T₁ follow well the $\sin^2\theta$ curve.

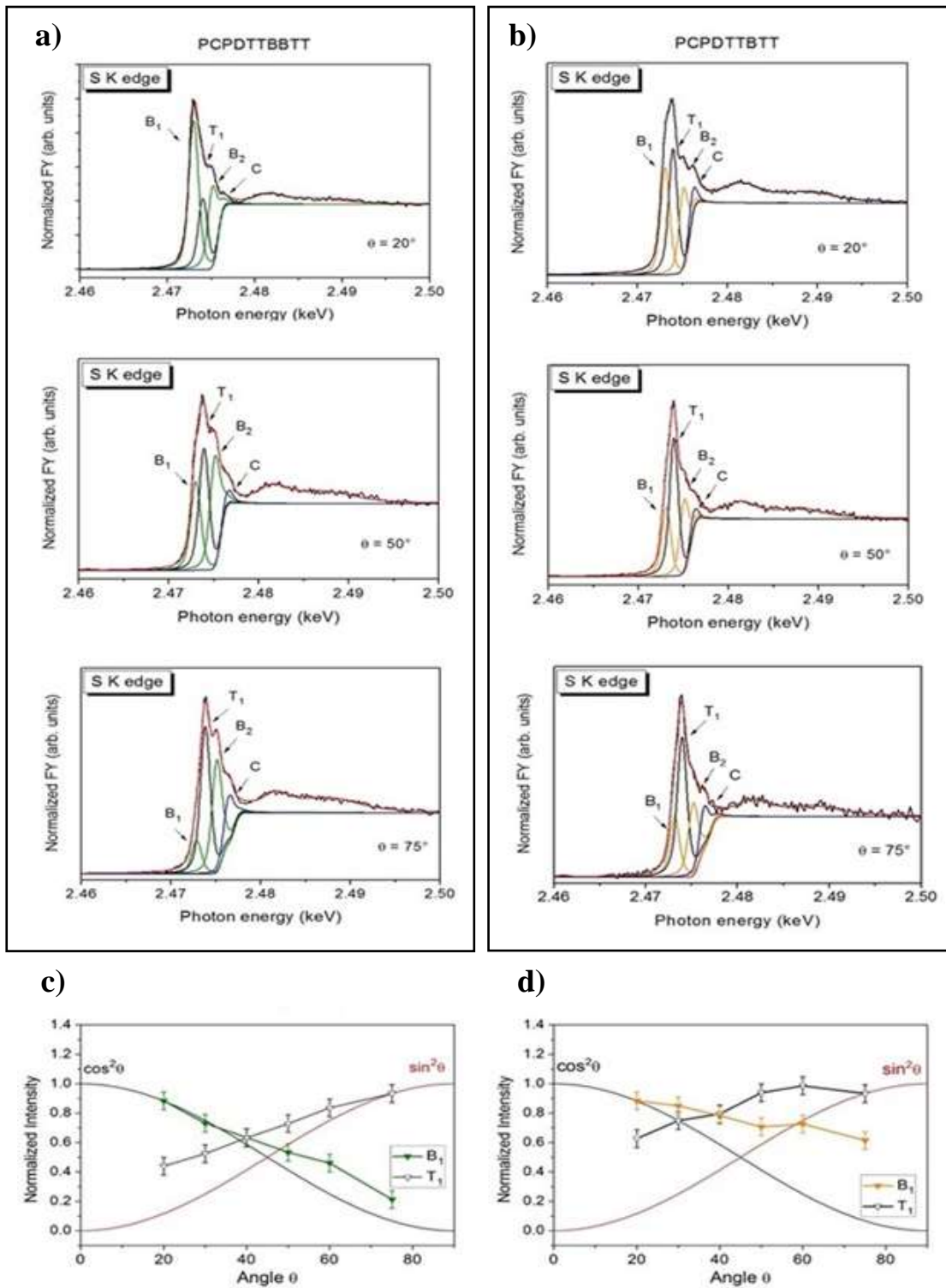


Figure 5.24: Example for a peak fit of S1s excitation spectra: (a) PCPDTTBTT and b) PCPDTTBTT films on ITO, with θ equals 20, 50 and 75 degrees. Peaks are coloured according to their origin from particular polymer subunits as shaded in corresponding insets (Fig 5.23b and d). Angular dependence of the intensity of T_1 and B_1 peaks shown in (c) and (d). The expected intensity profiles for out of plane transitions of perfectly lying and standing molecules are indicated by black ($\cos^2\theta$) and red ($\sin^2\theta$) lines, respectively. Assuming that T_1 corresponds to a transition polarized parallel to the polymer backbone, the data points for PCPDTTBTT follow well the curve expected for molecules with their π -conjugated backbone oriented perpendicular to the substrate surface. The figure is adapted from the reference³.

This indicates that the thiophene moieties of the polymer backbone are preferably oriented parallel to the sample surface, either “flat-lying” or “edge on”. In contrast, B_1 shows the reversed trend in comparison to T_1 for both polymers and increases with a decrease of the incidence angle, as visible from Figure 5.24 (c and d). This behaviour reminds on that found for PCPDTBT and Si-PCPDTBT polymers in the thin films.^{99, 287} The angular dependence of B_1 peak, which has maximal intensity at grazing incidence, points to a preferred flat lying or “face-on” orientation of the benzobisthiadiazole moieties. However, a distinct twist between BBT and all thiophene moieties is unlikely because such a twist would result in a strong reduction of the effective conjugation length and as a consequence in a poor efficiency of these materials in devices. Moreover, for PCPDTBT in the thin films has been found a remarkably high exciton diffusion length.²⁹⁶ Comparing PCPDTTBBTT and PCPDTTBTT, it is clearly visible that the data points for T_1 and B_1 in Figure 5.24 (c and d) tend to follow $\sin^2\theta$ and $\cos^2\theta$, respectively, as expected for molecules with a preferred orientation. Nonetheless, the variation of intensity is stronger in the case of PCPDTTBBTT indicating a preferred orientation of the backbone, thus a high degree of ordering. In contrast, for PCPDTTBTT the addition of thiophenes moieties without hexyl side chains results in a loss of the preferred orientation observed for PCPDTBT.

The empirical curve fitting has shown notable success in the determination of how much order is present in films and the molecular orientation of the polymer. Nonetheless, the calculations may additionally help with the identification of the angular dependence of transitions and their potential overlapping. Calculations based on Density Functional Theory (DFT) are now at a stage where this can be attempted for closed shell systems. Hence, for the sake of better understanding of the molecular orientation, for polymers PCPDTBT and PCPDTTBBTT which have shown high degree of ordering in the thin film, two fits: an orthogonal two component tilt single film and three film simple texture model, are performed.⁴ The theoretical analysis was

essentially done by Dr. David Batchelor from ANKA synchrotron light source facility at Karlsruhe Institute of Technology, but discussed together within our team. From the calculations might be inferred that intensity around T_1 is mainly polarized in the plane, parallel to the polymer backbone (denoted x'), i.e. their intensity is a maximum if the electric field vector E of the radiation is parallel to the polymer chain. In contrast, the intensity close to B_1 is mainly defined by out of plane transitions (z') and in the energy range of B_2 in plane transitions, perpendicular to the backbone (y') were observed (see ref.⁴). Used axis can be seen in Figure 5.25. Assuming 100% linear polarization of the incoming light and a perfect “edge-on” orientation of the polymer chain, the angular dependence of T_1 transition should follow a simple $\sin^2\theta$ function and a $\cos^2\theta$ dependence is expected for z' polarized transitions (B_1), supporting findings obtained above from the empirical curve fitting of the data (compare with ref.¹⁷¹).

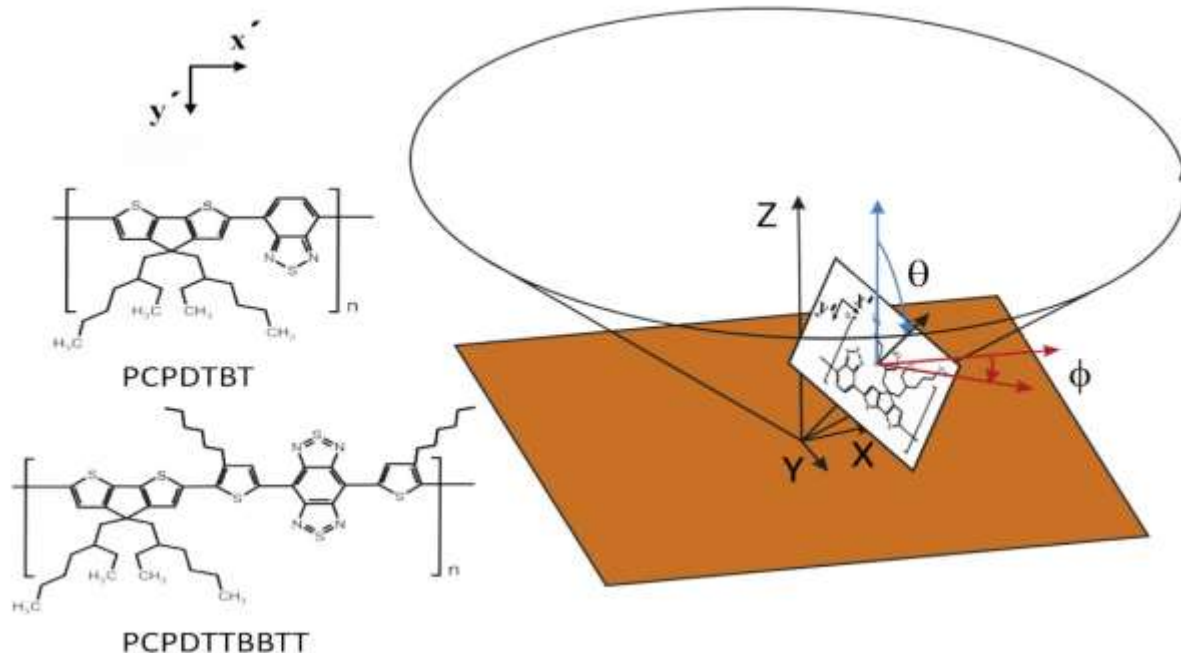


Figure 5.25: Polymers for which DFT calculations and fits to experimental data have been done, PCPDTBT and PCPDTTBTT, are shown on the left side of figure. The axes relevant to the calculations are shown on the right side drawing; the z' axis is out of the plane of the paper and y' axis down the page. Diagram illustrating the rotation (ϕ) and tilt (θ) with respect to the surface normal (Z) and X axis used for the modelling. Text and figure are adapted from the reference⁴.

Detailed analysis of simulated spectra for different polarizations has shown a preferred “face-on” orientation for PCPDTTBBTT, hence, it is in agreement with the discussion above. On the other side, for PCPDTBT polymer, calculations have shown equal amounts of “face-on” and “edge-on” orientations.⁴

Hence, turning back to the thin films of PCPDTTBBTT and PCPDTTBT polymers, the higher degree of orientation was found for the former polymer. This observation might be further supported by AFM measurements. The AFM today is frequently used for the morphology studies of the polymer thin films, allowing insight into the correlation between preparation procedure (usage of different solvents, additives, post-deposition thermal annealing, and etc.) and morphology, which is of crucial importance for the performance of the semiconductive π -conjugated polymers as materials applied in organic electronic device. Being initially developed for probing non-conductive surfaces, modern AFM provides three-dimensional topography at sub-nanometer of conductors and insulators (even biological samples), in the air or under vacuum, having a lateral resolution around 1 nm and vertical resolution at sub-angstrom level. The AFM images of the thin films of four polymers are shown in Figure 5.26, where can be seen that the grain-like structures, which can be interpreted as crystallites, are visible only for PCPDTTBBTT and PCPDTBT. Thus, the conclusion is that the introduction of hexylthiophene for PCPDTBBT/PCPDTTBBTT results in better ordering, whereas for PCPDTBT/PCPDTTBT the ordering is practically lost after the introduction of thiophene. Here it should be mentioned, that for P3HT was reported how/that the molecular weight can affect the crystallinity of polymers to certain extent.^{94, 297} However, in neat P3HT, films the fraction of the aggregated polymer over the total polymer varied only by about 5 % for a broad range of the molecular weight ($M_w=11-91$ kg/mol).²⁹⁷ Therefore, in the case presented here a conclusion may be that the alkyl chains might play a leading role in the orientation and ordering in thin films. On the other side, the addition of thiophene spacer rings without hexyl side chains

might affect the rigidity of the polymer backbone leading to a loss of the preferred molecular orientation in thin films. In general, the interplay between chemical structure and the tendency for self-organization is complex and still under investigation. Furthermore, it was shown that the length and position of side chains have a significant impact on the self-organization behaviour of polymers in the thin films.²⁵ Thus, from the presented data, we may conclude that in particular the introduction of alkylthiophene moieties is a promising way to optimize the orientation and ordering in thin films.

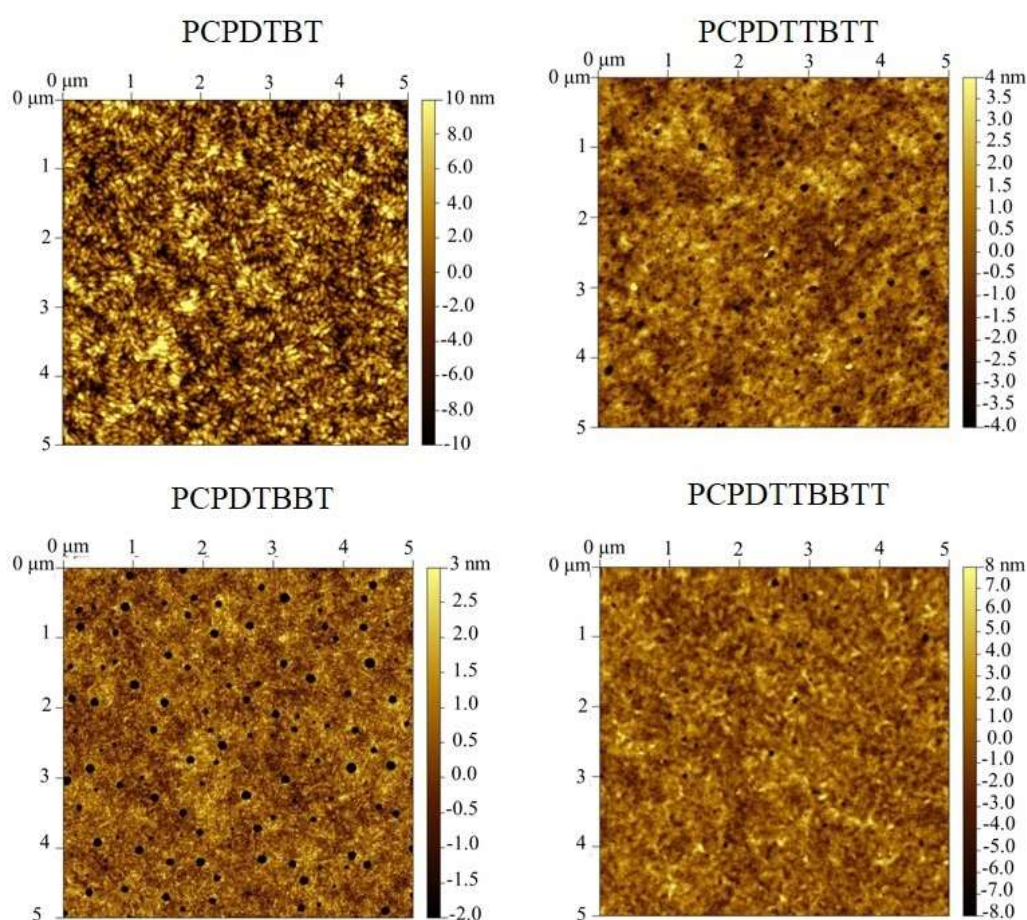


Figure 5.26: The AFM images (taken in tapping mode) of the two polymer pairs PCPDTBT & PCPDTTBTT (top) and PCPDTBBT & PCPDTTBTT (bottom). Pronounced crystalline structures are visible for PCPDTTBTT and PCPDTBT, only. Thus, the introduction of hexylthiophene for PCPDTBBT/PCPDTTBTT results in a higher ordering, whereas the ordering is practically lost after the introduction of thiophene to PCPDTBT. The crystallinity appears to correlate well with the preferred orientation found by NEXAFS. In presented images, a presence of holes in the thin films might be deduced. However, we believe that the presence of holes do not substantially affect the message we want to convey about the morphology of prepared films. The images were taken in tapping (non-contact) mode at a high-resolution multimode AFM device NanoScope IIIa. The figure is taken from the reference³.

5.4.2. Molecular orientation of PCPDTTBTT and PCPDTTBTT polymers in 1:1 blend films with PCBM – the effect of blending

As commented in the preceding section, for the application of LBG polymers in BHJ based solar cells, their properties and behaviour in the active layer (donor-acceptor blend) are of high significance. Therefore, the impact of mixing with the fullerene PCBM (ratio 1:1) on the molecular orientation of the two polymers PCPDTTBTT and PCPDTTBTT, is studied. In Figure 5.27 angle dependent S K edge absorption spectra for PCPDTTBTT/PCBM and PCPDTTBTT/PCBM blends are shown together with the evaluation of the intensity of T_1 and B_1 .

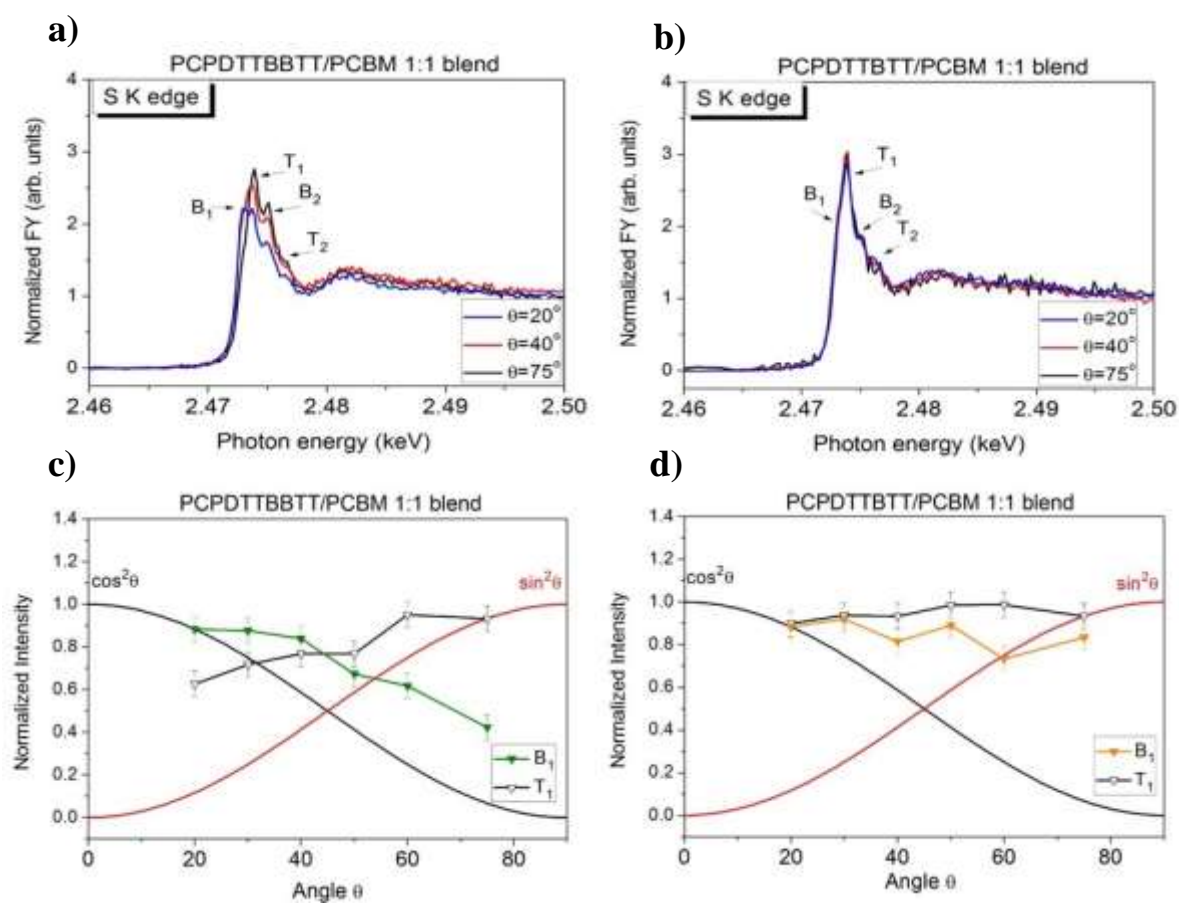


Figure 5.27: The S1s excitation spectra of PCPDTTBTT and PCPDTTBTT in blend films with PCBM (1:1) as a function of θ (a and b). The angle dependence of the intensity for T_1 and B_1 (cf. Fig. 5.51) is summarized in (c and d). Generally, the dichroism is less pronounced after blending with PCBM pointing to a weaker ability for self-organization.

For the PCPDTTBTT/PCBM blend, the change of the peak shape and the trend of data points are reminiscent to that of the pure polymer (cf. Figure 5.23c), but with clearly weaker dichroism. Thus, in spite of that the presence of PCBM molecules disrupt the π - π interaction of polymer chains, the preferred orientation of PCPDTTBTT is at least partially preserved. On the other hand, the (weaker) dichroism of pristine PCPDTTBTT (cf. Figure 5.23d) is hardly visible in the PCPDTTBTT/PCBM blend. This indicates that the blending with PCBM most likely weakens self-organization properties of the polymers. This conclusion is in good agreement with what was found for related polymer systems PCPDTBT and PCPDTBBT (as well as P3HT), utilizing NEXAFS and complementary methods, such as X-ray diffraction.^{287, 298} Previously reported structural investigations upon blend films, utilizing NEXAFS spectroscopy and X-ray diffraction method^{287, 298-300} showed that introduced PCBM prevents self-organization of polymers which appear then disordered (amorphous polymer/PCBM domains were found).²⁸⁷ In general, it can be concluded that blending with fullerene derivative PCBM results in weaker preferred molecular orientation of polymers PCPDTTBTT and PCPDTTBTT in the blend thin films, which is similar to what is found for LBG polymers previously studied.²⁸⁷

5.4.3. The effect of post-deposition thermal annealing on molecular orientation of PCPDTTBTT and PCPDTTBTT polymers in pristine and blend films

The post-deposition annealing is a proven method for tailoring the morphology of the BHJ active layer thin film through separation and reorganization of the donor and the acceptor

phases,³⁰¹⁻³⁰² it has been demonstrated to improve the long-range order and thus hole transport within the polymer,^{120, 303-304} and consequently increases the photovoltaic efficiency of BHJ based OPVs.^{120, 305-308} It has been shown for related blend systems that the dichroism of the sulfur absorption edge increases upon annealing, finally comparable to the pure polymer.²⁸⁷ Hence, here will be discussed in more detail how the post-process annealing influences molecular orientation and self-ordering of polymers PCPDTTBTT and PCPDTTBTT in neat and blend films. In Figure 5.28 are presented angle dependent S K excitation spectra of PCPDTTBTT and PCPDTTBTT after annealing at 120 °C, and evaluation of B_1 and T_1 intensities of the latter two spectra.

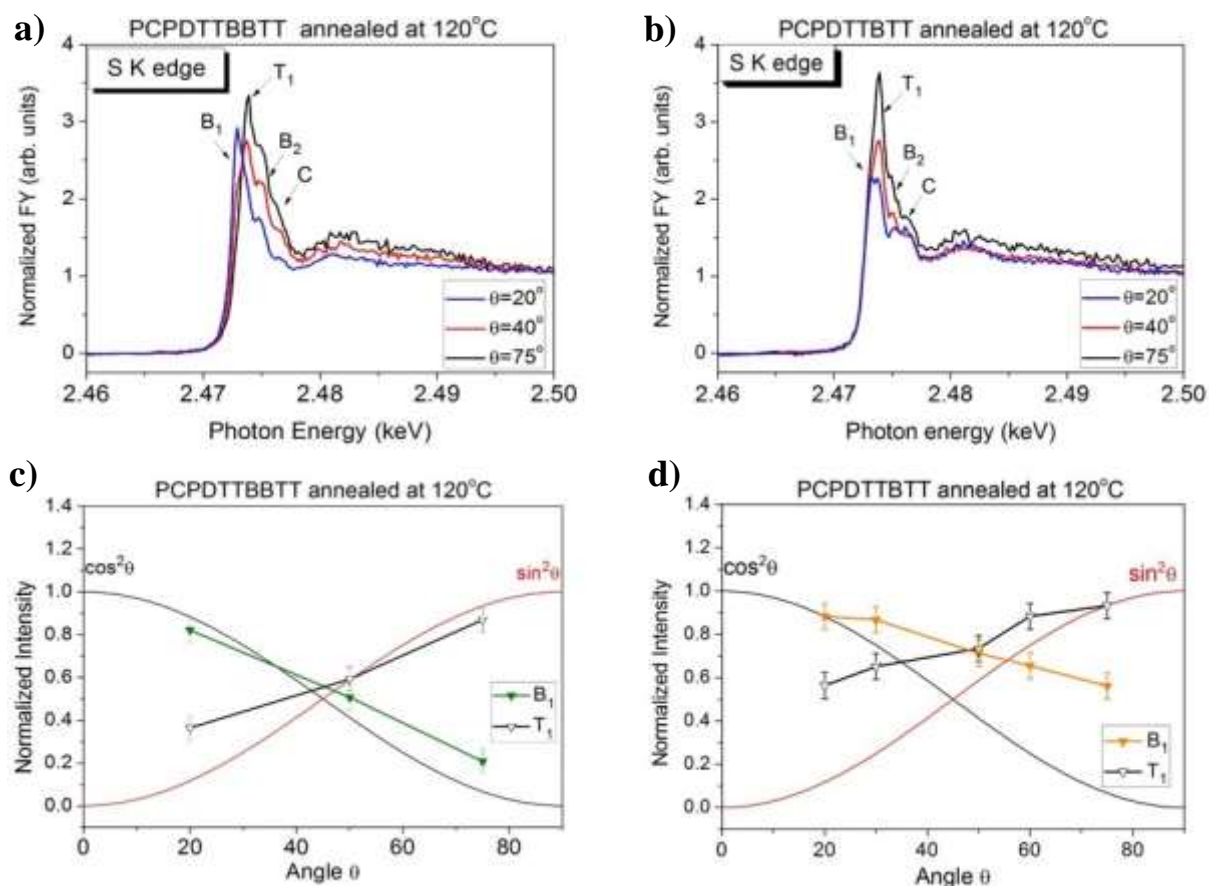


Figure 5.28: The S1s excitation spectra of PCPDTTBTT and PCPDTTBTT films annealed at 120 °C as a function of angle θ (a and b). The angle dependence of the intensity for T_1 and B_1 is summarized in (c and d).

It can be clearly seen, that the angular dependence of B_1 and T_1 features for both polymers is very similar to the situation before annealing (cf. Figure 5.23c and 5.23d) indicating only minor changes of the molecular orientation. Still, the small improvement of molecular orientation is noticeable for the PCPDTTBTT film. Furthermore, it will be discussed how the post-deposition annealing affects an ordering and orientation of polymer in the blend, for PCPDTTBTT/PCBM and PCPDTTBTT/PCBM blends with 1:1 ratio. In Figure 5.29 can be seen S-K absorption spectra of the PCPDTTBTT/PCBM blend 1:1 sample as deposited and corresponding blend samples annealed at 120°C, and 180°C.

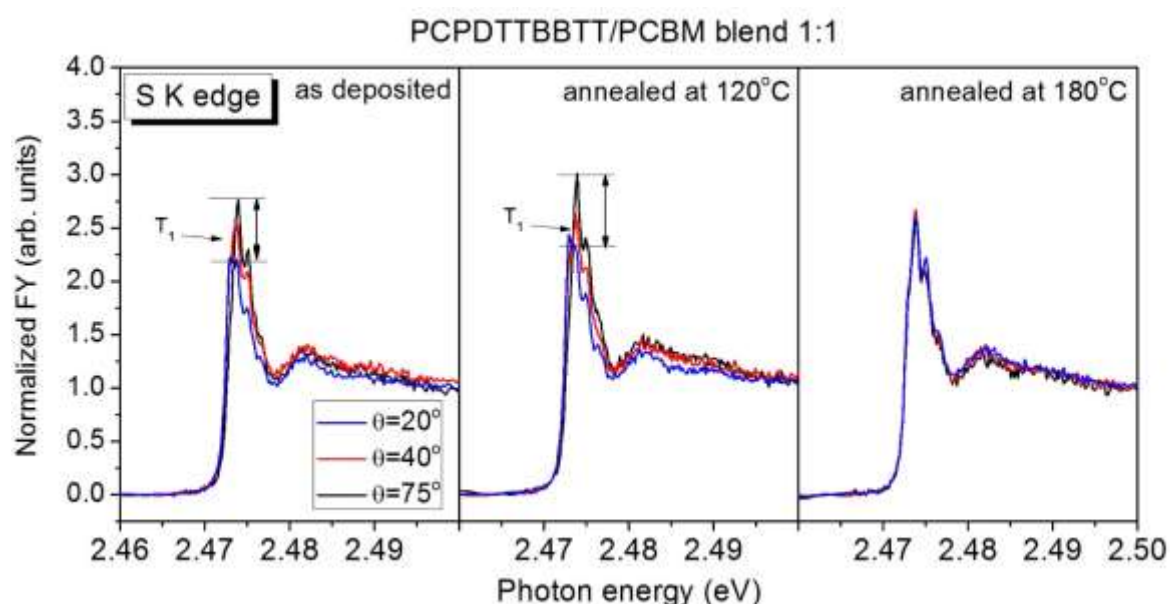


Figure 5.29: Angle dependent S K excitation spectra of PCPDTTBTT:PCBM 1:1 blends before annealing and after annealing to 120 °C and 180 °C. The figure is adapted from the reference³.

After the annealing at 120°C minor changes can be observed in the spectra, therefore, the annealing at 120°C has an only minor influence on the preferred orientation of π -conjugated system of PCPDTTBTT in the blend film. Thus, the degree of orientation is still lower comparing to the neat material thin film. Phase separation and the diffusion of molecules in the blend are necessary for an improvement of the orientation and ordering. Also, the temperature of annealing which may improve the molecular orientation of polymer under consideration might be significantly higher than 120°C; an important parameter in this context is e.g. the respective

glass transition temperature, which is not known for materials presented here. Nevertheless, after the second annealing step at 150°C (not shown here) no further changes can be observed, and upon the last annealing step at 180°C complete loss of the orientation happens. The reason for the weak improvement of polymer ordering in the blend after annealing steps at 120°C and 150°C may be found in the polymer matrix of PCPDTTBBTT which preserves diffusion of fullerene PCBM molecules. Succeeding complete loss of the angular dichroism of the absorption spectra, hence loss of orientation, after annealing at 180°C might be explained by the occurrence of a degradation of the polymer which happens due to potentially too high temperature used for the annealing process. The same experiment was performed for the PCPDTTBBTT/PCBM 1:1 blend shown in Figure 5.30, and upon thermal annealing at three temperatures 120°C, 150 °C (not shown here) and 180 °C no effect on the angular dependence of the absorption spectra, hence, no improvement of ordering can be observed in the case of PCPDTTBBTT.

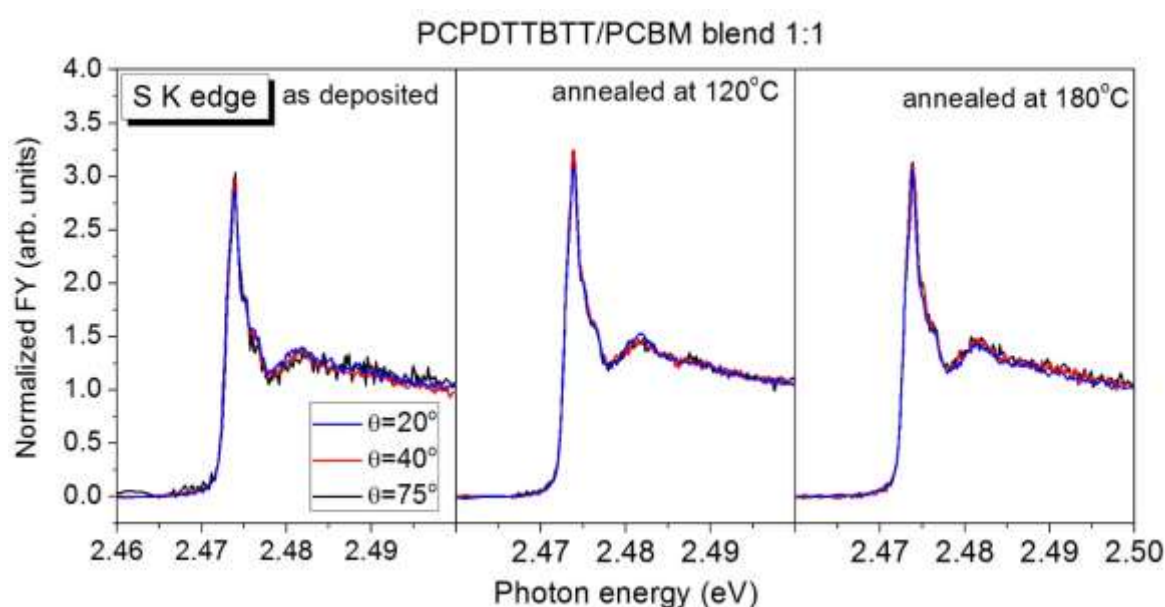


Figure 5.30: Angle dependent S K excitation spectra of PCPDTTBBTT:PCBM 1:1 blend films before annealing and after annealing to 120 °C and 180 °C. The figure is adapted from the reference³.

An explanation could be that even higher temperature than 180°C is necessary for the improvement of ordering for the polymer in the blend film, nevertheless, what can be clearly seen from everything afore presented is that PCPDTTBTT in general shows very weak degree of orientation in the thin films. On the other hand, the related polymer PCPDTBT in 1:1 blend with PCBM, has shown to be much more sensitive to the annealing process. Apparent changes in the dichroism of spectra after annealing step at 150°C and even further at 175°C, may indicate about improved molecular ordering of PCPDTBT film, similar to the neat film.²⁸⁷ Therefore, the summary of this section is, that the annealing of PCPDTTBTT and PCPDTTBTT thin films as well as of the corresponding blends with PCBM, results only in minor changes in the molecular orientation and ordering in the thin films.

5.4.4. Summary of Section 5.4.

In this chapter, the influence of the introduction of additional (hexyl)thiophene subunits in LGB polymers on the molecular orientation in the thin films, was studied. Concretely, the effect of the introduction of additional hexylthiophene spacer rings in the case of PCPDTBBT and PCPDTTBTT polymer pair, and thiophene rings without alkyl side chains for PCPDTBT and PCPDTTBTT pair, was studied. Obtained results show that in the case of BBT polymer pair, that the dichroism of the NEXAFS spectra is more pronounced after the introduction of additional hexylthiophene spacer rings, whereas introduction of thiophene in the case of BT polymer pair cause an almost complete loss of the preferred orientation. It was commented that the presence of the alkyl side chains might have a substantial influence on the self-organization ability of polymers in the thin films. The blending with PCBM in 1:1 ratio, was shown to inhibit the self-organization properties of both polymers, which is good agreement with NEXAFS experiments previously performed on PCPDTBT and PCPDTBBT.^{99, 287} The post-deposition

annealing of the thin films of PCPDTTBBTT and PCPDTTBTT, along with corresponding blends was performed. The XAS experiments showed that the annealing has a small influence on the orientation of the polymers, resulting in only minor changes. Therefore, the conclusion might be drawn that the introduction of alkyl-thiophene moieties shows an encouraging potential to be utilized as the method to optimize film forming properties in the thin films of LBG polymers.

Chapter 6

General summary

The donor-acceptor (D-A) conjugated copolymers have gained huge interest in recent years for the application in organic photovoltaic cells. Through the fine molecular and supramolecular design, the chemical structure of polymers can be finely tuned in order to adjust their electronic structure and ordering properties in the solid state (thin films), hence, improve their performance in devices. The goal of the presented study was to correlate the difference in chemical structure within LBG polymer pairs PCPDTBT & PCPDTTBTT and PCPDTBBT & PCPDTTBTT and in between them, with their electronic structure, interaction at different interfaces and self-organization properties in the thin films.

Accordingly, the Chapter 5 named Results and Discussion is divided into four parts:

1. donor/electrode interfaces
2. donor/acceptor interfaces in PHJ and BHJ
3. influence of the p-doping on donor/electrode and donor/acceptor interfaces
4. molecular orientation of polymers in the neat and blend thin films

In the first part, UV-Vis-NIR spectroscopy measurements showed that polymer pair PCPDTBBT and PCPDTTBTT have about twice narrower optical band gaps than the

counterparts PCPDTBT and PCPDTTBTT, respectively. This outcome was subscribed to the presence of stronger electron withdrawing subunit BBT in the chemical structure of former polymers. Hence, it was further discussed that the electronic band gap (HOMO-LUMO gap) is also expected to be lower for the BBT-holding polymer pair. On the other hand, within one polymer pair, optical band gaps show very similar values, not substantially affected by the difference in the chemical structure of two polymers, hence, it is expected that E_g holds similar values for two polymers. The photoemission measurements showed that the ionization potential (IP) within one polymer pair is the same. However, different IP values were measured between two polymer pairs, which was again subscribed to the presence of different electron accepting subunit in their structures. Next, the thin film of PCPDTTBTT shows the FLP regime with the same parameters as PCPDTBT at the interfaces with two substrates with highest work functions, which can suggest that the difference in their chemical structure between them does not have substantial influence on the electronic structure (the HOMO and derived state positions) of these polymers relevant for the application in OPVs as donor materials. On the other side, it was found that the ELA scenarios with two substrates with the lowest work functions, where the LUMO level position is expected to be an important parameter for the determination of ELA (interaction) at the interface, is different for PCPDTBT (VLA) and PCPDTTBTT (FLP). For the BBT polymer pair, the FLP regime is found for both polymer thin films prepared on five used substrates. In all cases, the substrate E_F is found pinned in the middle of band gaps of polymers, at positions recognized as negative and positive polaronic levels, which show similar values. All these ELA outcomes suggest that PCPDTBBT and PCPDTTBTT indeed have the ultralow band gaps which can be interesting for their application in OPV devices.

In the second part, interfaces made by the organic acceptors, fullerene C_{60} and PCBM were explored firstly. Thin films of the latter two molecules were prepared on several substrates in

order to assess their electronic structure important for the ELA of these as acceptor materials. Then, the donor/acceptor interface in planar and bulk heterojunctions was studied. For that purpose, firstly, the thin film of fullerene C_{60} was deposited onto three PCPDTTBTT/electrode stacks. After the study of three C_{60} /PCPDTTBTT interfaces, an important thing might be concluded, that the E_F pinning in PCPDTTBTT prepared on PEI/ITO and ZnO is rather induced by trap states within the polymer band gap than the LUMO derived states, which is further indirectly supported by NEXAFS measurements. Thereafter, the donor/acceptor interfaces are created by deposition of fullerene C_{60} onto the PCPDTBBT covered PEI/ITO and AuO_x/Au substrates. Obtained information support the idea about ultralow band gap in polymers with BBT subunit. For the presented donor/acceptor interfaces in PHJ, it was found that ELA of these is highly affected/determined by the ELA at donor/substrate interface. Generally, it was shown that the ELA and energetics at all studied PHJ interfaces are well explainable by the ICT model for weakly interacting interfaces. On the other hand, the ELA regimes in studied PCPDTBT:PCBM blends are found to be not easily interpretable via ICT model, and different than what had been expected from the separate experiments with neat materials. Different ELA of the polymer and PCBM in blend, might be understood as a result of the blending/mixing of materials, more precisely, different electrostatic environment (interaction between materials) in BHJ than in PHJ.

The next part dealt with the p-doping of PCPDTBT by F4-TCNQ molecule, i.e. with its effect on ELA in a prototype organic solar cell structure prepared with ITO (anode) and fullerene C_{60} (acceptor material). Unfavourable ELA scenario for the device functioning depicted in the large Δ_h at the PCPDTBT/ITO interface, was found to be much improved at the PCPDTBT:F4-TCNQ/ITO interface, where quasi-Ohmic contact between the donor material and electrode is perceived. Additionally, it was demonstrated that doping of the donor material does not have an influence on the ELA with the acceptor material. Also, the measurements showed that F4-

TCNQ is accumulated closer to the interface with the ITO substrate than the surface of polymer film, which might be the reason for successful doping at the latter interface.

In the last part, the implications of the difference in chemical structure within polymer pairs on the molecular orientation of these in the thin films, were explored by NEXAFS spectroscopy. It is found that addition of hexylthiophene spacer rings to PCPDTBBT which leads to the new structure of PCPDTTBBTT polymer, also leads to the improved self-orientation properties in the thin film of the new polymer. On the other side, the introduction of thiophene rings without alkyl side chains into the structure of PCPDTBT giving PCPDTTBTT, had opposite effect on the molecular orientation of the derived polymer. The conclusion was made that the presence of side chains may have a strong influence on self-organization ability of polymers in the thin films. Further, the self-organization of PCPDTTBBTT and PCPDTTBTT in the blend films were hindered by the presence of PCBM, which had been earlier demonstrated for other two polymers PCPDTBT and PCPDTBBT. Finally, the post-deposition annealing of the thin films of PCPDTTBBTT and PCPDTTBTT along with corresponding blend films with PCBM, was performed, resulting in only minor improvements of the orientation of the polymers.

The experimental results shown in this thesis raise additional questions for the future investigation. One of them is the effect of the different side chains (in polarity, structure, length, position and etc.) on the electronic structure and self-organization properties of the same polymer backbone. Moreover, an influence of the doping (with different kind of dopants), on the polymer thin film morphology, electronic structure, and interaction at interfaces, ought to be further scrutinized. By answering these questions, important new avenues towards a deeper understanding of the interplay between the chemical structure on the one side, and electronic and structural properties of conjugated polymers in the thin films on the other, might be opened.

Appendix

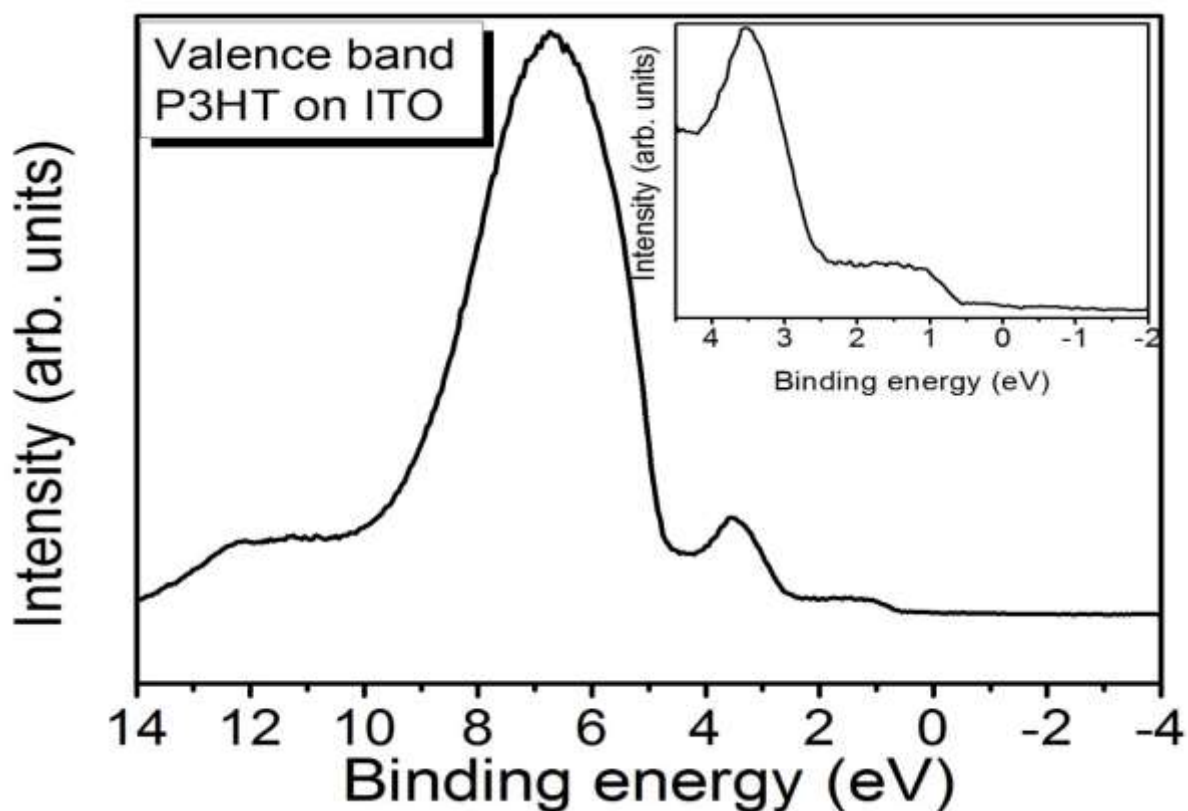


Figure A1: UPS valence band spectrum of P3HT thin film prepared on ITO. Inset presents zoom in into the HOMO onset region of the spectrum. Extended spectral feature with lower binding energy (between approximately 0.5 and 2.5 eV) is subscribed to delocalized frontier π -band, which originates mainly from C 2p and partly from S 3p atomic orbitals. On the other side, signal at around 3.5 eV is expected to stem from localized π -band. This localized π -state is composed of S3p and less of C2s atomic orbitals.

References:

1. Friedrich, R.; Stefan, H., Photoemission Spectroscopy—from Early Days to Recent Applications. *New Journal of Physics* **2005**, *7*, 97.
2. Franciosi, A.; Van de Walle, C. G., Heterojunction Band Offset Engineering. *Surface Science Reports* **1996**, *25*, 1-140.
3. Ivanović, M., et al., Electronic Structure and Self-Organization Properties of Low Band Gap Polymers: The Effect of the Introduction of Additional Thiophene Moieties. *Solar Energy Materials and Solar Cells* **2016**, *157*, 286-294.
4. Batchelor, D. R.; Aygül, U.; Dettinger, U.; Ivanovic, M.; Tournebize, A.; Mangold, S.; Forster, M.; Scherf, U.; Peisert, H.; Chassé, T., Insight into the Orientation of Lbg Polymer Films by Xanes Experiment and Calculation. *European Polymer Journal* **2016**, *81*, 686-693.
5. Chiang, C. K.; Fincher, C. R.; Park, Y. W.; Heeger, A. J.; Shirakawa, H.; Louis, E. J.; Gau, S. C.; MacDiarmid, A. G., Electrical Conductivity in Doped Polyacetylene. *Physical Review Letters* **1977**, *39*, 1098-1101.
6. Shirakawa, H.; Louis, E. J.; MacDiarmid, A. G.; Chiang, C. K.; Heeger, A. J., Synthesis of Electrically Conducting Organic Polymers: Halogen Derivatives of Polyacetylene, (Ch). *Journal of the Chemical Society, Chemical Communications* **1977**, 578-580.
7. Jun, T.; Akio, T.; Kikuko, K., Structure and Electrical Properties of Polyacetylene Yielding a Conductivity of 10⁵ S/Cm. *Japanese Journal of Applied Physics* **1990**, *29*, 125.
8. Tsukamoto, J., Recent Advances in Highly Conductive Polyacetylene. *Advances in Physics* **1992**, *41*, 509-546.
9. Friend, R. H., et al., Electroluminescence in Conjugated Polymers. *Nature* **1999**, *397*, 121.
10. Burroughes, J. H.; Bradley, D. D. C.; Brown, A. R.; Marks, R. N.; Mackay, K.; Friend, R. H.; Burns, P. L.; Holmes, A. B., Light-Emitting Diodes Based on Conjugated Polymers. *Nature* **1990**, *347*, 539.
11. Brown, A. R.; Greenham, N. C.; Gymer, R. W.; Pichler, K.; Bradley, D. D. C.; Friend, R. H.; Burn, P. L.; Kraft, A.; Holmes, A. B., Conjugated Polymer Light-Emitting Diodes. In *Intrinsically Conducting Polymers: An Emerging Technology*, Aldissi, M., Ed. Springer Netherlands: Dordrecht, 1993; pp 87-106.
12. Ellen, M., Conjugated Polymer Blends: Linking Film Morphology to Performance of Light Emitting Diodes and Photodiodes. *Journal of Physics: Condensed Matter* **2002**, *14*, 12235.
13. Yu, G.; Gao, J.; Hummelen, J. C.; Wudl, F.; Heeger, A. J., Polymer Photovoltaic Cells: Enhanced Efficiencies Via a Network of Internal Donor-Acceptor Heterojunctions. *Science* **1995**, *270*, 1789-1791.
14. Brabec, C. J.; Sariciftci, N. S.; Hummelen, J. C., Plastic Solar Cells. *Advanced Functional Materials* **2001**, *11*, 15-26.
15. Hoppe, H.; Sariciftci, N. S., Organic Solar Cells: An Overview. *Journal of Materials Research* **2011**, *19*, 1924-1945.
16. Sirringhaus, H.; Tessler, N.; Friend, R. H., Integrated, High-Mobility Polymer Field-Effect Transistors Driving Polymer Light-Emitting Diodes. *Synthetic Metals* **1999**, *102*, 857-860.
17. Sirringhaus, H.; Kawase, T.; Friend, R. H.; Shimoda, T.; Inbasekaran, M.; Wu, W.; Woo, E. P., High-Resolution Inkjet Printing of All-Polymer Transistor Circuits. *Science* **2000**, *290*, 2123-2126.
18. Sirringhaus, H., Device Physics of Solution-Processed Organic Field-Effect Transistors. *Advanced Materials* **2005**, *17*, 2411-2425.
19. Benavides, C. M., et al., High-Performance Organic Photodetectors from a High-Bandgap Indacenodithiophene-Based π -Conjugated Donor-Acceptor Polymer. *ACS Applied Materials & Interfaces* **2018**, *10*, 12937-12946.

20. Hide, J. G. F.; Wang, H., Efficient Photodetectors and Photovoltaic Cells from Composites of Fullerenes and Conjugated Polymers: Photoinduced Electron Transfer. *Synthetic Metals* **1997**, *84*, 979-980.
21. Potyrailo, R. A.; Nagraj, N.; Tang, Z.; Mondello, F. J.; Surman, C.; Morris, W., Battery-Free Radio Frequency Identification (Rfid) Sensors for Food Quality and Safety. *Journal of Agricultural and Food Chemistry* **2012**, *60*, 8535-8543.
22. Singh, R.; Singh, E.; Nalwa, H. S., Inkjet Printed Nanomaterial Based Flexible Radio Frequency Identification (Rfid) Tag Sensors for the Internet of Nano Things. *RSC Advances* **2017**, *7*, 48597-48630.
23. Facchetti, A., Π -Conjugated Polymers for Organic Electronics and Photovoltaic Cell Applications. *Chemistry of Materials* **2011**, *23*, 733-758.
24. Chong, L.-W.; Chou, Y.-N.; Lee, Y.-L.; Wen, T.-C.; Guo, T.-F., Hole-Injection Enhancement of Top-Emissive Polymer Light-Emitting Diodes by P3ht/Fnab Modification of Ag Anode. *Organic Electronics* **2009**, *10*, 1141-1145.
25. Bolognesi, A.; Botta, C.; Mercogliano, C.; Marinelli, M.; Porzio, W.; Angiolini, L.; Salatelli, E., Oriented Thin Films from Soluble Polythiophenes. *Polymers for Advanced Technologies* **2003**, *14*, 537-543.
26. Ohkita, H., et al., Charge Carrier Formation in Polythiophene/Fullerene Blend Films Studied by Transient Absorption Spectroscopy. *Journal of the American Chemical Society* **2008**, *130*, 3030-3042.
27. Hamadani, B. H.; Gundlach, D. J.; McCulloch, I.; Heeney, M., Undoped Polythiophene Field-Effect Transistors with Mobility of $1\text{cm}^2\text{v}^{-1}\text{s}^{-1}$. *Applied Physics Letters* **2007**, *91*, 243512.
28. Jahnke, A. A.; Djukic, B.; McCormick, T. M.; Buchaca Domingo, E.; Hellmann, C.; Lee, Y.; Seferos, D. S., Poly(3-Alkyltellurophene)S Are Solution-Processable Polyheterocycles. *Journal of the American Chemical Society* **2013**, *135*, 951-954.
29. Patra, A.; Bendikov, M., Polyselenophenes. *Journal of Materials Chemistry* **2010**, *20*, 422-433.
30. Bredas, J.-L., Mind the Gap! *Materials Horizons* **2014**, *1*, 17-19.
31. Sensfuss, S. A.-I., M., Optoelectronic Properties of Conjugated Polymer/Fullerene Binary Pairs with Variety of Lumo Level Differences. In *Organic Photovoltaics: Mechanisms, Materials, and Devices* Sariciftci, N. S. S. S.-S., Ed. CRC Press Taylor&Francis: Boca Raton, Florida, 2005; pp 529-557.
32. Henckens, A.; Knipper, M.; Polec, I.; Manca, J.; Lutsen, L.; Vanderzande, D., Poly(Thienylene Vinylene) Derivatives as Low Band Gap Polymers for Photovoltaic Applications. *Thin Solid Films* **2004**, *451-452*, 572-579.
33. Brabec, C. J.; Winder, C.; Sariciftci, N. S.; Hummelen, J. C.; Dhanabalan, A.; Hal, P. A. v.; Janssen, R. A. J., A Low-Bandgap Semiconducting Polymer for Photovoltaic Devices and Infrared Emitting Diodes. *Advanced Functional Materials* **2002**, *12*, 709-712.
34. Roncali, J., Synthetic Principles for Bandgap Control in Linear Π -Conjugated Systems. *Chemical Reviews* **1997**, *97*, 173-206.
35. Peet, J.; Heeger, A. J.; Bazan, G. C., "Plastic" Solar Cells: Self-Assembly of Bulk Heterojunction Nanomaterials by Spontaneous Phase Separation. *Accounts of Chemical Research* **2009**, *42*, 1700-1708.
36. Cahen, D.; Kahn, A., Electron Energetics at Surfaces and Interfaces: Concepts and Experiments. *Advanced Materials* **2003**, *15*, 271-277.
37. Kahn, A., Fermi Level, Work Function and Vacuum Level. *Materials Horizons* **2016**, *3*, 7-10.
38. Jakobi, K., 3.1.1.2 the Jellium Model. In *Electronic and Vibrational Properties*, Chiarotti, G., Ed. Springer Berlin Heidelberg: Berlin, Heidelberg, 1994; pp 29-31.
39. Lang, N. D.; Kohn, W., Theory of Metal Surfaces: Work Function. *Physical Review B* **1971**, *3*, 1215-1223.
40. Strayer, R. W.; Mackie, W.; Swanson, L. W., Work Function Measurements by the Field Emission Retarding Potential Method. *Surface Science* **1973**, *34*, 225-248.
41. Egelhoff, W. F., Core-Level Binding-Energy Shifts at Surfaces and in Solids. *Surface Science Reports* **1987**, *6*, 253-415.
42. Bagus, P. S.; Staemmler, V.; Wöll, C., Exchangelike Effects for Closed-Shell Adsorbates: Interface Dipole and Work Function. *Physical Review Letters* **2002**, *89*, 096104.

43. Chen, Y. C.; Cunningham, J. E.; Flynn, C. P., Dependence of Rare-Gas-Adsorbate Dipole Moment on Substrate Work Function. *Physical Review B* **1984**, *30*, 7317-7319.
44. Bagus, P. S.; Hermann, K.; Wöll, C., The Interaction of C₆H₆ and C₆H₁₂ with Noble Metal Surfaces: Electronic Level Alignment and the Origin of the Interface Dipole. *The Journal of Chemical Physics* **2005**, *123*, 184109.
45. Witte, G.; Lukas, S.; Bagus, P. S.; Wöll, C., Vacuum Level Alignment at Organic/Metal Junctions: "Cushion" Effect and the Interface Dipole. *Applied Physics Letters* **2005**, *87*, 263502.
46. Watkins, N. J.; Yan, L.; Gao, Y., Electronic Structure Symmetry of Interfaces between Pentacene and Metals. *Applied Physics Letters* **2002**, *80*, 4384-4386.
47. Li, H.; Duan, Y.; Coropceanu, V.; Bredas, J.-L., Electronic Structure of the Pentacene–Gold Interface: A Density-Functional Theory Study. *Organic Electronics* **2009**, *10*, 1571-1578.
48. Fahlman, M.; Crispin, A.; Crispin, X.; Henze, S. K. M.; Jong, M. P. d.; Osikowicz, W.; Tengstedt, C.; Salaneck, W. R., Electronic Structure of Hybrid Interfaces for Polymer-Based Electronics. *Journal of Physics: Condensed Matter* **2007**, *19*, 183202.
49. Tengstedt, C.; Osikowicz, W.; Salaneck, W. R.; Parker, I. D.; Hsu, C.-H.; Fahlman, M., Fermi-Level Pinning at Conjugated Polymer Interfaces. *Applied Physics Letters* **2006**, *88*, 053502.
50. Yoshimura, D.; Yokoyama, T.; Ito, E.; Ishii, H.; Ouchi, Y.; Hasegawa, S.; Seki, K., Electronic Structure of Alq₃/LiF/Al Interfaces Studied by Uv Photoemission. *Synthetic Metals* **1999**, *102*, 1145-1146.
51. Samanta, M. P.; Tian, W.; Datta, S.; Henderson, J. I.; Kubiak, C. P., Electronic Conduction through Organic Molecules. *Physical Review B* **1996**, *53*, R7626-R7629.
52. Bumm, L. A.; Arnold, J. J.; Cygan, M. T.; Dunbar, T. D.; Burgin, T. P.; Jones, L.; Allara, D. L.; Tour, J. M.; Weiss, P. S., Are Single Molecular Wires Conducting? *Science* **1996**, *271*, 1705-1707.
53. Braun, S.; Salaneck, W. R.; Fahlman, M., Energy-Level Alignment at Organic/Metal and Organic/Organic Interfaces. *Advanced Materials* **2009**, *21*, 1450-1472.
54. Ivanco, J.; Netzer, F. P.; Ramsey, M. G., On Validity of the Schottky-Mott Rule in Organic Semiconductors: Sexithiophene on Various Substrates. *Journal of Applied Physics* **2007**, *101*, 103712.
55. Kahn, A.; Koch, N.; Gao, W., Electronic Structure and Electrical Properties of Interfaces between Metals and π -Conjugated Molecular Films. *Journal of Polymer Science Part B: Polymer Physics* **2003**, *41*, 2529-2548.
56. Koch, N., Organic Electronic Devices and Their Functional Interfaces. *ChemPhysChem* **2007**, *8*, 1438-1455.
57. Garcia-Belmonte, G.; Boix, P. P.; Bisquert, J.; Sessolo, M.; Bolink, H. J., Simultaneous Determination of Carrier Lifetime and Electron Density-of-States in P3ht:Pcbm Organic Solar Cells under Illumination by Impedance Spectroscopy. *Solar Energy Materials and Solar Cells* **2010**, *94*, 366-375.
58. Garcia-Belmonte, G.; Bisquert, J., Open-Circuit Voltage Limit Caused by Recombination through Tail States in Bulk Heterojunction Polymer-Fullerene Solar Cells. *Applied Physics Letters* **2010**, *96*, 113301.
59. Arkhipov, V. I.; Heremans, P.; Emelianova, E. V.; Bäessler, H., Effect of Doping on the Density-of-States Distribution and Carrier Hopping in Disordered Organic Semiconductors. *Physical Review B* **2005**, *71*, 045214.
60. Silver, M.; Pautmeier, L.; Bäessler, H., On the Origin of Exponential Band Tails in Amorphous Semiconductors. *Solid State Communications* **1989**, *72*, 177-180.
61. Schubert, M.; Preis, E.; Blakesley, J. C.; Pingel, P.; Scherf, U.; Neher, D., Mobility Relaxation and Electron Trapping in a Donor/Acceptor Copolymer. *Physical Review B* **2013**, *87*, 024203.
62. Rivnay, J.; Noriega, R.; Northrup, J. E.; Kline, R. J.; Toney, M. F.; Salleo, A., Structural Origin of Gap States in Semicrystalline Polymers and the Implications for Charge Transport. *Physical Review B* **2011**, *83*, 121306.
63. Liu, Y.; Guo, J.; Zhu, E.; Liao, L.; Lee, S.-J.; Ding, M.; Shakir, I.; Gambin, V.; Huang, Y.; Duan, X., Approaching the Schottky–Mott Limit in Van Der Waals Metal–Semiconductor Junctions. *Nature* **2018**, *557*, 696-700.

64. Hill, I. G.; Rajagopal, A.; Kahn, A.; Hu, Y., Molecular Level Alignment at Organic Semiconductor-Metal Interfaces. *Applied Physics Letters* **1998**, *73*, 662-664.
65. Vázquez, H.; Gao, W.; Flores, F.; Kahn, A., Energy Level Alignment at Organic Heterojunctions: Role of the Charge Neutrality Level. *Physical Review B* **2005**, *71*, 041306.
66. Vázquez, H.; Flores, F.; Kahn, A., Induced Density of States Model for Weakly-Interacting Organic Semiconductor Interfaces. *Organic Electronics* **2007**, *8*, 241-248.
67. Flores, F.; Ortega, J.; Vazquez, H., Modelling Energy Level Alignment at Organic Interfaces and Density Functional Theory. *Physical Chemistry Chemical Physics* **2009**, *11*, 8658-8675.
68. Vázquez, H.; Oszwaldowski, R.; Pou, P.; Ortega, J.; Pérez, R.; Flores, F.; Kahn, A., Dipole Formation at Metal/Ptcds Interfaces: Role of the Charge Neutrality Level. *Europhys. Lett.* **2004**, *65*, 802-808.
69. Hill, I. G.; Rajagopal, A.; Kahn, A., Energy-Level Alignment at Interfaces between Metals and the Organic Semiconductor 4,4'-N,N'-Dicarbazolyl-Biphenyl. *Journal of Applied Physics* **1998**, *84*, 3236-3241.
70. Hill, I. G.; Schwartz, J.; Kahn, A., Metal-Dependent Charge Transfer and Chemical Interaction at Interfaces between 3,4,9,10-Perylenetetra-carboxylic Bisimidazole and Gold, Silver and Magnesium. *Organic Electronics* **2000**, *1*, 5-13.
71. Braun, S.; de Jong, M. P.; Osikowicz, W.; Salaneck, W. R., Influence of the Electrode Work Function on the Energy Level Alignment at Organic-Organic Interfaces. *Applied Physics Letters* **2007**, *91*, 202108.
72. Fahlman, M.; Sehati, P.; Osikowicz, W.; Braun, S.; de Jong, M. P.; Brocks, G., Photoelectron Spectroscopy and Modeling of Interface Properties Related to Organic Photovoltaic Cells. *Journal of Electron Spectroscopy and Related Phenomena* **2013**, *190*, Part A, 33-41.
73. Bao, Q.; Sandberg, O.; Dagnelund, D.; Sandén, S.; Braun, S.; Aarnio, H.; Liu, X.; Chen, W. M.; Österbacka, R.; Fahlman, M., Trap-Assisted Recombination Via Integer Charge Transfer States in Organic Bulk Heterojunction Photovoltaics. *Advanced Functional Materials* **2014**, *24*, 6309-6316.
74. Sehati, P.; Braun, S.; Fahlman, M., Energy Level Alignment in Au/Pentacene/Ptcds Trilayer Stacks. *Chemical Physics Letters* **2013**, *583*, 38-41.
75. Koch, N.; Elschner, A.; Rabe, J. P.; Johnson, R. L., Work Function Independent Hole-Injection Barriers between Pentacene and Conducting Polymers. *Advanced Materials* **2005**, *17*, 330-335.
76. Hill, I. G.; Kahn, A.; Cornil, J.; dos Santos, D. A.; Brédas, J. L., Occupied and Unoccupied Electronic Levels in Organic π -Conjugated Molecules: Comparison between Experiment and Theory. *Chemical Physics Letters* **2000**, *317*, 444-450.
77. Hill, I. G.; Kahn, A.; Soos, Z. G.; Pascal, J. R. A., Charge-Separation Energy in Films of π -Conjugated Organic Molecules. *Chemical Physics Letters* **2000**, *327*, 181-188.
78. Crispin, A.; Crispin, X.; Fahlman, M.; Berggren, M.; Salaneck, W. R., Transition between Energy Level Alignment Regimes at a Low Band Gap Polymer-Electrode Interfaces. *Applied Physics Letters* **2006**, *89*, 213503.
79. Brocks, G.; Çakır, D.; Bokdam, M.; de Jong, M. P.; Fahlman, M., Charge Equilibration and Potential Steps in Organic Semiconductor Multilayers. *Organic Electronics* **2012**, *13*, 1793-1801.
80. Osikowicz, W.; de Jong, M. P.; Salaneck, W. R., Formation of the Interfacial Dipole at Organic-Organic Interfaces: C60/Polymer Interfaces. *Advanced Materials* **2007**, *19*, 4213-4217.
81. Koch, N.; Duhm, S.; Rabe, J. P.; Vollmer, A.; Johnson, R. L., Optimized Hole Injection with Strong Electron Acceptors at Organic-Metal Interfaces. *Physical Review Letters* **2005**, *95*, 237601.
82. Koch, N.; Duhm, S.; Rabe, J. P.; Rentenberger, S.; Johnson, R. L.; Klankermayer, J.; Schreiber, F., Tuning the Hole Injection Barrier Height at Organic/Metal Interfaces with (Sub-) Monolayers of Electron Acceptor Molecules. *Applied Physics Letters* **2005**, *87*, 101905.
83. Ge, Y.; Whitten, J. E., Energy Level Alignment between Sexithiophene and Buckminsterfullerene Films. *Chemical Physics Letters* **2007**, *448*, 65-69.
84. Elumalai, N. K.; Uddin, A., Open Circuit Voltage of Organic Solar Cells: An in-Depth Review. *Energy & Environmental Science* **2016**, *9*, 391-410.

85. Min, Y.; Akbulut, M.; Kristiansen, K.; Golan, Y.; Israelachvili, J., The Role of Interparticle and External Forces in Nanoparticle Assembly. *Nature Materials* **2008**, *7*, 527.
86. Kesters, J.; Verstappen, P.; Raymakers, J.; Vanormelingen, W.; Drijkoningen, J.; D'Haen, J.; Manca, J.; Lutsen, L.; Vanderzande, D.; Maes, W., Enhanced Organic Solar Cell Stability by Polymer (Pcpdtbt) Side Chain Functionalization. *Chemistry of Materials* **2015**, *27*, 1332-1341.
87. Schulz, G. L.; Fischer, F. S. U.; Trefz, D.; Melnyk, A.; Hamidi-Sakr, A.; Brinkmann, M.; Andrienko, D.; Ludwigs, S., The Pcpdtbt Family: Correlations between Chemical Structure, Polymorphism, and Device Performance. *Macromolecules* **2017**, *50*, 1402-1414.
88. Aygül, U.; Egelhaaf, H. J.; Nagel, P.; Merz, M.; Schuppler, S.; Eichele, K.; Peisert, H.; Chassé, T., Photodegradation of C-Pcpdtbt and Si-Pcpdtbt: Influence of the Bridging Atom on the Stability of a Low-Band-Gap Polymer for Solar Cell Application. *ChemPhysChem* **2015**, *16*, 428-435.
89. Fischer, F. S. U.; Tremel, K.; Saur, A. K.; Link, S.; Kayunkid, N.; Brinkmann, M.; Herrero-Carvajal, D.; Navarrete, J. T. L.; Delgado, M. C. R.; Ludwigs, S., Influence of Processing Solvents on Optical Properties and Morphology of a Semicrystalline Low Bandgap Polymer in the Neutral and Charged States. *Macromolecules* **2013**, *46*, 4924-4931.
90. Rogers, J. T.; Schmidt, K.; Toney, M. F.; Kramer, E. J.; Bazan, G. C., Structural Order in Bulk Heterojunction Films Prepared with Solvent Additives. *Advanced Materials* **2011**, *23*, 2284-2288.
91. Peet, J.; Cho, N. S.; Lee, S. K.; Bazan, G. C., Transition from Solution to the Solid State in Polymer Solar Cells Cast from Mixed Solvents. *Macromolecules* **2008**, *41*, 8655-8659.
92. Liu, F.; Chen, D.; Wang, C.; Luo, K.; Gu, W.; Briseno, A. L.; Hsu, J. W. P.; Russell, T. P., Molecular Weight Dependence of the Morphology in P3ht:Pcbm Solar Cells. *ACS Applied Materials & Interfaces* **2014**, *6*, 19876-19887.
93. Joshi, S.; Grigorian, S.; Pietsch, U., X-Ray Structural and Crystallinity Studies of Low and High Molecular Weight Poly(3-Hexylthiophene). *physica status solidi (a)* **2008**, *205*, 488-496.
94. Zen, A., et al., Effect of Molecular Weight on the Structure and Crystallinity of Poly(3-Hexylthiophene). *Macromolecules* **2006**, *39*, 2162-2171.
95. Ma, W.; Kim, J. Y.; Lee, K.; Heeger, A. J., Effect of the Molecular Weight of Poly(3-Hexylthiophene) on the Morphology and Performance of Polymer Bulk Heterojunction Solar Cells. *Macromolecular Rapid Communications* **2007**, *28*, 1776-1780.
96. Erb, T.; Zhokhavets, U.; Gobsch, G.; Raleva, S.; Stühn, B.; Schilinsky, P.; Waldauf, C.; Brabec, C. J., Correlation between Structural and Optical Properties of Composite Polymer/Fullerene Films for Organic Solar Cells. *Advanced Functional Materials* **2005**, *15*, 1193-1196.
97. Morana, M.; Wegscheider, M.; Bonanni, A.; Kopidakis, N.; Shaheen, S.; Scharber, M.; Zhu, Z.; Waller, D.; Gaudiana, R.; Brabec, C., Bipolar Charge Transport in Pcpdtbt-Pcbm Bulk-Heterojunctions for Photovoltaic Applications. *Advanced Functional Materials* **2008**, *18*, 1757-1766.
98. Fischer, F. S. U., et al., Highly Crystalline Films of Pcpdtbt with Branched Side Chains by Solvent Vapor Crystallization: Influence on Opto-Electronic Properties. *Advanced Materials* **2015**, *27*, 1223-1228.
99. Aygül, U.; Batchelor, D.; Dettinger, U.; Yilmaz, S.; Allard, S.; Scherf, U.; Peisert, H.; Chassé, T., Molecular Orientation in Polymer Films for Organic Solar Cells Studied by Nexafs. *The Journal of Physical Chemistry C* **2012**, *116*, 4870-4874.
100. Mollinger, S. A.; Krajina, B. A.; Noriega, R.; Salleo, A.; Spakowitz, A. J., Percolation, Tie-Molecules, and the Microstructural Determinants of Charge Transport in Semicrystalline Conjugated Polymers. *ACS Macro Letters* **2015**, *4*, 708-712.
101. Hwang, H.; Lee, H.; Shafian, S.; Lee, W.; Seok, J.; Ryu, K.; Yeol Ryu, D.; Kim, K., Thermally Stable Bulk Heterojunction Prepared by Sequential Deposition of Nanostructured Polymer and Fullerene. *Polymers* **2017**, *9*, 456.
102. Ma, J.; Hashimoto, K.; Koganezawa, T.; Tajima, K., End-on Orientation of Semiconducting Polymers in Thin Films Induced by Surface Segregation of Fluoroalkyl Chains. *Journal of the American Chemical Society* **2013**, *135*, 9644-9647.
103. Mayer, A. C.; Scully, S. R.; Hardin, B. E.; Rowell, M. W.; McGehee, M. D., Polymer-Based Solar Cells. *Materials Today* **2007**, *10*, 28-33.

104. Carsten, D.; Vladimir, D., Polymer–Fullerene Bulk Heterojunction Solar Cells. *Reports on Progress in Physics* **2010**, *73*, 096401.
105. Scharber, M. C.; Sariciftci, N. S., Efficiency of Bulk-Heterojunction Organic Solar Cells. *Progress in Polymer Science* **2013**, *38*, 1929-1940.
106. Lee, J. K.; Ma, W. L.; Brabec, C. J.; Yuen, J.; Moon, J. S.; Kim, J. Y.; Lee, K.; Bazan, G. C.; Heeger, A. J., Processing Additives for Improved Efficiency from Bulk Heterojunction Solar Cells. *Journal of the American Chemical Society* **2008**, *130*, 3619-3623.
107. Balsara, N. P.; Lin, C.; Hammouda, B., Early Stages of Nucleation and Growth in a Polymer Blend. *Physical Review Letters* **1996**, *77*, 3847-3850.
108. Cahn, J. W.; Hilliard, J. E., Free Energy of a Nonuniform System. I. Interfacial Free Energy. *The Journal of Chemical Physics* **1958**, *28*, 258-267.
109. Björström, C. M.; Nilsson, S.; Bernasik, A.; Budkowski, A.; Andersson, M.; Magnusson, K. O.; Moons, E., Vertical Phase Separation in Spin-Coated Films of a Low Bandgap Polyfluorene/Pcbm Blend—Effects of Specific Substrate Interaction. *Applied Surface Science* **2007**, *253*, 3906-3912.
110. Anthony, M. H.; Simon, J. M.; Richard, L. T.; John, C.; Monika, V.; David, G. L.; Richard, A. L. J.; Mark, G., Surface Segregation and Self-Stratification in Blends of Spin-Cast Polyfluorene Derivatives. *Journal of Physics: Condensed Matter* **2005**, *17*, 1319.
111. Ton-That, C.; Shard, A. G.; Teare, D. O. H.; Bradley, R. H., Xps and Afm Surface Studies of Solvent-Cast Ps/Pmma Blends. *Polymer* **2001**, *42*, 1121-1129.
112. Schmidt-Hansberg, B., et al., Structure Formation in Low-Bandgap Polymer:Fullerene Solar Cell Blends in the Course of Solvent Evaporation. *Macromolecules* **2012**, *45*, 7948-7955.
113. Yang, X.; Alexeev, A.; Michels, M. A. J.; Loos, J., Effect of Spatial Confinement on the Morphology Evolution of Thin Poly(P-Phenylenevinylene)/Methanofullerene Composite Films. *Macromolecules* **2005**, *38*, 4289-4295.
114. Park, S. K.; Jackson, T. N.; Anthony, J. E.; Mourey, D. A., High Mobility Solution Processed 6,13-Bis(Triisopropyl-Silylethynyl) Pentacene Organic Thin Film Transistors. *Applied Physics Letters* **2007**, *91*, 063514.
115. Rogers, J. T.; Schmidt, K.; Toney, M. F.; Bazan, G. C.; Kramer, E. J., Time-Resolved Structural Evolution of Additive-Processed Bulk Heterojunction Solar Cells. *Journal of the American Chemical Society* **2012**, *134*, 2884-2887.
116. Peet, J.; Kim, J. Y.; Coates, N. E.; Ma, W. L.; Moses, D.; Heeger, A. J.; Bazan, G. C., Efficiency Enhancement in Low-Bandgap Polymer Solar Cells by Processing with Alkane Dithiols. *Nature Materials* **2007**, *6*, 497.
117. Gu, Y.; Wang, C.; Russell, T. P., Multi-Length-Scale Morphologies in Pcpdtbt/Pcbm Bulk-Heterojunction Solar Cells. *Advanced Energy Materials* **2012**, *2*, 683-690.
118. Li, G.; Yao, Y.; Yang, H.; Shrotriya, V.; Yang, G.; Yang, Y., “Solvent Annealing” Effect in Polymer Solar Cells Based on Poly(3-Hexylthiophene) and Methanofullerenes. *Advanced Functional Materials* **2007**, *17*, 1636-1644.
119. Treat, N. D.; Shuttle, C. G.; Toney, M. F.; Hawker, C. J.; Chabynyc, M. L., In Situ Measurement of Power Conversion Efficiency and Molecular Ordering During Thermal Annealing in P3ht:Pcbm Bulk Heterojunction Solar Cells. *Journal of Materials Chemistry* **2011**, *21*, 15224-15231.
120. Ma, W.; Yang, C.; Gong, X.; Lee, K.; Heeger, A. J., Thermally Stable, Efficient Polymer Solar Cells with Nanoscale Control of the Interpenetrating Network Morphology. *Advanced Functional Materials* **2005**, *15*, 1617-1622.
121. Li, G.; Shrotriya, V.; Huang, J.; Yao, Y.; Moriarty, T.; Emery, K.; Yang, Y., High-Efficiency Solution Processable Polymer Photovoltaic Cells by Self-Organization of Polymer Blends. *Nature Materials* **2005**, *4*, 864.
122. Schwabegger, G.; Ullah, M.; Irimia-Vladu, M.; Baumgartner, M.; Kanbur, Y.; Ahmed, R.; Stadler, P.; Bauer, S.; Sariciftci, N. S.; Sitter, H., High Mobility, Low Voltage Operating C60 Based N-Type Organic Field Effect Transistors. *Synthetic Metals* **2011**, *161*, 2058-2062.
123. Zhang, X.-H.; Kippelen, B., High-Performance C60 N-Channel Organic Field-Effect Transistors through Optimization of Interfaces. *Journal of Applied Physics* **2008**, *104*, 104504.

124. Anthopoulos, T. D.; Singh, B.; Marjanovic, N.; Sariciftci, N. S.; Ramil, A. M.; Sitter, H.; Cölle, M.; Leeuw, D. M. d., High Performance N-Channel Organic Field-Effect Transistors and Ring Oscillators Based on C60 Fullerene Films. *Applied Physics Letters* **2006**, *89*, 213504.
125. Haldi, A.; Sharma, A.; Jr., W. J. P.; Kippelen, B., Equivalent Circuit Model for Organic Single-Layer Diodes. *Journal of Applied Physics* **2008**, *104*, 064503.
126. Zhao, Y. Q.; Huang, C. J.; Ogundimu, T.; Lu, Z. H., Transparent Conducting C60:Lif Nanocomposite Thin Films for Organic Light-Emitting Diodes. *Applied Physics Letters* **2007**, *91*, 103109.
127. Sai, N.; Gearba, R.; Dolocan, A.; Tritsch, J. R.; Chan, W.-L.; Chelikowsky, J. R.; Leung, K.; Zhu, X., Understanding the Interface Dipole of Copper Phthalocyanine (Cupc)/C60: Theory and Experiment. *The Journal of Physical Chemistry Letters* **2012**, *3*, 2173-2177.
128. Wang, W.; Placencia, D.; Armstrong, N. R., Planar and Textured Heterojunction Organic Photovoltaics Based on Chloroindium Phthalocyanine (Clinpc) Versus Titanyl Phthalocyanine (Tiopc) Donor Layers. *Organic Electronics* **2011**, *12*, 383-393.
129. Haddock, J.; Domercq, B.; Kippelen, B., Fullerene Based N-Type Organic Thin-Film Transistors. *MRS Proceedings* **2011**, *871*, I3.11.
130. Shaheen, S. E.; Brabec, C. J.; Sariciftci, N. S.; Padinger, F.; Fromherz, T.; Hummelen, J. C., 2.5% Efficient Organic Plastic Solar Cells. *Applied Physics Letters* **2001**, *78*, 841-843.
131. Shakhmin, A. L.; Khodorkovskii, A. M.; Murashov, S. V.; Artamonova, T. O.; Golod, A. V., Electron Structure of Thin Fullerene Films Deposited by Various Methods. *Technical Physics Letters* **2001**, *27*, 87-89.
132. Khodorkovskii, M. A.; Murashov, S. V.; Artamonova, T. O.; Shakhmin, A. L.; Belyaeva, A. A., The Binding Energy of Molecules in Thin Fullerene Films. *Technical Physics Letters* **2004**, *30*, 129-130.
133. Zou, X.; Zhu, S.; Xie, J.; Feng, J., Low-Temperature Synthesis of C60 Thin Films by Ionized Cluster Beam Deposition Technique. *Journal of Crystal Growth* **1999**, *200*, 441-445.
134. Katz, E. A.; Faiman, D.; Shtutina, S.; Isakina, A., Deposition and Structural Characterization of High Quality Textured C60 Thin Films. *Thin Solid Films* **2000**, *368*, 49-54.
135. Gimzewski, J. K.; Modesti, S.; Schlittler, R. R., Cooperative Self-Assembly of Au Atoms and C_{60} on Au(110) Surfaces. *Physical Review Letters* **1994**, *72*, 1036-1039.
136. Yan, D.-W.; Liu, W.; Wang, H.-Z.; Wang, C.-R., Preparation of Fullerene Polycrystalline Films on Different Substrates by Physical Vapor Deposition. *MATERIALS TRANSACTIONS* **2007**, *48*, 700-703.
137. Itaka, K.; Yamashiro, M.; Yamaguchi, J.; Haemori, M.; Yaginuma, S.; Matsumoto, Y.; Kondo, M.; Koinuma, H., High-Mobility C60 Field-Effect Transistors Fabricated on Molecular- Wetting Controlled Substrates. *Advanced Materials* **2006**, *18*, 1713-1716.
138. Salzmann, I.; Duhm, S.; Opitz, R.; Johnson, R. L.; Rabe, J. P.; Koch, N., Structural and Electronic Properties of Pentacene-Fullerene Heterojunctions. *Journal of Applied Physics* **2008**, *104*, 114518.
139. McAfee, T.; Apperson, A.; Ade, H.; Dougherty, D. B., Growth of Thermally Stable Crystalline C60 Films on Flat-Lying Copper Phthalocyanine. *Journal of Materials Chemistry A* **2016**, *4*, 1028-1032.
140. Chen, W.; Zhang, H. L.; Xu, H.; Tok, E. S.; Loh, K. P.; Wee, A. T. S., C60 on Sic Nanomesh. *The Journal of Physical Chemistry B* **2006**, *110*, 21873-21881.
141. Zhong, J. Q.; Huang, H.; Mao, H. Y.; Wang, R.; Zhong, S.; Chen, W., Molecular-Scale Investigation of C60/P-Sexiphenyl Organic Heterojunction Interface. *The Journal of Chemical Physics* **2011**, *134*, 154706.
142. Hinderhofer, A.; Gerlach, A.; Broch, K.; Hosokai, T.; Yonezawa, K.; Kato, K.; Kera, S.; Ueno, N.; Schreiber, F., Geometric and Electronic Structure of Templated C60 on Diindenoperylene Thin Films. *The Journal of Physical Chemistry C* **2013**, *117*, 1053-1058.
143. Zhang, F. J.; Vollmer, A.; Zhang, J.; Xu, Z.; Rabe, J. P.; Koch, N., Energy Level Alignment and Morphology of Interfaces between Molecular and Polymeric Organic Semiconductors. *Organic Electronics* **2007**, *8*, 606-614.
144. Evans, S. D.; Ulman, A., Surface Potential Studies of Alkyl-Thiol Monolayers Adsorbed on Gold. *Chemical Physics Letters* **1990**, *170*, 462-466.

145. Yuan, L.-F.; Yang, J.; Wang, H.; Zeng, C.; Li, Q.; Wang, B.; Hou, J. G.; Zhu, Q.; Chen, D. M., Low-Temperature Orientationally Ordered Structures of Two-Dimensional C₆₀. *Journal of the American Chemical Society* **2003**, *125*, 169-172.
146. Nakayama, M.; Kautz, N. A.; Wang, T.; Sibener, S. J., Formation of Rectangular Packing and One-Dimensional Lines of C₆₀ on 11-Phenoxyundecanethiol Self-Assembled Monolayers on Au(111). *Langmuir* **2012**, *28*, 4694-4701.
147. David, T.; Gimzewski, J. K.; Purdie, D.; Reihl, B.; Schlittler, R. R., Epitaxial Growth of C₆₀ on Ag(110) Studied by Scanning Tunneling Microscopy and Tunneling Spectroscopy. *Physical Review B* **1994**, *50*, 5810-5813.
148. Sakurai, T.; Wang, X. D.; Hashizume, T.; Nishina, Y.; Shinohara, H.; Saito, Y., Fullerene (C₆₀) Adsorption on Si Surfaces. *Applied Surface Science* **1993**, *67*, 281-285.
149. Saito, Y.; Yoshikawa, T.; Ishikawa, Y.; Nagashima, H.; Shinohara, H., Electron Microscopy of Fullerene Thin Films Grown on Solid Surfaces. *Materials Science and Engineering: B* **1993**, *19*, 18-24.
150. Burke, S. A.; Topple, J. M.; Grütter, P., Molecular Dewetting on Insulators. *Journal of Physics: Condensed Matter* **2009**, *21*, 423101.
151. Katz, E. A.; Faiman, D.; Iakoubovskii, K.; Isakina, A.; Yagotintsev, K. A.; Strzhemechny, M. A.; Balberg, I., Effect of the Disorder/Order Phase Transition on the Electrical and Photoelectrical Properties of C₆₀ Thin Films. *Journal of Applied Physics* **2003**, *93*, 3401-3406.
152. Kosugi, N.; Kuroda, H., Equivalent-Core Basis Functions to Study Core-Ionized and Excited States. *Chemical Physics Letters* **1983**, *94*, 377-382.
153. Salaneck, W. R.; Bigelow, R. W.; Freund, H. J.; Plummer, E. W., X-Ray Photoelectron Spectroscopy of Gaseous and Solid C₆₀: Ion-State-Enhanced Intermolecular Interactions. *Physical Review B* **1981**, *24*, 2403-2411.
154. Berglund, C. N.; Spicer, W. E., Photoemission Studies of Copper and Silver: Theory. *Physical Review* **1964**, *136*, A1030-A1044.
155. Hüfner, S., *Photoelectron Spectroscopy: Principles and Applications*; Springer, 2003.
156. Aronniemi, M.; Sainio, J.; Lahtinen, J., Chemical State Quantification of Iron and Chromium Oxides Using Xps: The Effect of the Background Subtraction Method. *Surface Science* **2005**, *578*, 108-123.
157. Van der Heide, P., *X-Ray Photoelectron Spectroscopy: An Introduction to Principles and Practices*; WILEY Hoboken, New Jersey, 2012.
158. Seah, M. P.; Dench, W. A., Quantitative Electron Spectroscopy of Surfaces: A Standard Data Base for Electron Inelastic Mean Free Paths in Solids. *Surface and Interface Analysis* **1979**, *1*, 2-11.
159. Yeh, J. J.; Lindau, I., Atomic Subshell Photoionization Cross Sections and Asymmetry Parameters: $1 \leq Z \leq 103$. *Atomic Data and Nuclear Data Tables* **1985**, *32*, 1-155.
160. Knut, R.; Lindblad, R.; Gorgoi, M.; Rensmo, H.; Karis, O., High Energy Photoelectron Spectroscopy in Basic and Applied Science: Bulk and Interface Electronic Structure. *Journal of Electron Spectroscopy and Related Phenomena* **2013**, *190*, 278-288.
161. Scofield, J. H., Hartree-Slater Subshell Photoionization Cross-Sections at 1254 and 1487 Ev. *Journal of Electron Spectroscopy and Related Phenomena* **1976**, *8*, 129-137.
162. Electron Spectroscopy for Chemical Analysis. In *Surface Analysis – the Principal Techniques*.
163. Photoelectron Spectroscopy Applications to Materials Science. In *Handbook of Spectroscopy*.
164. Bianconi, A., Surface X-Ray Absorption Spectroscopy: Surface Exafs and Surface Xanes. *Applications of Surface Science* **1980**, *6*, 392-418.
165. Bianconi, A.; Dell'Araccia, M.; Durham, P. J.; Pendry, J. B., Multiple-Scattering Resonances and Structural Effects in the X-Ray-Absorption near-Edge Spectra of Fe II and Fe III Hexacyanide Complexes. *Physical Review B* **1982**, *26*, 6502-6508.
166. Koch, E. E.; Kunz, C.; Sonntag, B., Electronic States in Solids Investigated by Means of Synchrotron Radiation. *Physics Reports* **1977**, *29*, 153-231.
167. Stöhr, J.; Outka, D. A., Determination of Molecular Orientations on Surfaces from the Angular Dependence of near-Edge X-Ray-Absorption Fine-Structure Spectra. *Physical Review B* **1987**, *36*, 7891-7905.

168. Zahn, D. R. T.; Gavrilă, G. N.; Salvan, G., Electronic and Vibrational Spectroscopies Applied to Organic/Inorganic Interfaces. *Chemical Reviews* **2007**, *107*, 1161-1232.
169. Hemraj-Benny, T., et al., Near-Edge X-Ray Absorption Fine Structure Spectroscopy as a Tool for Investigating Nanomaterials. *Small* **2006**, *2*, 26-35.
170. Watts, B.; Swaraj, S.; Nordlund, D.; Lüning, J.; Ade, H., Calibrated Nexafs Spectra of Common Conjugated Polymers. *The Journal of Chemical Physics* **2011**, *134*, 024702.
171. Stöhr, J., *Nexafs Spectroscopy*; Springer, 1992.
172. Tirsell, K. G.; Karpenko, V. P., A General Purpose Sub-Kev X-Ray Facility at the Stanford Synchrotron Radiation Laboratory. *Nuclear Instruments and Methods in Physics Research Section A: Accelerators, Spectrometers, Detectors and Associated Equipment* **1990**, *291*, 511-517.
173. Losego, M. D.; Guske, J. T.; Efremenko, A.; Maria, J.-P.; Franzen, S., Characterizing the Molecular Order of Phosphonic Acid Self-Assembled Monolayers on Indium Tin Oxide Surfaces. *Langmuir* **2011**, *27*, 11883-11888.
174. Casu, M. B.; Schöll, A.; Bauchspiess, K. R.; Hübner, D.; Schmidt, T.; Heske, C.; Umbach, E., Nucleation in Organic Thin Film Growth: Perylene on Al₂O₃/Ni₃Al(111). *The Journal of Physical Chemistry C* **2009**, *113*, 10990-10996.
175. Hahner, G., Near Edge X-Ray Absorption Fine Structure Spectroscopy as a Tool to Probe Electronic and Structural Properties of Thin Organic Films and Liquids. *Chemical Society Reviews* **2006**, *35*, 1244-1255.
176. Mikhnenko, O. V.; Blom, P. W. M.; Nguyen, T.-Q., Exciton Diffusion in Organic Semiconductors. *Energy & Environmental Science* **2015**, *8*, 1867-1888.
177. Gélinas, S.; Rao, A.; Kumar, A.; Smith, S. L.; Chin, A. W.; Clark, J.; van der Poll, T. S.; Bazan, G. C.; Friend, R. H., Ultrafast Long-Range Charge Separation in Organic Semiconductor Photovoltaic Diodes. *Science* **2014**, *343*, 512-516.
178. Mas-Torrent, M.; Rovira, C., Role of Molecular Order and Solid-State Structure in Organic Field-Effect Transistors. *Chemical Reviews* **2011**, *111*, 4833-4856.
179. T.Ohta, K. A., T.Yokoyama,, Application to Surface Structure Analyses. In *Applications of Synchrotron Radiation to Materials Analysis*, H.Saisho, Y. G., Ed. Elsevier: Amsterdam, The Netherlands, 1996; pp 307-351.
180. Chassé, T.; Casu, M. B., Nexafs Studies at Surfaces. In *Handbook of Spectroscopy*, WILEY-VCH: 2014; Vol. 3, pp 1485-1505.
181. Hoheisel, M.; Heller, S.; Mrotzek, C.; Mitwalsky, A., Advanced Transparent Conductive Oxide Electrode for Optoelectronic Thin-Film Devices. *Solid State Communications* **1990**, *76*, 1-3.
182. Shizuo Fujita; Takeshi Sakamoto; Kentaro Ueda; Kazuki Ohta; Shigeo Fujita, Surface Treatment of Indium-Tin-Oxide Substrates and Its Effects on Initial Nucleation Processes of Diamine Films. *Japanese Journal of Applied Physics* **1997**, *36*, 350.
183. Fehse, K.; Olthof, S.; Walzer, K.; Leo, K.; Johnson, R. L.; Glowatzki, H.; Bröker, B.; Koch, N., Energy Level Alignment of Electrically Doped Hole Transport Layers with Transparent and Conductive Indium Tin Oxide and Polymer Anodes. *Journal of Applied Physics* **2007**, *102*, 073719.
184. Hu, T.; Zhang, F.; Xu, Z.; Zhao, S.; Yue, X.; Yuan, G., Effect of Uv-Ozone Treatment on Ito and Post-Annealing on the Performance of Organic Solar Cells. *Synthetic Metals* **2009**, *159*, 754-756.
185. Destruel, P.; Bock, H.; Séguy, I.; Jolinat, P.; Oukachmih, M.; Bedel-Pereira, E., Influence of Indium Tin Oxide Treatment Using Uv-Ozone and Argon Plasma on the Photovoltaic Parameters of Devices Based on Organic Discotic Materials. *Polymer International* **2006**, *55*, 601-607.
186. Zhou, Y., et al., A Universal Method to Produce Low-Work Function Electrodes for Organic Electronics. *Science* **2012**, *336*, 327-332.
187. Yun, J. H.; Lee, I.; Kim, T.-S.; Ko, M. J.; Kim, J. Y.; Son, H. J., Synergistic Enhancement and Mechanism Study of Mechanical and Moisture Stability of Perovskite Solar Cells Introducing Polyethylene-Imine into the CH₃NH₃PbI₃/HTM Interface. *Journal of Materials Chemistry A* **2015**, *3*, 22176-22182.
188. Min, X.; Jiang, F.; Qin, F.; Li, Z.; Tong, J.; Xiong, S.; Meng, W.; Zhou, Y., Polyethylenimine Aqueous Solution: A Low-Cost and Environmentally Friendly Formulation to Produce Low-Work-

- Function Electrodes for Efficient Easy-to-Fabricate Organic Solar Cells. *ACS Applied Materials & Interfaces* **2014**, *6*, 22628-22633.
189. Kim, J.-H.; Song, C. E.; Kim, H. U.; Grimsdale, A. C.; Moon, S.-J.; Shin, W. S.; Choi, S. K.; Hwang, D.-H., High Open Circuit Voltage Solution-Processed Tandem Organic Photovoltaic Cells Employing a Bottom Cell Using a New Medium Band Gap Semiconducting Polymer. *Chemistry of Materials* **2013**, *25*, 2722-2732.
190. Zhou, Y.; Fuentes-Hernandez, C.; Khan, T. M.; Liu, J.-C.; Hsu, J.; Shim, J. W.; Dindar, A.; Youngblood, J. P.; Moon, R. J.; Kippelen, B., Recyclable Organic Solar Cells on Cellulose Nanocrystal Substrates. *Scientific Reports* **2013**, *3*, 1536.
191. Höfle, S.; Schienle, A.; Bruns, M.; Lemmer, U.; Colmann, A., Enhanced Electron Injection into Inverted Polymer Light-Emitting Diodes by Combined Solution-Processed Zinc Oxide/Polyethylenimine Interlayers. *Advanced Materials* **2014**, *26*, 2750-2754.
192. Sun, B.; Hong, W.; Aziz, H.; Li, Y., A Pyridine-Flanked Diketopyrrolopyrrole (Dpp)-Based Donor-Acceptor Polymer Showing High Mobility in Ambipolar and N-Channel Organic Thin Film Transistors. *Polymer Chemistry* **2015**, *6*, 938-945.
193. Sun, Y.; Seo, J. H.; Takacs, C. J.; Seifert, J.; Heeger, A. J., Inverted Polymer Solar Cells Integrated with a Low-Temperature-Annealed Sol-Gel-Derived ZnO Film as an Electron Transport Layer. *Advanced Materials* **2011**, *23*, 1679-1683.
194. Wilken, S.; Parisi, J.; Borchert, H., Role of Oxygen Adsorption in Nanocrystalline ZnO Interfacial Layers for Polymer–Fullerene Bulk Heterojunction Solar Cells. *The Journal of Physical Chemistry C* **2014**, *118*, 19672-19682.
195. Prosa, M., et al., Enhanced Ultraviolet Stability of Air-Processed Polymer Solar Cells by Al Doping of the ZnO Interlayer. *ACS Applied Materials & Interfaces* **2016**, *8*, 1635-1643.
196. Sun, Y.; Seo, J. H.; Takacs, C. J.; Seifert, J.; Heeger, A. J., Inverted Polymer Solar Cells Integrated with a Low-Temperature-Annealed Sol-Gel-Derived ZnO Film as an Electron Transport Layer. *Advanced Materials* **2011**, *23*, 1679-1683.
197. Crispin, X.; Geskin, V.; Crispin, A.; Cornil, J.; Lazzaroni, R.; Salaneck, W. R.; Brédas, J.-L., Characterization of the Interface Dipole at Organic/ Metal Interfaces. *Journal of the American Chemical Society* **2002**, *124*, 8131-8141.
198. Rentenberger, S.; Vollmer, A.; Zojer, E.; Schennach, R.; Koch, N., Uv/Ozone Treated Au for Air-Stable, Low Hole Injection Barrier Electrodes in Organic Electronics. *Journal of Applied Physics* **2006**, *100*, 053701.
199. Nguyen, T. P.; Le Rendu, P.; Long, P. D.; De Vos, S. A., Chemical and Thermal Treatment of Pedot:Pss Thin Films for Use in Organic Light Emitting Diodes. *Surface and Coatings Technology* **2004**, *180-181*, 646-649.
200. Aernouts, T.; Vanlaeke, P.; Geens, W.; Poortmans, J.; Heremans, P.; Borghs, S.; Mertens, R.; Andriessen, R.; Leenders, L., Printable Anodes for Flexible Organic Solar Cell Modules. *Thin Solid Films* **2004**, *451-452*, 22-25.
201. Li, T.-C.; Chang, R.-C., Improving the Performance of Ito Thin Films by Coating Pedot:Pss. *International Journal of Precision Engineering and Manufacturing-Green Technology* **2014**, *1*, 329-334.
202. Kim, W. H.; Kushto, G. P.; Kim, H.; Kafafi, Z. H., Effect of Annealing on the Electrical Properties and Morphology of a Conducting Polymer Used as an Anode in Organic Light-Emitting Devices. *Journal of Polymer Science Part B: Polymer Physics* **2003**, *41*, 2522-2528.
203. Tada, A.; Geng, Y.; Wei, Q.; Hashimoto, K.; Tajima, K., Tailoring Organic Heterojunction Interfaces in Bilayer Polymer Photovoltaic Devices. *Nature Materials* **2011**, *10*, 450.
204. Greczynski, G.; Kugler, T.; Salaneck, W. R., Characterization of the Pedot-Pss System by Means of X-Ray and Ultraviolet Photoelectron Spectroscopy. *Thin Solid Films* **1999**, *354*, 129-135.
205. Greczynski, G.; Kugler, T.; Keil, M.; Osikowicz, W.; Fahlman, M.; Salaneck, W. R., Photoelectron Spectroscopy of Thin Films of Pedot–Pss Conjugated Polymer Blend: A Mini-Review and Some New Results. *Journal of Electron Spectroscopy and Related Phenomena* **2001**, *121*, 1-17.
206. Kirchmeyer, S.; Reuter, K., Scientific Importance, Properties and Growing Applications of Poly(3,4-Ethylenedioxythiophene). *Journal of Materials Chemistry* **2005**, *15*, 2077-2088.

207. Vitoratos, E.; Sakkopoulos, S.; Dalas, E.; Paliatsas, N.; Karageorgopoulos, D.; Petraki, F.; Kennou, S.; Choulis, S. A., Thermal Degradation Mechanisms of Pedot:Pss. *Organic Electronics* **2009**, *10*, 61-66.
208. Howatt, G. N.; Breckenridge, R. G.; Brownlow, J. M., Fabrication of Thin Ceramic Sheets for Capacitors*. *Journal of the American Ceramic Society* **1947**, *30*, 237-242.
209. Xiong, K.; Hou, L.; Wu, M.; Huo, Y.; Mo, W.; Yuan, Y.; Sun, S.; Xu, W.; Wang, E., From Spin Coating to Doctor Blading: A Systematic Study on the Photovoltaic Performance of an Isoindigo-Based Polymer. *Solar Energy Materials and Solar Cells* **2015**, *132*, 252-259.
210. Kowarik, S.; Gerlach, A.; Schreiber, F., Organic Molecular Beam Deposition: Fundamentals, Growth Dynamics, and in Situ Studies. *Journal of Physics: Condensed Matter* **2008**, *20*, 184005.
211. Forrest, S. R., Ultrathin Organic Films Grown by Organic Molecular Beam Deposition and Related Techniques. *Chemical Reviews* **1997**, *97*, 1793-1896.
212. Krause, B.; Dürr, A. C.; Schreiber, F.; Dosch, H.; Seeck, O. H., Thermal Stability and Partial Dewetting of Crystalline Organic Thin Films: 3,4,9,10-Perylenetetracarboxylic Dianhydride on Ag(111). *The Journal of Chemical Physics* **2003**, *119*, 3429-3435.
213. Andreasson, M.; Ilver, L.; Kanski, J.; Andersson, T. G., Organic Molecular Beam Deposition System and Initial Studies of Organic Layer Growth. *Physica Scripta* **2006**, *2006*, 1.
214. Pinotti, E.; Sassella, A.; Borghesi, A., Thermal Model of Knudsen Cells for Organic Molecular Beam Deposition. *Journal of Vacuum Science & Technology A: Vacuum, Surfaces, and Films* **2001**, *19*, 878-882.
215. Ritley, K. A.; Krause, B.; Schreiber, F.; Dosch, H., A Portable Ultrahigh Vacuum Organic Molecular Beam Deposition System for in Situ X-Ray Diffraction Measurements. *Review of Scientific Instruments* **2001**, *72*, 1453-1457.
216. Brazovskii, S.; Kirova, N.; Bishop, A. R.; Klimov, V.; McBranch, D.; Barashkov, N. N.; Ferraris, J. P., Excitations and Optical Properties of Phenylene-Based Conjugated Polymers and Oligomers. *Optical Materials* **1998**, *9*, 472-479.
217. Hadziioannou, G.; Geoghegan, M., *Polymer Electronics*; Oxford University Press: Oxford, 2013.
218. Hsin-Fei, M., Overview of Semiconducting Conjugated Polymers. In *Polymer Electronics*, Pan Stanford CRC Press
- Taylor & Francis Group: Boca Raton, Florida, 2013; pp 9-43.
219. Fung, S. D. D.; Wallace, C. H. C., Introduction to Organic Solar Cells. In *Organic Solar Cells - Materials and Device Physics* Wallace, C. H. C., Ed. Springer: 2013; pp 1-16.
220. Moses, D.; Wang, J.; Heeger, A. J.; Kirova, N.; Brazovski, S., Singlet Exciton Binding Energy in Poly(Phenylene Vinylene). *Proceedings of the National Academy of Sciences* **2001**, *98*, 13496-13500.
221. Conwell, E. M., Definition of Exciton Binding Energy for Conducting Polymers. *Synthetic Metals* **1996**, *83*, 101-102.
222. Conwell, E. M., Photophysics of Conducting Polymers. In *Organic Electronic Materials Conjugated Polymers and Low Molecular Weight Organic Solids*, Farchioni, R. G., Giuseppe Ed. Springer: Berlin Heidelberg, 2001; pp 127-180.
223. Yuen, J. D.; Fan, J.; Seifert, J.; Lim, B.; Hufschmid, R.; Heeger, A. J.; Wudl, F., High Performance Weak Donor-Acceptor Polymers in Thin Film Transistors: Effect of the Acceptor on Electronic Properties, Ambipolar Conductivity, Mobility, and Thermal Stability. *Journal of the American Chemical Society* **2011**, *133*, 20799-20807.
224. Brédas, J. L., Relationship between Band Gap and Bond Length Alternation in Organic Conjugated Polymers. *The Journal of Chemical Physics* **1985**, *82*, 3808-3811.
225. Mitsumoto, R., et al., Electronic Structures and Chemical Bonding of Fluorinated Fullerenes Studied by Nexafs, Ups, and Vacuum-Uv Absorption Spectroscopies. *The Journal of Physical Chemistry A* **1998**, *102*, 552-560.
226. Peisert, H.; Knupfer, M.; Schwieger, T.; Fuentes, G. G.; Olligs, D.; Fink, J.; Schmidt, T., Fluorination of Copper Phthalocyanines: Electronic Structure and Interface Properties. *Journal of Applied Physics* **2003**, *93*, 9683-9692.

227. Ishii, H.; Sugiyama, K.; Ito, E.; Seki, K., Energy Level Alignment and Interfacial Electronic Structures at Organic/Metal and Organic/Organic Interfaces. *Advanced Materials* **1999**, *11*, 605-625.
228. Chen, W.; Qi, D. C.; Huang, Y. L.; Huang, H.; Wang, Y. Z.; Chen, S.; Gao, X. Y.; Wee, A. T. S., Molecular Orientation Dependent Energy Level Alignment at Organic–Organic Heterojunction Interfaces. *The Journal of Physical Chemistry C* **2009**, *113*, 12832-12839.
229. Salaneck, W. R.; Inganäs, O.; Thémans, B.; Nilsson, J. O.; Sjögren, B.; Österholm, J. E.; Brédas, J. L.; Svensson, S., Thermochromism in Poly(3-Hexylthiophene) in the Solid State: A Spectroscopic Study of Temperature-Dependent Conformational Defects. *The Journal of Chemical Physics* **1988**, *89*, 4613-4619.
230. Hao, X. T.; Hosokai, T.; Mitsuo, N.; Kera, S.; Sakamoto, K.; Okudaira, K. K.; Ueno, N., Surface Electronic Structures of Polythiophene Derivatives. *Macromolecular Symposia* **2007**, *249-250*, 493-497.
231. Hao, X. T.; Hosokai, T.; Mitsuo, N.; Kera, S.; Mase, K.; Okudaira, K. K.; Ueno, N., Electronic Density Tailing Outside π -Conjugated Polymer Surface. *Applied Physics Letters* **2006**, *89*, 182113.
232. Wykes, M.; Milián-Medina, B.; Gierschner, J., Computational Engineering of Low Bandgap Copolymers. *Frontiers in Chemistry* **2013**, *1*.
233. Peisert, H.; Petr, A.; Dunsch, L.; Chassé, T.; Knupfer, M., Interface Fermi Level Pinning at Contacts between Pedot: Pss and Molecular Organic Semiconductors. *ChemPhysChem* **2007**, *8*, 386-390.
234. Ivanco, J.; Haber, T.; Krenn, J. R.; Netzer, F. P.; Resel, R.; Ramsey, M. G., Sexithiophene Films on Ordered and Disordered TiO₂(110) Surfaces: Electronic, Structural and Morphological Properties. *Surface Science* **2007**, *601*, 178-187.
235. Duhm, S.; Heimel, G.; Salzmänn, I.; Glowatzki, H.; Johnson, R. L.; Vollmer, A.; Rabe, J. P.; Koch, N., Orientation-Dependent Ionization Energies and Interface Dipoles in Ordered Molecular Assemblies. *Nat Mater* **2008**, *7*, 326-332.
236. Chen, W.; Huang, H.; Chen, S.; Huang, Y. L.; Gao, X. Y.; Wee, A. T. S., Molecular Orientation-Dependent Ionization Potential of Organic Thin Films. *Chemistry of Materials* **2008**, *20*, 7017-7021.
237. Bao, Q.; Liu, X.; Braun, S.; Gao, F.; Fahlman, M., Energetics at Doped Conjugated Polymer/Electrode Interfaces. *Advanced Materials Interfaces* **2015**, *2*, n/a-n/a.
238. Braun, S.; Salaneck, W. R., Fermi Level Pinning at Interfaces with Tetrafluorotetracyanoquinodimethane (F4-Tcnq): The Role of Integer Charge Transfer States. *Chemical Physics Letters* **2007**, *438*, 259-262.
239. Hwang, J.; Amy, F.; Kahn, A., Spectroscopic Study on Sputtered Pedot · Pss: Role of Surface Pss Layer. *Organic Electronics* **2006**, *7*, 387-396.
240. Havinga, E. E.; ten Hoeve, W.; Wynberg, H., Alternate Donor-Acceptor Small-Band-Gap Semiconducting Polymers; Polysquaraines and Polycroconaines. *Synthetic Metals* **1993**, *55*, 299-306.
241. Knupfer, M.; Peisert, H., Electronic Properties of Interfaces between Model Organic Semiconductors and Metals. *physica status solidi (a)* **2004**, *201*, 1055-1074.
242. Rosén, A.; Wästberg, B., Buckminsterfullerene C₆₀ — a Surface with Curvature and Interesting Properties. *Surface Science* **1992**, *269-270*, 1121-1128.
243. Yu, S.; Frisch, J.; Opitz, A.; Cohen, E.; Bendikov, M.; Koch, N.; Salzmänn, I., Effect of Molecular Electrical Doping on Polyfuran Based Photovoltaic Cells. *Applied Physics Letters* **2015**, *106*, 203301.
244. Mao, H. Y.; Wang, R.; Huang, H.; Wang, Y. Z.; Gao, X. Y.; Bao, S. N.; Wee, A. T. S.; Chen, W., Tuning of C₆₀ Energy Levels Using Orientation-Controlled Phthalocyanine Films. *Journal of Applied Physics* **2010**, *108*, 053706.
245. Ruoff, R. S.; Tse, D. S.; Malhotra, R.; Lorents, D. C., Solubility of Fullerene (C₆₀) in a Variety of Solvents. *The Journal of Physical Chemistry* **1993**, *97*, 3379-3383.
246. Nápoles-Duarte, J. M.; Reyes-Reyes, M.; Ricardo-Chavez, J. L.; Garibay-Alonso, R.; López-Sandoval, R., Effect of Packing on the Cohesive and Electronic Properties of Methanofullerene Crystals. *Physical Review B* **2008**, *78*, 035425.
247. Hudhomme, P., An Overview of Molecular Acceptors for Organic Solar Cells. *EPJ Photovolt.* **2013**, *4*, 40401.

248. Yoshida, H., Low-Energy Inverse Photoemission Study on the Electron Affinities of Fullerene Derivatives for Organic Photovoltaic Cells. *The Journal of Physical Chemistry C* **2014**, *118*, 24377-24382.
249. Akaike, K.; Kanai, K.; Yoshida, H.; Tsutsumi, J. y.; Nishi, T.; Sato, N.; Ouchi, Y.; Seki, K., Ultraviolet Photoelectron Spectroscopy and Inverse Photoemission Spectroscopy of [6,6]-Phenyl-C61-Butyric Acid Methyl Ester in Gas and Solid Phases. *Journal of Applied Physics* **2008**, *104*, 023710.
250. Nakanishi, R.; Nogimura, A.; Eguchi, R.; Kanai, K., Electronic Structure of Fullerene Derivatives in Organic Photovoltaics. *Organic Electronics* **2014**, *15*, 2912-2921.
251. Guan, Z.-L.; Kim, J. B.; Wang, H.; Jaye, C.; Fischer, D. A.; Loo, Y.-L.; Kahn, A., Direct Determination of the Electronic Structure of the Poly(3-Hexylthiophene):Phenyl-[6,6]-C61 Butyric Acid Methyl Ester Blend. *Organic Electronics* **2010**, *11*, 1779-1785.
252. Wang, C.; Turinske, A. J.; Gao, Y., Orientation-Dependent Ionization Potential of Cupc and Energy Level Alignment at C60/Cupc Interface. *Applied Physics B* **2013**, *113*, 361-365.
253. Zhong, S.; Zhong, J. Q.; Mao, H. Y.; Zhang, J. L.; Lin, J. D.; Chen, W., The Role of Gap States in the Energy Level Alignment at the Organic–Organic Heterojunction Interfaces. *Physical Chemistry Chemical Physics* **2012**, *14*, 14127-14141.
254. Sueyoshi, T.; Fukagawa, H.; Ono, M.; Kera, S.; Ueno, N., Low-Density Band-Gap States in Pentacene Thin Films Probed with Ultrahigh-Sensitivity Ultraviolet Photoelectron Spectroscopy. *Applied Physics Letters* **2009**, *95*, 183303.
255. Zuo, G.; Li, Z.; Andersson, O.; Abdalla, H.; Wang, E.; Kemerink, M., Molecular Doping and Trap Filling in Organic Semiconductor Host–Guest Systems. *The Journal of Physical Chemistry C* **2017**, *121*, 7767-7775.
256. El-Sayed, A., et al., Understanding Energy-Level Alignment in Donor–Acceptor/Metal Interfaces from Core-Level Shifts. *ACS Nano* **2013**, *7*, 6914-6920.
257. Aygül, U.; Hintz, H.; Egelhaaf, H.-J.; Distler, A.; Abb, S.; Peisert, H.; Chassé, T., Energy Level Alignment of a P3ht/Fullerene Blend During the Initial Steps of Degradation. *The Journal of Physical Chemistry C* **2013**, *117*, 4992-4998.
258. Xu, Z.; Chen, L.-M.; Chen, M.-H.; Li, G.; Yang, Y., Energy Level Alignment of Poly(3-Hexylthiophene): [6,6]-Phenyl C61 Butyric Acid Methyl Ester Bulk Heterojunction. *Applied Physics Letters* **2009**, *95*, 013301.
259. Li, Y.-Q.; Wang, Q.-K.; Ou, Q.-D.; Tang, J.-X., Interface Energetics and Engineering of Organic Heterostructures in Organic Photovoltaic Cells. *Science China Chemistry* **2016**, 1-13.
260. Sweetnam, S.; Vandewal, K.; Cho, E.; Risko, C.; Coropceanu, V.; Salleo, A.; Brédas, J.-L.; McGehee, M. D., Characterizing the Polymer:Fullerene Intermolecular Interactions. *Chemistry of Materials* **2016**, *28*, 1446-1452.
261. Marchiori, C. F. N.; Koehler, M., Density Functional Theory Study of the Dipole across the P3ht : Pcbm Complex: The Role of Polarization and Charge Transfer. *Journal of Physics D: Applied Physics* **2014**, *47*, 215104.
262. Johansson, F. O. L.; Ivanović, M.; Svanström, S.; Cappel, U. B.; Peisert, H.; Chassé, T.; Lindblad, A., Femtosecond and Attosecond Electron-Transfer Dynamics in Pcpdtbt:Pcbm Bulk Heterojunctions. *The Journal of Physical Chemistry C* **2018**, *122*, 12605-12614.
263. Zampetti, A., et al., Influence of the Interface Material Layers and Semiconductor Energetic Disorder on the Open Circuit Voltage in Polymer Solar Cells. *Journal of Polymer Science Part B: Polymer Physics* **2015**, *53*, 690-699.
264. Wang, F.; Sun, G.; Li, C.; Liu, J.; Hu, S.; Zheng, H.; Tan, Z. a.; Li, Y., Finding the Lost Open-Circuit Voltage in Polymer Solar Cells by Uv-Ozone Treatment of the Nickel Acetate Anode Buffer Layer. *ACS Applied Materials & Interfaces* **2014**, *6*, 9458-9465.
265. Mihailtchi, V. D.; Blom, P. W. M.; Hummelen, J. C.; Rispen, M. T., Cathode Dependence of the Open-Circuit Voltage of Polymer:Fullerene Bulk Heterojunction Solar Cells. *Journal of Applied Physics* **2003**, *94*, 6849-6854.
266. Brabec, C. J.; Cravino, A.; Meissner, D.; Sariciftci, N. S.; Fromherz, T.; Rispen, M. T.; Sanchez, L.; Hummelen, J. C., Origin of the Open Circuit Voltage of Plastic Solar Cells. *Advanced Functional Materials* **2001**, *11*, 374-380.

267. Blakesley, J. C.; Clubb, H. S.; Greenham, N. C., Temperature-Dependent Electron and Hole Transport in Disordered Semiconducting Polymers: Analysis of Energetic Disorder. *Physical Review B* **2010**, *81*, 045210.
268. Ma, H.; Yip, H.-L.; Huang, F.; Jen, A. K. Y., Interface Engineering for Organic Electronics. *Advanced Functional Materials* **2010**, *20*, 1371-1388.
269. Ju, H.; Knesting, K. M.; Zhang, W.; Pan, X.; Wang, C.-H.; Yang, Y.-W.; Ginger, D. S.; Zhu, J., Interplay between Interfacial Structures and Device Performance in Organic Solar Cells: A Case Study with the Low Work Function Metal, Calcium. *ACS Applied Materials & Interfaces* **2016**, *8*, 2125-2131.
270. Cheng, P.; Zhan, X., Stability of Organic Solar Cells: Challenges and Strategies. *Chemical Society Reviews* **2016**, *45*, 2544-2582.
271. Gwinner, M. C.; Pietro, R. D.; Vaynzof, Y.; Greenberg, K. J.; Ho, P. K. H.; Friend, R. H.; Sirringhaus, H., Doping of Organic Semiconductors Using Molybdenum Trioxide: A Quantitative Time-Dependent Electrical and Spectroscopic Study. *Advanced Functional Materials* **2011**, *21*, 1432-1441.
272. Deschler, F.; Riedel, D.; Deák, A.; Ecker, B.; von Hauff, E.; Da Como, E., Imaging of Morphological Changes and Phase Segregation in Doped Polymeric Semiconductors. *Synthetic Metals* **2015**, *199*, 381-387.
273. Kahn, A.; Zhao, W.; Gao, W.; Vázquez, H.; Flores, F., Doping-Induced Realignment of Molecular Levels at Organic–Organic Heterojunctions. *Chemical Physics* **2006**, *325*, 129-137.
274. Gao, W.; Kahn, A., Controlled P-Doping of Zinc Phthalocyanine by Coevaporation with Tetrafluorotetracyanoquinodimethane: A Direct and Inverse Photoemission Study. *Applied Physics Letters* **2001**, *79*, 4040-4042.
275. Loiudice, A.; Rizzo, A.; Biasiucci, M.; Gigli, G., Bulk Heterojunction Versus Diffused Bilayer: The Role of Device Geometry in Solution P-Doped Polymer-Based Solar Cells. *The Journal of Physical Chemistry Letters* **2012**, *3*, 1908-1915.
276. Han, X.; Wu, Z.; Sun, B., Enhanced Performance of Inverted Organic Solar Cell by a Solution-Based Fluorinated Acceptor Doped P3ht:Pcbm Layer. *Organic Electronics* **2013**, *14*, 1116-1121.
277. Zhang, Y.; Zhou, H.; Seifert, J.; Ying, L.; Mikhailovsky, A.; Heeger, A. J.; Bazan, G. C.; Nguyen, T.-Q., Molecular Doping Enhances Photoconductivity in Polymer Bulk Heterojunction Solar Cells. *Advanced Materials* **2013**, *25*, 7038-7044.
278. Guillain, F.; Endres, J.; Bourgeois, L.; Kahn, A.; Vignau, L.; Wantz, G., Solution-Processed P-Dopant as Interlayer in Polymer Solar Cells. *ACS Applied Materials & Interfaces* **2016**.
279. Li, J.; Rochester, C. W.; Jacobs, I. E.; Friedrich, S.; Stroeve, P.; Riede, M.; Moulé, A. J., Measurement of Small Molecular Dopant F4tcnq and C60f36 Diffusion in Organic Bilayer Architectures. *ACS Applied Materials & Interfaces* **2015**, *7*, 28420-28428.
280. Chen, L.-M.; Xu, Z.; Hong, Z.; Yang, Y., Interface Investigation and Engineering - Achieving High Performance Polymer Photovoltaic Devices. *Journal of Materials Chemistry* **2010**, *20*, 2575-2598.
281. Katz, E. A.; Faiman, D.; Tuladhar, S. M.; Kroon, J. M.; Wienk, M. M.; Fromherz, T.; Padinger, F.; Brabec, C. J.; Sariciftci, N. S., Temperature Dependence for the Photovoltaic Device Parameters of Polymer-Fullerene Solar Cells under Operating Conditions. *Journal of Applied Physics* **2001**, *90*, 5343-5350.
282. Mukherjee, A. K.; Thakur, A. K.; Takashima, W.; Kaneto, K., Minimization of Contact Resistance between Metal and Polymer by Surface Doping. *Journal of Physics D: Applied Physics* **2007**, *40*, 1789.
283. Meerheim, R.; Olthof, S.; Hermenau, M.; Scholz, S.; Petrich, A.; Tessler, N.; Solomeshch, O.; Lüssem, B.; Riede, M.; Leo, K., Investigation of C60f36 as Low-Volatility P-Dopant in Organic Optoelectronic Devices. *Journal of Applied Physics* **2011**, *109*, 103102.
284. Euvrard, J.; Revaux, A.; Bayle, P.-A.; Bardet, M.; Vuillaume, D.; Kahn, A., The Formation of Polymer-Dopant Aggregates as a Possible Origin of Limited Doping Efficiency at High Dopant Concentration. *Organic Electronics* **2018**, *53*, 135-140.
285. Tumbleston, J. R.; Collins, B. A.; Yang, L.; Stuart, A. C.; Gann, E.; Ma, W.; You, W.; Ade, H., The Influence of Molecular Orientation on Organic Bulk Heterojunction Solar Cells. *Nat Photon* **2014**, *8*, 385-391.

286. Osaka, I.; Takimiya, K., Backbone Orientation in Semiconducting Polymers. *Polymer* **2015**, *59*, A1-A15.
287. Aygül, U., et al., Molecular Orientation in Polymer/Fullerene Blend Films and the Influence of Annealing. *Solar Energy Materials and Solar Cells* **2014**, *128*, 119-125.
288. Sirringhaus, H., et al., Two-Dimensional Charge Transport in Self-Organized, High-Mobility Conjugated Polymers. *Nature* **1999**, *401*, 685.
289. Chang, J.-F.; Sun, B.; Breiby, D. W.; Nielsen, M. M.; Sölling, T. I.; Giles, M.; McCulloch, I.; Sirringhaus, H., Enhanced Mobility of Poly(3-Hexylthiophene) Transistors by Spin-Coating from High-Boiling-Point Solvents. *Chemistry of Materials* **2004**, *16*, 4772-4776.
290. Bao, Z.; Dodabalapur, A.; Lovinger, A. J., Soluble and Processable Regioregular Poly(3-Hexylthiophene) for Thin Film Field-Effect Transistor Applications with High Mobility. *Applied Physics Letters* **1996**, *69*, 4108-4110.
291. McCullough, R. D.; Tristram-Nagle, S.; Williams, S. P.; Lowe, R. D.; Jayaraman, M., Self-Orienting Head-to-Tail Poly(3-Alkylthiophenes): New Insights on Structure-Property Relationships in Conducting Polymers. *Journal of the American Chemical Society* **1993**, *115*, 4910-4911.
292. Schöll, A.; Fink, R.; Umbach, E.; Mitchell, G. E.; Urquhart, S. G.; Ade, H., Towards a Detailed Understanding of the Nexafs Spectra of Bulk Polyethylene Copolymers and Related Alkanes. *Chemical Physics Letters* **2003**, *370*, 834-841.
293. Pettersson, L. G. M.; Ågren, H.; Schürmann, B. L.; Lippitz, A.; Unger, W. E. S., Assembly and Decomposition of Building Blocks to Analyze Polymer Nexafs Spectra. *International Journal of Quantum Chemistry* **1997**, *63*, 749-765.
294. Hesse, R.; Weiß, M.; Szargan, R.; Streubel, P.; Denecke, R., Comparative Study of the Modelling of the Spectral Background of Photoelectron Spectra with the Shirley and Improved Tougaard Methods. *Journal of Electron Spectroscopy and Related Phenomena* **2013**, *186*, 44-53.
295. Peisert, H.; Chassé, T.; Streubel, P.; Meisel, A.; Szargan, R., Relaxation Energies in Xps and Xaes of Solid Sulfur Compounds. *Journal of Electron Spectroscopy and Related Phenomena* **1994**, *68*, 321-328.
296. Mikhnenko, O. V.; Azimi, H.; Scharber, M.; Morana, M.; Blom, P. W. M.; Loi, M. A., Exciton Diffusion Length in Narrow Bandgap Polymers. *Energy & Environmental Science* **2012**, *5*, 6960-6965.
297. Spoltore, D., et al., Effect of Molecular Weight on Morphology and Photovoltaic Properties in P3ht:Pcbm Solar Cells. *Organic Electronics* **2015**, *21*, 160-170.
298. Yin, W.; Dadmun, M., A New Model for the Morphology of P3ht/Pcbm Organic Photovoltaics from Small-Angle Neutron Scattering: Rivers and Streams. *ACS Nano* **2011**, *5*, 4756-4768.
299. Gomez, E. D.; Barteau, K. P.; Wang, H.; Toney, M. F.; Loo, Y.-L., Correlating the Scattered Intensities of P3ht and Pcbm to the Current Densities of Polymer Solar Cells. *Chemical Communications* **2011**, *47*, 436-438.
300. Rivnay, J.; Toney, M. F.; Zheng, Y.; Kauvar, I. V.; Chen, Z.; Wagner, V.; Facchetti, A.; Salleo, A., Unconventional Face-on Texture and Exceptional in-Plane Order of a High Mobility N-Type Polymer. *Advanced Materials* **2010**, *22*, 4359-4363.
301. Xue, B.; Vaughan, B.; Poh, C.-H.; Burke, K. B.; Thomsen, L.; Stapleton, A.; Zhou, X.; Bryant, G. W.; Belcher, W.; Dastoor, P. C., Vertical Stratification and Interfacial Structure in P3ht:Pcbm Organic Solar Cells. *The Journal of Physical Chemistry C* **2010**, *114*, 15797-15805.
302. Germack, D. S.; Chan, C. K.; Kline, R. J.; Fischer, D. A.; Gundlach, D. J.; Toney, M. F.; Richter, L. J.; DeLongchamp, D. M., Interfacial Segregation in Polymer/Fullerene Blend Films for Photovoltaic Devices. *Macromolecules* **2010**, *43*, 3828-3836.
303. Motaung, D. E.; Malgas, G. F.; Arendse, C. J.; Mavundla, S. E.; Oliphant, C. J.; Knoesen, D., The Influence of Thermal Annealing on the Morphology and Structural Properties of a Conjugated Polymer in Blends with an Organic Acceptor Material. *Journal of Materials Science* **2009**, *44*, 3192-3197.
304. Wu, W.-R.; Jeng, U. S.; Su, C.-J.; Wei, K.-H.; Su, M.-S.; Chiu, M.-Y.; Chen, C.-Y.; Su, W.-B.; Su, C.-H.; Su, A.-C., Competition between Fullerene Aggregation and Poly(3-Hexylthiophene) Crystallization Upon Annealing of Bulk Heterojunction Solar Cells. *ACS Nano* **2011**, *5*, 6233-6243.

305. Huang, Y.; Kramer, E. J.; Heeger, A. J.; Bazan, G. C., Bulk Heterojunction Solar Cells: Morphology and Performance Relationships. *Chemical Reviews* **2014**, *114*, 7006-7043.
306. Padinger, F.; Rittberger, R. S.; Sariciftci, N. S., Effects of Postproduction Treatment on Plastic Solar Cells. *Advanced Functional Materials* **2003**, *13*, 85-88.
307. Qiao, F.; Liu, A.; Hu, Z.; Liu, Y.; Yu, S.; Zhou, Z., Improved Photovoltaic Properties of Solar Cells Based on Poly [9, 9'-Dioctyl-Fluorene-Co-Bithiophene] and a Soluble Fullerene by Microwave Annealing. *Journal of Materials Science* **2009**, *44*, 3462-3465.
308. Ng, A.; Liu, X.; To, C. H.; Djurišić, A. B.; Zapien, J. A.; Chan, W. K., Annealing of P3ht:Pcbm Blend Film—the Effect on Its Optical Properties. *ACS Applied Materials & Interfaces* **2013**, *5*, 4247-4259.